PROPERTIES OF REDOX POLYMER MODIFIED ELECTRODES

AND

AN INVESTIGATION OF THE CLAIMS OF COLD FUSION

by

DAVID ALBAGLI

Bachelor of Science and Engineering, Princeton University
1985

SUBMITTED TO THE DEPARTMENT OF CHEMISTRY
IN PARTIAL FULFILLMENT OF THE REQUIREMENTS FOR THE
DEGREE OF DOCTOR OF PHILOSOPHY

at the

MASSACHUSETTS INSTITUTE OF TECHNOLOGY

June 1990

Signature of Author.....
Department of Chemistry
May 25, 1990

Certified by.....
Mark S. Wrighton
Thesis Supervisor

Accepted by.....
Glenn A. Berchtold
Chairman, Departmental Committee on Graduate Students

This doctoral thesis has been examined by a Committee of the Department of Chemistry as follows:

Professor Alan Davison.....
Chairman

Professor Mark S. Wrighton.....
Thesis Supervisor

Professor Hans-Conrad zur Loye.....

PROPERTIES OF REDOX POLYMER MODIFIED ELECTRODES

AND

AN INVESTIGATION OF THE CLAIMS OF COLD FUSION

by

DAVID ALBAGLI

Submitted to the Department of Chemistry
on May 24, 1990 in partial fulfillment
of the requirements for the
Degree of Doctor of Philosophy in Chemistry

ABSTRACT

Chapter I

A brief overview of the field of chemically modified electrodes is given. The relation of the work presented here to the general goals of the field is pointed out.

Chapter II

The synthesis and application of 1,1'-di(4-triethoxysilylbutyl)octamethylferrocene, **1**, as an electrode derivatizing reagent is presented. Electrode-confined electroactive polymers are formed by hydrolysis and condensation of the triethoxysilyl groups to give a siloxane polymer, cross-linked to the oxide surface of the electrode. This peralkylated ferrocene reagent yields hydrophobic films with a redox potential negative of SCE, -0.090 V. The current response of electrode-confined films of **1** significantly decreases, or becomes nonexistent, upon switching the electrode from a nonaqueous cell to an aqueous cell. This loss in the ability to pass charge is reversible. On n-Si, films of **1** cannot be oxidized in the dark. Upon photonic excitation of n-Si with $h\nu > E_{band\ gap}$, **1** is oxidized with a photovoltage of 450 mV. The contact angle of water droplets on films of **1** approaches 90° for electrodes with a coverage of **1** of 6.4×10^{-9} mol cm^{-2}. In comparison, polyvinylferrocene films have a contact angle of 61°, and show a larger faradaic response in aqueous cells.

Chapter III

The preparation of well-defined redox active polymers and block polymers is presented. The polymers were prepared in a living polymerization by ring-opening metathesis of norbornene derivatives using $Mo(CHR)(O\text{-}t\text{-}Bu)_2(NAr)$ (Ar = 2,6-diisopropylphenyl) as the initiator. Redox active

monomers, containing ferrocene and phenothiazine, have been made and were used to prepare a series of polymers and block polymers with norbornene. The polymers have been characterized by NMR, gel permeation chromatography, differential scanning calorimetry, and field desorption mass spectrometry. The solution electrochemical behavior was studied by cyclic voltammetry and normal pulse voltammetry, and was shown to be influenced by the block formation with norbornene. Unique functionalities were incorporated into the polymer as end groups. Redox active end groups were incorporated into the starting end group using Mo(CHFc)(O-*t*-Bu)$_2$(NAr), a Mo ferrocenylmethylidene, to initiate, and into the capping end group using octamethylferrocenecarboxaldehyde to terminate the polymerization. The emission properties of pyrene-capped polymers was studied. Pyrene emission was quenched in ferrocene and phenothiazine polymers. When a phenothiazine block was adjacent to the pyrene end group, pyrene emission was quenched by exiplex formation.

Chapter IV

Polymers were made by the methods described in Chapter III that contain functional groups capable of binding to electrode surfaces. The surface binding groups were incorporated as monomers or as end groups. Block polymers made with the monomer triethoxysilylnorbornene, a silane coupling reagent, and a redox-active monomer could be used to derivatize Pt, In(Sn)O_2, and n-Si electrodes. Polymers end-capped using pyrenecarboxaldehyde were examined for adsorption into C surfaces via the pyrene group. Homopolymers of the ferrocene and phenothiazine monomers were found to adsorb to C irrespective of the presence of a pyrene end group. Electroactive polymers end-capped with a nucleophilic group, pyridine, or an electrophilic group, a benzylhalide, were reacted with electrode surfaces that had been treated with silane reagents containing the complimetnary reactant, a benzylhalide or pyridine, respectively, to produce a derivatized electrode surface.

Chapter V

The background to the experiments done at MIT to try to duplicate the claims of cold fusion by Pons, Fleischmann, and Hawkins is given.

Chapter VI

Results of experiments intended to reproduce cold fusion phenomena originally reported by Fleischmann, Pons, and Hawkins are presented. These experiments were performed on a pair of matched electrochemical cells containing 0.1 x 9 cm pd rods that were operated for 10 days. The cells were analyzed by the following means: 1) constant temperature

calorimetry; 2) neutron counting and γ-ray spectroscopy; 3) mass spectral analysis of ^4He in effluent gases, and ^4He and ^3He within the Pd metal; 4) tritium analysis of the electrolyte solution; and 5) X-ray photoelectron spectroscopy of the Pd cathode surface. Within our estimated levels of accuracy, no excess power output or any other evidence of fusion products was detected.

Chapter VII

An 80 MeV/c negative muon beam from the Alternating Gradient Synchrotron at Brookhaven National Laboratory was used to investigate the stopping of muons inside Pd, Ti and Y targets saturated with deuterium. Neutron emission from the targets was measured with an array of ^3He detectors, and in some runs, the temperature of the target was monitored as a function of time, with and without a flux of muons on the target. The neutron rates were also measured for Pd cathodes in an active electrochemical cell similar in design to those used in "cold fusion" experiments, and the electrolyte solution was analyzed for excess tritium. No evidence was found for muon catalyzed fusion at rates consistent with those claimed in cold fusion experiments. Neutron production from catalyzed fusion due to the presence of deuterium in palladium deuteride, $PdD_{0.7}$, exposed to muons was determined to be 0.0 ± 0.03 (stat.) ± 0.25 (syst.) neutrons per stopped muon.

Thesis Supervisor: Mark S. Wrighton
Title: Department Head and CIBA-GEIGY Professor of Chemistry

To my parents, and the rest of our family
who all brought me to this point.
And to Feng-Yi...

ACKNOWLEDGMENTS

I would like to acknowledge the assistance of the Whitesides group in the Chemistry Department at Harvard Univerity, and the use of their facility, for performing the contact angle measurements described in Chapter II.

Field-desorption mass spectroscopy, presented in Chapter III, was carried out at the NIH Regional Facility for mass spectroscopy at MIT, by Dr. C. Costello.

The work presented in Chapter III and IV resulted from a collaboration with Professor R. R. Schrock and his student, Gui Bazan. This collaboration combined the methodology developed by the Schrock group for ring-opening metathesis polymerization using Mo alkylidene initiators, with our interest in the properties of electroactive polymers.

The experimental testing of the claims of cold fusion by Pons and Fleischmann by the group at MIT is documented in Part 2. The lists of coauthors in these projects are given on the title pages of Chapters VI and VII.

I would like to express my thanks to my co-workers throughout the years. You Wrighton group members, present and past, (that timeline was never constructed, so we'll have to guess who was here when) have made this lab a great place, if not an amusing place, to work. A special word of thanks to Dr. Dick Crooks and Dr. Richard Giasson for showing me (some of the) the elementary ropes in electrochemical and synthetic techniques, respectively.

I cannot leave out the Schrock group (we're all here for the same purpose anyway); thanks for the help, the discussions, etc. Enjoy the 4th floor.

I would like to thank Professor R. R. Schrock for an enjoyable collaboration.

Finally, I thank Professor Mark S. Wrighton for his support and guidance, and for allowing the freedom to develop new projects. His approach to science is exemplary, and stands for me as one to aspire to.

BIOGRAPHICAL NOTE

The author was born on December 11, 1962, in East Orange, NJ. After graduating from Governor Livingston Regional High School in Berkeley Heights, NJ, in 1981, he attended Princeton University. At Princeton, he developed an interest in chemistry, doing his senior thesis with Professor Maitland Jones in the Chemistry Department, but receiving a BSE degree in Chemical Engingeering, in 1985. He finally left New Jersey to attend the Massachusetts Institute of Technology, to pursue those chemical interests.

TABLE OF CONTENTS

LIST OF FIGURES

Number Page

Chapter II

Chapter III

Chapter VII

LIST OF SCHEMES

Number Page

Chapter II

Chapter III

Chapter IV

LIST OF CHARTS

Number Page

Chapter III

Chapter IV

LIST OF TABLES

Number Page

Chapter II

Chapter III

Chapter VI

PART 1

POLYMER MODIFIED ELECTRODES

Chapter I

Introduction

The study of the electrochemical behavior of modified electrodes has yet to reach its 20th anniversary but in this brief history there has been remarkable progress and work now aims toward what was unimaginable at the start. The field began with efforts to exploit the adsorption of certain compounds onto metal electrodes,[1] a situation first considered to be a complication in solution electrochemical studies. The idea of exploiting adsorption phenomena gave way to purposeful modification of an electrode surface via a variety of techniques, including specific adsorption,[2] covalent bonding,[3] electrostatic binding,[4] or precipitation.[5] Now, discussion focuses on tailoring an electrode surface for a specific, supermolecular purpose such as photoinduced unidirectional charge transport.

Early work in this field by A. T. Hubbard, F. C. Anson, L. L. Miller and R. W. Murray, researchers who are still active, addressed such topics as the structure and properties of the double layer, electrocatalysis, chiral induction in electroorganic synthesis, and analytical detection. The scope of applications soon increased and polymers began to be used to derivatize electrodes.[6] With polymer modified electrodes, the number of electroactive sites available to the electrode is significantly increased over monolayer coverages of molecular species, consequently there is a larger signal-to-background ratio (faradaic to ohmic current) and a more easily detected response. However, charge transport through the polymer coating is a

more complex process than at a conductor-solution interface and the nature of the charge-compensating electrolyte and the solvent influences the performance of the polymer modified electrode. A basic understanding of the mechanism of charge transport in such films became a goal in itself. Modified electrodes were also applied toward problems ranging from mediation of biological redox compounds, to improvements in solar energy conversion through photosensitization or photo-anode corrosion suppression.[7] R. W. Murray's review[6] in 1984 represents a comprehensive survey to that date, and is the best entry into the literature in this field.

In recent years, turning polymer modified electrodes into functional materials such as secondary batteries, information storage devices, and display devices has been of interest. Such topics are explored in a recent review entitled "Polymer-Coated Electrodes: New Materials for Science and Technology".[8] Also, long-range projects being discussed include artificial photosynthetic systems[9] and molecular memory devices.[10] Basic building blocks in the development of such systems have been of particular interest to the Wrighton group. The assembly of complex systems such as these will require the synthesis of well-defined macromolecule(s) and the ability to spatially assemble and orient such macromolecule(s) at the electrode interface in order to achieve the intended supermolecular function. These are the new demands on the ability to control the

chemical modification of electrode surfaces.

In Part 1 of this thesis studies of various kinds of polymer modified electrodes are presented. Chapter II details work on films of a peralkylated ferrocene derivative. Ferrocene polymers represent the most often studied class of redox polymers and are usually used as the prototypic redox polymer in work using new techniques to study these polymers. For the most part, the ferrocene center is a mono- or disubstituted derivative,[11] and there are only a few examples of penta- or hexasubstituted ferrocene-based redox polymers.[12] A reason for increasing the number of substituents on the cyclopentadienyl rings is to shift the redox potential to more negative values. Decamethylferrocene has a redox potential of -0.1 V vs. SCE, which is approximately 0.5 V negative of ferrocene. Peralkylated derivatives then can be used to reversibly mediate to a variety of biological redox compounds since their redox potentials are more nearly matched, or, in electron transfer chains with ferrocene derivatives where there would be a ~0.4 V driving force for electron transfer. The peralkylated ferrocene-based polymer studied here is the first example of such a redox polymer. A consequence of peralkylation, however, is an increase in the hydrophobicity of the ferrocene center. This has a large effect on the charge transport properties of the film in different solvents.

Chapter III presents work on the properties and

electrochemical behavior of well-defined polymers and block polymers prepared by ring-opening metathesis polymerization (ROMP). Because ROMP is a living process the polymer produced has a narrow molecular weight range. The living polymerization process allows a polymer to be built up into blocks from different monomers, which may be electroactive, may bind to electrode surfaces, or may have other functional groups which affect solubility, for example. ROMP provides a new class of electroactive polymers with a well-defined primary structure that can be characterized by a variety of methods used in polymer analysis prior to electrode attachment.

In Chapter IV, methods for confining polymers prepared by ROMP to electrode surfaces are presented. Functional groups that are capable of binding to electrode surfaces can be incorporated into these polymers either in monomer units or as end groups. In both cases the location of the binding group is well-defined in terms of the primary structure of the polymer. First, the utility of the binding groups are determined, then the consequences of attaching these polymers to electrodes can be studied.

References

1. (a) Lane, R. F.; Hubbard, A. T. *J. Phys. Chem.* **1973**, *77*, 1401. (b) Lane, R. F.; Hubbard, A. T. *J. Phys. Chem.* **1973**, *77*, 1411.

2. Brown, A. P.; Koval, C.; Anson, F. C. *J. Electroanal. Chem.* **1976**, *72*, 379.

3. (a) Moses, P. R.; Wier, L.; Murray, R. W. *Anal. Chem.* **1975**, *47*, 1882. (b) Watkins, B. F.; Behling, J. R.; Kariv, E.; Miller, L. L. *J. Am. Chem. Soc.* **1975**, *97*, 3549.

4. Oyama, N.; Anson, F. C. *J. Electrochem. Soc.* **1980**, *127*, 247.

5. Merz, A.; Bard, A. J. *J. Am. Chem. Soc.* **1978**, *100*, 3222.

6. Murray, R. W. In *Electroanalytical Chemistry;* Bard, A. J., Ed.; Dekker: New York, NY, 1984; Vol. 13, p 191 and references therein.

7. Wrighton, M. S. *ACS Symp. Ser.* **1982**, No. 192, 99.

8. Kaneko, M.; Wöhrle, D. *Adv. Polym. Sci.* **1988**, *84*, 141.

9. Wrighton, M. S. *Comments Inorg. Chem.* **1985**, *4*, 269.

10. Hopfield, J. J.; Onuchic, J.; Beraten, D. N. *J. Phys. Chem.* **1989**, *93*, 6350.

11. (a) Rockett; B. W., Marr, G. *J. Organomet. Chem.* **1988**, *357*, 247 and preceding Annual Survey issues noted. (b) Shimidzu, T.; Iyoda, T. *Kagaku (Kyoto)* **1983**, *38*, 661.

12. Chao, S; Robbins, J. L.; Wrighton, M. S. *J. Am. Chem. Soc.* **1983**, *105*, 181.

13. Calvert, J. M.; Schmehl, R. H.; Sullivan, B. P.; Facci, J. S.; Meyer, T. J.; Murray, R. W. *Inorg. Chem.* **1983**, *22*, 2151.

14. Fawcett, A. H. In *Encyclopedia of Polymer Science and Technology;* Kroschwitz, J. I., Ed.; Wiley-Interscience: New York, NY, 1985; Vol. 10, p 408.

Chapter II

Characteristics of Decaalkylferrocene-Modified Electrodes: Hydrophobic Electroactive Films

Introduction

This chapter details the synthesis and application of the peralkylated ferrocene, 1,1'-di(4-triethoxysilylbutyl) octamethylferrocene, **1**, as a hydrophobic electrode

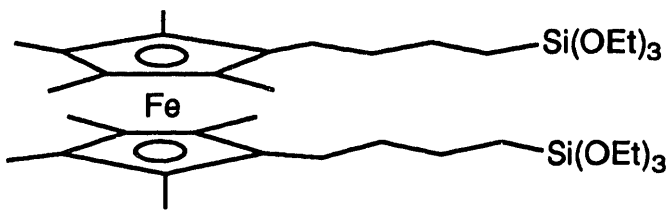

1

derivatizing reagent. The consequences of the hydrophobicity is that in aqueous electrolyte solutions the cyclic voltammetric behavior of the electrode-confined decaalkylferrocene film is poor. For electrodes with coverages at least 10 monolayers thick (~2 x 10^{-9} mol cm^{-2}) there is relatively little faradaic current, in contrast to other ferrocene polymers in which the film passes its full complement of charge. In organic solutions the behavior is significantly improved, exhibiting a nearly ideal response[1] for a surface-bound, fast electron transfer reagent. In aqueous electrolyte solutions the characteristics of the redox wave of decaalkylferrocene can approach that of the ideal case by covalently binding an organic solvent within the polysiloxane film. The contact angle formed by water on electrode-confined polymers of **1** was measured to assess the hydrophobicity of what is the polymer-solution interface.

Charge Transport in Redox Polymers. Ferrocenes have been widely studied as surface derivatizing reagents in work on

chemically modified electrodes since they possess many of the qualities wanted in a redox couple and they can be synthetically tailored to suit almost any purpose. Because the ferrocene unit is a fast, outer-sphere, one electron redox couple, both halves of which are stable, and also, since the redox potential is nearly invariant in all solvents, it has been proposed by IUPAC for use as a reference redox couple.[2] The hundreds of ferrocene derivatives that have been made indicates the synthetic versatility. This versatility is augmented by the fact that the redox potential can be adjusted over a range of 1.0 V by varying the ring substituents.[3] Thus the ferrocene "active site" can serve in most any system.

The charge transport properties of polymer modified electrodes depends on many more factors than just the electron transfer properties in the redox couple. Factors such as the structure of the monomer, the degree of cross-linking, polymer flexibility or rigidity, porosity, and the mobility of charge compensating ions all affect the overall rate of charge transport.[4] The solvent is also a factor; it must be able to solvate the polymer film since it must facilitate ion motion at the electrode-polymer interface, the point where the charged sites in the film are created or annihilated.[5]

The passage of charge through a polymer modified electrode is a diffusional process[6] with an associated constant, D_{ct} [cm^2 s^{-1}]. There have been many studies to determine what

the rate limiting process is for charge transport in redox polymer films.[4a] For the same polymer system diffusional rates can be highly dependent on solvent. The importance of the solvent is illustrated in Figure 1 with a poly(vinylferrocene) modified electrode.[7] The solvent dramatically alters the charge transport dynamics. In most systems the amount of charge passed diminishes and slower kinetics are obtained with poorer solvents.

Synthesis of Peralkylated Ferrocenes. One of the limitations of ferrocene redox polymers is that in the oxidized state ferrocenium is not stable in the presence of many nucleophiles[8] and restricts these polymers from use in certain applications.[9] The oxidized state is stabilized by the presence of electron donating groups in the ring.[10] So, by alkylating the cyclopentadienyl rings a more durable redox center is obtained. In the limit, a peralkylated ferrocene, the redox center is not as sensitive to nucleophilic decomposition, and also the electron self-exchange rate is ~10 times faster than for ferrocene.[11] Given this, and the opportunity to mediate electron transfer in a more negative potential range, peralkylated ferrocene derivative-based polymer modified electrodes are worth investigating.

There are fewer synthetic routes to persubstituted derivatives than for simpler derivatives of ferrocene, although this cannot be considered a limitation. Three good routes into nona- and decaalkyl derivatives are shown in

Figure 1. Cyclic voltammograms of poly(vinylferrocene) modified Pt electrodes in three different solvents, adapted from Ref. 6. (a) CH_3CN; scan rate 10 mV s^{-1}; S = 12 μA cm^{-2}. (b) 1:1 EtOH/H_2O; 50 mV s^{-1}; S = 120 μA cm^{-2}. (c) H_2O; 10 mV s^{-1}; S = 32 μA cm^{-2}. The potential scale is in volts vs. SCE. The electrolyte is 0.1 M $LiClO_4$, and three different electrodes with coverages ~5 x 10^{-9} mol cm^{-2} were used.

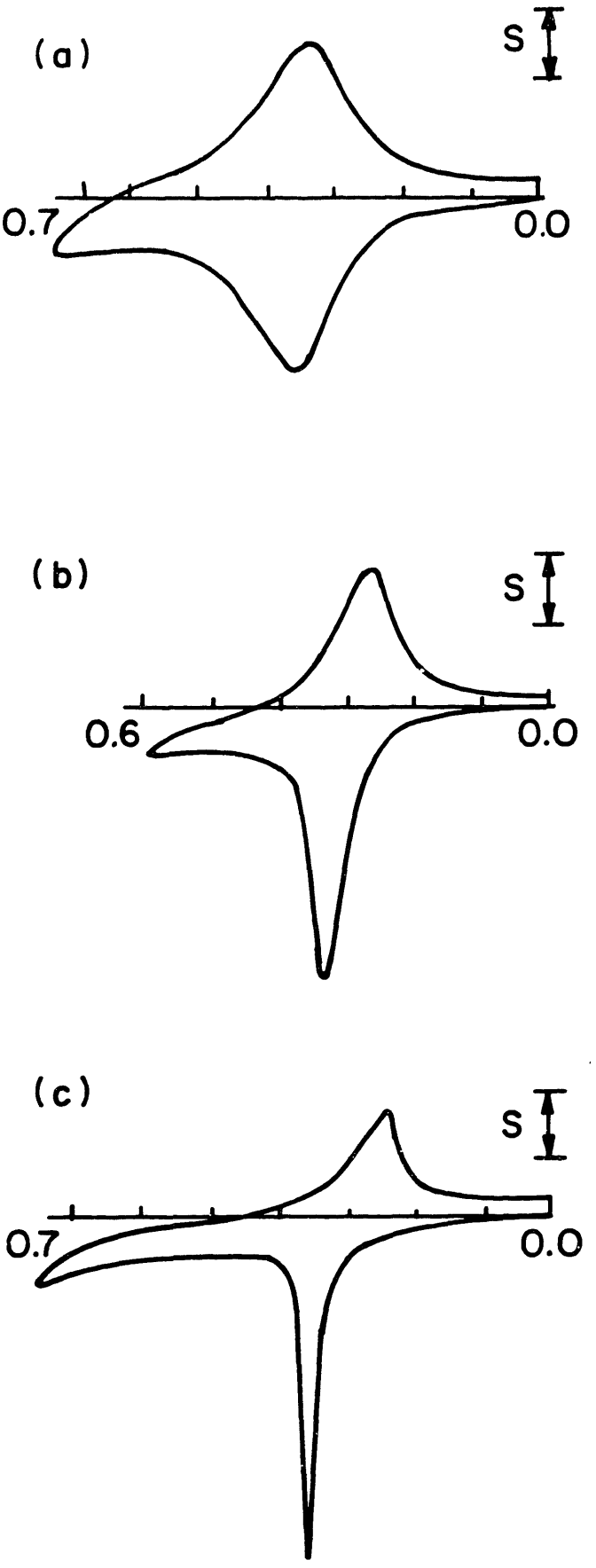
(a)
S
0.7
0.0
(b)
S
0.6
0.0
(c)
S
0.7
0.0

Scheme I. Route 1[12] is a simple modification of Bercaw's C_5Me_5H synthesis in which an appropriately functionalized ester is used in place of the acetate ester. Route 2[13] turns what was a competing side reaction in earlier procedures into the desired reaction pathway, resulting in improved yields. Whereas when nucleophiles are added to tetramethylcyclopentadiene abstraction of the α proton to form the enol is a competitive side reaction to 1,2 addition, in route 2 the enol is formed and reacted with the appropriate electrophile. The ligands made in these two reactions directly lead to symmetric peralkylated ferrocenes. There are procedures reported for the formation of asymmetric metallocenes in better than a statistical yield which can be applied to these ligands.[14] However, the benefit of route 3[15] is that it is a simpler and more efficient way to make asymmetric polyalkylated derivatives.

Contact Angles. The contact angle of a liquid on a solid arises from a balancing of the interfacial free energies at the solid-liquid-vapor interfaces[16] as shown in Figure 2 and expressed by equation 1:

$$\gamma_{LV}\cos\theta = \gamma_{SV} + \gamma_{SL} \qquad (1)$$

where γ is the interfacial free energy between the various solid (S), liquid (L) and vapor (V) phase boundaries. The thermodynamics of real systems are more complicated, but this simple mechanical balance, first derived in 1805[17] is widely used and does describe the thermodynamic equilibrium in the ideal case.[18] The macroscopic drop is formed from

Scheme I. Three synthetic routes to polyalkylated ferrocene derivatives.

Reaction 1

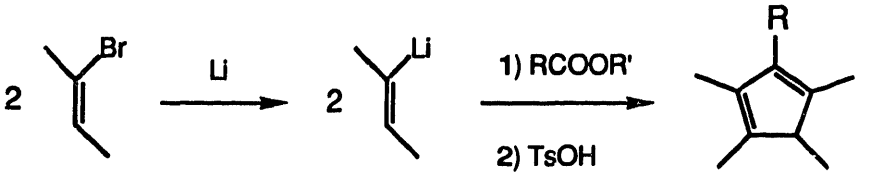

Reaction 2

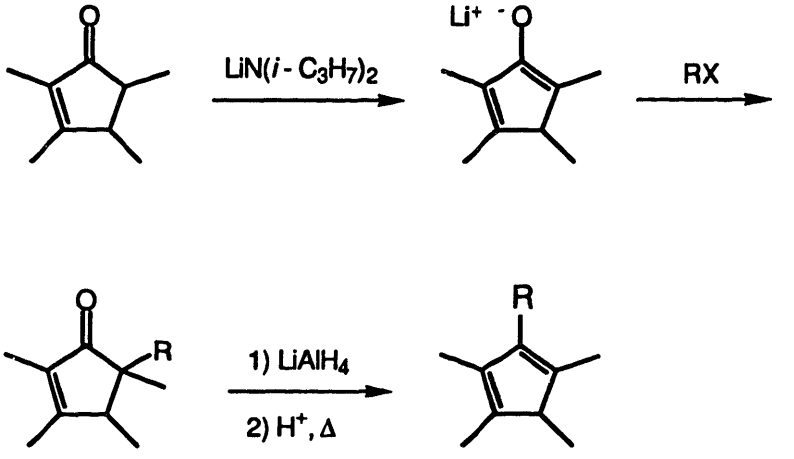

Reaction 3

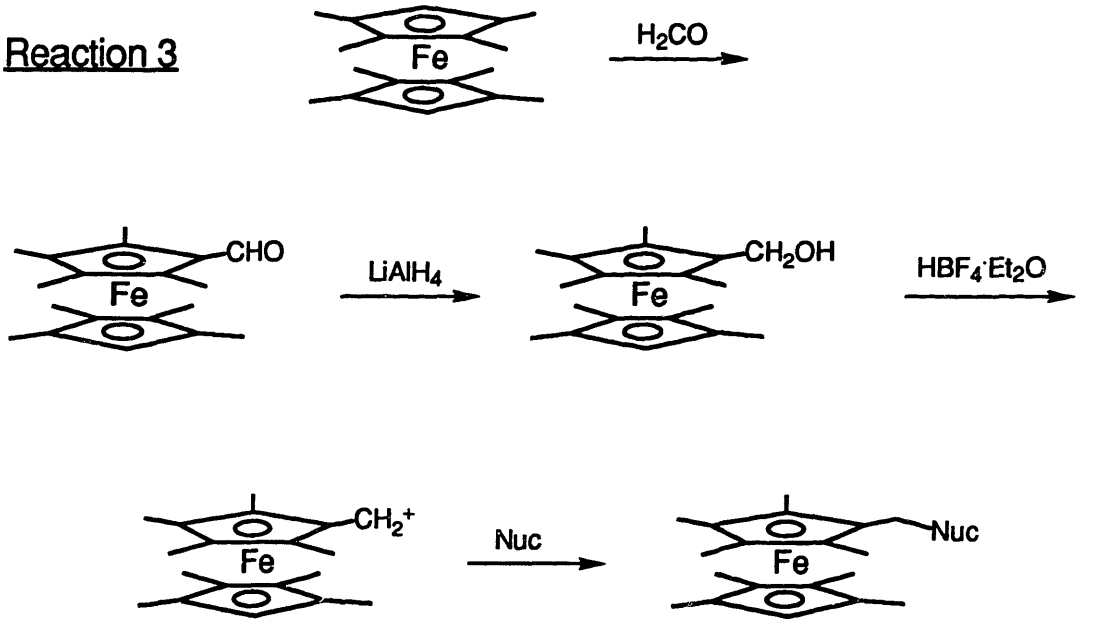

Figure 2. The interfacial forces that determine the wetting properties of a liquid on a solid substrate. The contact angle is denoted as θ.

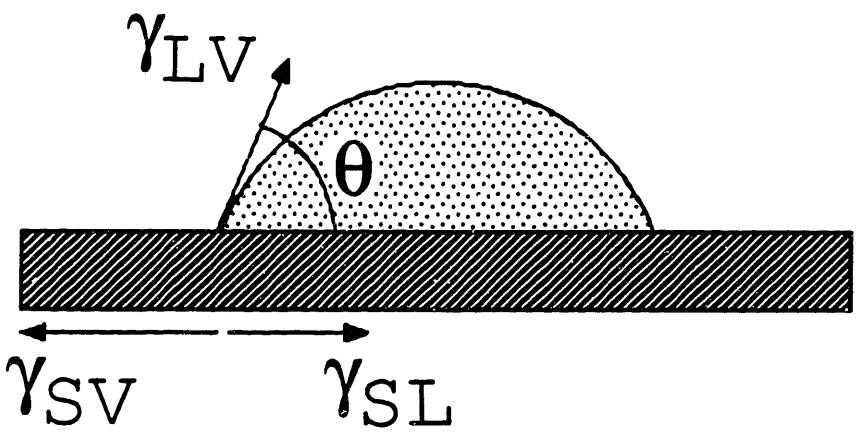
γ_{LV}
θ
γ_{SV}
γ_{SL}

contributions of the molecular properties and the microscopic structure in the surface of the solid to the interfacial free energy. The angle between the tangent normal to the drop at the interface and the surface of the solid can be easily measured by a variety of techniques.[19] This measurement is widely used in industry as a simple and convenient method to characterize surfaces. The interpretation is largely empirical, though the effects of some surface complexity can be modelled. Deriving a detailed understanding of the surface structure from this measurement is difficult. Only recently have there been experiments that have tried to correlate wetting properties with the structure at the molecular level.[20]

Experimental

Electrochemistry. Electrochemical experiments were performed with a PAR 173 potentiostat and a PAR 175 universal programmer, or a Pine Instruments RDE-4 bipotentiostat. Current-potential traces were recorded on a Houston Instruments X-Y recorder or a Kipp and Zonen BD 91 X-Y recorder. All experiments were performed at ambient temperatures, 23°C.

All electrolyte salts were reagent grade; $NaClO_4$ and $LiClO_4$ were used as received and $[n\text{-}Bu_4N]ClO_4$ was recrystallized from EtOH and dried in vacuo at 80°C for 48 h. Absolute EtOH, spectral grade isooctane, HPLC grade CH_2Cl_2, glass distilled deionized H_2O, and butyronitrile (Aldrich) were used as received. 3-Cyanopropyltriethoxysilane (Petrarch) was handled under N_2 in a dry box. Glass-distilled CH_3CN (EM Science) was passed through a column of activated alumina and collected under N_2 in a dry bottle containing 4Å molecular sieves for storage.

Electrochemical measurements were made using a conventional one-compartment, three electrode cell. In aqueous and ethanolic solutions an SCE reference electrode was used. In all other solvents a 0.01 M Ag^+/Ag reference electrode was used. The counter electrode was Pt gauze. The working electrode was a Pt disk (Pt wire sealed in soft glass), a Pt flag, or a Pt gauze electrode. For the latter two electrical contacts were made by joining a Cu wire to the Pt with Ag epoxy, insulating the contact with white

epoxy (Hysol), and passing the Cu wire through a glass tube for support. To reuse the Pt disk electrodes they were soaked in concentrated HNO_3 for 5 min, and repolished with 3μ and 1μ Metadi diamond paste (Buehler) to a mirror-like finish. Before use the electrodes were electrochemically pretreated by anodization at +2.0 V vs. SCE in 1 N H_2SO_4 for 15 s, followed by continuously cycling the potential between -0.27 and +1.30 V at 100 mV s^{-1} until the i-V trace was constant. If the electrode was to be derivatized with a triethoxysilyl reagent the electrode was finally anodized to form an oxide layer on the surface by holding the potential at +1.30 V until the current decayed to the background level, and then removing it from potential control. Electrodes not to be derivatized were removed from potential control at +0.4 V. The electrodes were then rinsed thoroughly with H_2O, EtOH, and then the next solvent in which they were to be used. Derivatization was accomplished by soaking pretreated electrodes in a ~10 mM isooctane solution of the triethoxysilyl reagent(s) for times ranging from 30 s to 48 h. The electrodes were rinsed thoroughly with isooctane, CH_3CN, and EtOH prior to use.

n-Si electrodes were fabricated from single-crystal, P-doped, (100 orientation) n-Si wafers with resistivities between 0.5 and 1.5 Ω/cm that were obtained from Monsanto. Electrodes were made from ~0.25 cm^2 pieces cut from the wafer. Ohmic contact to the n-Si was made by scratching the Si surface and applying Ga-In eutectic. The Cu lead was

secured to the Ga-In with Ag epoxy. The Cu lead was supported in a glass tube, and all but the polished Si face was insulated with 1C White epoxy (Hysol, Seabrook, NH).

n-Si electrodes were pretreated for derivatization with triethoxysilyl reagents by soaking in concentrated HF for 30 s, rinsing with H_2O, soaking in 10 M NaOH for 60 s, rinsing with H_2O, CH_3CN, and the solvent used for the derivatization solution. The electrodes were then immediately placed into the derivatization solution. The derivatized electrodes were rinsed with the soaking solvent and EtOH before being used in electrochemical experiments. For photoelectrochemical experiments with n-Si, the electrodes were irradiated with a 5 mW He-Ne laser emitting at 632.8 nm with the beam expanded to cover the electrode area (0.25 cm^2).

Contact Angle Measurements. Measurements were made on a Ramé-Hart Model 100 contact angle goniometer equipped with an environmental chamber using a 1 μL drop of doubly distilled water. The chamber atmosphere was maintained at 100% humidity by filling the wells in the chamber with distilled water. The contact angle was determined by measuring the tangent normal to the sessile drop at the liquid-solid interface. The substrates used were Pt flag electrodes derivatized with triethoxysilyl reagents as described above. The electrodes were first examined electrochemically to assess the coverage and were removed from the cell in the reduced state, and rinsed thoroughly

with CH_3CN and EtOH. After determining the contact angle on the reduced samples, the films were oxidized by soaking in a stirred CH_3CN solution of ferrocenium tetrafluoroborate for approximately 15 min. Each value reported represents an average of at least 8 different drops from various locations on the substrate. The substrate was rinsed with absolute EtOH and dried with a stream of N_2 between sets of measurements.

Synthesis. All chemicals used were reagent grade. Tetrahydrofuran was distilled from $LiAlH_4$ under N_2, and anhydrous ethyl ether (Mallinckrodt) and the solvents used in chromatography (Mallinckrodt) were used as received. The alumina used in chromatography was Woelm Alumina, neutral, Akt. I, from ICN Biomedicals. 2-Bromo-2-butene was from Columbia Organic Chemical Company, *n*-butyl lithium (*n*-BuLi) and anhydrous ferrous chloride ($FeCl_2$) were from Alfa Products, and all other chemicals were from Aldrich Chemical Company.

^1H NMR spectra were recorded on a Bruker 250 MHz or a Varian XL-300 MHz FT spectrometer. Electronic absorption spectra were obtained on a Hewlett-Packard 8541A diode array spectrometer or a Cary 17 spectrometer using 1 cm pathlength quartz cuvettes. Spectral grade solvents were used without further purification. Mass spectrometry was done with a Finnigan MAT System 8200 with a double focusing magnetic sector by electron impact (70 eV). Melting points were obtained with a Thomas capillary melting point apparatus,

and are uncorrected. Elemental analyses were done by Schwarzkopf Microanalytical Laboratory, Woodside, NY.

Methyl 4-pentenoate. According to the literature,[21] to 25.5 mL (0.25 mol) of 4-pentenoic acid was added 1.14 g (0.006 mol) of *p*-TsOH·H_2O dissolved in 10 mL (0.25 mol) of CH_3OH followed by 34.4 mL (0.28 mol) of 2,2-dimethoxypropane, added in one portion. The solution was stirred at room temperature. After 20 h, the solution was washed with saturated aqueous $NaHCO_3$, and then saturated aqueous KCl. The organic solution was dried with $MgSO_4$, filtered, and the solvents were removed in a simple distillation apparatus. A 5 cm Vigreux column was added to the distillation apparatus, and 21.5 g (0.19 mol) of the ester was collected by distillation as a clear, colorless oil at 127-129°C (Lit.[22] bp 128°C). ^1H NMR ($CDCl_3$) δ 2.32 (m, 4 H), 3.60 (s, 3 H), 4.94 (m, 2 H), 5.74 (m, 1 H).

1-(3-butenyl)-2,3,4,5-tetramethylcyclopentadiene. According to the literature,[11] a 500 mL three-neck round bottom flask was equipped with a gas inlet, addition funnel, condenser fitted with a gas outlet and a stir bar, and then flame dried under a flow of Ar. Li wire (99.9%) was wiped clean of its protective mineral oil with a hexane soaked tissue, scraped with a razor to expose a shiny surface and then added to a tared beaker containing xylene to be weighed. Under a stream of Ar, 5.30 g (0.765 mol) Li was added to the flask by cutting the wire into 0.5 cm segments. Via cannula, 250 mL Et_2O was added to the flask. A portion, 7.1

mL (0.07 mol), of freshly distilled 2-bromo-2-butene was cannulated into the addition funnel and added dropwise to the stirred Li suspension, causing the Et_2O to gently reflux and a white precipitate to form. The remainder, 28.9 mL (0.28 mol) of the 2-bromo-2-butene and 20.20 g (0.177 mol) of methyl 4-pentenoate were cannulated into the addition funnel. This mixture was added dropwise at a rate that maintained a gentle reflux of the Et_2O. Addition was complete after 2.5 h. After stirring the mixture for an additional 2 h, 150 mL saturated aqueous NH_4Cl was added slowly, dropwise to the reaction mixture, causing the Et_2O to reflux. The phases were separated, and the aqueous phase was extracted (2 x 125 mL) with Et_2O. The organic phases were combined, dried with $MgSO_4$, filtered and concentrated to 50 mL. The ethereal solution was added dropwise to a stirred solution of 3 g *p*-TsOH·H_2O in 100 mL Et_2O. The solution was stirred another 15 min and then poured into 200 mL saturated aqueous $NaHCO_3$ containing 2.5 g of Na_2CO_3. The phases were separated and the aqueous phase was extracted (2 x 100 mL) with Et_2O. The organic phases were combined, dried with $MgSO_4$, filtered and concentrated to give 25 mL of a clear, yellow oil as the crude product. Purification by distillation was not effective. Instead, 12 g of the product was obtained by column chromatography using alumina eluted with hexane. TLC R_f 0.95 (hexane); ^1H NMR ($CDCl_3$) major isomer: δ 1.0 (d, 3 H), 1.55 (m, 2 H), 1.78 (m, 9 H), 2.11 (m, 2 H), 2.27 (q, 1 H), 4.94 (m, 2 H), 5.82 (m, 1 H).

1,1'-di(3-butenyl)octamethylferrocene (2). According to the literature,[23] in a dry box, 4.0 g (22.5 mmol) of 1-(3-butenyl)-2,3,4,5-tetramethylcyclopentadiene was added to 80 mL Et_2O in a 250 mL beaker. To the stirred ethereal solution was added 9 mL of 2.6 M *n*-BuLi (hexane solution), forming a white precipitate. After stirring the mixture an additional 15 min the solid was collected on a fritted funnel and washed with Et_2O to give 2.6 g of an off-white solid (14.1 mmol of LiCp'). The solid was dissolved in tetrahydrofuran and added to a stirred solution of 0.89 g (7.06 mmol) of $FeCl_2$ in tetrahydrofuran. The color soon turned yellow, and then brown. After 48 h the brown liquid was concentrated to a solid by evaporation. The residue was taken up in pentane and chromatographed on an alumina column eluted with pentane. The yellow band moving with the solvent front was collected and concentrated to give 2.1 g of crude product. The product was purified by sublimation at 95°C/0.07 mm Hg to give 1.73 g of **2**. MP 67°C; ^1H NMR (C_6D_6) δ 1.64 (s, 6 H; 3-Me, 4-Me), 1.67 (s, 6 H; 2-Me, 5-Me), 2.08 (m, 2 H; $CH_2CH=CH_2$), 2.30 (m, 2 H; $CH_2CH_2CH=$), 4.97 (m, 1 H; CH=C*H*H, *E*) 5.06 (m, 1 H; CH=CH*H*, *Z*), 5.84 (m, 1 H; C*H*=CHH); ^{13}C NMR (C_6D_6) δ 9.73 (3-Me, 4-Me), 9.84 (2-Me, 5-Me), 25.75 ($CH_2CH_2CH=$), 35.63 ($CH_2CH=CH_2$), 78.21 (Cp ring C 3,4), 79.03 (Cp ring C 2,5), 82.42 (Cp ring C 1), 114.53 ($CH=CH_2$), 139.05 ($CH=CH_2$); MS *m/e* (relative abundance) 406 (M^+, 55), 365 (M - $CH_2CH=CH_2^+$, 15), 350 (M - $CH_2CH_2CH=CH_2^+$, 26), 176 (Cp' + 1^+, 17), 175 (Cp'^+, 23), 174

(Cp' - 1^+, 29), 135 ($C_{10}H_{15}^+$, 51) 133 ($C_{10}H_{13}^+$, 100); UV-vis (isooctane) λ_{max}/nm (log ε) 422 nm (2.09), 286 (sh), 264 (sh), 222 (4.54); Anal. Calcd. for $C_{26}H_{38}Fe$: C, 76.84; H, 9.42; Fe, 13.74. Found: C, 77.07; H, 8.91; Fe, 13.37.

1,1'-di(4-triethoxysilylbutyl)octamethylferrocene (1). According to the literature,[24] to 1 mL of tetrahydrofuran in a 1 cm d. tube with an O-ring joint was added 400 mg (0.98 mmol) of **2** and 370 μL (1.96 mmol) of triethoxysilane. To this was added 0.019 mg (5×10^{-5} mmol) of H_2PtCl_6 as a freshly prepared 0.1 mM solution in tetrahydrofuran. The tube was fitted with a CAPFE coated O-ring (Ace Glass, Vineland, NJ) and clamped shut. The closed reactor was heated in a water bath at 70°C for 2 days. The solvent was removed under vacuum and the silylated product was taken up in isooctane and stored as a solution. ^1H NMR (C_6D_6) δ 0.78 (2 H, t), 1.18 (9 H, m), 1.50 (2 H, m), 1.66 (12 H, m), 2.09 (2 H, m), 2.29 (2 H, m), 3.81 (6 H, m); UV-vis (isooctane) λ_{max}/nm 422.

Results and Discussion

Synthesis of **1** and Electrochemistry of Electrodes Modified With **1** in Non-Aqueous Media. The synthesis of **1** is summarized in Scheme II. The electrode derivatizing reagent, **1**, stored as an isooctane solution in a dry box, was stable for more than one year; there was no color change, no visible precipitation, and electrodes could be derivatized.

The solution electrochemistry of this decaalkylferrocene derivative was investigated first by studying 1,1'-di(3-butenyl) octamethylferrocene, **2**, the precursor to **1**. In CH_3CN/0.1 M $LiClO_4$ solutions using Pt electrodes, **2** shows reversible cyclic voltammograms at $E'^{\circ} = -0.405$ V vs. 0.01 M Ag^+/Ag. In other organic solvents, (EtOH, CH_2Cl_2, butyronitrile), the behavior is qualitatively the same, and is that characteristic of a reversibly redox active solution species. The oxidized state of **2** is soluble in water, though its solution electrochemistry is not reversible owing to the precipitation of the reduced form onto the electrode. In CH_3CN/0.1 M $LiClO_4$ the redox potential of **2** is 520 mV negative of that of ferrocene, consistent with the observation that each alkyl substituent on ferrocene shifts the redox potential negative by roughly 50 mV.[25]

Polymer films of **1** on electrodes are achieved by hydrolysis of the triethoxysilyl groups to form a cross-linked and surface bound siloxane polymer.[26] Pt electrodes can be derivatized with **1** by soaking a pretreated electrode

Scheme II. Synthetic route to the electrode derivatizing reagent 1,1'-(4-triethoxysilylbutyl)octamethylferrocene, **1**. (a) CH_3OH, $(CH_3)_2C(OCH_3)_2$, *p*-TsOH, 75%, Ref. 21; (b) Li, 2-bromo-2-butene, methyl 4-pentenoate, then *p*-TsOH, 36%, Ref. 11; (c) *n*-BuLi, then $FeCl_2$, 37%, Ref. 23; (d) $HSi(OEt)_3$, H_2PtCl_6, Ref. 24.

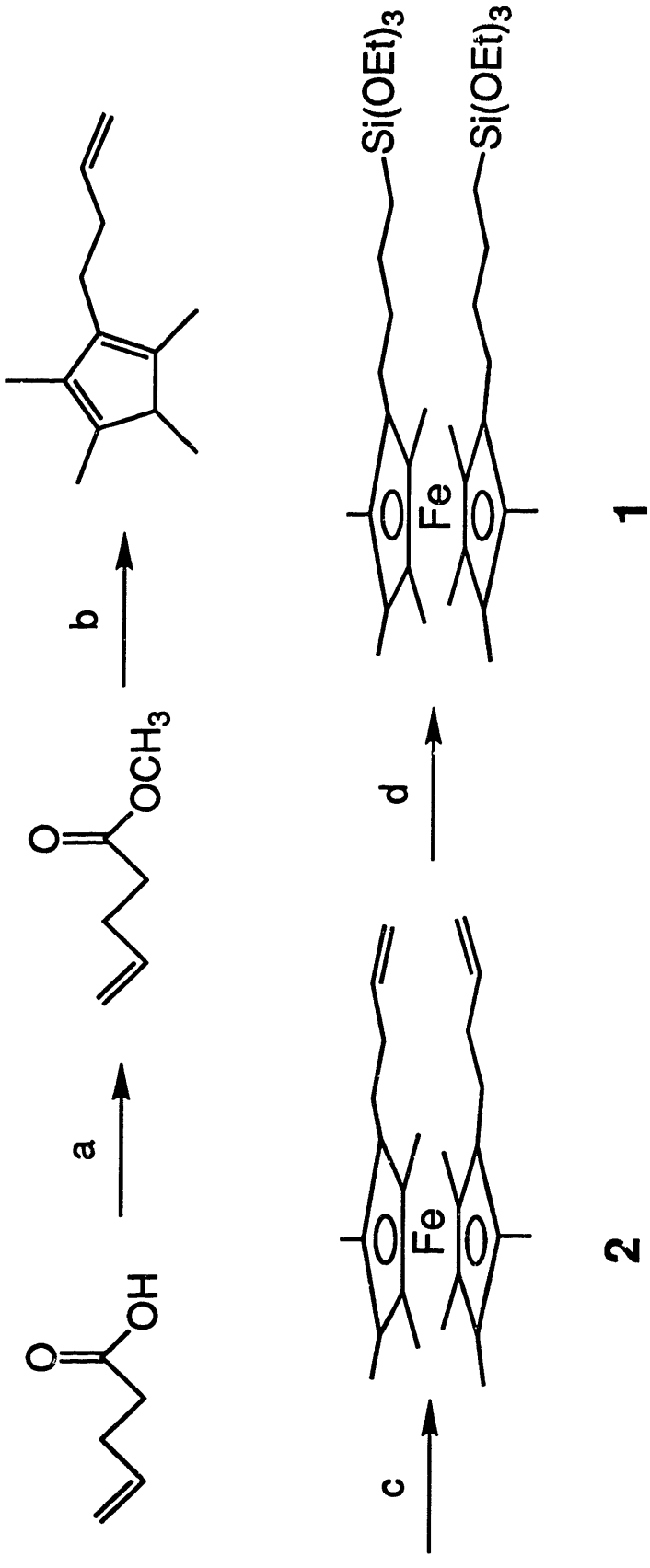
OH
O
a
OCH3
O
b
Si(OEt)3
Si(OEt)3
Fe
d
1
Fe
c
2

in an alkane solution of **1** for at least 30 s. This provides a monolayer (~2 x 10^{-10} mol cm^{-2}) of **1** bound to the electrode. The largest coverage observed was 1.7 x 10^{-7} mol cm^{-2}, obtained upon soaking for 26 h. In general, thicker films are obtained with longer soaking times and coverage is roughly proportional to time. The derivatized electrodes are durable. They can be left exposed to air for two weeks or cycled through its redox wave for 18 h (3,330 cycles) with <5% loss in activity. Scanning electron micrographs shown in Figure 3 reveal a continuous coating of material containing amorphous globules interspersed over the surface. Globules presumably are a consequence of aggregates, formed in the liquid phase by trialkoxysilyl condensation polymerization, depositing on the electrode.[27]

In CH_3CN/0.1 M [*n*-Bu_4N]ClO_4 solutions, Pt electrodes derivatized with **1**, (Pt/**1**), exhibit a reversible wave with a redox potential of $E^{1\circ}$ = -0.350 V vs. Ag^+/Ag (-0.090 V vs. SCE). In other organic solvents, EtOH and butyronitrile, the behavior is qualitatively the same. The cyclic voltammetry of Pt/**1** is that typical for a surface-confined redox couple. The wave is symmetric, the peak splitting is small (<30 mV at moderate scan rates), the anodic charge equals the cathodic charge, and E_{FWHM} is 90-120 mV. The cyclic voltammogram for a surface-confined redox couple is analytically described by the same equation as for thin-layer conditions for a solution species. The peak current is given by:

Figure 3. Scanning electron micrograph of a Pt electrode derivatized with the decaalkylferrocene reagent **1**. The scale bar applies to the picture on the right. The rectangular inset is magnified 10x on the left.

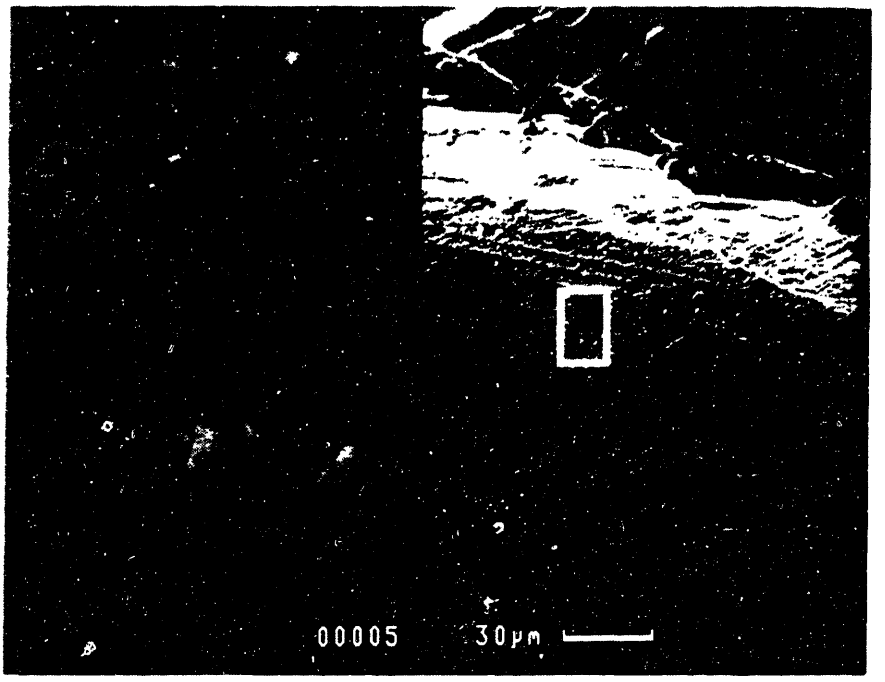
00005
30µm

$$i_p = n^2F^2\nu VC/4RT \qquad (2)$$

where n is the number of equivalents of electrons per redox molecule, F is the Faraday, ν is the scan rate, V is the volume of film, and C is the concentration of redox molecules in the film. Measuring the peak current at appropriate scan rates yields the number of moles of electroactive species (VC = N). Comparing this value with the number of moles of electroactive material determined by integrating the i-V curve gives an indication of the quality of the waveshape, which in turn is indicative of interactions between the redox sites. The ratio of $N_{calc}/N_{integral}$ found was 0.91 ± 0.07, for electrodes representing a wide range in area and coverage. To obtain a ratio lower than 1.0, the integrated area may be systematically high, by inclusion of some of the capacitive current, or the peak current may be lower than for ideal behavior. The latter is more likely the case, since E_{FWHM} averages to be 110 mV, not the ideal 90 mV.[1] Together, this indicates that the surface wave for Pt/**1** is slightly wider and shorter than for an ideal surface wave.

The scan rate dependence of the i-V characteristics of Pt/**1** (5.3×10^{-9} mol cm^{-2}) is shown in Figure 4. At slower scan rates ΔE_p is small (10 mV) and constant and the current maxima are proportional to the scan rate, as expected for thin layer behavior. At scan rates faster than 100 mV/s, the linear relationship between i_p and $\nu^{1/2}$ indicates that charge transport in the film is now a

Figure 4. Scan rate dependence of the cyclic voltammetry for a Pt electrode derivatized with **1** in CH_3CN/0.1 M [*n*-Bu_4N]ClO_4 at (a) slow scan rates and (b) fast scan rates. The coverage of **1** is 5.3 x 10^{-9} mol cm^{-2} as determined by integration of the current at slow scan rate.

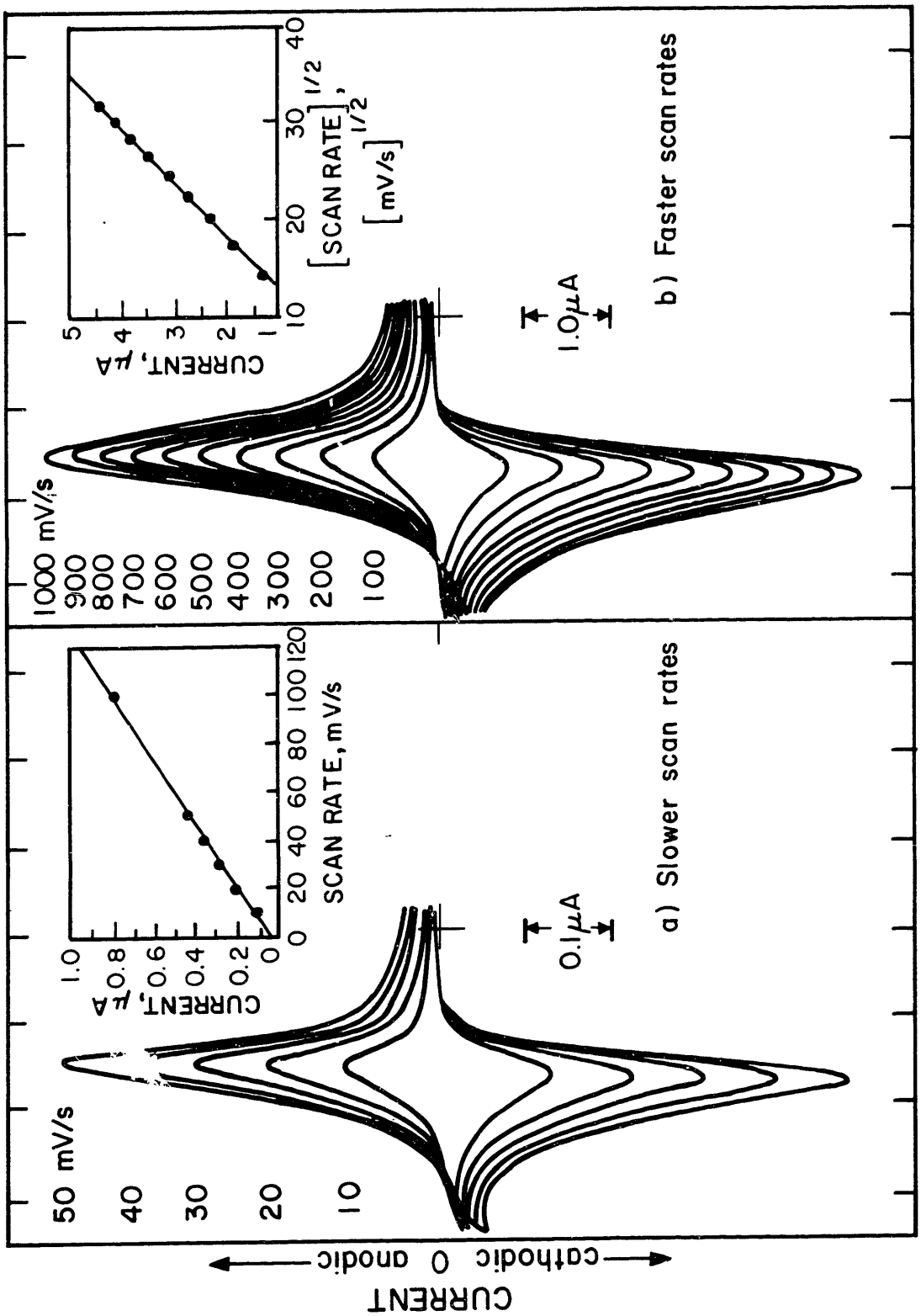
Pt/I⁻ in CH3CN/0.1M [n-Bu4N]ClO4
CURRENT
cathodic 0 anodic
50 mV/s
40
30
20
10
0.1μA
a) Slower scan rates
CURRENT, μA
SCAN RATE, mV/s
1000 mV/s
900
800
700
600
500
400
300
200
100
1.0μA
b) Faster scan rates
[SCAN RATE]^1/2, [mV/s]^1/2
POTENTIAL, V vs. Ag+/Ag
POTENTIAL, V vs. Ag+/Ag

diffusion controlled process. The diffusion coefficient, D_{Ct}, can be estimated using the Randles-Sevcik equation

$$i_p = (2.69 \times 10^5) n^{3/2} FACD^{1/2} \nu^{1/2} \quad (3)$$

from the slope of the plot i_p vs. $\nu^{1/2}$. First, $D_{Ct}{}^{1/2}C$ is determined to be 1.04×10^{-8} mol cm^{-2} $s^{-1/2}$. Without an accurate value for the concentration, D_{Ct} can only be estimated. One way to estimate the concentration is to convert the coverage (mol cm^{-2}) into mass and then assume a density for the polymer film. The density of decamethylferrocene is 1.2 g cm^{-3}; the density of ferrocene sites in the polymer film is not known, but a value of ρ = 1.0 g cm^{-3} can be assumed. With this value, it is found C = 1.8×10^{-3} mol cm^{-3}, and $D_{Ct} = 3.5 \times 10^{-11}$ cm^2 s^{-1}. To check this result two different determinations of the film thickness, δ, can be compared. From Γ/C, δ = 300 Å, but from estimating the diffusion layer thickness, $\delta \sim (Dt)^{1/2}$, for t = 2 s (time for a single sweep at 300 mV s^{-1}) δ = 830 Å. This means the boundary condition of semi-infinite linear diffusion is not satisfied and equation 3 does not apply. Qualitatively, this can be inferred from the waveshape; the current does not decay with a $t^{-1/2}$ dependence following the peak. Thus, the value of D_{Ct} obtained is a lower limit.

Pretreated n-Si electrodes were derivatized by soaking the electrode in an alkane solution of **1**. Derivatized n-Si electrodes, n-Si/**1**, show no faradaic current in the dark. Upon illumination with energetic enough photons (E > band

gap = 1.1 eV) reversible, symmetric cyclic voltammograms characteristic of a surface bound redox couple are observed. As shown in Figure 5, for an illuminated (15 mW/cm^2 at 632.8 nm) n-Si/**1** electrode in EtOH/0.1 M $[n\text{-}Bu_4N]ClO_4$, the anodic peak for **1** is -0.490 V vs. SCE, representing a negative shift of 450 mV compared to **1** on Pt. The 450 mV shift represents the photovoltage, or the extent to which light is used to drive the oxidation of **1** in a thermodynamically uphill sense. If the light is turned off at the positive scan limit following photooxidation of **1**, the reduction of **1** in the dark is observed, but thereafter no faradaic current passes. The behavior is that expected for a molecule whose redox potential is between the conduction and valence band edges of the semiconductor electrode in contact with the electrolyte solution.[28]

Evidence that **1** can form continuous pin-hole free films is that derivatized electrodes can block solution species from the electrode. In CH_3CN/0.1 M $[n\text{-}Bu_4N]ClO_4$ with 2.0 mM $Fe(C_5H_4Me)_2$, a bare Pt electrode shows the redox wave of 1,1'-dimethylferrocene at +0.280 V vs. SCE. For a Pt/**1** electrode ($\Gamma = 9 \times 10^{-9}$ mol cm^{-2}) in the same solution there is no current at that potential, as shown in Figure 6. Oxidation of 1,1'-dimethylferrocene by **1** is thermodynamically disfavored so the surface-bound film cannot mediate to the solution species. The absence of a wave for 1,1'-dimethylferrocene also indicates that the solution ferrocene can not penetrate the film to undergo

Figure 5. Cyclic voltammetric behavior of an n-Si electrode derivatized with **1** in EtOH/0.1 M [*n*-Bu_4N]ClO_4 in the dark (- - - -), illuminated with 632.8 nm light (————), and with the light source turned off at the positive sweep limit (——·——·). The coverage of **1** is 1.6 x 10^{-10} as determined by integration of the current at slow scan rate.

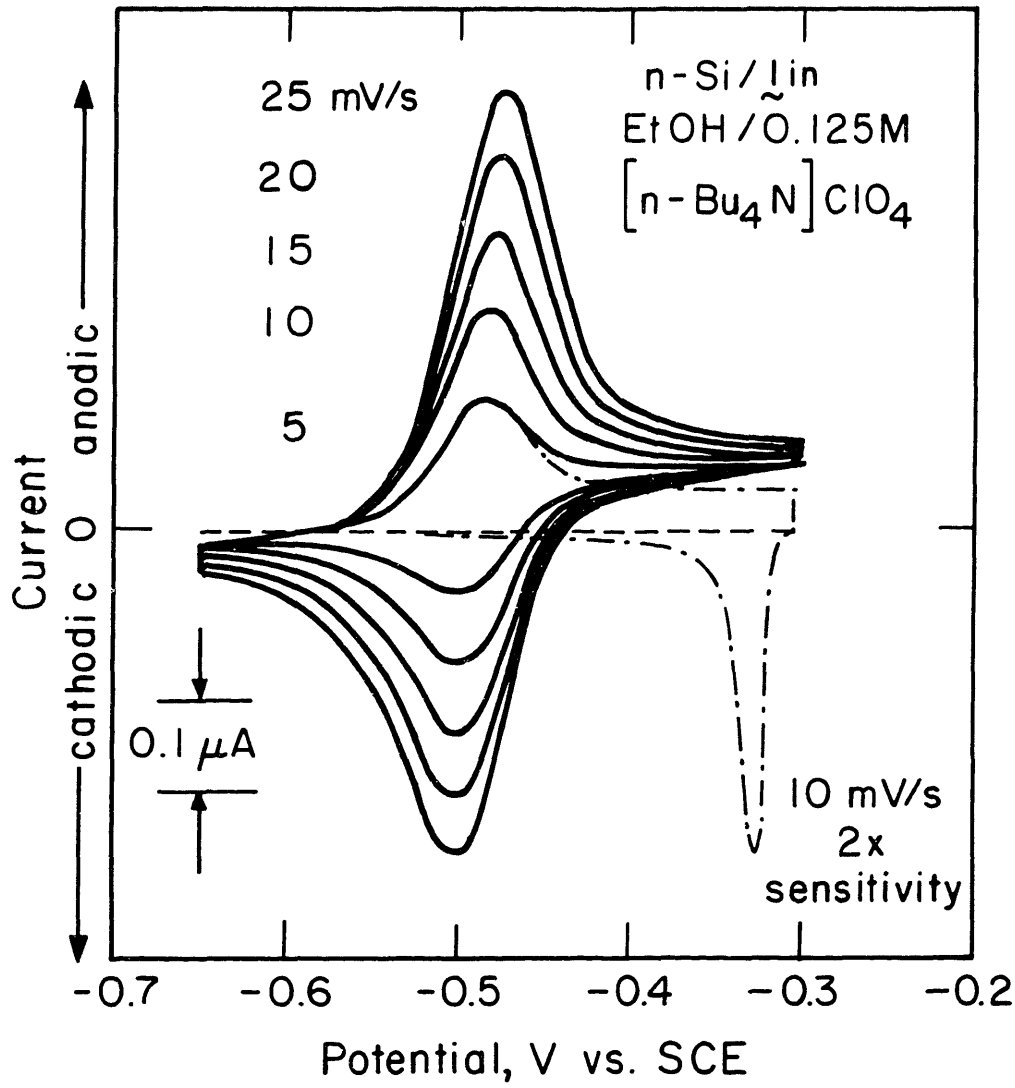
25 mV/s
20
15
10
5
n-Si/I⁻in
EtOH/0.125M
[n-Bu4N]ClO4
Current
anodic
0
cathodic
0.1 μA
10 mV/s
2x
sensitivity
-0.7
-0.6
-0.5
-0.4
-0.3
-0.2
Potential, V vs. SCE

Figure 6. Cyclic voltammetry of 2.0 mM $Fe(C_5H_4Me)_2$ in CH_3CN/0.1 M [*n*-Bu_4N]ClO_4 at a bare Pt electrode (- - -) and a Pt/**1** modified electrode (———), $\Gamma = 9 \times 10^{-9}$ mol cm^{-2}. The area of the bare electrode is 4 times greater than the area of the derivatized electrode.

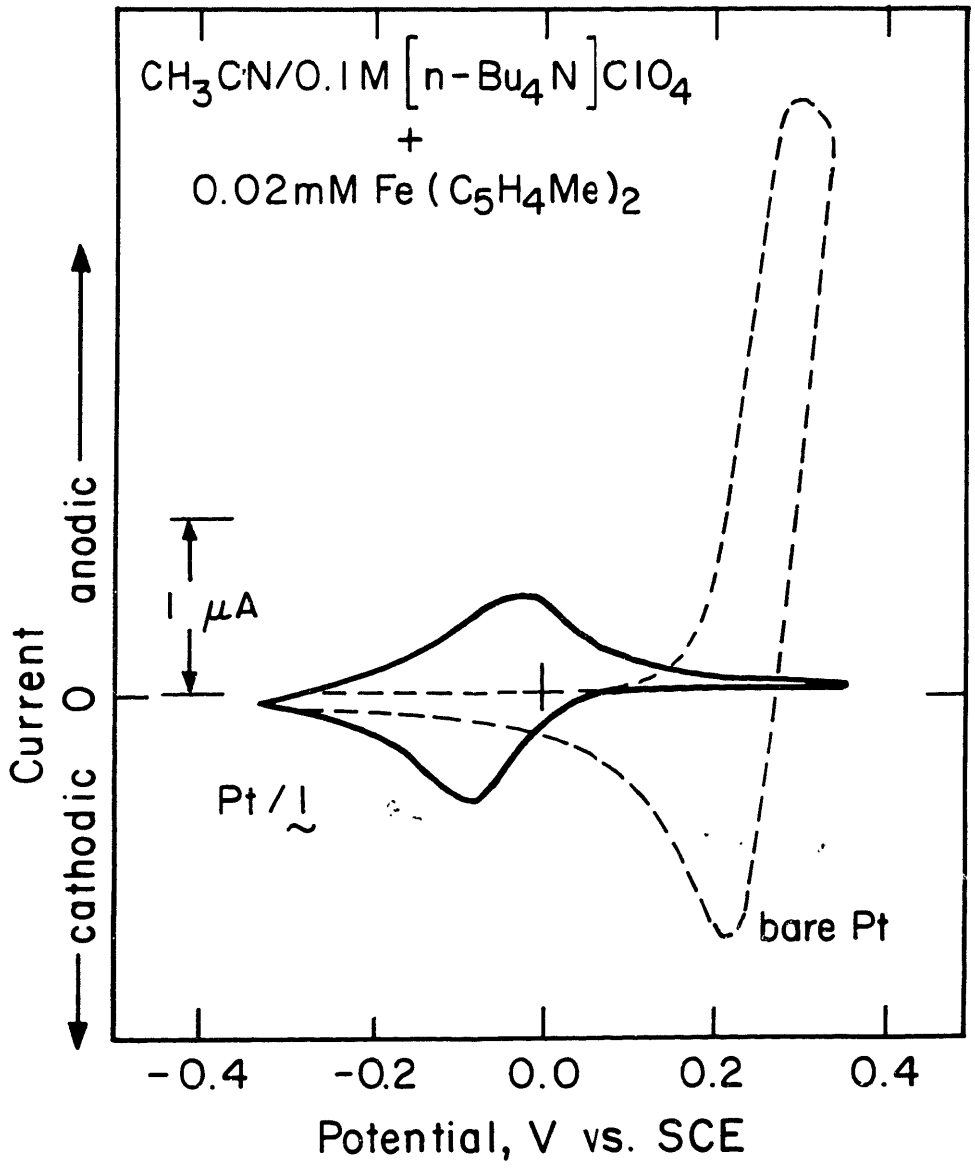
CH3CN/0.1M [n-Bu4N]ClO4
+
0.02mM Fe(C5H4Me)2
Current
anodic
cathodic
0
1 μA
Pt / I
bare Pt
-0.4
-0.2
0.0
0.2
0.4
Potential, V vs. SCE

electron transfer at the Pt surface.

Reduction of pentamethylferrocenium by **1** is thermodynamically possible, and mediation to this solution species is observed, as shown in Figure 7. However, there is no cathodic current until the film of **1** (Γ = 1.7 x 10^{-8} mol cm^{-2}) undergoes reduction, 150 mV negative of E'° of pentamethylferrocene. These mediation experiments show that the polymer films from **1** can be pin-hole free and are able to resist the diffusion of neutral or cationic redox reagents into the film. Obviously, the film is not impervious to ions, as charge compensating counterions must penetrate upon redox cycling.

Electrochemical Response of Electrodes Modified With **1** in Aqueous Electrolytes. In aqueous electrolytes, Pt/**1** electrodes depart from their well-behaved response in organic solvents. Freshly derivatized electrodes behave poorly in aqueous electrolyte solutions as judged by cyclic voltammetry. The peak shapes are broad and short with large peak-to-peak separations, and in some instances the peaks are difficult to discern above the charging current. These traits are seen to be deficiencies since the same electrodes, when transferred to CH_3CN/0.1 M $LiClO_4$ solutions, pass more charge and display the normal characteristics of a surface-bound electroactive film. Figure 8 shows derivatized electrodes repeatedly switched between an CH_3CN/electrolyte and H_2O/electrolyte alternatively giving normal and poor cyclic voltammetric

Figure 7. Mediated reduction of $Fe(C_5H_5)(C_5Me_5)^+BF_4^-$ at a Pt/**1** modified electrode: (a) Pt/**1** electrode, $\Gamma = 9 \times 10^{-9}$ mol cm^{-2}, in CH_3CN/0.1 M [*n*-Bu_4N]ClO_4, (b) bare Pt electrode in CH_3CN/electrolyte containing 5 mM $Fe(C_5H_5)(C_5Me_5)^+BF_4^-$, and (c) Pt/**1** in stirred CH_3CN/electrolyte containing 5 mM $Fe(C_5H_5)(C_5Me_5)^+BF_4^-$.

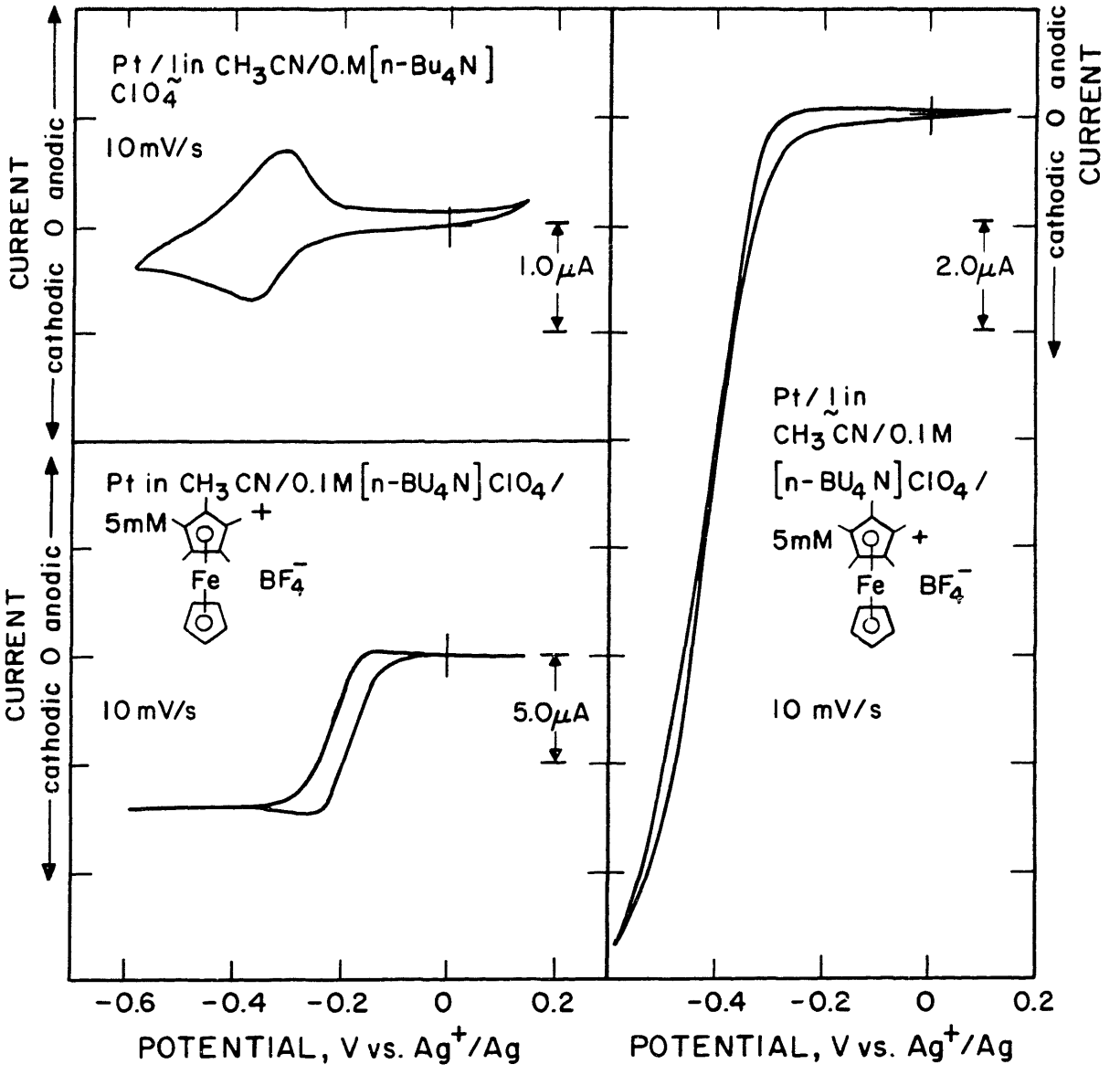
Pt / 1 in CH3CN/0.M[n-Bu4N]ClO4
10mV/s
1.0μA
Pt in CH3CN/0.1M[n-BU4N]ClO4/
5mM
Fe
BF4
10 mV/s
5.0μA
Pt/ 1 in CH3CN/0.1M [n-BU4N]ClO4/
5mM
Fe
BF4
10 mV/s
2.0μA
CURRENT
cathodic O anodic
-0.6 -0.4 -0.2 0 0.2
POTENTIAL, V vs. Ag+/Ag
-0.4 -0.2 0 0.2
POTENTIAL, V vs. Ag+/Ag

Figure 8. Cyclic voltammograms of a Pt/**1** modified electrode transferred back and forth between CH_3CN/0.1 M $LiClO_4$ and H_2O/0.1 M $NaClO_4$ solutions: (a) Cyclic voltammetry in CH_3CN/electrolyte before (———) and after (- - -) the cyclic voltammograms recorded in (b) the H_2O/electrolyte. The electrode was removed from potential control at the positive limit prior to transfer. Coverage of **1** was 4×10^{-9} as measured in CH_3CN/electrolyte.

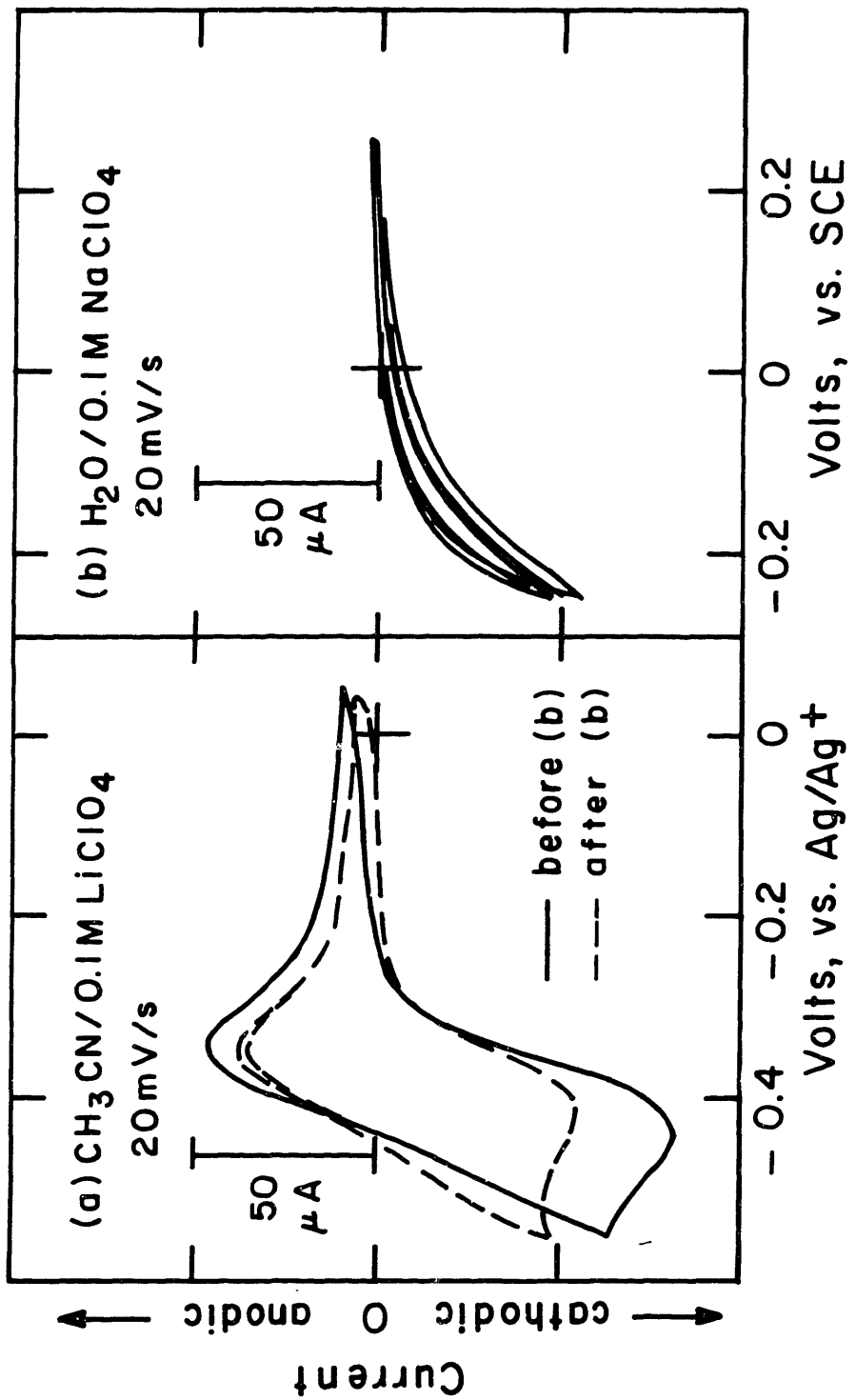
(a) CH_3CN/0.1M $LiClO_4$
20mV/s
50 μA
before (b)
after (b)
(b) H_2O/0.1M $NaClO_4$
20mV/s
50 μA
Current
cathodic 0 anodic
Volts, vs. Ag/Ag+
Volts, vs. SCE
-0.4
-0.2
0
-0.2
0
0.2

responses. Similar behavior is found when switching n-Si electrodes between EtOH/electrolyte and H_2O/electrolyte. Transfer of modified electrodes from H_2O/electrolyte to organic solvent/electrolyte initially shows some differences compared to the original characteristics in the nonaqueous medium. The peaks shift ~100 mV positive and the amount of charge and current maxima are lower, but on continued cycling the cyclic voltammogram regains its original form.

Of several ways tried to induce a good electrochemical response for polymers from **1** in the presence of H_2O/electrolyte, none succeeded. For example, freshly derivatized electrodes were first cycled in CH_3CN/electrolyte solutions to "break in" the film and then transferred to an aqueous cell. The electrode was also potentiostated prior to transfer at the positive scan limit to completely oxidize the film, and a "broken in" electrode was soaked overnight in aqueous electrolyte. The effect on the electrochemistry of Pt/**1** of adding water to an CH_3CN/electrolyte is shown in Figure 9. The addition of H_2O/0.25 M $NaClO_4$ to a stirred CH_3CN/0.5 M $LiClO_4$ solution resulted in a continuous loss of activity, and, when the solution was 63% CH_3CN only 34% of the initial (no H_2O) amount of charge passed.

The poor electrochemical behavior in H_2O/electrolyte for electrodes derivatized with **1** is presumably due to the inability of water to solvate the film to facilitate counterion transport. Solvent effects have been often noted

Figure 9. The effect on the cyclic voltammetry of Pt/**1** by the addition of H_2O to a CH_3CN electrolyte solution: (a) CH_3CN/0.5 M $LiClO_4$, (b) increasing amounts of H_2O/0.25 M $NaClO_4$ added to (a) to give 12%, 21%, 37% and 50% by volume aqueous solutions, and (c) electrochemical response in pure H_2O/0.25 M $NaClO_4$.

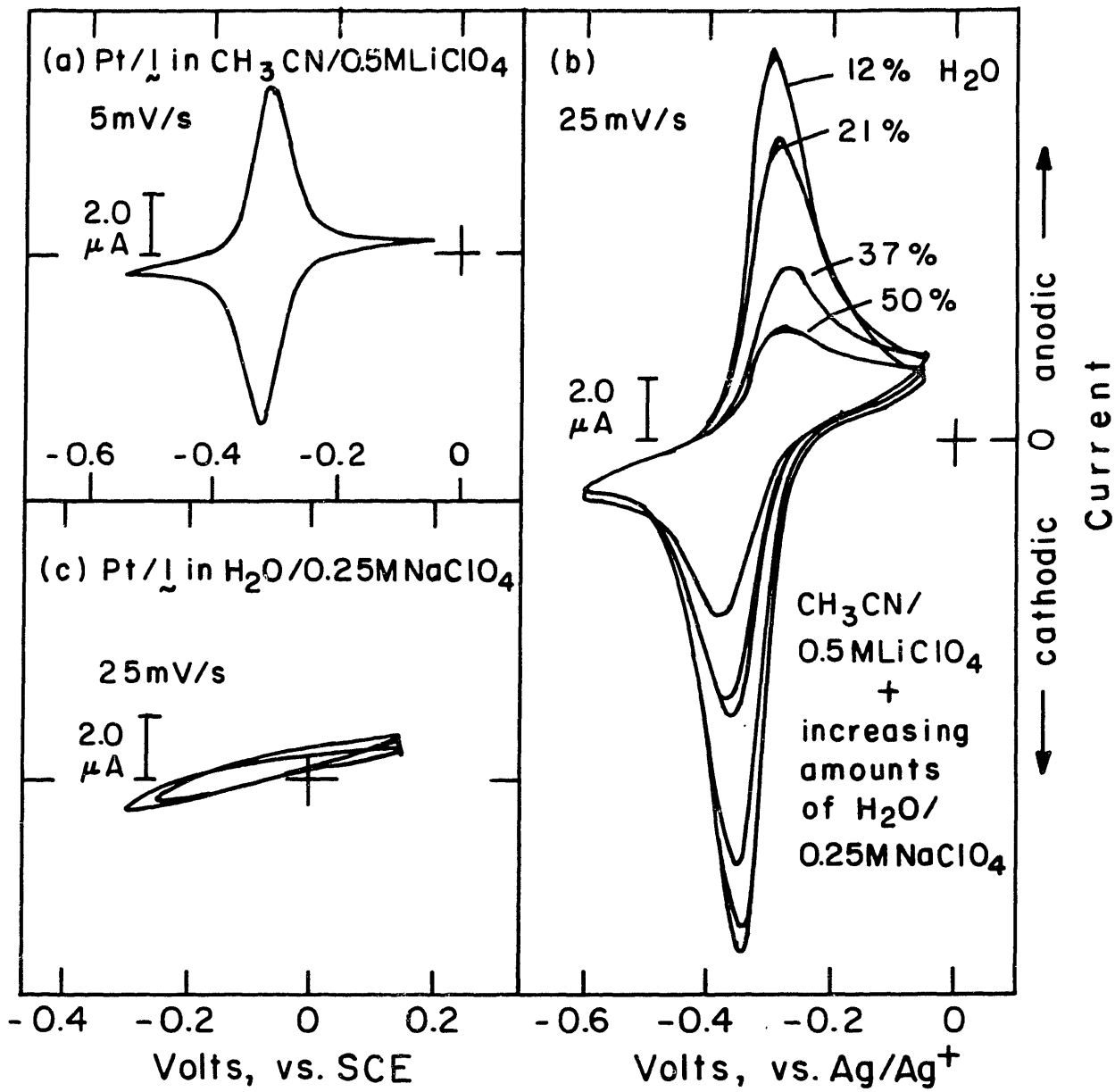
(a) Pt/I in CH3CN/0.5MLiClO4
5mV/s
2.0 μA
-0.6 -0.4 -0.2 0
(c) Pt/I in H2O/0.25M NaClO4
25mV/s
2.0 μA
-0.4 -0.2 0 0.2
Volts, vs. SCE
(b)
25mV/s
12% H2O
21%
37%
50%
2.0 μA
CH3CN/ 0.5MLiClO4 + increasing amounts of H2O/ 0.25M NaClO4
-0.6 -0.4 -0.2 0
Volts, vs. Ag/Ag+
cathodic 0 anodic
Current

and rationalized by differing interaction parameters between reduced and oxidized states.[29] A comparison is offered by pentamethylferrocene-based modified electrodes; however, though solvent differences are observed they are not so pronounced as for films of **1**.[30] There is evidence that solvation is a problem. An electrode with a coverage of 1.6 x 10^{-9} mol cm^{-2}, which showed no faradaic current in aqueous cells, was removed from potential control in the reduced state and treated with a drop of butyronitrile. After a minute the excess was shaken off, the electrode was placed in an aqueous electrolyte solution and a cyclic voltammogram recorded immediately. As shown in Figure 10, the amount of charge passed had greatly increased, and the peak shape of the cyclic voltammogram was that expected for a well-behaved electrode-confined redox couple. Upon continued cycling the improved performance was maintained until the butyronitrile diffused out of the film into the bulk water. Reapplying a drop restored the improvement.

By derivatizing Pt electrodes in the presence of both **1** and 3-cyanopropyltriethoxysilane, **3**, the effect that the drop of butyronitrile had could be made permanent. Cyclic voltammograms in both H_2O and CH_3CN cells of an electrode derivatized in a solution of **1** and **3** is shown in Figure 11. The voltammetric behavior in aqueous electrolyte solution is now improved, though the integrated current is only 60% of that for the electrode in CH_3CN. This indicates that a copolymer of **1** and **3** forms with the cyanopropyl group acting

Figure 10. Cyclic voltammetry of Pt/**1** in (a) H_2O/0.1 M $[Et_4N]Br$, (b) the same electrode in the same electrolyte solution after adding 1 drop of butyronitrile directly to the electrode film, $\Gamma_{app} = 1.6 \times 10^{-9}$ mol cm^{-2}, (c) the same electrode in H_2O/0.25 M NaOTs after adding 1 drop of butyronitrile directly to the electrode film, $\Gamma_{app} = 9.6 \times 10^{-10}$ initially, and (d) in CH_3CN/0.1 M $LiClO_4$, $\Gamma_{app} = 1.6 \times 10^{-9}$. In (c) the current began to decay after 10 min of cycling, and by 35 min had reached the smallest level shown, $\Gamma_{app} = 1.8 \times 10^{-10}$.

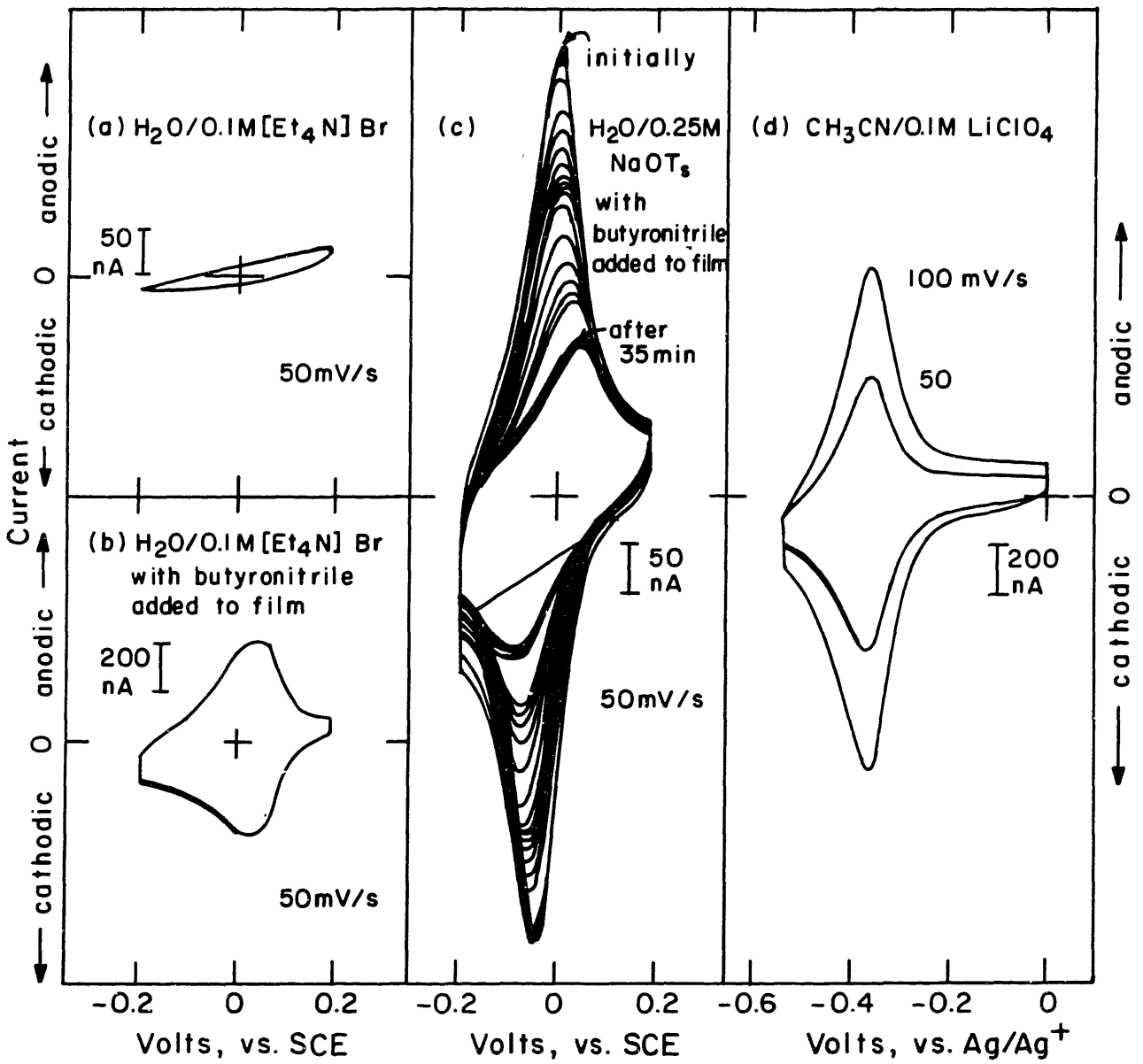
(a) H_2O/0.1M[Et_4N] Br
50 nA
50mV/s
(b) H_2O/0.1M[Et_4N] Br with butyronitrile added to film
200 nA
50mV/s
(c)
H_2O/0.25M $NaOT_s$ with butyronitrile added to film
initially
after 35min
50 nA
50mV/s
(d) CH_3CN/0.1M $LiClO_4$
100 mV/s
50
200 nA
Current
anodic
cathodic
0
-0.2
0
0.2
-0.6
-0.4
Volts, vs. SCE
Volts, vs. SCE
Volts, vs. Ag/Ag^+

Figure 11. Cyclic voltammograms of a Pt electrode derivatized in the presence of **1** and 3-cyanopropyltriethoxysilane, **3**, in (a) CH_3CN/electrolyte and (b) H_2O/electrolyte. The apparent coverages are 2.4×10^{-9} and 1.4×10^{-9} mol cm^{-2}, respectively.

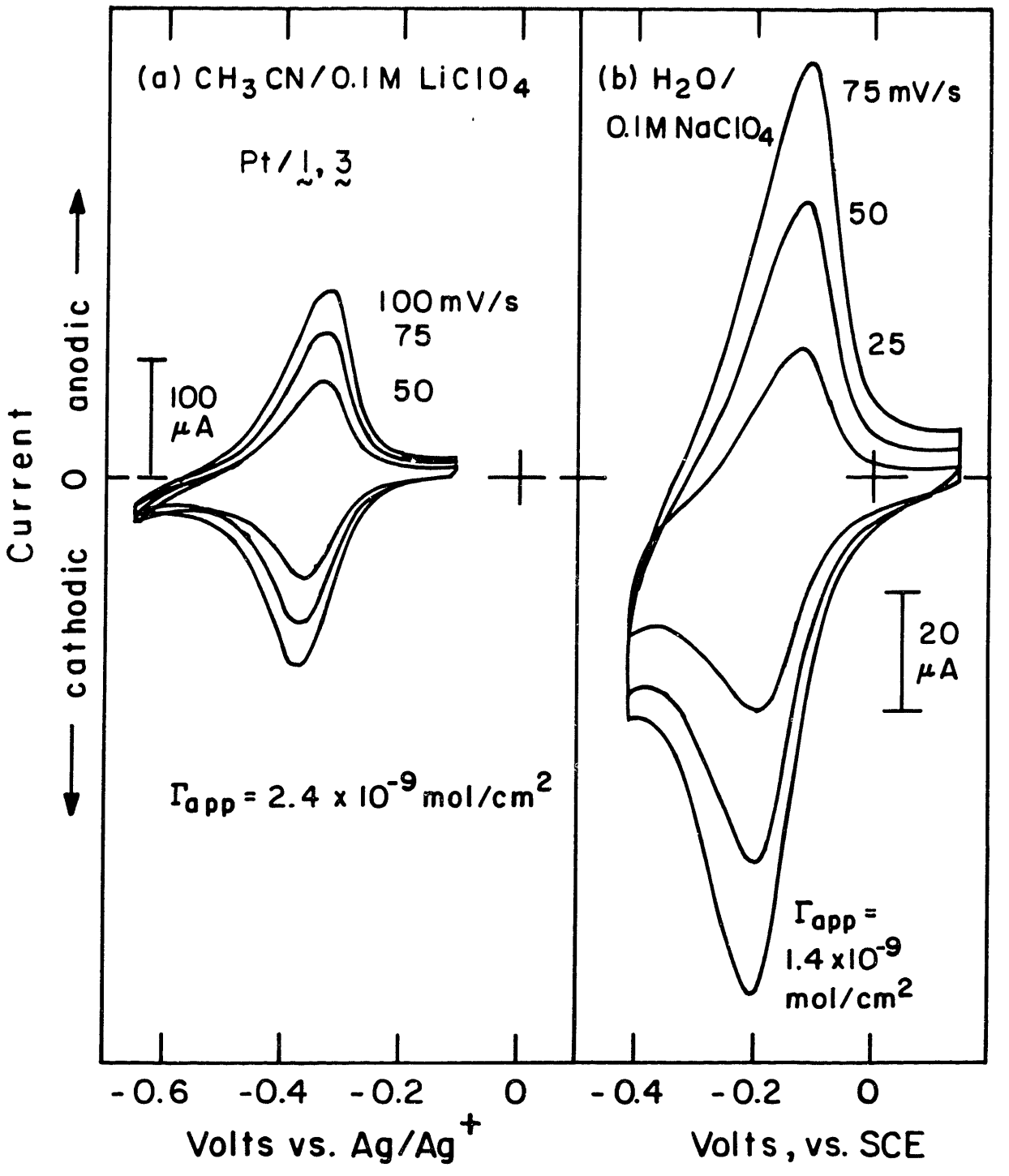
(a) CH3CN/0.1M LiClO4
Pt/1, 3
100 mV/s
75
50
100 μA
Γapp = 2.4 x 10-9 mol/cm2
(b) H2O/
0.1M NaClO4
75 mV/s
50
25
20 μA
Γapp = 1.4 x 10-9 mol/cm2
Current
anodic
0
cathodic
-0.6
-0.4
-0.2
0
Volts vs. Ag/Ag+
-0.4
-0.2
0
Volts, vs. SCE

as a "solvent", fixed in the film, supporting counter-ion and charge transport through the film. Though, for this particular film composition, a portion of the film is still not accessible for charge transport.

Contact Angle Measurements for Oxidized and Reduced Films From **1**. To more quantitatively assess the hydrophobic nature of the film of **1**, the contact angle of water on Pt/**1** electrodes was measured.[16] In Table I, the contact angle is shown for a water drop resting on the film of **1** in its reduced and oxidized states, versus coverage. Despite the presence of polar groups, Si-O, (six per monomer unit) in the film the observed contact angles are remarkably high. In comparison, contact angles on poly(vinylferrocene) films[31] which presumably only consist of C, H, and Fe are nearly 30° smaller. It has been demonstrated in one case that the contact angles on a molecular film are sensitive to only the outer ~3 Å of the film.[32] With decaalkylferrocene groups dominating the interface and the siloxane bonds located in the next layer such high contact angles for Pt/**1** can be reasonably expected. The increase in the contact angle with increasing coverage probably indicates that the coverage is not uniform, leaving exposed sections of the Pt oxide surface in the thinner films. Surface roughness is an important factor, but for angles (θ_{true}) which are less than 90°, the observed angle ($\theta_{apparent}$) is smaller than θ_{true}.[16] A similar change in the contact angle upon oxidation of the substrate was observed for a polyacetylene film measured

Table I. Contact Angle of H_2O on Pt/**1** Electrodes

Polymer	Γ (mol cm^{-2})	Contact Angle (°)[a]	
		Red.[b]	Ox.[c]
1	4.0×10^{-10}	53	30
1	7.6×10^{-10}	54	40
1	1.6×10^{-9}	75	64
1	5.2×10^{-9}	82	71
1	6.4×10^{-9}	89	70
1/3	2.4×10^{-9}	73	60
PVFc[d]		61	52

[a]Values are averages of at least 8 measurements, ± 3°. [b]Polymer in reduced state. [c]Polymer in oxidized state. The polymer was oxidized by immersing the reduced sample into a stirred solution of $Fc^+BF_4^-$ for 15 min. [d]Data from Ref. 31.

before and after doping with I_2.[33] In the reduced state the film can only interact with water via dipole and dispersion forces, resulting in a larger contact angle. When Pt/**1** is oxidized, the charged sites in the film increase the surface free energy of the film, resulting in a smaller contact angle due to electrostatic interaction between H_2O and the film.

The contact angle observed on Pt/**1**,**3** is not significantly lower than for Pt/**1** with a similar coverage of electroactive material. The effect of **3** is therefore not an increase in the hydrophilicity. Its effect on the electrochemistry must be to increase the fluidity of the polymer film and to solvate ions within the film.

For contact angles $\geq 90°$ the liquid is said to "not wet" the substrate. It is this property that prevents a liquid from entering capillary pores in a substrate. At typical coverages of the decaalkylferrocene redox polymer, 2×10^{-9} mol cm^{-2}, the contact angle observed indicates the film of **1** to be rather hydrophobic, supporting the hypothesis that H_2O can not properly solvate this film.

Conclusion

A decaalkylferrocene, **1**, containing trialkoxysilyl groups can be used to derivatize electrodes to yield durable, pinhole free electroactive films. On Pt electrodes in non-aqueous solvents, films from **1** have $E'^{\circ} = -0.09$ V vs. SCE. On illuminated n-Si electrodes, photovoltages of 450 mV for the oxidation of **1** can be observed. Derivatized electrodes have pronounced solvent effects upon switching from non-aqueous to aqueous electrolyte media, an effect ascribed to the hydrophobicity of peralkylated ferrocenes. In aqueous media the faradaic current significantly decreases, or may become nonexistent.

By covalently incorporating a propylnitrile into the decaalkylferrocene film the electrode response in aqueous media can be maintained at levels comparable to those in non-aqueous media.

Contact angle measurements of H_2O on decaalkylferrocene films approach 90°, showing that the decaalkylferrocene-modified electrode/solution interface is hydrophobic, supporting the hypothesis that the poor electrochemical behavior in aqueous media is because H_2O cannot solvate these films.

References

1. Bard, A. J; Faulkner, L. R. *Electrochemical Methods;* Wiley: New York, NY, 1980; pp 521-524.

2. Gritzner, G.; Kuta, J. *Pure Appl. Chem.* **1982**, *54*, 1527; **1984**, *56*, 461.

3. Sabbatini, M. M.; Cesarotti, E. *Inorg. Chim. Acta* **1977**, *24*, L9.

4 (a) Chapter I, Ref. 6, pp 334-338. (b) Oh, S. M.; Faulkner, L. R. *J. Electroanal. Chem.* **1989**, *269*, 77. (c) Oh, S. M.; Faulkner, L. R. *J. Am. Chem. Soc.* **1989**, *111*, 5613.

5 (a) Daum, P.; Murray, R. W. *J. Phys. Chem.* **1981**, *85*, 389. (b) Francis, C. V.; Joo, P.; Chambers, J. Q. *J. Phys. Chem.* **1987**, *91*, 6315.

6. (a) Andrieux, C. P.; Savéant, J. M. *J. Electroanal. Chem.* **1980**, *111*, 377. (b) Oyama, N.; Anson, F. C. *J. Electrochem. Soc.* **1980**, *127*, 640. (c) Daum, P.; Lenhard, J. R.; Rolison, D.; Murray, R. W. *J. Am. Chem. Soc.* **1980**, *102*, 4649.

7. Daum, P.; Murray, R. W. *J. Electroanal. Chem.* **1979**, *103*,

289.

8. Prins, R.; Korswagen, A. R.; Kortbeek A. G. T. G. *J. Organomet. Chem.* **1972**, *39*, 335.

9. (a) Chapter I, Ref. 12. (b) Wrighton, M. S.; Palazzotto, M. C.; Bocarsly, A. B.; Bolts, J. M.; Fischer, A. B.; Nadjo, L *J. Am. Chem. Soc.* **1978**, *100*, 7264. (c) Lenhard, J. R.; Murray, R. W. *J. Am. Chem. Soc.* **1978**, *100*, 7870.

10. Hüttner, G.; Fischer, E. O. *J. Organomet. Chem.* **1967**, *8*, 299.

11. Yang, E. S.; Chan, M-S.; Wahl, A. C. *J. Phys. Chem.* **1980**, *84*, 3094.

12. (a) Threlkel, R. S.; Bercaw, J. E. *J. Organomet. Chem.* **1977**, *136*, 1. (b) Manriquez, J. M.; Fagan, P. J.; Schertz, L. D.; Marks, T. J. *Inorg Synth.* **1982**, *21*, 181.

13. Mintz, E. A.; Pando, J. C.; Zervos, I. *J. Org. Chem.* **1987**, *52*, 2948.

14. (a) Bunel, E. E.; Valle, L.; Manriquez, J. M. *Organometallics* **1985**, *4*, 1680. (b) Kolle, U.; Fuss, B.; Khouzami, F.; Gersdorf, J. *J. Organomet. Chem.* **1985**, *290*,

77.

15. Zou, C. F.; Wrighton, M. S. submitted for publication in *J. Am. Chem. Soc.*

16. Adamson, A. W. *Physical Chemistry of Surfaces*, 4th ed.; Wiley: New York, NY, 1982; Chapter X.

17. Young, T. *Philos. Trans. R. Soc. London* **1805**, *95*, 15.

18. Johnson, R. E. Jr. *J. Phys. Chem.* **1959**, *63*, 1655.

19. Neumann A. W. and Good, R. J. *Surfaces and Colloid Science*, Vol. 2; Good, R. J. and Stromberg, R. R. Eds.; Plenum: New York, NY, 1979.

20. (a) Holmes-Farley, S. R.; Reamey, R. H.; McCarthy, T. J.; Deutch, J.; Whitesides, G. M. *Langmuir*, **1985**, *1*, 725. (b) Holmes-Farley, S. R.; Whitesides, G. M. *Langmuir*, **1987**, *3*, 62.

21. Lorette, N. B.; Brown, J. H., Jr. *J. Org. Chem.* **1959**, *24*, 261.

22. McCreer, D. E.; Chiv, N. W. K.; *Can. J. Chem.* **1968**, *46*, 2217.

23. Feitler, D.; Whitesides, G. M. *Inorg. Chem.* **1976**, *15*, 466.

24. Speier, J. L.; Webster, J. A.; Barnes, G. H. *J. Am. Chem. Soc.* **1957**, *79*, 974.

25. Robbins, J. L.; Edelstein, N.; Spencer, B.; Smart, J. C. *J. Am. Chem. Soc.* **1982**, *104*, 1882.

26. (a) Deschler, U.; Kleinschmit, P.; Danster, P. *Angew. Chem. Int. Ed. Eng.* **1986**, *25*, 236. (b) Moses, P. R.; Weir, L.; Murray, R. W. *Anal. Chem.* **1975**, *47*, 1882.

27. Haller, I. *J. Am. Chem. Soc.* **1978**, *100*, 8050.

28. Wrighton, M. S. *Acc. Chem. Res.* **1979**, *12*, 303.

29. Brown, A. P.; Anson, F. C. *Anal. Chem.* **1977**, *49*, 1589.

30. Chao, S.; Robbins, J. L; Wrighton, M. S. *J. Am. Chem. Soc.* **1983**, *105*, 181.

31. Willman, K. W.; Murray, R. W. *Anal. Chem.* **1983**, *55*, 1139.

32. Holmes-Farley, S. R.; Bain, C. D.; Whitesides, G. M. *Langmuir* **1988**, *4*, 921.

33. Guiseppi-Elie, A.; Wnek, G. E.; Wesson, S. P. *Langmuir*, **1986**, *2*, 509.

Chapter III

Preparation and Properties of Well-Defined Redox Active Polymers and Block Polymers Made by a Living Ring-Opening Metathesis Polymerization

Introduction

The ability to exert more control over the behavior and properties of surface-modified electrodes is an ever present goal. The study of electrodes modified by the attachment of electroactive polymers has largely focused on the electrochemical response, and not on the properties of the polymer. To learn more about the modifying electroactive polymer and to be able to incorporate a variety of functional units in an organized manner, the polymer must be synthesized first. Following preparation the material could then be characterized, both prior to and after electrode derivatization.

In-situ polymerization techniques for the formation of modified electrodes preclude the chance to fully characterize the polymer that is formed. Also, molecules which are not electroactive will not be able to propagate the polymerization as the film grows from the electrode interface. Step-wise synthetic techniques allow for the precise formation and characterization of surface derivatizing reagents. These reagents may be applied as molecules for monolayer derivatization or as monomers to be cross-linked for multilayer formation. Such assemblies can achieve "molecular electronic" functions such as pH-dependent charge trapping and chemical sensing.[1] A drawback to this approach is the synthetic effort required as the target molecule increases in complexity.

In contrast to in-situ polymerization and step-wise

synthesis, living polymerization techniques offer several advantages for the preparation of a new class of electroactive polymers. Large molecules consisting of a variety of functional groups can be prepared, characterized, and stored in a bottle as a batch. Slight variations in their structure can readily accomplished, facilitating structure vs. function and control experiments.

Living polymerization techniques enable a high level of control in the primary structure of the polymer. An illustration of the types of structures that can be made is shown in Scheme I. The nature of the starting end group is determined by the catalyst used. Formation of segments in the polymer chain uniquely consisting of one type of monomer is possible, and the number of monomers in each of these blocks is controllable. Finally, the polymer chain can be capped with a molecule chosen specifically for a variety of purposes.

As in any polymer synthesis, the material prepared is comprised of a range of chain lengths; unlike step-wise synthesis a unique compound is not made. Instead polymers are described by their average molecular weight and a polydispersity index, PDI, which indicates the size of the range over which different chain lengths have been produced. The PDI is the ratio of the weight average molecular weight, M_w, to the number average molecular weight, M_n. In most polymerization mechanisms, the product has a broad molecular weight range, characterized by a polydispersity of 2 or

Scheme I. Schematic showing the primary structure in a block polymer with a starting end group derived from the initiator and a capping end group introduced in the termination reaction.

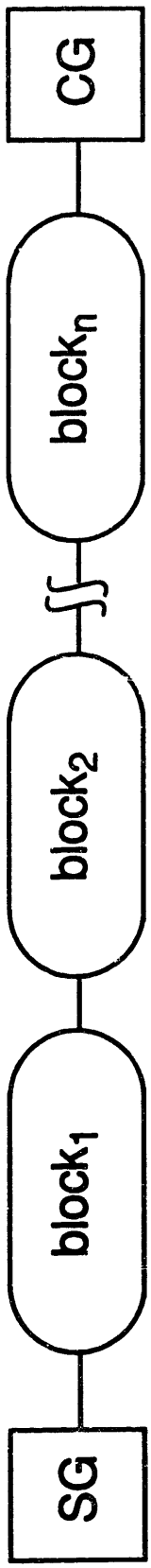
SG
block1
block2
blockn
CG

more, whereas for living polymerizations a narrow distribution about a controllable average molecular weight is produced.[2] Polydispersity values ideally approach 1.01 as the average chain length increases, but even for short chain lengths, or unfavorable kinetics the values are typically 1.10-1.30.[3] The reason for both the degree of control over the polymer composition and the narrow molecular weight distribution is that the only reactions that occur are initiation and propagation.[4] Chain termination is controlled by the addition of a capping reagent, and there is no chain-biting, depolymerization, or chain-transfer observed for the system presented here.

The polymerization kinetics depend only on the rate of initiation and the rate of propagation for each block in a living polymerization. The dispersity in the molecular weight of the polymer depends on the kinetics. Narrower dispersities are produced when the rate of initiation is the same as or faster than the propagation step. When the initiation step is relatively slow, initiated chains propagate faster than new chains are initiated. This widens the difference in the degree of polymerization between the chains which are the first and the last to be initiated. (It is difficult to understand the significance of a polydispersity value without a graphic representation; refer to the Results and Discussion for more details.)

A variety of living polymerization techniques have been developed, including anionic,[5] cationic,[6] group transfer,[7]

and more recently ring opening metathesis polymerization, ROMP, of cyclic olefins.[8] The first example of metathesis polymerization, found 20 years ago, used $TiCl_4/LiAl(C_7H_{15})_4$ to make polynorbornene.[9] This and other metal halides with various promoters are now referred to as "classical" catalysts for metathesis polymerization. These catalysts have not been amenable to structural characterization in their active forms and they do not produce living polymerizations. Nonetheless, they are applied in industrial processes.[10]

In the meantime the chemistry of alkene and alkyne metathesis reactions at the metal of organometallic compounds was being explored. With the work of Osborne, Schrock and Grubbs, among others, in the last five years well-defined organometallic compounds capable of a living metathesis polymerization have been found.[8]

Metathesis polymerization catalysts of the type $M(=CHR)(OR')_2(NAr)$, M = Mo, W, have been developed and studied by the Schrock group.[11] ROMP proceeds quickly at room temperature with quantitative conversion of monomer to polymer. An important difference between the two metals, Mo and W, is that the Mo initiator is more tolerant of functional groups. With an efficient synthetic route to the Mo catalyst now available, the catalyst can be more widely applied.[12]

The living metathesis polymerization process is outlined in Scheme II. The Mo alkylidene first forms a

Scheme II. Polymerization reaction pathways for ring opening metathesis polymerization of strained cyclic olefins with metal alkylidene initiators. The other ligands coordinated to Mo have been omitted. See Chart I for the structure of the Mo compound.

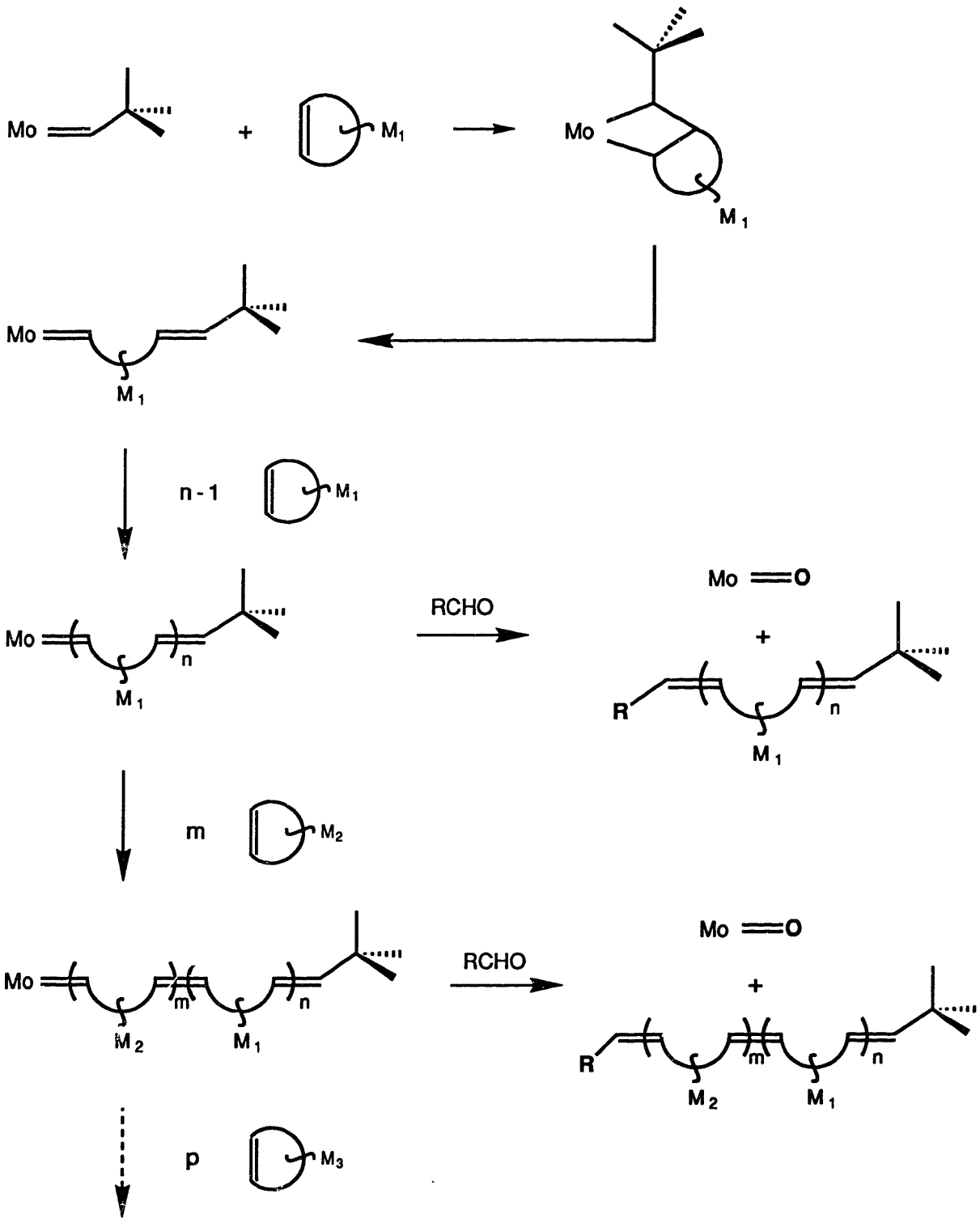
Mo
+
M1
Mo
M1
Mo
M1
n - 1
M1
Mo
n
M1
RCHO
Mo
O
+
R
n
M1
m
M2
Mo
m
n
M2
M1
RCHO
Mo
O
+
R
m
n
M2
M1
p
M3

metallocyclobutane intermediate with the cyclic olefin monomer, which can reversibly breakup to form the reactants, or produce the monoinsertion product. This new alkylidene reacts similarly with monomers until there are no free monomers. This Mo alkylidene species is said to be a living polymer, since the active chain carrying intermediate is present and the addition of more monomer would continue the growth of the polymer. At this point a different monomer could be introduced to produce a new polymeric block linked to the first. The third option is to terminate the polymerization by reacting the Mo alkylidene species with an aldehyde. In a Wittig-like reaction, the intermediate metallooxocyclobutane cleaves to give a metal oxo compound separated from the polymer.[13] As indicated by Scheme II new monomers can be sequentially introduced to produce block polymers.

Applying the methodology in Scheme II to the formation of redox polymers provides a new class of electroactive polymers. The primary structure is variable in that different monomers can be incorporated, and this variability is controllable on the order of the size of a block segment. In the context of redox polymers for electrode surface modification there are certain different properties which one would like to incorporate into the monomers. Monomers with a stable, reversible redox active substituent are the primary concern. Electroactive polymers themselves can be placed on electrodes using any of the usual deposition or

casting methods. As an alternative, block polymers made with a monomer that is capable of binding to the electrode surface can be used to provide a way to specifically attach the polymer. Also, monomers with other functionalities can be used to alter the solubility, hydrophobicity, or morphology of the polymers. Unique functional groups can be positioned at the end of the polymer chain through the termination reaction. Since there can be only one such cap per chain, and it occupies a special position at the chain end, it can be exploited as a probe of the polymerization reaction and of the conformation of the polymer.

Experimental

Chemicals. Norbornene, pivaldehyde, ferrocenecarboxaldehyde, 1-pyrenecarboxyaldehyde, *p*-(dimethylamino)-benzaldehyde and 10-methylphenothiazine were obtained from Aldrich Chemical Co. Norbornene was distilled from molten Na, pivaldehyde was distilled from molecular sieves under N_2, ferrocenecarboxaldehyde and 1-pyrenecarboxaldehyde were recrystallized and *p*-(dimethylamino)benzaldehyde was passed through a 5 cm column of activated alumina prior to use. Octamethylferrocenecarboxaldehyde[14] and *p*-(trimethylsilyl)-benzaldehyde[15] were prepared and purified as previously described. 10-Methylphenothiazine was recrystallized from EtOH.

Polymer Preparation. Polymer syntheses were carried out under a N_2 atmosphere in a Vacuum Atmospheres drybox. The general procedure was as follows. A Mo catalyst (5-10 mg) was dissolved in 1 mL tetrahydrofuran (THF) that was freshly distilled from Na benzophenone ketyl under N_2. The appropriate number of equivalents of a monomer were dissolved in THF and injected into the well-stirred catalyst solution. After an appropriate reaction time, either a second monomer was added to the living polymer in a similar manner, or the living polymer was terminated by the addition of 3-5 equivalents of an aldehyde. In cases where a series of related polymers were made the solution of the living polymer was split at the latest possible point. The polymers were purified by twice precipitating in hexane,

collected by centrifugation, and then dried under vacuum.

Polymer Characterization. Gel permeation chromatography (GPC) analyses were done using Shodex KF 802.5, 803, 804, 805, 800P columns, a Knauer differential refractometer, and a Spectroflow 757 absorbance detector. The samples were 0.1-0.3 w/v% CH_2Cl_2 solutions. The samples were filtered through a Millex-SR 0.5 μm filter. The GPC columns were calibrated with commercial polystyrene standards from Polymer Laboratories Ltd. ranging from 1.206×10^3 to 1.03×10^6 MW.

Differential scanning calorimetry (DSC) was done using a Perkin-Elmer DSC-4 interfaced with the Perkin-Elmer Thermal Analysis Data Station. For experiments requiring sub-ambient temperature operation the unit was cooled with dry ice under an N_2 atmosphere. The Al sample pan contained 4-8 mg of material and the reference pan contained an Al lid. The material was first annealed above its glass transition temperature for 10 min. Measurements were made heating the material at a rate of 20°C/min and then cooling it either slowly (≤20°C/min) or quickly (320°C/min) through the transition. Glass transitions were confirmed by repetition of the measurement on the same sample.

^1H NMR spectra were recorded on either a Varian XL 300 or XL 500 MHz FT spectrometer; ^{13}C NMR spectra were recorded on these instruments at 75.4 or 125 MHz, respectively. Chemical shifts were calibrated by a residual solvent resonance relative to Me_4Si, δ 0.0.

Field desorption mass spectrometry (FD-MS) was carried out on a JEOL HX110/HX110 instrument.

Electrochemistry. Electrochemical experiments were done using conventional 3-electrode cells. The electrolyte was sparged with Ar or N_2 before use. In the case of Mo alkylidene compounds, electrochemical experiments were done in a dry box in cells which had been heated to 110°C under 10^{-6} Torr vacuum. Cyclic voltammetric experiments were performed using a Pine Instruments RDE 4 bipotentiostat modified for low current sensitivity. Normal pulse voltammetry was done using a PAR 174 polarographic analyzer. Traces were recorded on a Kipp and Zonen BD 91 X-Y recorder. Pt working electrodes were prepared and pretreated as previously described.[16] The counter electrode was a large piece of Pt gauze. The Ag quasi-reference elelctrode was prepared by dipping a Ag wire in concentrated HNO_3, rinsing with H_2O and MeOH and drying. The reference potential was calibrated with ferrocene (0.380 V vs. SCE, 5 mM in CH_3CN/0.1 M [*n*-Bu_4N]PF_6) and converted to V vs. SCE.

[*n*-Bu_4N]AsF_6 was prepared by combining equimolar aqueous solutions of [*n*-Bu_4N]Br (Southwestern Analytical Chemicals, Austin, TX) and $LiAsF_6$ (Lithco, Bessemer City, NC). After 2 h at 4°C, the solid was collected by filtration and recrystallized from acetone and H_2O and dried at 110°C for 48 h, then stored in a dry box. MP 244°C (Lit[17] 245°C).

[*n*-Bu_4N]PF_6 (Aldrich Chem. Co.) was recrystallized from 95% EtOH twice and dried under vacuum. [*n*-Bu_4N]BF_4 (Aldrich

Chem. Co.) was recrystallized from acetone/H_2O and dried under vacuum.

Fluorescence Measurements. Fluorescence measurements were done on a Perkin-Elmer MPF-44 fluorescence spectrophotometer with a 150 W Xe arc lamp excitation source, 90° emission detection geometry, and a Hamamatsu R777 photomultiplier tube, in 1 cm fused silica fluorescence cuvettes. Traces were recorded with a Perkin-Elmer 56 strip chart recorder and a Nicolet 4094B digital storage oscilloscope. Relative quantum yields were determined with solutions matched in absorbance at the excitation wavelength, OD = 0.086 at 330 nm. Stern-Volmer quenching experiments were done using O_2 as the quencher. Samples were prepared with a concentration of 5 μM, deoxygenated with solvent-saturated Ar and the emission spectrum was recorded. The sample was then purged with solvent-saturated gases and the spectrum then remeasured in the order O_2, Ar, air, and Ar. All other spectra were made with Ar saturated samples ~5 μM in pyrene concentration.

Synthesis. All chemicals used were reagent grade. Tetrahydrofuran was distilled from CaH_2 under N_2 immediately prior to use. Pyridine was stored over 4Å molecular sieves. Benzene was stirred with concentrated H_2SO_4, decanted, and distilled under N_2. Anhydrous Et_2O and the solvents used in chromatography were used as received. Silica gel, 230-400 mesh, from Aldrich Chemical Co. was used in chromatography. N-Nitroso-N-methyl urea, stabilized with 10 wt% CH_3CO_2H, was

generously provided by Professor S. Masamune. Ethylene oxide was obtained from Eastman Kodak, dicyclopentadiene and pyrrolidine were obtained from Fluka AG, and all other reagents were from Aldrich Chemical Co.

^1H NMR spectra were recorded on either a Varian XL or Gemini 300 MHz FT spectrometer. ^{13}C NMR spectra were recorded at 75.4 MHz. Chemical shifts were calibrated by a residual solvent resonance relative to Me_4Si, δ 0.0. Electronic absorption spectra were obtained on a HP 8452A spectrophotometer using 1 cm pathlength quartz cuvettes. Mass spectrometry was done on a Finnigan MAT System 8200 with a double focusing magnetic sector by electron impact (70 eV). Melting points were obtained with a Thomas capillary melting point apparatus, and are uncorrected. Elemental analyses were done by Schwartzkopf Microanalytical Lab, Woodside, NY.

β-Ferrocenylacrylic acid (3) was prepared according to the literature[18] in 70% yield. Only the *trans* isomer was obtained. ^1H NMR ($CDCl_3$) δ 4.13 (5H, s), 4.38 (2H, m), 4.46 (2H, m), 6.02 (1H, d, 16 Hz), 7.56 (1H, d, 16 Hz).

***trans*-5-Norbornene-3-ferrocenyl-2-carboxylic acid (4).** The procedure was adapted from the literature.[19] β-Ferrocenylacrylic acid (1.6 g, 6.2 mmol) and *p*-hydroquinone (25 mg, 0.2 mmol) was added under a stream of Ar to 25 mL benzene in a flask fitted with a condenser and gas inlet, glass stoppers and a stir bar. Cyclopentadiene (cracked, collected at -70°C and stored at -80°C under Ar) was added

to the stirred refluxing solution in 1 mL (15 mmol) portions five times a day over seven days. The progress of the reaction was monitored by ^1H NMR of a sample obtained from the workup of a 1 mL aliquot. The reaction solution was cooled to room temperature, transferred to a separatory funnel and washed three times with 10% $NaHCO_3$. The orange aqueous solution was neutralized with 10% HCl and the resulting precipitate was extracted with Et_2O until the aqueous phase was colorless. The Et_2O extracts were dried over $MgSO_4$, filtered, and evaporated to give an orange solid. The reaction was run twice, to 80% and 94% conversion of the β-ferrocenylacrylic acid. Two diastereomers of the norbornene product were present in a 2:3 ratio both times. Isolation and purification of the product was deferred until after the next step. ^1H NMR (diastereomeric mixture) ($CDCl_3$) δ 1.48 (1H, m), 1.66 (0.6H, m), 1.82 (0.4H, m), 2.32 (0.4H, m), 2.75-2.90 (2.2H, m), 3.10 (0.4H, m), 3.23 (0.6H, m), 3.49 (0.4H, m) 4.08 (9H, m), 5.94 (0.4H, m), 6.08 (0.6H, m) 6.26 (0.4H, m), 6.39 (0.6H, m).

***trans*-(exo, endo)-2-Carbomethoxy-(endo, exo)-3-ferrocenyl-5-norbornene (5a,b).** Diazomethane was generated by adding N-nitroso-N-methyl urea in small portions to Et_2O and 50% aqueous KOH in a test tube cooled to 0°C. The yellow-green ether layer was transferred to an ice cooled, stirred ethereal solution of *trans*-5-norbornene-3-ferrocenyl-2-carboxylic acid. The progress of the reaction was monitored

by TLC (1:19 ethyl acetate:hexane). The Et_2O was removed by rotary evaporation and the yellow solid obtained was purified by flash chromatography (1:19 ethyl acetate:hexane).[20] The diastereomers were separable and on the basis of ^1H and ^{13}C NMR spectroscopy[19] assigned to be **5a**, *exo*-2-carbomethoxy-*endo*-3-ferrocenyl-5-norbornene, and **5b**, *endo*-2-carbomethoxy-*exo*-3-ferrocenyl-5-norbornene. Polymerizations were done using the mixture of diastereomers. R_f methyl β-ferrocenylacrylate, 0.24; **5b**, 0.33; **5a**, 0.39; ^1H NMR (C_6D_6) **5a** δ 1.42 (1H, m), 2.01 (1H, m), 2.36 (1H, m), 2.67 (1H, m), 2.91 (1H, m), 3.44 (3H, s), 3.62 (1H, m), 3.71 (1H, m), 3.92 (2H, m), 3.94 (1H, m), 4.06 (5H, s), 5.81 (1H, m), 6.00 (1H, m); **5b** δ 1.36 (1H, m), 1.51 (1H, m), 2.61 (1H, m), 2.80 (1H, m), 3.05 (1H, m), 3.11 (1H, m), 3.38 (3H, s), 3.96 (4H, m), 4.06 (5H, s), 6.04 (1H, m), 6.26 (1H, m); ^{13}C NMR (C_6D_6) **5a** δ 43.96, 47.89, 49.04, 49.68, 50.90, 51.52, 66.92, 67.64, 67.74, 68.75, 90.67, 136.22, 136.63, 176.02; **5b** δ 43.16, 46.42, 47.56, 51.02, 51.21, 51.66, 67.34, 67.83, 67.89, 69.01, 92.15, 133.77, 138.84, 174.36; UV-vis (THF) **5a,b** λ_{max}/nm (log ε) 440 (2.11), 324 (sh); MP **5a,b** 58-61°C; MS *m/e* (relative abundance) 336 (M^+, 18), 270 (M - $C_5H_6^+$, 100), 205 (M - C_5H_6 - $C_5H_5^+$, 25), 175 (M - C_5H_6 - C_5H_5 - OCH_3^+, 15), 121 ($FeC_5H_5^+$, 14); Anal. Calcd for $C_{19}H_{20}FeO_2$: C, 67.88; H, 6.00; Fe, 16.61; Found: C, 68.34; H, 6.12; Fe, 16.51.

10-(2-Hydroxyethyl)-phenothiazine (6). Phenothiazine, recrystallized from xylene, (4.95 g, 25 mmol) was dissolved

in 20 mL THF and added to a NaH oil dispersion (1.0 g of a 60% dispersion) in 80 mL THF. The mixture was refluxed for 2 h, then cooled to 0°C, ethylene oxide (2.4 mL, 50 mmol) was added via cannula. After stirring the mixture for 3 h at 0°C, it was transferred to a separatory funnel containing saturated aqueous NH_4Cl. The product was extracted with CH_2Cl_2 and the extract was washed twice with H_2O, dried over $MgSO_4$, filtered and concentrated by rotary evaporation. Kugelrohr vacuum distillation (168-175°C/0.15 mm Hg) yielded 5.0 g (83%) of product. ^1H NMR ($CDCl_3$) δ 2.00 (1H, m), 3.89 (2H, t), 4.10 (2H, t), 6.89-6.99 (4H, m), 7.14-7.21 (4H, m).

Bis(10-(2-ethyl)-phenothiazine)-*trans*-5-norbornene-2,3-dicarboxylate (7). A 250 mL 3 neck flask was assembled hot with a stopper, gas inlet, septum and stir bar and cooled under Ar. Via cannula, 60 mL THF and then a 20 mL THF solution of 10-(2-hydroxyethyl)-phenothiazine (5.35 g, 22 mmol) and pyridine (1.83 mL, 22 mmol) was added to the flask. *trans*-5-Norbornene-2,3-dicarbonyl chloride (1.56 mL, 10 mmol) was added dropwise via syringe to the stirred solution, yielding a purple solution. After 9 h, the THF was removed by rotary evaporation and the residue taken up in $CHCl_3$ and H_2O. The phases were separated, the organic phase washed with H_2O, and the aqueous phases extracted the $CHCl_3$. The combined organic solutions were dried over $MgSO_4$ and concentrated to a light green, viscous gum. The crude product was chromatographed with a graded elution solvent, from 3:7 to 3:1 ethyl acetate:hexane (EA:Hex). The

fractions containing **7** were taken up in CH_2Cl_2, combined and the solvent removed by rotary evaporation. The white solid was recrystallized from EtOH/$CHCl_3$ to give 3.03 g (48%) of **7**. R_f (3:7 EA:Hex) 0.39; (1:1 EA:Hex) 0.56; (7:3 EA:Hex) 0.82; MP 121°C; ^{1}H NMR ($CDCl_3$) δ 1.33 (1H, m), 1.44 (1H, m), 2.64 (1H, m), 3.04 (1H, m), 3.17 (1H, m), 3.32 (1H, m), 4.07 (2H, t), 4.14 (2H, t), 4.33 (2H, t), 4.41 (2H, t), 5.85 (1H, m), 6.14 (1H, m), 6.90 (8H, m), 7.12 (8H, m); ^{13}C NMR ($CDCl_3$) δ 45.8, 46.0, 47.1, 47.4, 47.6, 47.9, 61.0, 61.3, 115.3, 115.4, 122.9, 125.3, 125.4, 127.4, 127.6, 135.0, 137.6, 144.7, 173.2, 174.3; UV-vis (THF) λ_{max}/nm (log ε) 310 (3.97); MS *m/e* (relative abundance) 632 (M^+, 42), 566 (M - $C_5H_6^+$, 66), 283 ([M - C_5H_6]/2^+, 12), 226 ($PhzCH_2CH_2^+$, 22), 212 ($PhzCH_2^+$, 100), 198 (Phz^+, 91), 180 ([M - 2 $PhzCH_2CH_2$]$^+$, 43), 66 ($C_5H_6^+$, 45); Anal. Calcd for $C_{37}H_{32}N_2O_4S_2$: C, 70.23; H, 5.10; N, 4.43; S, 10.13; Found: C, 70.22; H, 5.12; N, 4.42; S, 10.24.

Mo(CH-*t*-Bu)(NAr)(O-*t*-Bu)$_2$, (Ar = 2,6-[di-isopropyl]phenyl) (1). Preparation of **1** has been described in detail elsewhere.[12]

Mo(CHFc)(NAr)(O-t-Bu)$_2$, (Fc = ferrocenyl; Ar = 2,6-[di-isopropyl]phenyl) (2). In a drybox, vinylferrocene (65 mg, 0.31 mmol) and **1** (150 mg, 0.31 mmol) were added together as solids and the minimum amount of toluene needed to dissolve the reactants was added (~1.5 mL). The solution color changed from dark orange to bright red as a light red solid precipatated. After stirring for 48 h, the solvent was

removed in vacuo. The red residue was extracted with pentane (1-2 mL) and the extracts were filtered through Celite. Recrystallization from a minimum amount of pentane at -40°C gave 83 mg (43%) of product as bright red needles in two crops. ^{1}H NMR (C_6D_6) δ 1.08 (12H, d), 1.35 (18H, s), 3.97 (2H, d of d), 4.00 (2H, sept), 4.09 (5H, s), 4.21 (2H,d of d), 7.05 (3H, m), 11.90 (1H, s, H_α); ^{13}C NMR (C_6D_6) δ 2.74 (C_α, J_{CH}=127 Hz), 27.8, 28.4, 32.0, 68.2, 69.3, 69.3, 77.2, 95.1, 123.1, 127.2, 155.5; Anal. Calcd for $C_{31}H_{45}FeMoNO_2$: C, 60.50; H, 7.37; N, 2.28; Found: C, 60.28; H, 7.44; N, 2.07.

Preparation of Polymers. The preparation of $(Nrb)_{60}(Fc)_{15}$ is given as a representative procedure. In a drybox, a solution of norbornene (115.8 mg, 1.23 x 10^{-3} mol) in THF (1.0 mL) was added quickly to a well-stirred solution of Mo(CH-t-Bu)(NAr)(O-t-Bu)$_2$, **1**, (10 mg, 2.05 x 10^{-5} mol) in THF (1.0 mL) and the solution was stirred for 5 min. Following this a solution of **5** (103.4 mg, 3.08 x 10-4 mol) in THF (1 mL) was added quickly to the reaction solution, and stirred for 5 min. The living polymerization was terminated by adding trimethylsilylbenzaldehyde (20 μL, 1.1 x 10^{-4} mol). As the yellow THF solution was added slowly to 100 mL stirred hexane the polymer precipitated. The light yellow precipitate was collected by centrifugation, reprecipitated in hexane, collected, and dried under vacuum. A yellow powder, 195 mg (90%) was obtained.

Results of GPC and DSC analyses for all of the polymers

are given in Tables I and II. The extent of conversion of the termination reactions were followed by ^1H NMR by monitoring the loss of the alkylidene proton resonance at ~11.6 ppm. The order of reactivity is trimethylsilylbenzaldehyde ~ pyrenecarboxyaldehyde > pivaldehyde >> octamethylferrocenecarboxaldehyde. The former two react completely in ~10 min, and the last requires 3 h for complete conversion.

1-Ethenylpyrene. To a stirred suspension of methyltriphenyl phosphonium bromide (1.43 g, 4.0 mmol) in 20 mL THF at 0°C under Ar was added *n*-butyllithium (4.4 mmol) in hexane. The resulting red solution was stirred for 15 min, followed by addition of 1-pyrenecarboxaldehyde (0.92 g, 4.0 mmol) in 5 mL THF. After stirring for 12 h at room temperature, the solution was treated with petroleum ether and H_2O, and the phases were separated. The organic layer was washed with H_2O and the combined aqueous solutions were extracted with petroleum ether. The combined organic solutions were dried with $MgSO_4$, filtered and the solvent was removed by rotary evaporation to give a pale yellow solid. The crude product was chromatographed on alumina (9:1 hexane:CH_2Cl_2) and recrystallized from EtOH to give 354 mg (40%) of 1-ethenylpyrene. R_f (9:1 hexane:CH_2Cl_2) 0.60; MP 88°C; ^1H NMR (CD_2Cl_2) δ 5.63 (1H, d of m), 6.02 (1H, d of m), 7.81 (1H, d of d), 7.99-8.41 (9H); ^{13}C NMR (CD_2Cl_2) δ 117.69, 123.61, 124.29, 125.46, 125.70, 125.92, 126.69, 127.92, 128.06, 128.20, 128.70, 131.58, 131.66, 132.17, 133.04, 134.77; UV-

vis (THF) λ_{max}/nm (log ε) 390 (2.96), 358 (4.62), 342 (4.55), 330 (sh); Anal. Calcd for $C_{18}H_{12}$: C, 94.70; H, 5.30; Found: C, 95.03; H, 5.60.

Results and Discussion

Functionality in the Polymers. The initiators used to make the polymers are shown in Chart I. The Mo neopentylidene, **1**, is a four-coordinate, tetrahedral complex that is isolable as a crystalline, air sensitive, orange solid. Its synthesis has been reported.[12] The Mo is considered to be in its highest oxidation state, Mo(VI), where the imido and alkylidene ligands are considered to be dianionic four electron donors. Though formally in its highest oxidation state the Mo neopentylidene, **1**, is reduced at a very negative potential. The cyclic voltammogram at a 25 μm Pt disk in THF/0.1 M [*n*-Bu_4N]AsF_6 is shown in Figure 1. The current-voltage characteristic for steady-state diffusion of a redox species is:[21]

$$E = E_{1/2} + (RT/nF) \log[(i_{lim} - i)/i] \quad (1)$$

Accordingly, a plot of E vs. $\log[(i_{lim} - i)/i]$ yields a line of slope RT/nF = 59/n mV for a reversible couple at room temperature. Shown in the inset in Figure 1, such a plot gives a line with a slope of +60 mV, indicating that the reduction is a reversible, one electron process. With a half-wave potential of -2.16 V vs. SCE the "oxidized" Mo initiator is stable towards reduction by many common redox molecules that might by incorporated in a monomer.

Chart I. Mo alkylidene compounds used for initiation of ring opening metathesis polymerization.

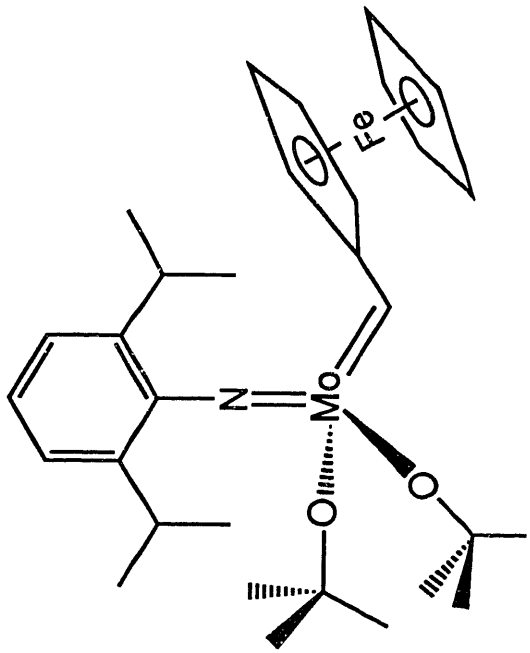

2

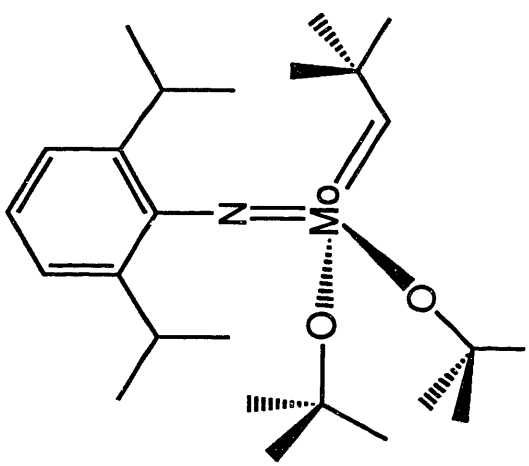

1

Figure 1. Cyclic voltammogram at 25 mV s^{-1} of **1** in THF/0.1 M [*n*-Bu_4N]AsF_6 at a 25 μm Pt disk electrode. A plot of electrode potential vs. $\log[(i_{lim} - i)/i]$ is shown in the inset.

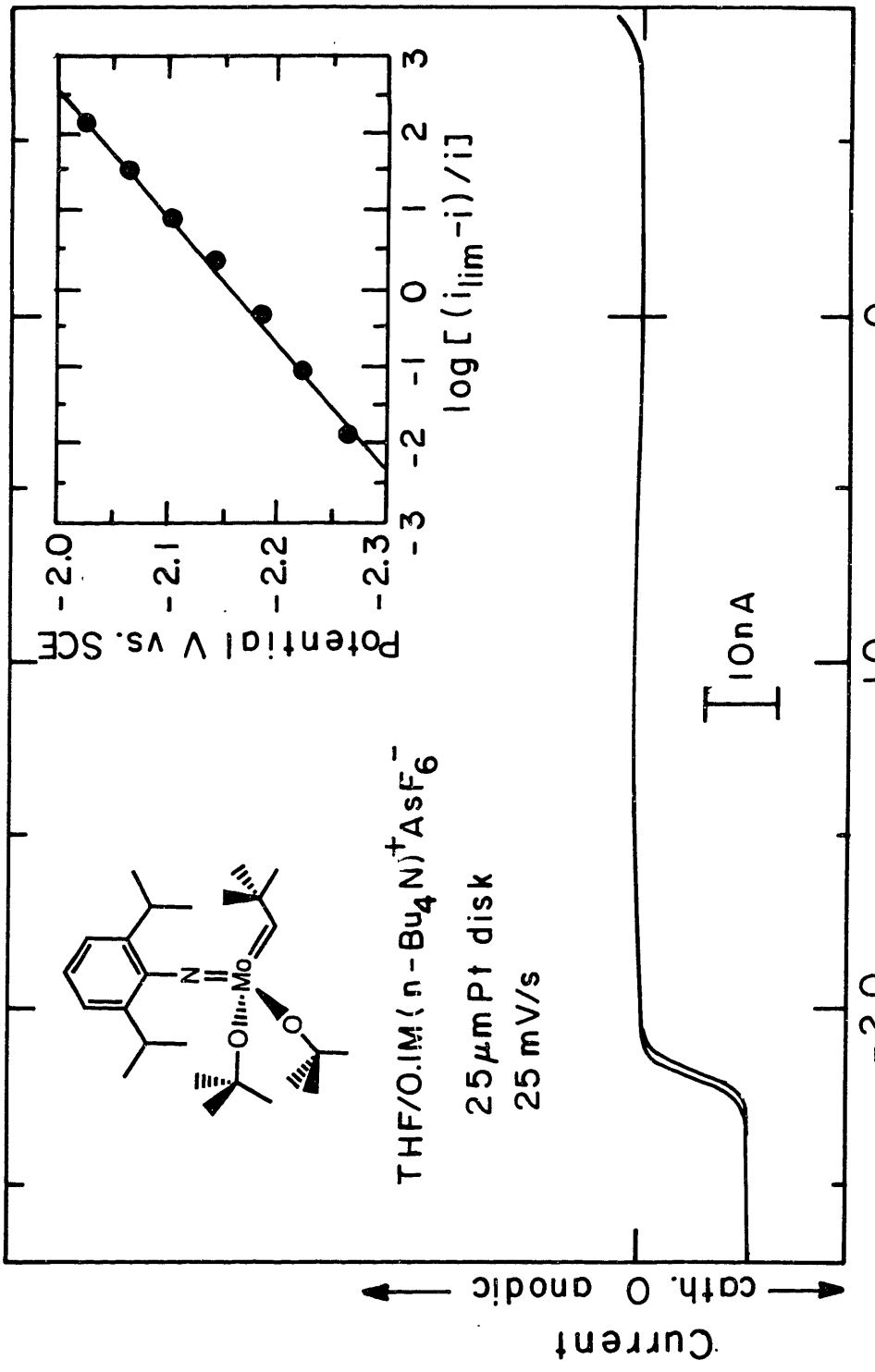
Current
cath. 0 anodic
Potential, V vs. SCE
-2.0
-1.0
0
10nA
THF/0.1M(n-Bu4N)+AsF6-
25μm Pt disk
25 mV/s
Potential V vs. SCE
-2.0
-2.1
-2.2
-2.3
log [(ilim-i)/i]
-3
-2
-1
0
1
2
3
N
Mo
O
O

The *t*-butyl group becomes the starting end group in polymers initiated with **1**. In ^{1}H NMR spectra of the resulting polymer the nine protons in this group exhibit a sharp singlet that generally does not overlap with other resonances in the polymer. Thus, it serves as a ^{1}H NMR probe for end group analysis. In addition the chemical shift of the *t*-butyl resonance depends on the geometry at the first double bond, providing information about the metathesis reaction.

Efforts to make a Mo initiator with a redpx active alkylidene have focused on the Mo ferrocenylmethylidene, **2**. This redox active initiator was prepared by alkene metathesis of vinylferrocene with **1** to produce neohexene and **2**, as a crystalline, air sensitive, red solid. This reaction proceeds in two days, whereas the reaction with styrene requires more than seven days,[22] and internal olefins (such as those in the polymers produced) do not react with the Mo alkylidene.

The cyclic voltammetry of **2** in THF/0.1 M [*n*-Bu_4N]AsF_6 and in CH_2Cl_2/0.1 M [*n*-Bu_4N]AsF_6 are shown in Figure 2. Out to -2.40 V vs. SCE there is no reduction wave for **2**. The ferrocenyl substituent is a stronger electron donor than the *t*-butyl group in **1**, thereby making the metal center more electron rich, and more difficult to reduce.

There is no oxidation wave for **1** out to the electrolyte background, whereas **2** shows what appears to be two overlapping oxidation waves. A ferrocene-centered, one-

Figure 2. Cyclic voltammetry of **2** in (a) THF/0.1 M [*n*-Bu_4N]AsF_6 at 100 mV s^{-1} at a 25 μm Pt disk electrode and (b) in CH_2Cl_2/0.1 M [*n*-Bu_4N]AsF_6 at 50 and 500 mV s^{-1} at a 500 μm Pt disk electrode.

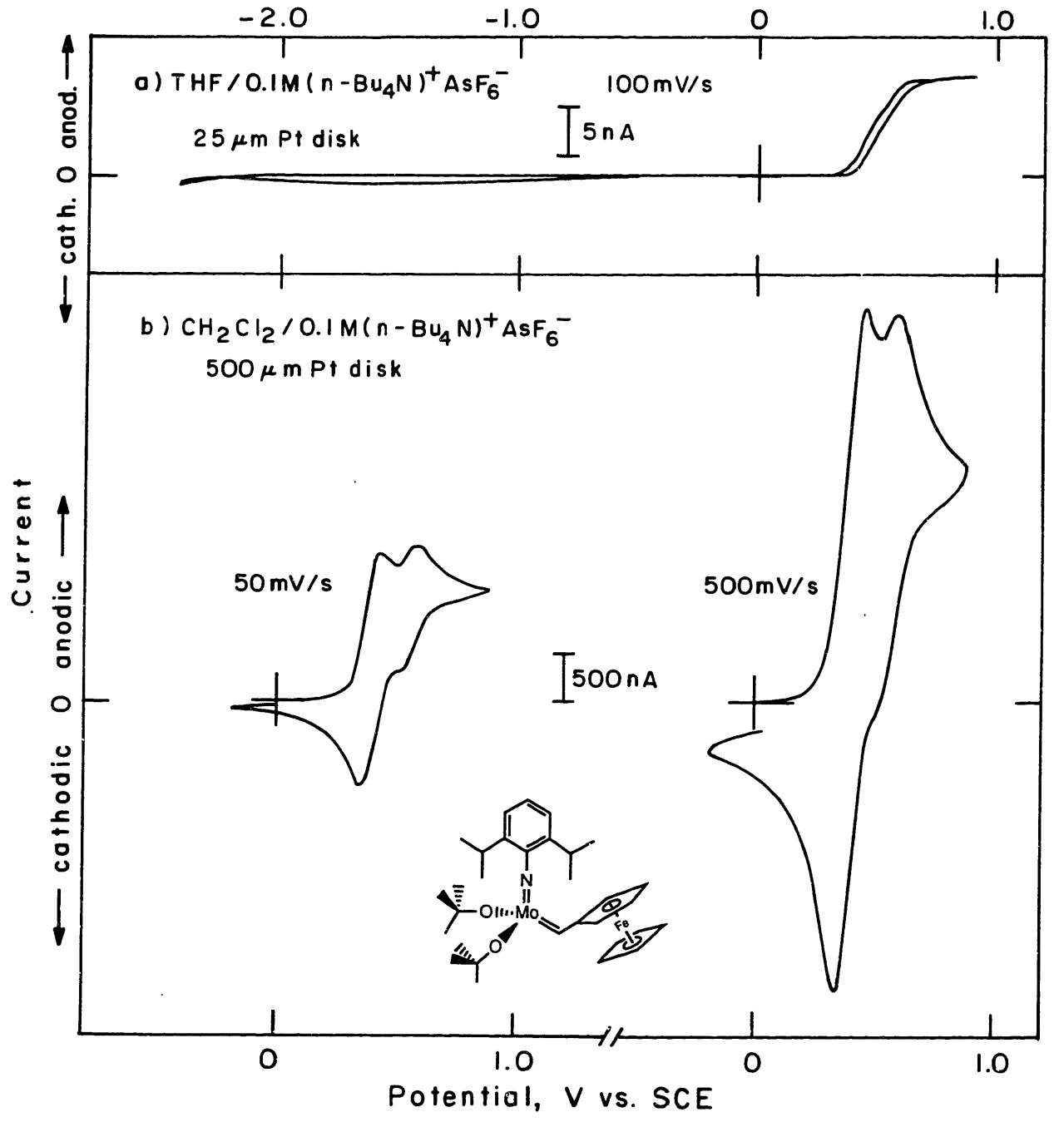
-2.0
-1.0
0
1.0
a) THF / 0.1M (n-Bu4N)+ AsF6−
100mV/s
25 μm Pt disk
5nA
cath. O anod.
b) CH2Cl2 / 0.1M (n-Bu4N)+ AsF6−
500 μm Pt disk
50mV/s
500mV/s
500nA
Current
cathodic O anodic
N
O
Mo
Fe
O
0
1.0
0
1.0
Potential, V vs. SCE

electron oxidation was expected. A possibe explanation for two waves is the presence of two different conformers with different redox potentials.[23] Electrochemically induced structural changes that produce isomers with different redox potentials have been observed for organometallic complexes,[24] and hindered olefins.[25] The two major conformers for compounds similar to **1** and **2** have the alkylidene substituent *syn* or *anti* to the imido ligand.[11] The rate of interconversion between the rotamers is found to be ~1 s^{-1} for similar alkylidene compounds.[26] For **2** this rate may be slower because of the larger size of the ferrocenyl group. This would seem to make the rate of interconversion slow enough that the voltammetric time scale, RT/Fv,[27] would be fast enough to observe only the major rotamer. However, the rate of rotation may increase upon oxidation of the ferrocene since the redox state of ferrocene probably controls the strength of the alkylidene π bond. In this case, if the other conformer has a more positive potential then there will be two waves,[28] as has been observed for **2**.

A second possibility is that the catalyst has reacted with itself or a trace impurity in electrolyte medium to form a ferrocene species with a different redox potential than the ferrocene in **2**. However, it is noted that 1) by ^1H NMR, **2** is present in 99% purity as ~95% one isomer, and 2) there is no change in the cyclic voltammetric wave of **2** in CH_2Cl_2/0.1 M [*n*-Bu_4N]AsF_6 over a 2 h period.

Using **2** to initiatate polymerization provides polymers with one ferrocene unit at one end of the polymer. The ferrocene serves as a unique redox probe. It is an internal, one electron standard. The average degree of polymerization of a redox active monomer can be determined by comparison of the current or charge passed in the redox waves of the monomer and the ferrocene starting group. Also, the ferrocene marks the polymer chain end. In cases where the polymer is attached to an electrode via a group at the opposite end of the chain, the ability of this ferrocene to exchange electrons with the electrode is an indication of the structure and the mobility of the surface confined film.

Strained cyclic olefins are used as the monomers in the ring opening metathesis polymerization by Mo alkylidenes. Ring strain in the olefin is required for the formation of metallocyclobutane intermediates. Unstrained internal olefins have not been observed to react with the Mo alkylidenes. The driving force for initiation and propagation is release of the strain energy. Conversely, depolymerization is disfavored due to the energy input required to reform the strained olefin. Norbornene, with a strain energy of 25 kcal/mol[29] is readily polymerized by **1** or **2**.

The norbornene skeleton is the preferred monomer, since many derivatives are commercially available or can be readily synthesized. The monomer is restricted to derivatives of norbornene with functional groups that the Mo

alkylidene can tolerate, groups that will not interfere with the course of the polymerization. Protic groups and isonitriles decompose the Mo compound, and aldehydes and ketones react with it. Polymerization can be done in the presence of ethers, esters, nitriles, thioethers, tertiary amines, alkyoxysilanes, dialkyl disulfides, and alkyl bromides. This was determined by polymerizing a monomer containing the functional group, or by polymerizing norbornene in the presence of an equimolar amount of the functional group. **1** and **2** are the most functionally tolerant set of initiators known for living metathesis polymerization.

The monomers used in this work are presented in Chart II. Norbornene, Nrb, produces a hydrophobic block segment of the elastomer polynorbornene. Ferrocenylcarbomethoxynorbornene, Fc, is an alkylferrocene with a redox potential of +0.380 V vs. SCE. The phenothiazine-containing norbornene derivative, Phz, has two phenothiazines per monomer. The monomer has one redox wave in which two electrons are transferred at +0.750 V vs. SCE. The ester groups increase the polarity of these monomers, aiding solubility in electrolyte media. Norbornene-2-methoxycarbonylferrocene, FcCE, is a ferrocenecarboxylate ester with a redox potential of +0.640 V vs. SCE, and triethoxysilylnorbornene, Si, is a surface coupling reagent[30] that works via hydrolytic formation of siloxane bonds with surface hydroxyl groups. These latter two monomers are discussed in Chapter IV.

Chart II. Norbornene derivatives used as monomers in the preparation of functionalized redox active polymers.

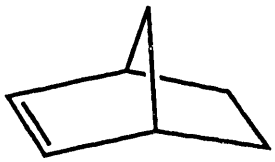

Nrb

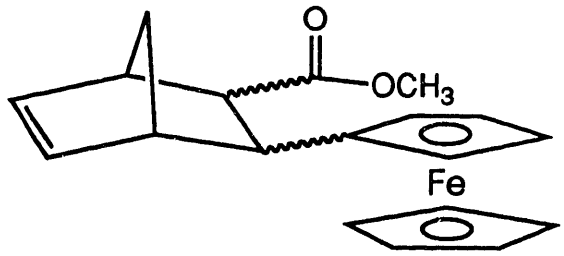

Fc

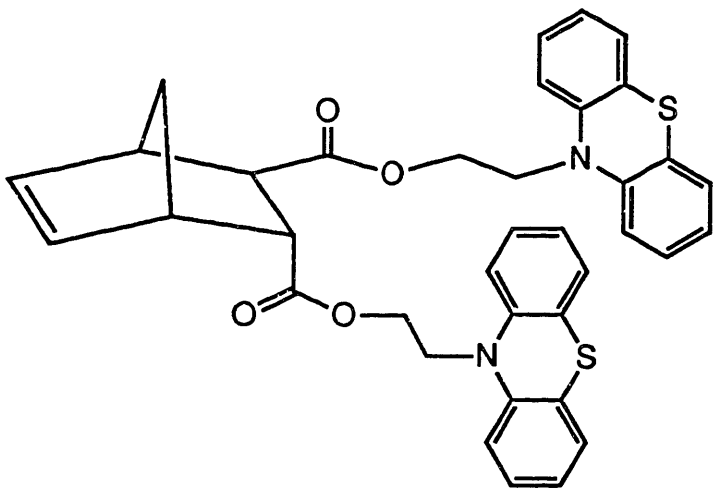

Phz

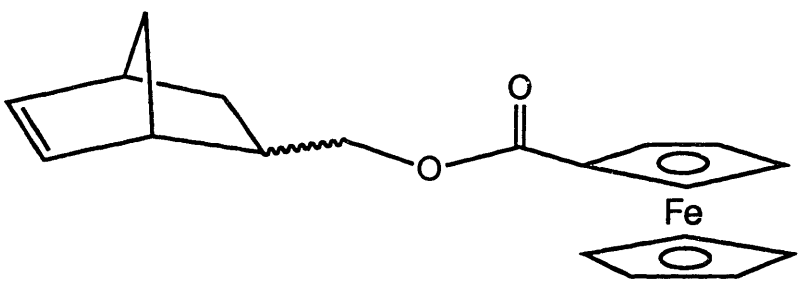

FcCE

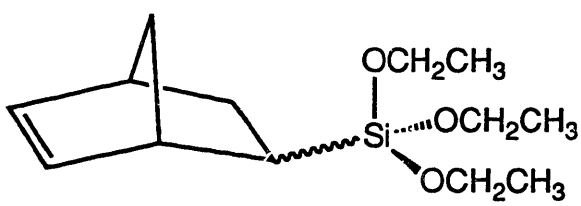

Si

A variety of functional groups can be introduced as the capping end group in the termination reaction of an aldehyde with the living Mo alkylidene. Quantitative reactions without side reactions are obtained with aldehydes lacking α protons, such as aryl aldehydes or pivaldehyde.[11] Aldehydes used as capping groups are shown in Chart III. Pivaldehyde and trimethylsilylbenzaldehyde are useful as ^{1}H NMR probes for end group analysis, as well as serving as 'nonfunctional' controls in contrast to other types of end groups. A unique redox active tag, such as octamethylferrocenecarboxaldehyde, can also be located at the end of the polymer. Pyrenecarboxaldehyde is an example of a polycyclic aromatic compound that binds to graphite surfaces,[31] luminesces,[32] and participates in excited state electron transfer reactions.[33] This capping group can thus be applied as a surface binding agent, an emissive probe of the polymer structure or as a component in an energy/electron transfer scheme. The last two, to be discussed in Chapter IV, pyridinecarboxaldehyde and α-bromo-*p*-tolualdehyde, have been investigated as reagents for surface linking reactions between the polymer and a functionalized electrode surface. Forming a bond between a surface confined electrophile or nucleophile and the complementary reagent introduced as the end group would give an electrode modifying polymer film with a unique, known point of attachment.

Ferrocene Polymers and Block Polymers. The synthetic route

Chart III. Aldehydes used in the termination reaction for the preparation of functionalized redox active polymers.

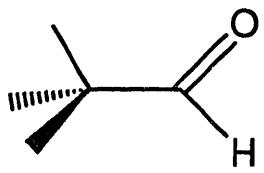
O
H

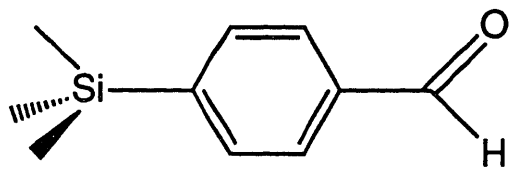
Si
O
H

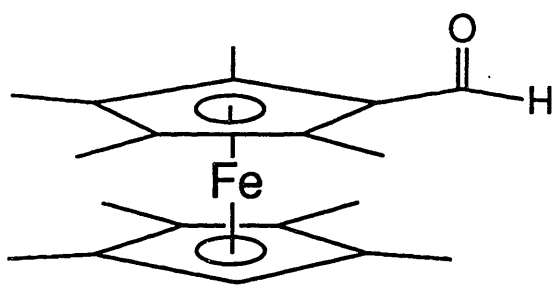
O
H
Fe

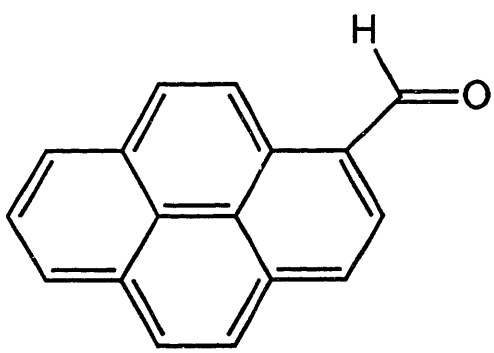
H
O

to the carbomethoxyferrocenylnorbornene monomer is shown is Scheme III. Formation of this norbornene bicycle is a slow reaction even at 110°C in toluene. Though the carboxylic acid is a good electron withdrawing group, ferrocene, a donating substituent, makes the olefin a relatively poor dienophile. The effect due to ferrocene is similar to that of a phenyl group since the reaction of cyclopentadiene with cinnamic acid occurs at a comparable rate.[19] Adding a Lewis acid catalyst, $AlCl_3$, to the reaction did not significantly change the rate. Running the reaction at elevated temperatures in a bomb caused decomposition of the ferrocene. The product obtained from the Diels-Alder reaction is best isolated after esterification. This last step also offers the chance to introduce other functionalities into this ferrocene monomer. The monomer can be separated into its two diastereomers by flash chromatography, however the mixture of isomers was used in the polymerizations.

A series of polymers and block polymers made with the monomer, Fc, and norbornene, Nrb, are shown in Chart IV. The number of repeat units indicated is the number of equivalents of monomer added to the Mo initiator; it will be shown (vide infra) that this is representative of the polymer that was made.

The course of the polymerization can be followed by ^1H NMR spectroscopy. The peaks of the monomer are replaced by the broadened peaks of the polymer and the signal of the

Scheme III. Synthetic route to 2-carbomethoxy-3-ferrocenyl-5-norbornene.

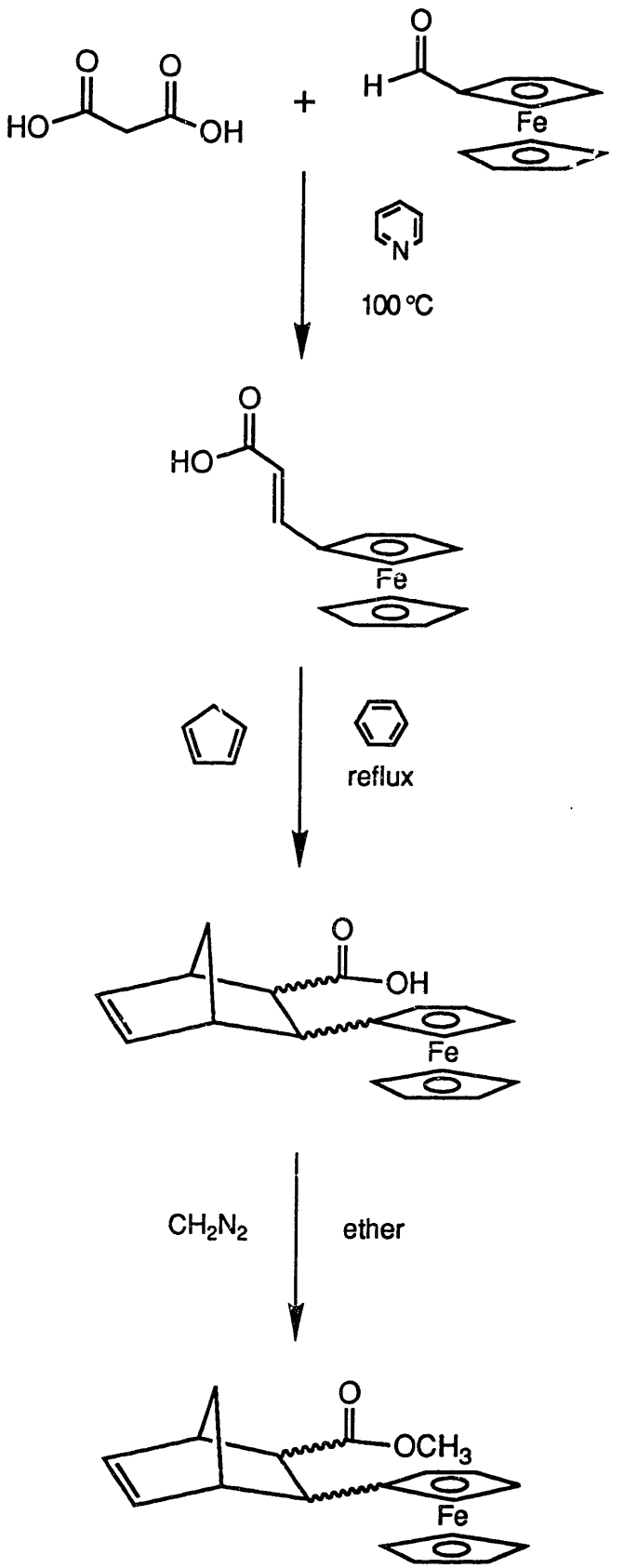

(3)

(4)

(5)

Chart IV. Ferrocene polymers and block polymers prepared by metathesis polymerization.

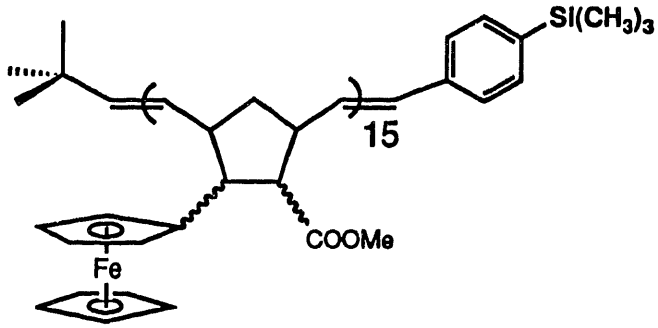

$(Fc)_{15}$

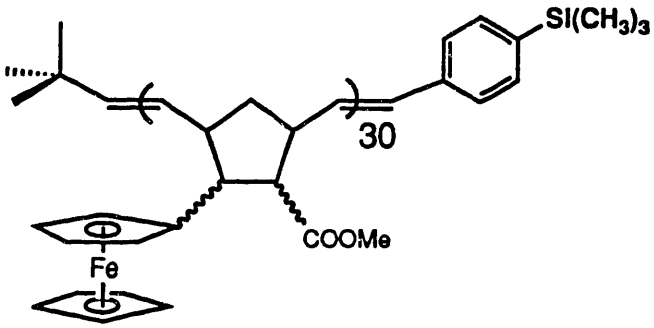

$(Fc)_{30}$

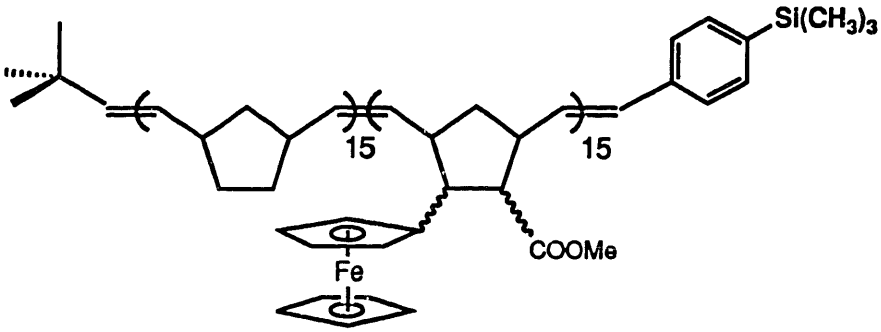

$(Nrb)_{15}(Fc)_{15}$

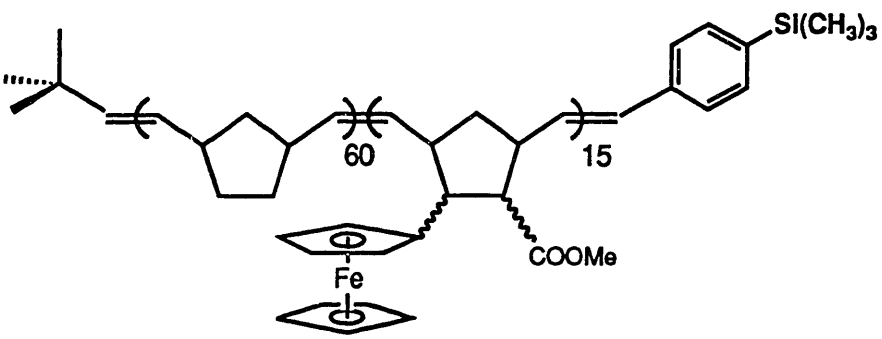

$(Nrb)_{60}(Fc)_{15}$

alkylidene proton of the initiator is replaced by the propagating alkylidene signal. The signal for this alkylidene, which is the chain-carrying species, has been observed to remain unchanged for more than 5 days at room temperature. Adding another monomer to the living alkylidene results in a new alkylidene signal and a set of broad peaks corresponding to a polymer of the new monomer. Addition of an aldehyde to the reaction results in loss of the alkylidene signal. A ^{1}H NMR spectrum of a block polymer is a superposition of the spectra of the corresponding homopolymers.

^{1}H NMR spectra yield the ratio of one end group to the other and the ratio of the average number of monomers incorporated to the end group(s). A 1:1 ratio of end groups confirms that all polymerizations that were initiated are finally terminated only by the aldehyde added as the capping group. If there was any chain transfer or back-biting into the polymer it would have to happen on the average only once per initiated chain. If there was such a competing side reaction it would be more apparent the longer the living alkylidene remained in solution, however the 1:1 ratio of end groups is found for capping reactions with rates that vary by a factor of 40.

The average degree of polymerization is found from the ratio of the olefinic protons to the end group. Since the peaks of the olefinic protons do not overlap with other peaks in the spectra the integral is uncomplicated. Within

the error of NMR integration the ratios obtained show that the average degree of polymerization is the same as the number of equivalents of monomer used.

As discussed above the only kinetic steps are initiation and propagation, and the ratio indicates the quality of the polydispersity produced. The individual rates are usually too fast to measure, but the ratio of the rates is readily determined.[34] By adding a small enough number of equivalents of monomer to an initiator, the ratio k_p/k_i is calculated from the final concentration of unreacted and reacted initiator and the initial monomer concentration.[35] For Fc with **1**, k_p/k_i is 10, while for Nrb with **1** k_p/k_i is 12. These values are not significantly different, so the order of addition for these monomers when making block polymers is not a concern.

Gel permeation chromatography (GPC) shows that unimodal, narrowly disperse polymers were made. Data from the GPC traces, the number average molecular weight, M_n, and the polydispersity, PDI, for these polymers are collected in Table I. The calculated molecular weight based on the number of equivalents of monomer added, MW_{calc}, is included for comparison. The low PDI's are indicative of a living polymerization.[4] The PDI's for the $(Nrb)_n(Fc)_m$ block polymers are lower than for the Fc homopolymers. This trend is in accord with an improvement in the PDI with longer chain length.[3] The GPC columns are calibrated with polystyrene standards so the M_n (and M_w) values determined

Table I. Characterization of Ferrocene Polymers and Block Polymers

Polymer	PDI[a]	M_n[b]	MW_{calc}[c]	T_g[d]
$(Fc)_{15}$	1.13	5090	5250	143
$(Fc)_{30}$	1.13	9030	10290	150
$(Nrb)_{15}(Fc)_{15}$	1.05	10460	6688	60, 123
$(Nrb)_{60}(Fc)_{15}$	1.07	16190	10930	43, 107

[a]Polydispersity index determined by gel permeation chromatography. [b]M_n as determined by GPC vs. polystyrene calibrant. [c]MW calculated for the number of equivalents added to the initiator. [d]Glass transition temperature determined by differential scanning calorimetry, scan rate 20°C/min.

correspond to the weight of a polystyrene chain that has the same hydrodynamic radius as the sample. Comparing M_n with MW_{calc} for the polymers and block polymers indicates that the size, and not the molecular weight of a sample is the governing factor. Also shown is that, within the regime of small polymers studied here the size of a $(Nrb)_n(Fc)_m$ block polymer is roughly equivalent to that of a homopolymer having n + m equivalents, in CH_2Cl_2 solution.

In Figure 3 is shown the GPC traces for $(Fc)_{15}$, $(Fc)_{30}$, and a coinjection of the two samples. In the coinjection the two polymer samples are not resolved, in agreement with a simple sum of the two individual traces. This unimodal curve is a testament to both the breadth of the range of chain lengths produced in the polymerization, and the limited resolving power of GPC columns. The M_n for this sample is calculated to correspond to a $(Fc)_{22}$ homopolymer, which is the average of the two individual samples. These numbers agree though because coinjection produces a unimodal distribution. Correspondingly, the PDI of the trace obtained in the coinjection is only 1.17, a seemingly low value, but if the sum of two Poisson distributions is unimodal then the calculated dispersity is expected to be in this low range.

In contrast to a living polymerization, radical polymerizations produce polymers with a broad distribution of chain lengths. As an illustration of what this means, Figure 4 shows the GPC trace of a sample of commercial

Figure 3. Gel permeation chromatograms of a coinjection of $(Fc)_{30}$ and $(Fc)_{15}$, and the individual traces of these two samples. The PDI's obtained were 1.18, 1.13, and 1.13, respectively.

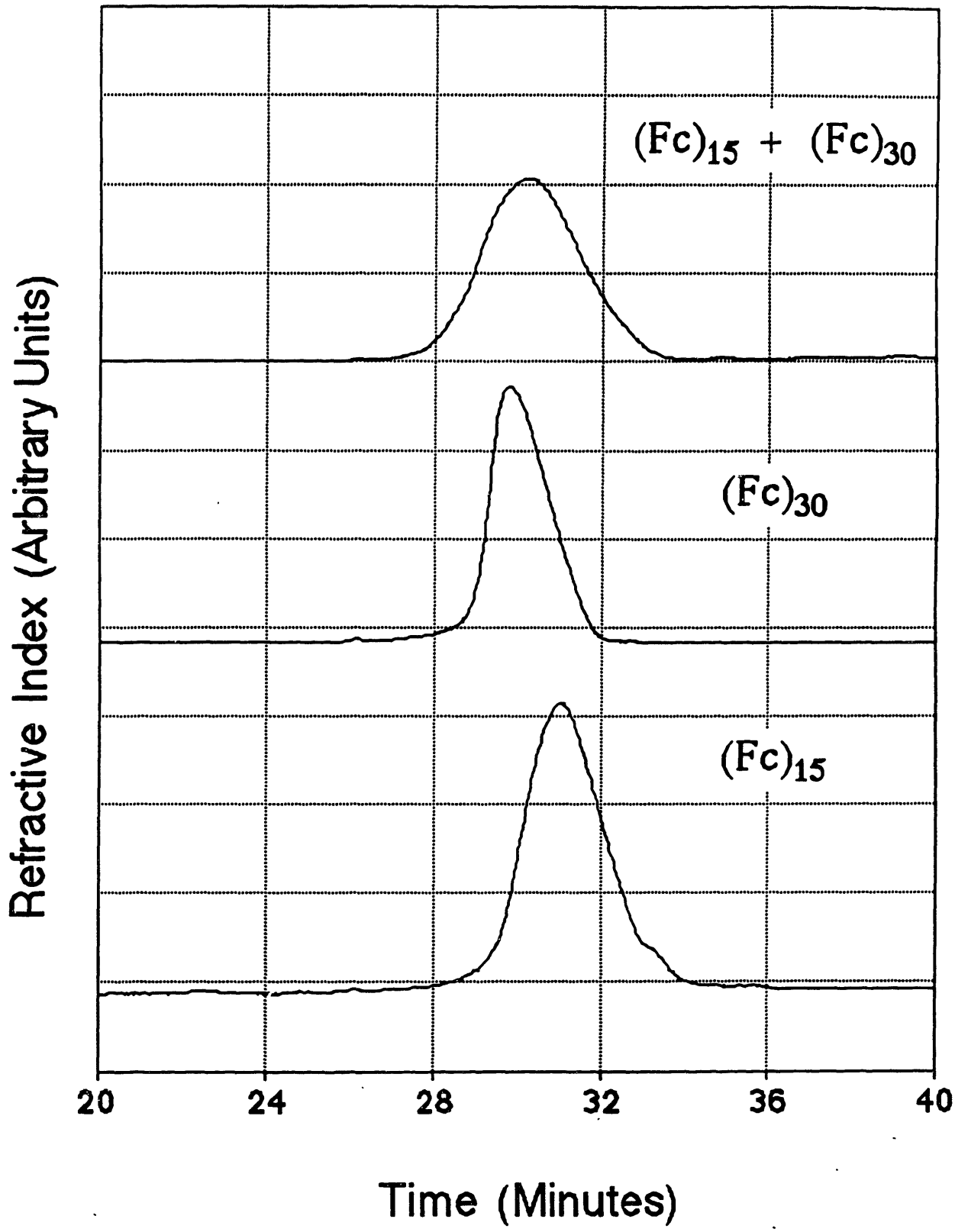
(Fc)15 + (Fc)30
(Fc)30
(Fc)15
Refractive Index (Arbitrary Units)
20
24
28
32
36
40
Time (Minutes)

Figure 4. Gel permeation chromatogram of commercially obtained polyvinylferrocene. The PDI was 3.54.

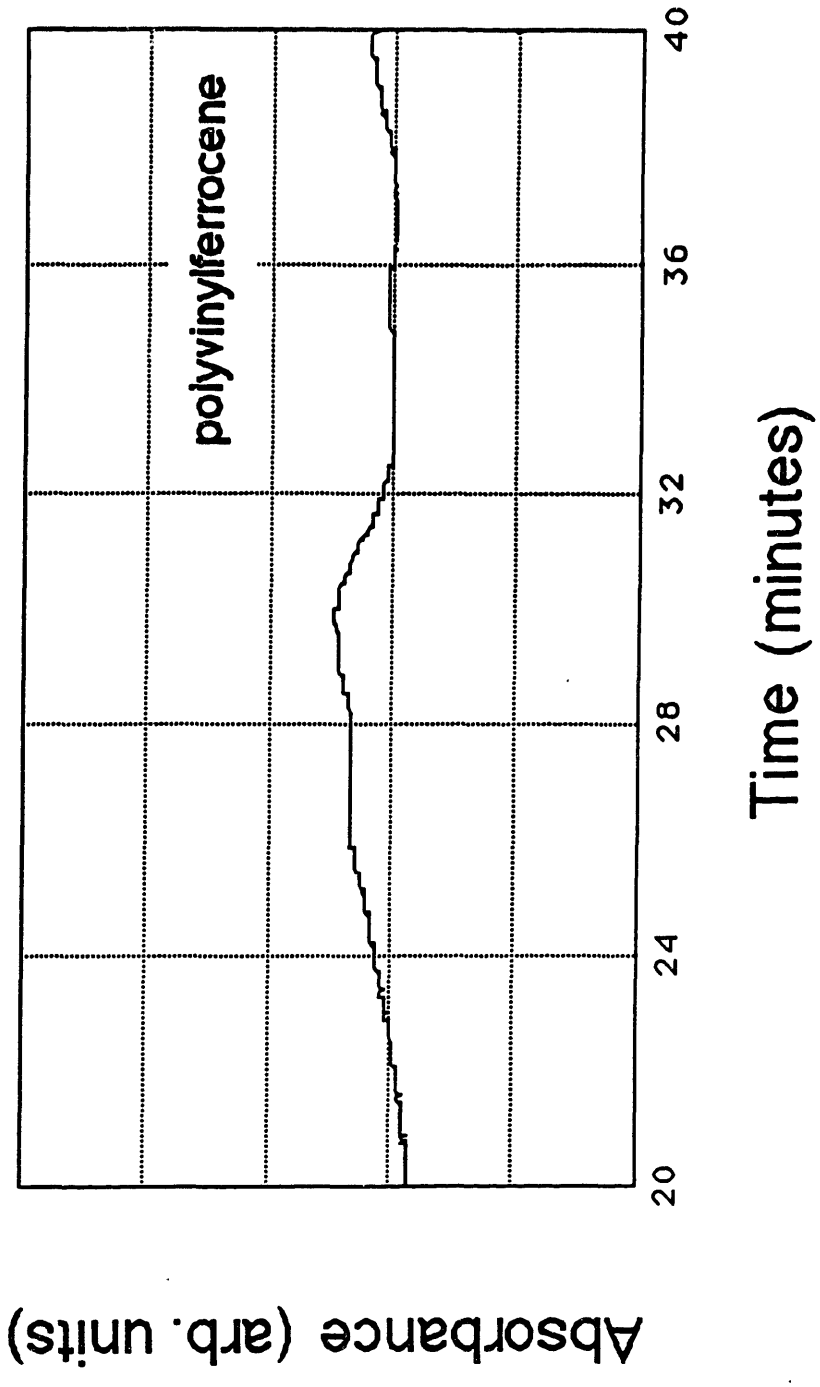
polyvinylferrocene
20
24
28
32
36
40
Time (minutes)
Absorbance (arb. units)

polyvinylferrocene. The calculated PDI of the main peak is 3.54. There is an additional peak at longer elution time, as well as some insoluble material that was filtered away before injection.

A more direct measure of the content of the polymer samples produced was obtained by field desorption mass spectroscopy (FD-MS). Recently FD-MS has been applied to polymer analysis of both synthetic and biological materials.[36] Interest in this technique arises from the fact that polar, high molecular weight, thermally unstable compounds can be induced to desorb with very little fragmentation.[37] Figure 5 shows the mass spectrum obtained from $(Fc)_{15}$. This spectrum shows the doubly charged manifold of peaks, ranging from n = 8 to n = 26. Spectra of a singly- and triply-charged manifold were obtained at different values of emitter current and have a similar range of peaks. In two cases the most abundant chain length was n = 14, and it was n = 15 in the other. Based on the abundance observed for each chain length the polydispersity was calculated to be 1.06. This value is in the range of that obtained by GPC, but it is not of particular importance since it is not known how well the spectrum of the desorbed material reflects the content of the sample. It is instructive, though, to see the range of chain lengths produced in a living polymerization by observing the molecular ions. Complete spectra of $(Fc)_{30}$ and $(Nrb)_{15}(Fc)_{15}$ could not be obtained by FD-MS.

Figure 5. Field desorption mass spectrum of $(Fc)_{15}$. Shown here is the doubly-charged manifold of peaks. A singly- and triply-charged manifold were observed at higher and lower emitter currents, respectively. The value of the polydispersity calculated from the relative abundances was 1.06. GPC, Figure 3, gives a PDI of 1.13.

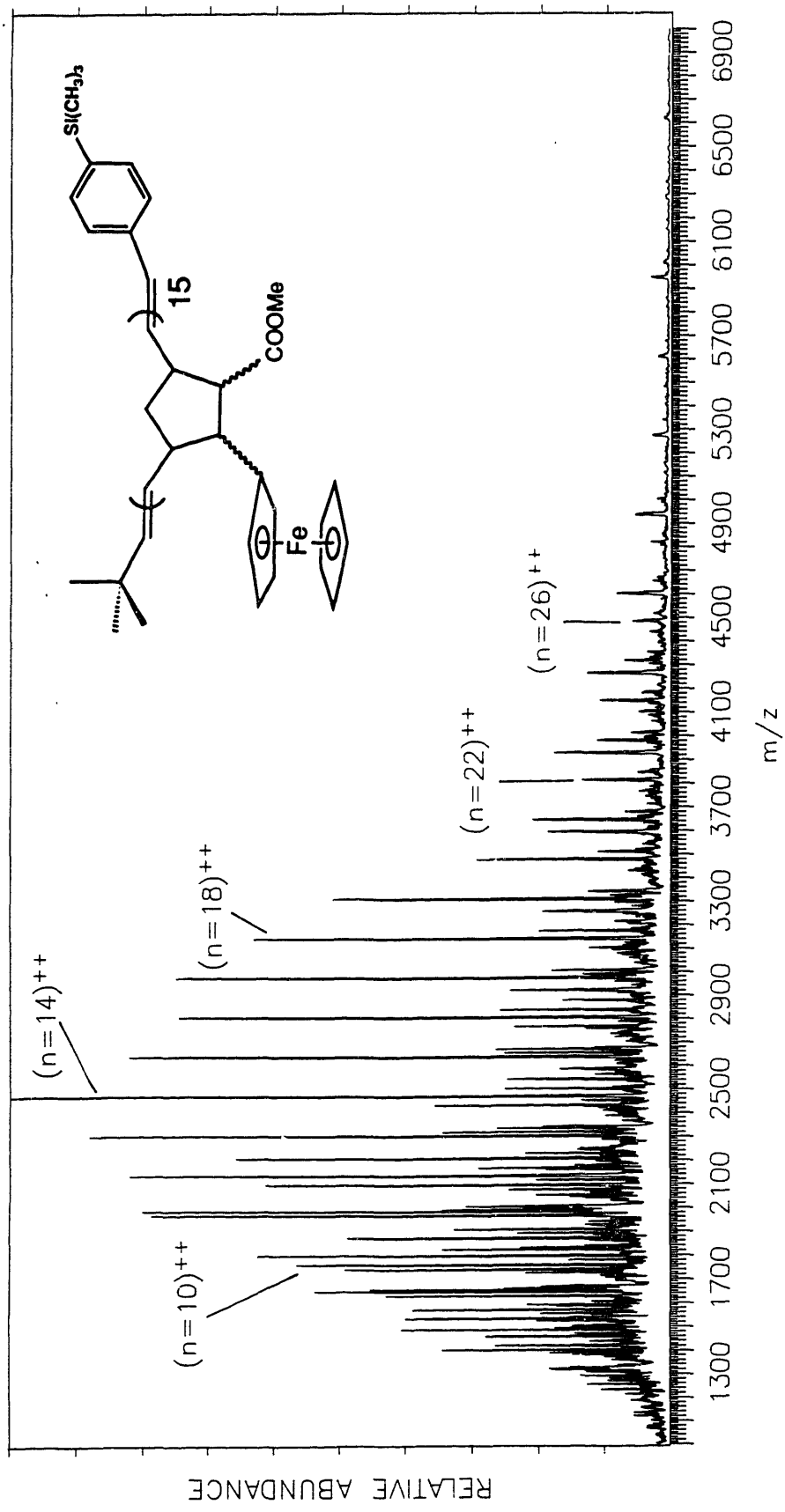
RELATIVE ABUNDANCE
m/z
1300
1700
2100
2500
2900
3300
3700
4100
4500
4900
5300
5700
6100
6500
6900
(n=10)++
(n=14)++
(n=18)++
(n=22)++
(n=26)++
Si(CH3)3
15
COOMe
Fe

To assess the effect of block formation on the structure of the polymer, the samples were analyzed by differential scanning calorimetry (DSC).[38] From DSC the phase transitions of a material are determined. With block polymers, if the blocks achieve microphase separation then phase transitions corresponding to each block are observed, instead of a transition that reflects the average of the block components. Microphase separation in block polymers is a well-known phenomenon, where blocks that are immiscible aggregate with the blocks of other polymer chains to form mutually exclusive domains. The DSC traces of $(Fc)_n$ and $(Nrb)_n(Fc)_m$ polymers are shown in Figure 6, and the observed glass transition temperatures are included in Table I. From these traces it is evident that the $(Nrb)_n$ and $(Fc)_m$ blocks phase separate, even having such short chain lengths. For the $(Fc)_n$ homopolymers, T_g increases with molecular weight as expected, since glass transition temperatures generally do not stop increasing until the molecular weight surpasses ~10,000.[39] In the block polymers the T_g ascribed to the $(Fc)_m$ phase is comparatively low. This is probably due the relatively small ratio of domain volume to interphase region resulting from small block sizes. The lower T_g material is of course linked to the higher T_g block. Consequently the motion in the polynorbornene unit increases the free volume of the $(Fc)_m$ phase and cooperativity of chain movements is mediated by the polymer chain between the phases.[40] As the relative block size of $(Nrb)_n$ to $(Fc)_m$ increases, the

Figure 6. Differential scanning calorimetry of the (Fc) polymers and (Nrb)(Fc) block polymers. Scan rate was 20°C/min. The samples were first annealed above the transition temperature for 10 min, and all measurements were repeated to confirm the transition.

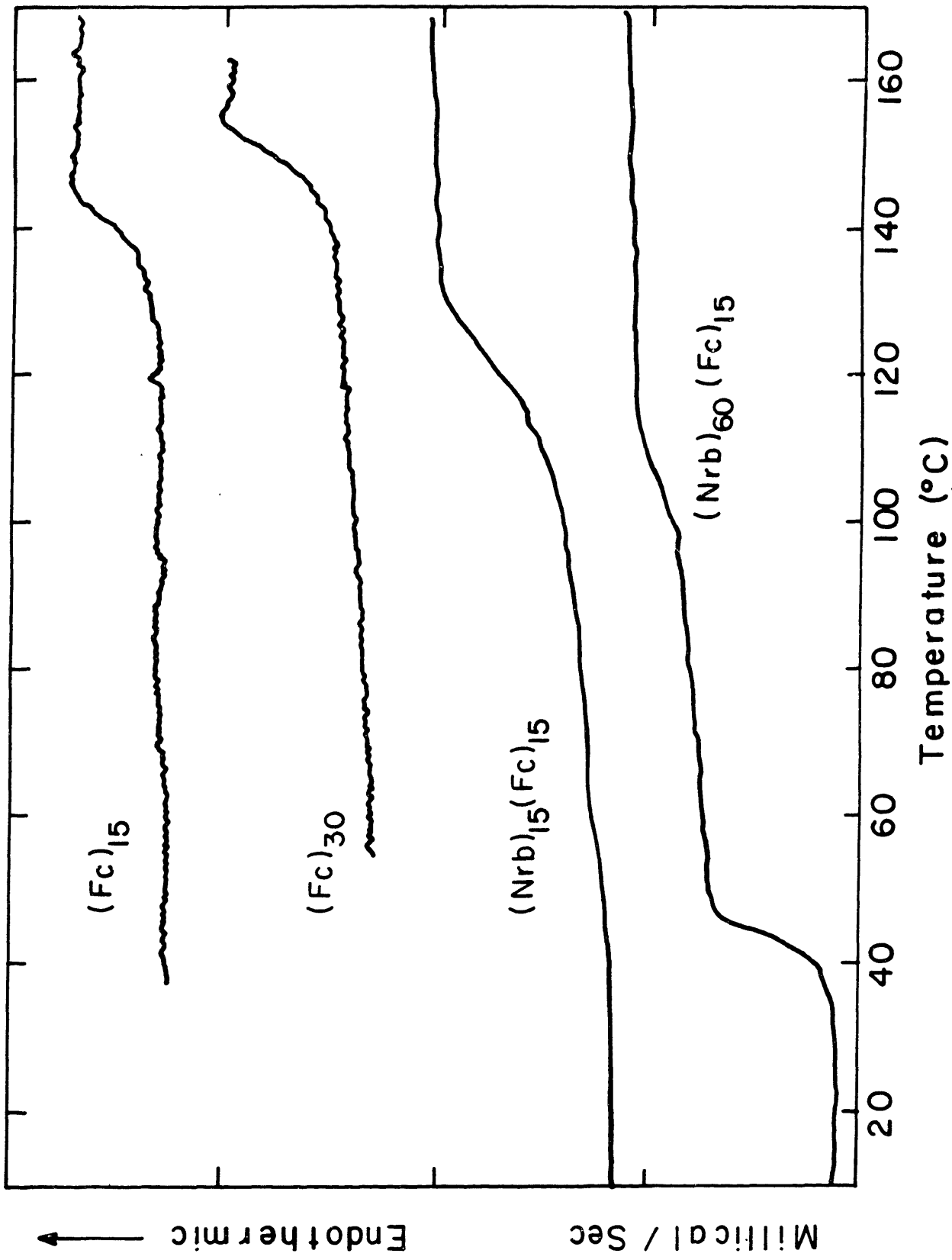
Endothermic
Milli cal / Sec
Temperature (°C)
20
40
60
80
100
120
140
160
(Fc)15
(Fc)30
(Nrb)15(Fc)15
(Nrb)60(Fc)15

magnitude of this effect is seen to increase; the higher T_g drops from 123°C to 107°C. Conversely, the lower T_g in block polymers is higher than for polynorbornene, which is 45°C. The presence of the higher T_g domains can act to lock in the chain motions in the nearby areas.[41] As the $(Nrb)_n$ block size increases the first T_g is observed at lower temperatures. This is consistent with the idea that high T_g domains should have less influence as the high T_g monomer becomes a smaller fraction of the polymer composition.

The electrochemistry of these redox active $(Fc)_n$ and $(Nrb)_n(Fc)_m$ polymers have been studied in solution and confined to the electrode surface. The surface-confined electrochemistry will be presented in Chapter IV. The solution electrochemical behavior of such redox polymers is governed by solubility. The solubility of these polymers depends on the state of charge of the ferrocene units. When in the reduced state the polymer is soluble in benzene, THF, CH_2Cl_2, and dimethylformamide, and insoluble in hexane, EtOH, CH_3CN, and H_2O. In the oxidized state, the polymer remains somewhat soluble in dimethylformamide, and it becomes insoluble in THF and CH_2Cl_2, and slightly soluble in CH_3CN.

The effects of the solubility properties on $(Fc)_{15}$ in DMF, THF, and CH_3CN are illustrated in Figure 7. As shown in Figure 7a, in DMF the cyclic voltammetric behavior is not greatly distorted from that for a soluble, reversible redox couple, except that the peak cathodic current is ~30% larger

Figure 7. Solvent dependence of the solution electrochemistry of $(Fc)_{15}$. (a) Scan rate dependence in dimethylformamide/0.1 M [*n*-Bu_4N]BF_4. (b) Cyclic voltammograms in THF, 1:1 THF:CH_3CN, and 1:6 THF:CH_3CN. The supporting electrolyte was 0.1 M [*n*-Bu_4N]BF_4.

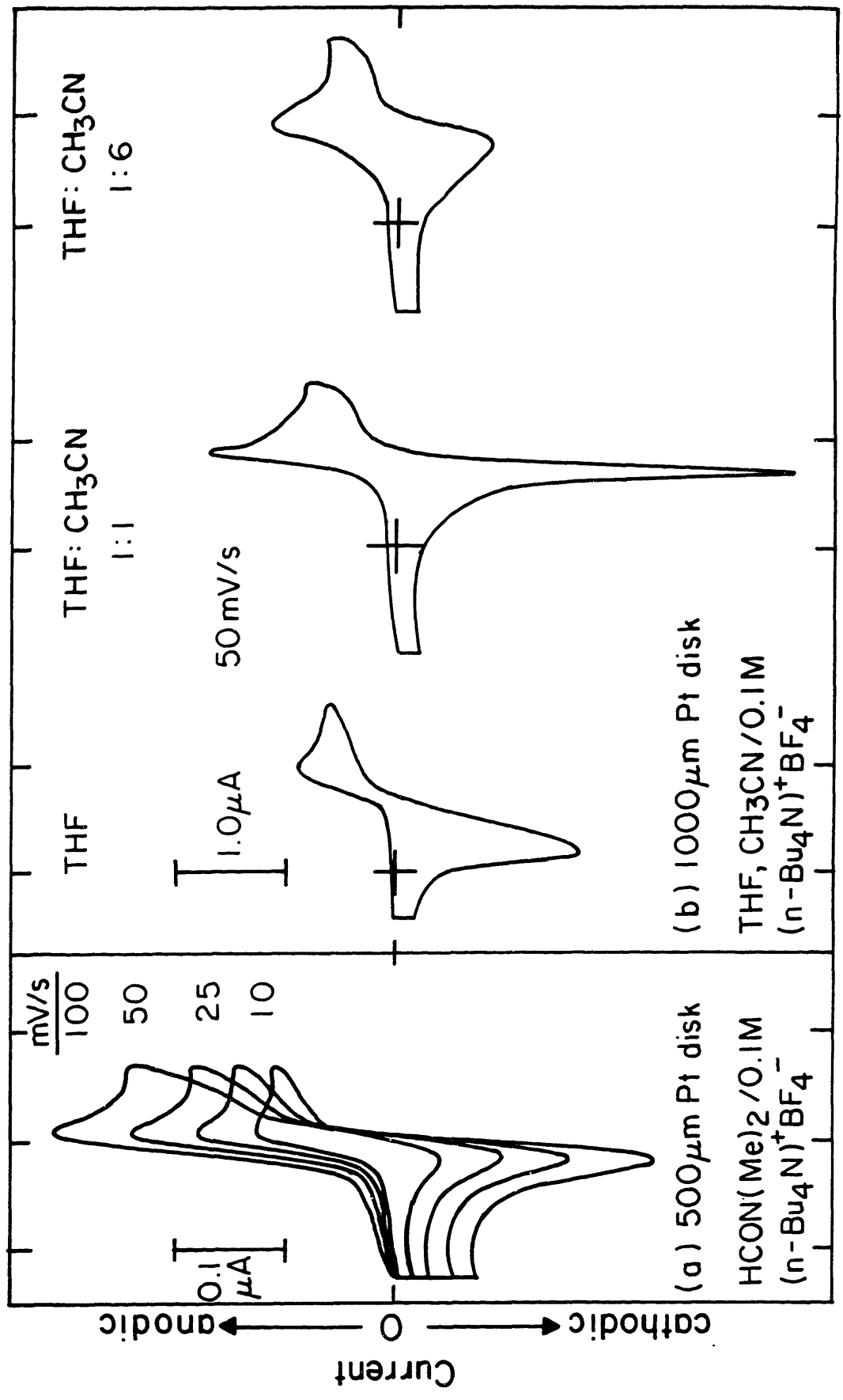
Current
cathodic
anodic
0
0.1 μA
mV/s
100
50
25
10
(a) 500μm Pt disk
HCON(Me)2 /0.1M
(n-Bu4N)+BF4-
THF
1.0μA
50 mV/s
(b) 1000μm Pt disk
THF, CH3CN/0.1M
(n-Bu4N)+BF4-
THF: CH3CN
1:1
THF: CH3CN
1:6
0.0
0.4
0.8
Potential, Volts vs. SCE

than the peak anodic current, rather than being equal.[42] In all other solvents studied the change in solubility with the change in oxidation state is more pronounced. For example, in THF, as for polyvinylferrocene,[43] oxidation of $(Fc)_n$ polymers results in precipitation of the polymer onto the electrode surface. During the reverse scan, as the polymer is reduced it redissolves into solution. Adding CH_3CN to the THF electrolyte medium changes the cyclic voltammetric behavior of $(Fc)_{15}$, as shown in Figure 7b. Since the oxidized state of the polymer is slightly soluble in CH_3CN, both of the redox states are soluble in this mixed solvent system. The cathodic stripping peak disappears, and the wave becomes more symmetric as the added CH_3CN keeps the oxidized form of the polymer in solution.

The solubility properties of a redox polymer also depend on the composition of the polymer. Diluting the number of charged sites per chain lowers the charge-to-mass ratio and results in a polymer whose solubility is less affected by the state of charge. Making a block polymer with a redox active monomer and a non-redox active monomer provides such a polymer with fewer charged sites per chain.

The effect of polymer composition on the solution electrochemical properties is shown in Figure 8, using the polymers listed in Chart IV. In solutions of equal ferrocene concentration, the cyclic voltammograms of the polymers are shown in contrast to that of ferrocene. The difference between the molecular and the polymeric behavior

Figure 8. Comparison of the cyclic voltammetric behavior in CH_2Cl_2/0.1 M [*n*-Bu_4N]PF_6 of ferrocene, $(Fc)_{15}$, $(Fc)_{30}$, $(Fc)_{15}(Nrb)_{15}$, and $(Fc)_{15}(Nrb)_{60}$. The concentration of ferrocene centers is the same for all solutions, 3.0 mM.

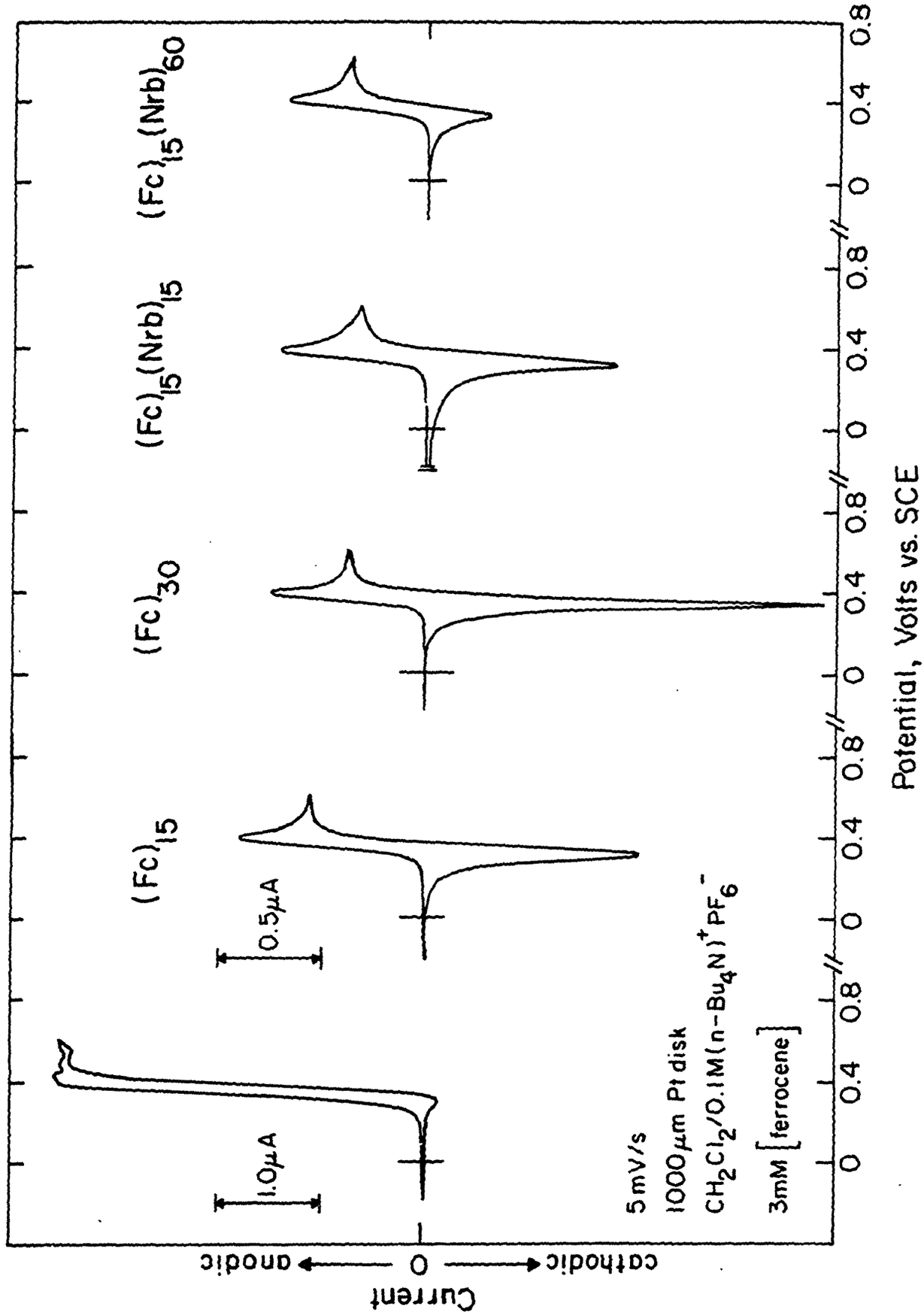
(Fc)15
(Fc)30
(Fc)15(Nrb)15
(Fc)15(Nrb)60
1.0μA
0.5μA
5mV/s
1000μm Pt disk
CH2Cl2/0.1M(n-Bu4N)+PF6-
3mM [ferrocene]
Current
cathodic ← 0 → anodic
0 0.4 0.8 // 0 0.4 0.8 // 0 0.4 0.8 // 0 0.4 0.8 // 0 0.4 0.8
Potential, Volts vs. SCE

is clear. The current for the polymer is diminished because of the smaller rate of diffusion. The $(Fc)_n$ polymers become insoluble in CH_2Cl_2 electrolyte upon oxidation, resulting in a cathodic stripping wave of the adsorbed polymer.[44] The shape of the wave changes with the size of the polymer and percent content of ferrocene.

The size, strictly the hydrodynamic radius, of the species determines its diffusion rate.[45] Together with the sweep rate and the electrode area, these three parameters determine the time and length scale of the experiment and thus the quality of the current-voltage curve. The information contained in the relationship among the parameters is expressed by the dimensionless number p:[46]

$$p = (nF/RT)^{1/2}(r^2v/D)^{1/2}$$

where r is a characteristic length of the electrode, v is the sweep rate, D is the diffusion coefficient and the other symbols have their usual meaning. The value of n needs to be considered carefully; for these multiredox center polymers n = 1 is appropriate. This point will be discussed later.

For $p > 13$ a cyclic voltammogram limited by semi-infinite linear diffusion is obtained, and for $p < 1$ a steady-state curve with radial diffusion is obtained.[46] For the data in Figure 8, in the case of ferrocene, $p = 4.5$, so intermediate behavior that approaches the steady-state response is observed as expected. For the polymers, D is much smaller. (Values of D can be estimated from a relation that has been

verified by experiment between D and the molecular weight.[47] See the following section.) Estimated values give p > 15, so cyclic voltammograms of the polymers are expected to be characterized by linear diffusion with the diffusional tail that decays as $t^{-1/2}$. Instead, the current peaks and then decays to a steady value. This behavior may be attributable to an equilibrium between oxidized polymers precipitated on the electrode and those in the diffusional boundary layer.

Adding a block of $(Nrb)_n$ to the $(Fc)_m$ polymer decreases the amount of material that deposits on the electrode upon oxidation. For $(Fc)_{15}(Nrb)_{60}$, the ratio of cathodic to anodic peak current is 1 at all sweep rates, notably the slower sweeps, from 5 to 500 mV s^{-1}. This is the ratio observed for ferrocene, and is the value expected for a reversible couple without adsorption.[21] The $(Fc)_n$ homopolymers are ~50% by weight ferrocene, whereas $(Fc)_{15}(Nrb)_{60}$, which does not precipitate when oxidized, is 25% by weight ferrocene.

In the block polymers, the charged sites are not actually "diluted", that is to say, homogeneously distributed along the chain. They retain the same structure as the homopolymers, and develop the same charge density in that block when oxidized. The solubilizing block attached somehow changes the oxidized block/solvent interaction to keep the polymer in solution. The effect would probably also occur for a random copolymer, but the solution structure of the oxidized block polymer is certainly

different.

Other points regarding the solution electrochemical properties of redox polymers will be presented in the following section on phenothiazine polymers.

Phenothiazine Polymers and Block Polymers. The synthetic route to the bis(10-(2-ethyl)-phenothiazine)-5-norbornene-2,3-dicarboxylate monomer, Phz, is shown in Scheme IV. This straightforward procedure can be carried out to provide gram quantities of the monomer.

A series of polymers and block polymers made with Phz and Nrb are shown in Chart V. The number of repeat units indicated is the number of equivalents of monomer added to the Mo initiator.

When forming block polymers the order of addition of the monomers will affect the dispersity of the polymer. Smaller dispersities are obtained when the monomer with the lowest value of k_p/k_i is used first. The initiation step for the second monomer, insertion into a living polynorbornene chain is faster than insertion into Mo neopentylidene, **1**, presumably because of less steric hindrance to the approach to the Mo. Thus the ratio k_p/k_i decreases and the overall dispersity is minimized. The ratio of k_p/k_i for Phz with **1** is 5, whereas the value for Nrb is 12. The $(Phz)_n(Nrb)_m$ block polymers were made by adding Phz first to **1**, followed by Nrb.

By GPC, unimodal, narrowly disperse polymers were made. This characteristic is indicative of a living

Scheme IV. Synthetic route to bis(10-(2-ethyl)-phenothiazine)-5-norbornene-2,3-dicarboxylate.

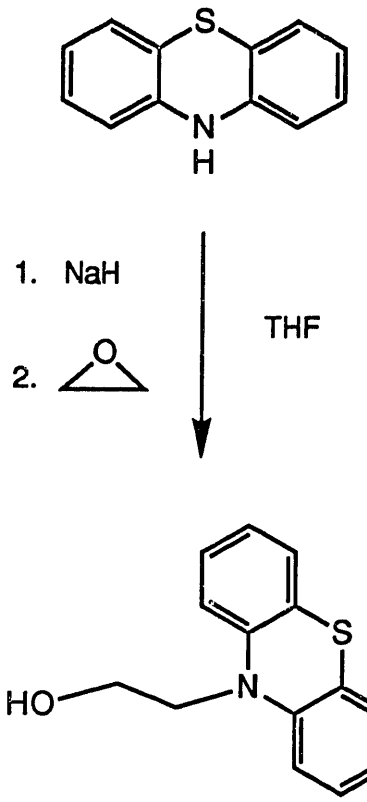

(6)

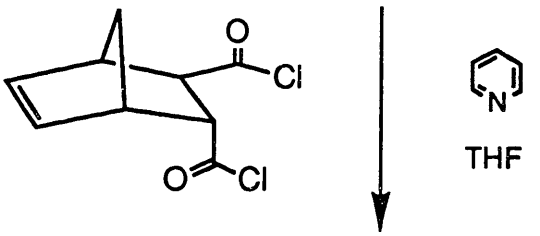

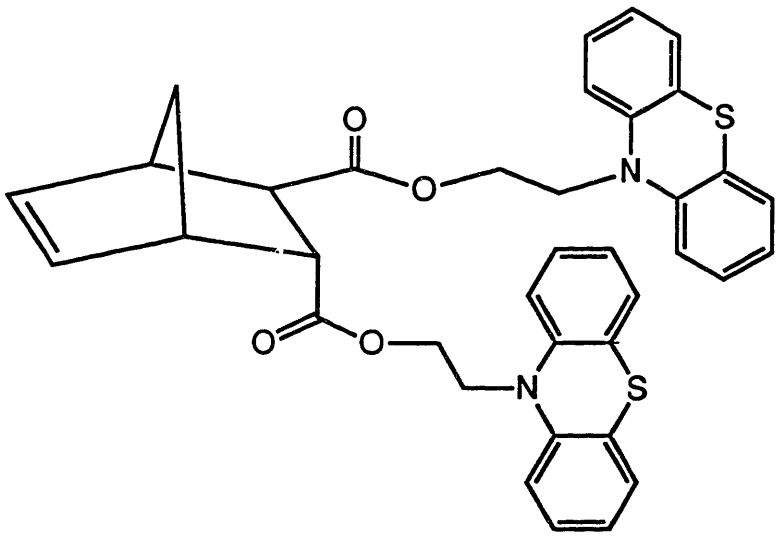

(7)

Chart V. Phenothiazine polymers and block polymers prepared by metathesis polymerization.

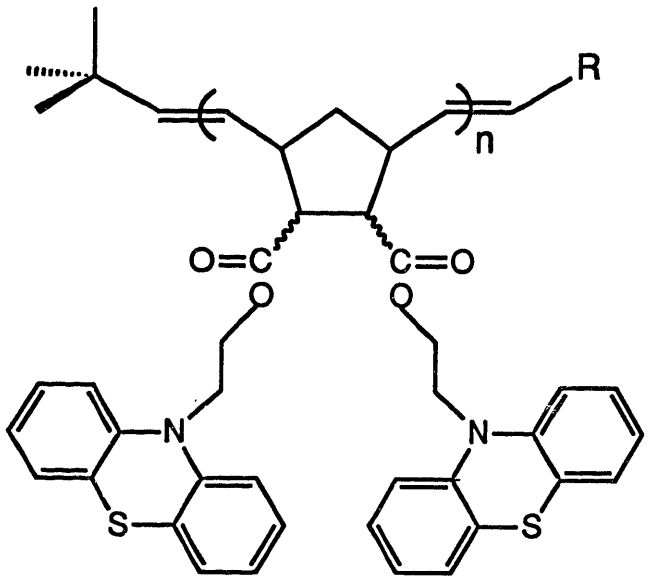

$(Phz)_{15}$

R =

$(Phz)_{30}$

R =

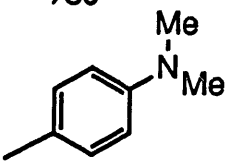

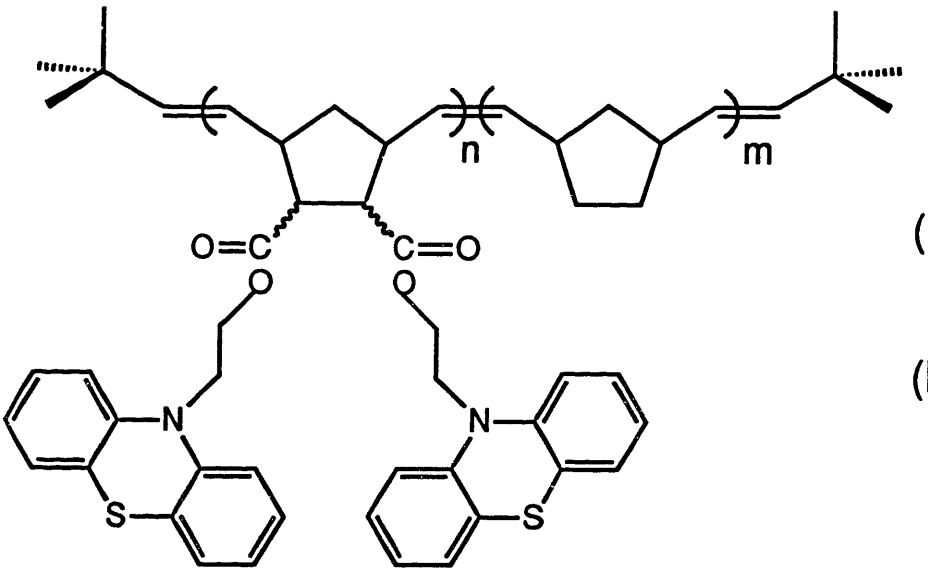

$(Phz)_{30}(Nrb)_{50}$

$(Phz)_{10}(Nrb)_{70}$

polymerization.[4] Values of PDI, M_n, and MW_{calc} are collected in Table II. The polydispersity is again observed to decrease as the degree of polymerization increases, as theory predicts.[3] The GPC traces for $(Phz)_{10}$, $(Phz)_{30}$, and a coinjection of the two samples are shown in Figure 9. In this case a bimodal chromatogram results from the coinjection, and appears to be a sum of the two individual traces. The PDI of the coinjection is 1.75, which is still a lower dispersity than polymers prepared by radical, ionic, or step-growth polymerization methods.[2]

A field desorption mass spectrum could not be obtained for any of these polymers. The smallest polymer, $(Phz)_{15}$, is nearly twice the average molecule weight of the polymer successfully characterized($(Fc)_{15}$) by FD-MS. Despite the fact that these polymers have relatively easily ionized redox groups, desorption of the polymer in the electric field is slower than decomposition.

The DSC analyses of $(Phz)_n$ and $(Phz)_n(Nrb)_m$ polymers are shown in Figure 10, and the observed glass transition temperatures are included in Table II. The blocks in $(Phz)_n(Nrb)_m$ are also observed to microphase separate at the small block sizes studied here. The glass transitions for the homopolymers are virtually superimposable despite a doubling of the average molecular weight from 10,000 to 20,000. As noted above, T_g generally does not increase as the molecular weight increases beyond 10,000.[39] In the block polymers the main change is the ~10°C decrease in the

Table II. Characterization of Phenothiazine Polymers and Block Polymers

Polymer	PDI[a]	M_n[b]	MW_{calc}[c]	T_g[d]
$(Phz)_{15}$	1.23	8360	9630	88
$(Phz)_{30}$	1.10	14750	19190	88
$(Phz)_{30}(Nrb)_{50}$	1.12	26740	23830	45, 91
$(Phz)_{10}(Nrb)_{70}$	1.08	35860	13060	50, 80
Fc-$(Phz)_5$	1.22	2700	3430	81

[a]Polydispersity index determined by gel permeation chromatography. [b]M_n as determined by GPC vs. polystyrene calibrant. [c]MW calculated for the number of equivalents added to the initiator. [d]Glass transition temperature determined by differential scanning calorimetry, scan rate 20°C/min.

Figure 9. Gel permeation chromatograms of a coinjection of $(Phz)_{30}$ and $(Phz)_{10}$, and the individual traces of these two samples. The PDI's obtained were 1.75, 1.10, and 1.23, respectively.

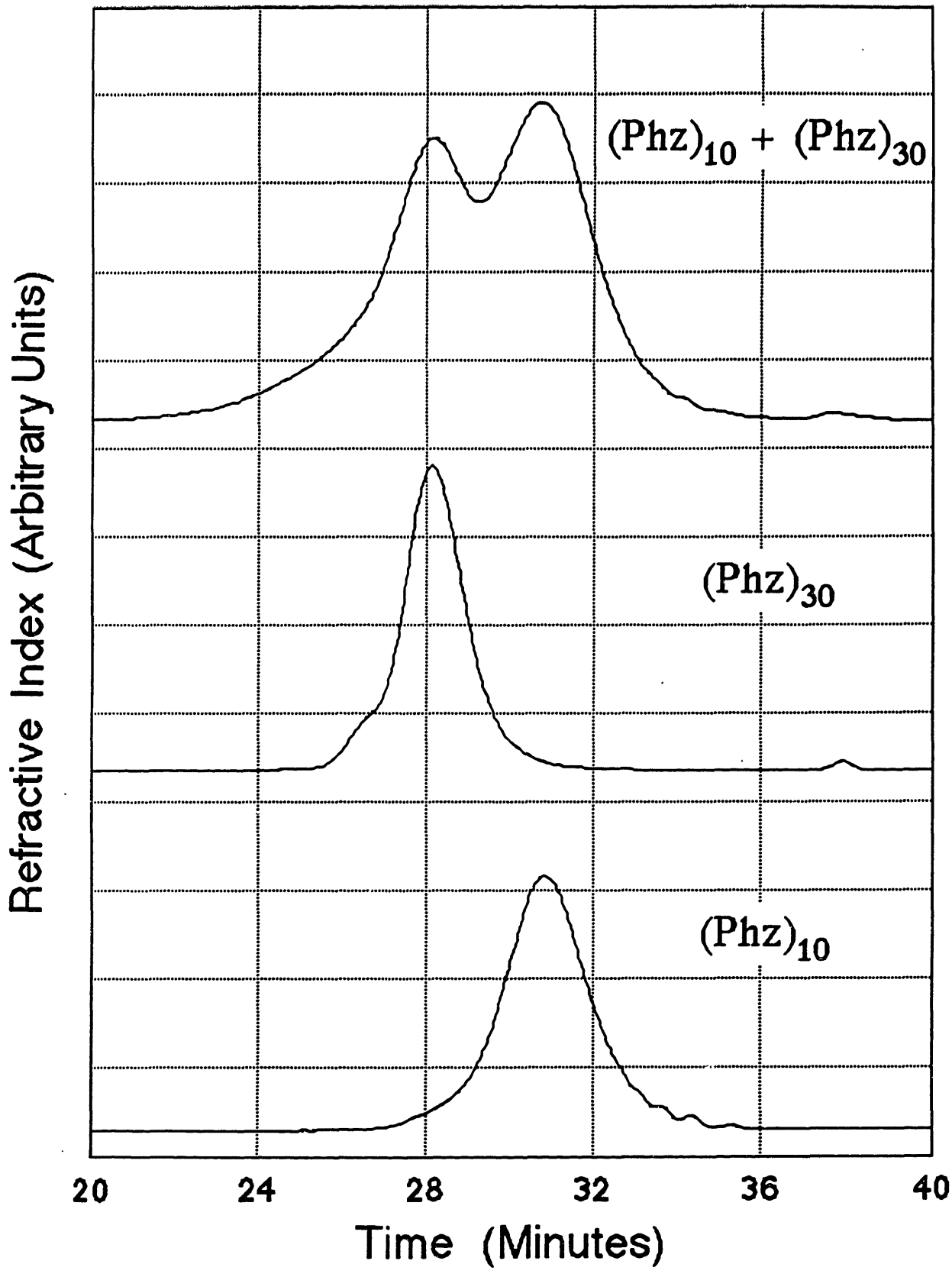
(Phz)10 + (Phz)30
(Phz)30
(Phz)10
Refractive Index (Arbitrary Units)
20
24
28
32
36
40
Time (Minutes)

Figure 10. Differential scanning calorimetry of the (Phz) polymers and (Phz)(Nrb) block polymers. Scan rate was 20°C/min. The samples were first annealed above the transition temperature for 10 min, and all measurements were repeated to confirm the transition.

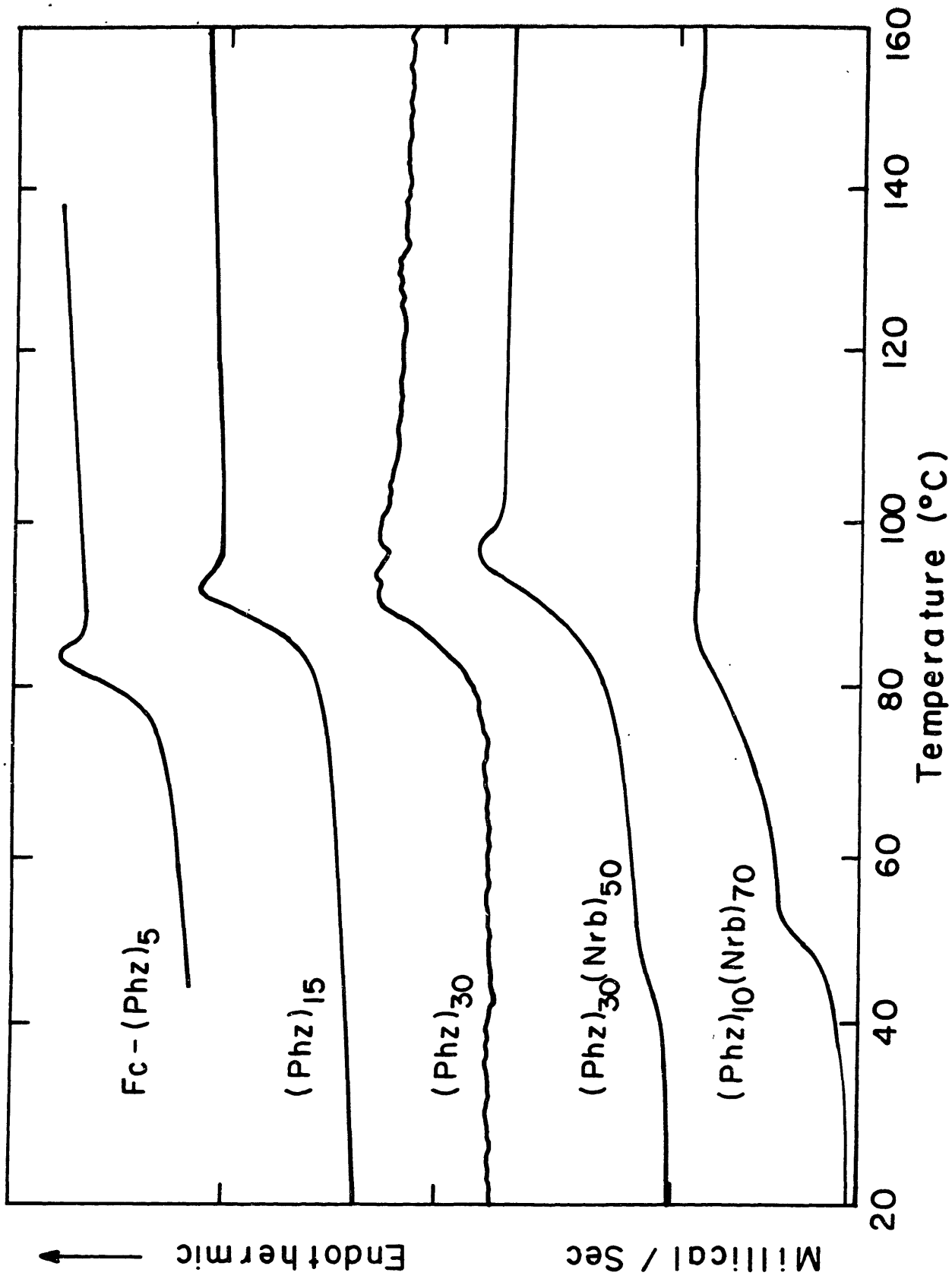
Fc-(Phz)5
(Phz)15
(Phz)30
(Phz)30(Nrb)50
(Phz)10(Nrb)70
20
40
60
80
100
120
140
160
Temperature (°C)
Endothermic
Milliical / Sec

higher T_g for $(Phz)_{10}(Nrb)_{70}$. The decrease is smaller than for the $(Nrb)_n(Fc)_m$ polymers and may indicate that a sharper phase separation exists in $(Phz)_n(Nrb)_m$ polymers.[38]

The glass transition of Phz blocks have a distinct endothermic peak, which increases in magnitude the slower the sample is cooled through the glass transition region. Slowly annealing the sample allows it time to approach a lower energy state. Upon heating more enthalpy is required to initiate segmental motion, at which point there is an exothermic relaxation to an amorphous state, resulting in a peak in the calorimetric measurement.[40,48]

The solubility properties of the $(Phz)_n$ and $(Phz)_n(Nrb)_m$ polymers are the same as those found for the Fc polymers. The solubilities are dependent on the state of charge of the phenothiazine units and the presence of a Nrb block, as discussed below.

The electrochemistry in CH_2Cl_2 of a set of Phz polymers, block polymers, and the Phz monomer was studied in solutions matched in phenothiazine concentration. The sweep rate dependence at moderate rates is shown in Figure 11. The Phz monomer exhibits the features characteristic of a reversible, Nernstian redox couple,[42] with a potential $E^{\circ\prime}$ = 0.75 V vs. SCE. The cyclic voltammograms of the polymers are marked by a reductive stripping wave due to precipitation of the oxidized material onto the electrode, as for the Fc polymers. The anodic wave maintains the qualities for linear diffusion of the electroactive

Figure 11. Scan rate dependence in CH_2Cl_2/0.1 M [*n*-Bu_4N]PF_6 of the phenothiazine monomer, $(Phz)_{15}$, $(Phz)_{30}(Nrb)_{50}$, and $(Phz)_{10}(Nrb)_{70}$. The concentration of phenothiazine centers is the same for all solutions, 0.2 mM

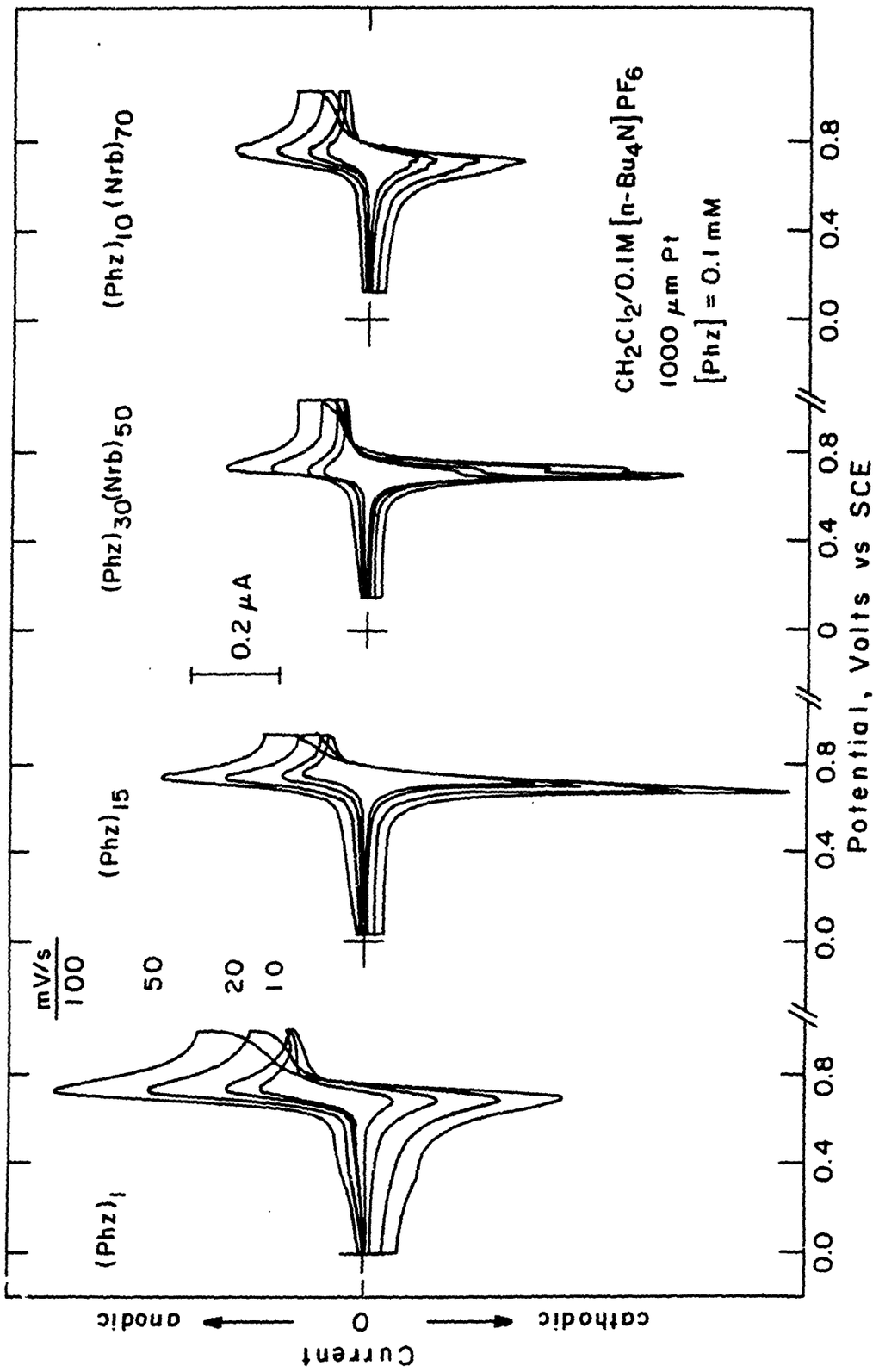
(Phz)1
(Phz)15
(Phz)30(Nrb)50
(Phz)10(Nrb)70
mV/s / 100
50
20
10
0.2 μA
CH2Cl2/0.1M [n-Bu4N]PF6
1000 μm Pt
[Phz] = 0.1 mM
0.0
0.4
0.8
0
Potential, Volts vs SCE
Current
cathodic
anodic
0

species.[42] The peak potential is independent of sweep rate (which is not true for chemically or electrochemically quasi- and irreversible processes) and the peak current scales linearly with the square root of the sweep rate up to 500 mV s^{-1}.

Note that the Phz monomer contains two phenothiazine units but there is a single redox wave and the peak separation, ΔE_p = 65 mV, is consistent with a value for n = 1 (59 mV), not n = 2 (29.5 mV).[42] Similarly, the cyclic voltammograms of the polymers have only one anodic wave, with no shoulders, and yet contain >20 phenothiazine units. It has been demonstrated for molecules with 2 identical redox sites,[49] and with ~1200 identical redox sites,[50] that the molecule undergoes reversible oxidation and reduction of 2 or 1200 electrons with a current-potential waveshape characteristic of a one-electron process. This multielectron wave can have a one-electron waveshape if the redox sites behave independently of one another.[43] It is the magnitude of the wave that is different, scaling with the number of electrons and the diffusion coefficient. Because of oxidative deposition of the (Phz) polymers in CH_2Cl_2 solvent, the peak-to-peak separation cannot be used as a criterion for whether the polymers have a one-electron voltammetric waveshape.

Problems with adsorption and precipitation of redox polymers can be overcome by employing normal pulse voltammetry (NPV) to study their solution properties.[43] In

NPV the applied potential is alternatively stepped between the initial potential at the foot of the wave, and a potential that increases with each pulse through the potential region of interest.[51] The duration of each pulse is short, 57 ms, which minimizes the precipitation of material. Since the potential then returns to the initial potential any material that might have deposited would be stripped away, and the initial conditions of the experiment recreated for the next potential pulse. The current is sampled over the last 17 ms of each potential pulse, meaning that transient currents such as double-layer charging have decayed, so the majority of the signal measured is faradaic current. NPV is a form of sampled-current voltammetry, and for reversible couples provides information about the formal potential, the concentration profile, diffusion coefficients and number of electrons in the process.[21]

Normal pulse voltammograms of the Phz polymers and the monomer are shown in Figure 12. Data from the curves, the limiting current, i_{lim}, half-wave potential, $E_{1/2}$, slope of the plot E vs. $\log[(i_{lim} - i)/i]$, and the diffusion coefficient, D_{NPV}, are given in Table III.

In the plot of the Heyrovsky-Ilkovic equation, eq 1, the slope is RT/nF and n represents the number of electrons characterizing the waveshape. For n = 1, the slope is 59 mV. The slopes determined for all the (Phz) samples agree quite well with this value. Thus the multiple redox sites behave independently, and polymer passes its electrons in a

Figure 12. Normal pulse voltammograms of the phenothiazine monomer, $(Phz)_{15}$, $(Phz)_{30}(Nrb)_{50}$, and $(Phz)_{10}(Nrb)_{70}$ in CH_2Cl_2/0.1 M [*n*-Bu_4N]PF_6. The current was sampled over the last 17 ms of a 57 ms pulse. Sweep rate, 10 mV s^{-1}; 'Drop time', 1 s.

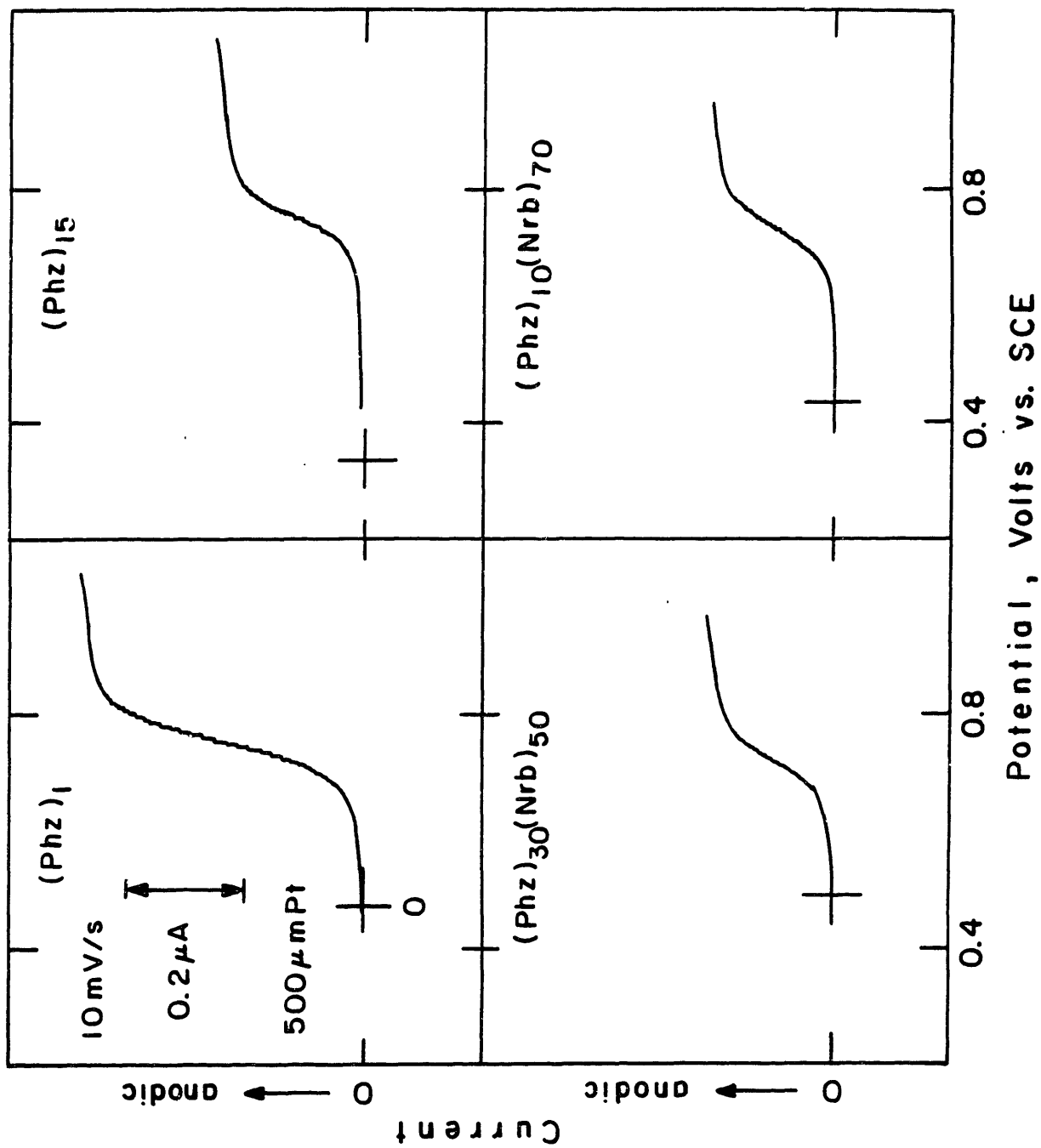
(Phz)15
(Phz)10(Nrb)70
(Phz)1
(Phz)30(Nrb)50
10mV/s
0.2μA
500μmPt
0
anodic
Current
0.4
0.8
Potential, Volts vs. SCE

wave characteristic of a one-electron process. That the polymer passes all of its electrons per redox unit will be shown in the next section using polymers with a redox active end group.

The diffusion coefficient for a randomly coiled, spherical polymer has been shown to be related to the molecular weight according to:[47]

$$D \propto MW^{-0.55} \tag{2}$$

for both biological and synthetic materials. This relation can be re-expressed as:

$$\log(D) = -0.55\log(MW) + \log(C) \tag{3}$$

where log(C) arises from the proportionality constant in eq 2. A log-log plot of the diffusion coefficient and molecular weight should yield a line with slope -0.55.

Values for D have been calculated in three ways, the results are included in Table III. D_{CV} was determined from the cyclic voltammetric sweep rate dependence shown in Figure 11. The slope of the plot $i_{p,a}$ vs. $v^{1/2}$ is given by:[42]

$$\text{slope} = (2.69 \times 10^5)n^{3/2}ACD^{1/2} \tag{4}$$

where A is the electrode area and C is the concentration of phenothiazine units, and n = 1. D_{SS} was determined from the steady-state current, i_{SS}, in voltammetric sweeps at a 25 μm Pt disk electrode from the relation:[52]

$$i_{SS} = 4nFrDC \tag{5}$$

where r is the electrode radius and the other symbols defined us usual. D_{NPV} was obtained from the limiting

Table III. Data From Normal Pulse Voltammetric Oxidation of Phenothiazine Monomer, Polymers and Block Polymers

Species	i_{lim} μA	$E_{1/2}$[a] mV	slope[b] mV	D_{NPV}[c]	D_{ss}[d]	D_{CV}[e]
				$cm^2s^{-1} \times 10^6$		
Phz monomer	0.44	750	-61	9.4	11.0	25.0
$(Phz)_{15}$	0.21	740	-62	2.6	3.4	12.0
$(Phz)_{30}(Nrb)_{50}$	0.16	740	-58	1.3	2.1	4.4
$(Phz)_{10}(Nrb)_{70}$	0.19	750	-61	1.9	2.8	4.6

[a]vs. SCE. [b]slope of the plot E vs. $\log[(i_{lim} - i)/i]$. [c]Calculated from eq 6. [d]Calculated from eq 5. [e]Calculated from eq 4.

current, i_{lim}, in a normal pulse voltammogram from the simplification of the i-V relation for the limiting current, which is just the Cottrell equation:[53]

$$i_{lim} = nFAC(D/\pi t)^{1/2} \quad (6)$$

where t is the time at which the current is sampled after a potential pulse.

Equation 3 is plotted in Figure 13 for the three sets of diffusion coefficients. The slopes agree well with the theoretical value of -0.55. The data derived from NPV are probably the most reliable. Normal pulse measurements minimize transient currents, since the electrode potential is constant during the measurement. The reproducibility of the measurement manifests itself with each successive pulse in the voltammogram. Because measurements of i_{lim} can be highly accurate, NPV is a good method for determining molecular properties such as diffusion coefficients.[51b] With a potential sweep technique there is the possibility of surface adsorption or precipitation during the sweep, changing the observed current and thus the diffusion coefficient from its true value. The good agreement with the theoretical power relationship, $MW^{-0.55}$ eq 2, supports the assumption that the polymers assume a randomly coiled spherical conformation in solution.[47]

Redox Active End Groups. Using Mo ferrocenylmethylidene, **2**, to initiate polymerizations produces polymers that have a ferrocene located at the end of the chain. Using octamethylferrocenecarboxaldehyde to terminate the reaction

Figure 13. Log-log plot of the diffusion coefficient vs. the molecular weight of a series of phenothiazine polymers, and a least-squares fit of the data. The diffusion coefficients were obtained experimentally by cyclic voltammetry, steady-state cyclic voltammetry, and normal pulse voltammetry.

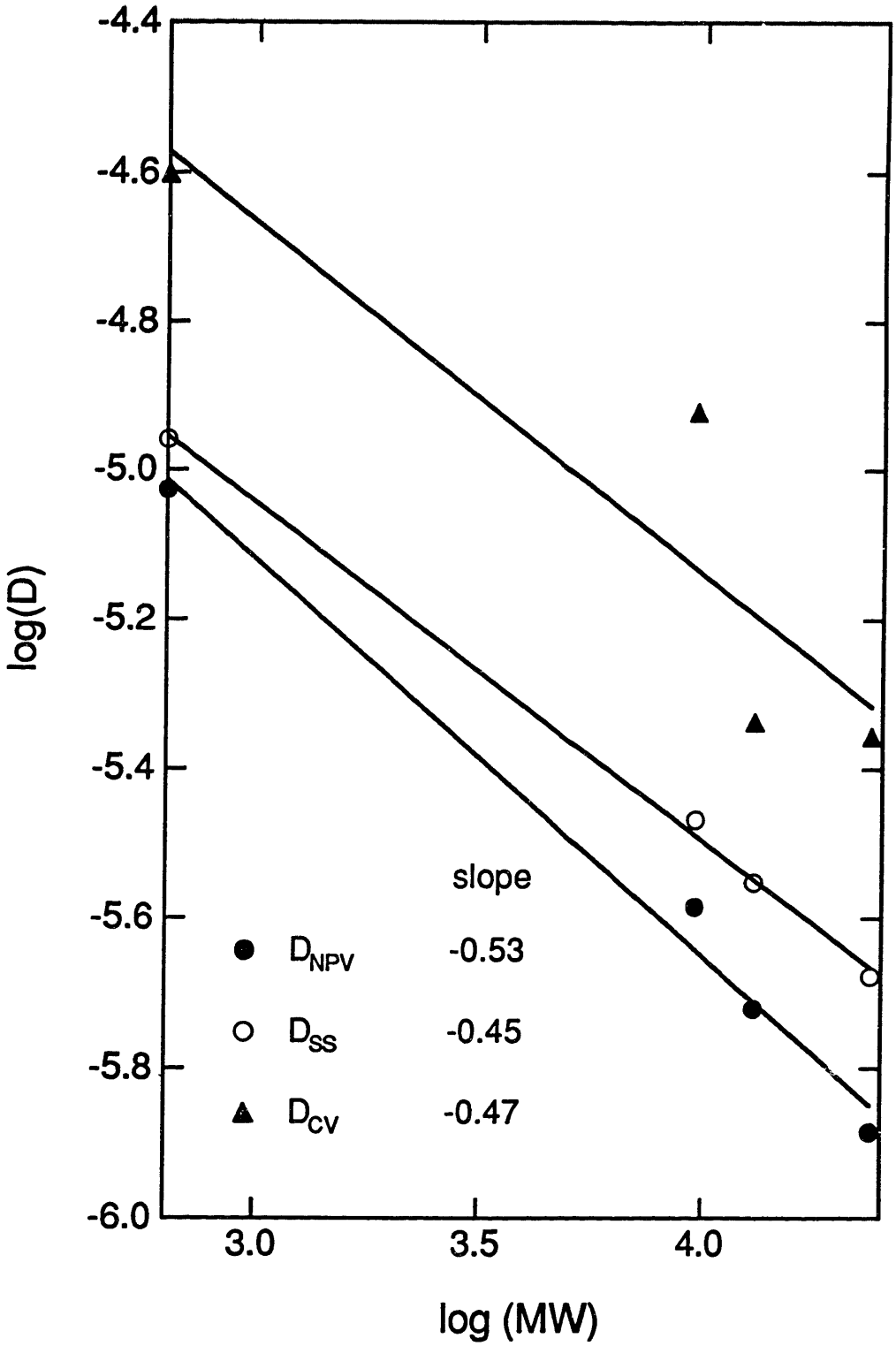
-4.4
-4.6
-4.8
-5.0
-5.2
-5.4
-5.6
-5.8
-6.0
log(D)
3.0
3.5
4.0
log (MW)
slope
D_{NPV} -0.53
D_{SS} -0.45
D_{CV} -0.47

produces polymers end-capped with a polyalkylferrocene. In this way two distinct redox tags can be incorporated into polymers prepared by ROMP. To demonstrate this ability the polymers shown in Chart VI were prepared. Small polymers were made to more clearly illustrate the redox properties of these materials.

The ferrocenylmethylidene, **2**, was found to be a better initiator than **1**. Monomers insert more readily into **2** leading to lower ratios of k_p/k_i. Thus polymers prepared from **2** will intrinsically be more narrowly disperse than the polymer initiated with **1**.[3] For Phz, k_p/k_i decreased to 2 for initiator **2**, a factor of 2.5 better than initiation with **1**. To prepare these polymers the solution of the living 5mer of (Phz) was divided in half and added to solutions of the different aldehyde capping reagents. Thus the polymers are identical in all respects except for the capping end group.

The results of the GPC and DSC analyses are given in Table II. These small polymers elute within the calibrated range of the GPC columns. For their short length, the PDI is very good. In the DSC trace of (Phz)-Fc, shown in Figure 10, the T_g is lower than the limiting T_g value observed for the larger $(Phz)_n$ polymers by 7°C. The glass transition temperature is expected to decrease as the molecular weight of the polymer becomes smaller.

The polymers with redox active end groups were studied by cyclic voltammetry and normal pulse voltammetry. The cyclic

Chart VI. Polymers prepared with redox active end groups.

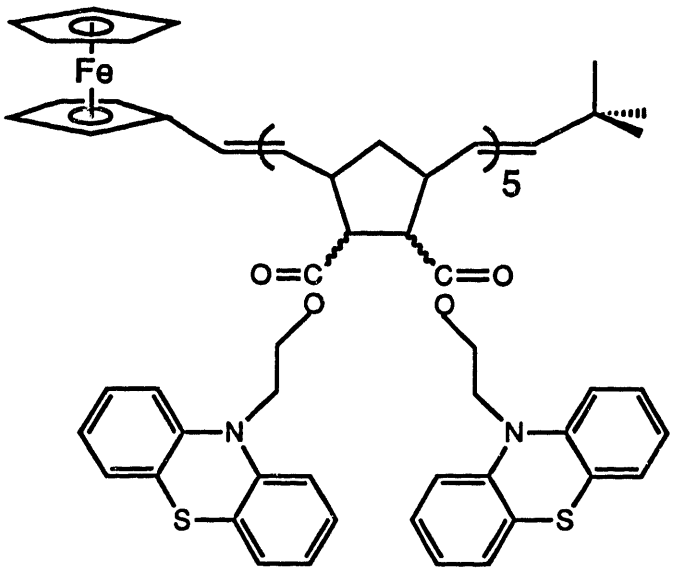

Fc-(Phz)$_5$

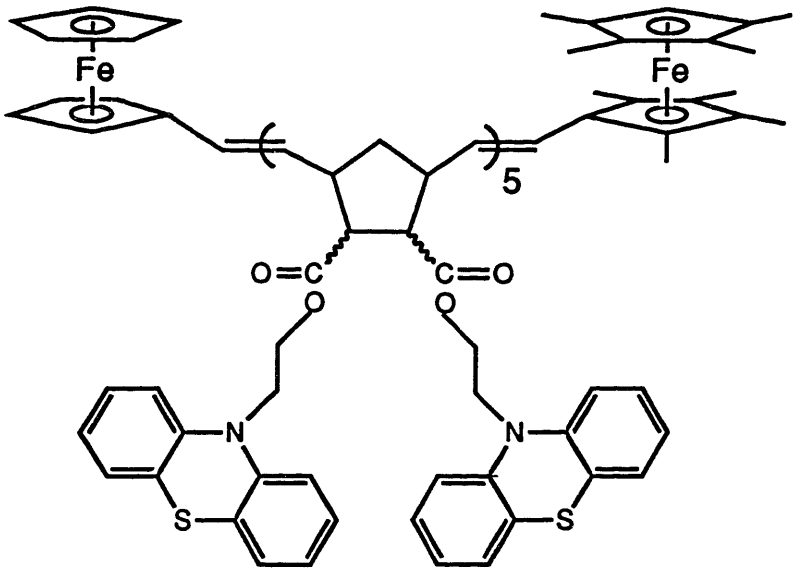

Fc-(Phz)$_5$-OMFc

voltammograms are shown in Figure 14. The redox waves of monoalkylferrocene and nonaalkylferrocene clearly indicate the presence of the end groups in the polymer. The redox waves for these end groups have the characteristics of a one-electron, reversible, solution couple; the peak potential is independent of scan rate, the peak current is linearly proportional to the square root of the scan rate, and the ratio of peak anodic current to peak cathodic current is roughly one.[42]

For Fc-$(Phz)_5$-OMFc, a comparison of the peak currents in each wave indicates the ratio of starting group Fc to capping group OMFc is ~1.06. Oxidation and reduction of these singular couples does not affect the solubility of the polymer, the solubility is controlled by the larger phenothiazine block. The phenothiazine reduction wave is a spike, indicating that the oxidized material deposits on the electrode. Because of the small size of these polymers precipitation is less pronounced, but it still occurs for polymers that on average consist of five phenothiazine monomer units and have a molecular weight of ~3400. The peak currents for the phenothiazine and each of the ferrocene waves yields a ratio of ~12:1. With five repeat units of the Phz monomer, each containing two phenothiazine centers, the ratio expected is 10:1. The meaning of the higher-than expected ratio is debatable, though, because the phenothiazine wave is not a simple reversible process for this polymer in CH_2Cl_2.

Figure 14. Cyclic voltammograms of Fc-$(Phz)_5$ and Fc-$(Phz)_5$-OMFc in CH_2Cl_2/0.1 M [*n*-Bu_4N]AsF_6 at a 500 μm Pt disk electrode. In the first cycle the potential sweep was reversed at +0.50 V, and in the second cycle the potential sweep was reversed at +1.00 V.

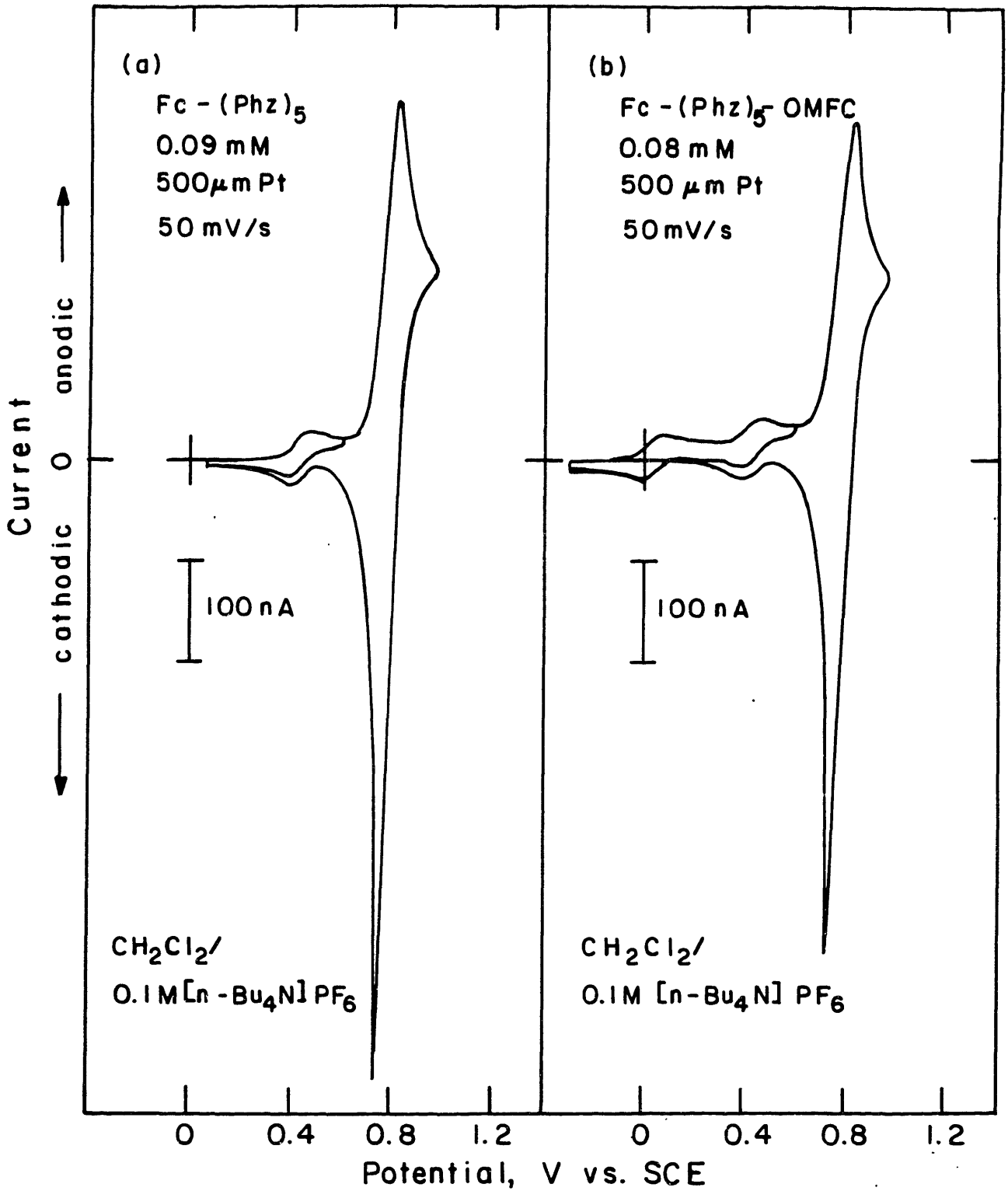
(a)
Fc - (Phz)5
0.09 mM
500μm Pt
50 mV/s
100 nA
CH2Cl2/
0.1M [n-Bu4N] PF6
(b)
Fc - (Phz)5 - OMFC
0.08 mM
500 μm Pt
50 mV/s
100 nA
CH2Cl2/
0.1M [n-Bu4N] PF6
Current
anodic
0
cathodic
0
0.4
0.8
1.2
Potential, V vs. SCE

The normal pulse voltammogram of Fc-$(Phz)_5$-OMFc is shown in Figure 15. Values of the limiting currents, half-wave potentials, slopes of the plots E vs. $\log[(i_{lim} - i)/i]$, and diffusion coefficients are given in Table IV. The ratio of the components in the redox polymers is more clearly defined in NPV since adsorption and precipitation are avoided. At each potential where a pulse is applied the diffusion limited current is proportional to the number of redox sites per polymer that can be oxidized at that potential. At +0.25 V only OMFc can be oxidized, at +0.55 V, OMFc and Fc can be oxidized, and at +0.90 V, OMFc, Fc, and Phz are all oxidized. From the diffusion limited currents at these potentials (Table IV), the ratio of the components are determined to be 0.92:1.0:9.6. Similarly, for Fc-$(Phz)_5$ the ratio determined was 1.0:10.2. Thus, results from NPV are in accord with the expected stoichiometry. As for the (Phz) and (Phz)(Nrb) polymers, the slopes of the curves closely correspond to the value for a Nernstian multielectron species that has noninteracting redox centers.

How are the number of electrons, n, and the concentration, C, assigned values for these polymers? Since the limiting current is linear with respect to the number of redox centers in the polymer, it can only be accounted for once between n and C. One can say that the concentration of phenothiazine is ten times greater, so that the current reflects ten times the concentration of n = 1 electron waves. Or, the concentration of the polymer can be taken as

Figure 15. Normal pulse voltammogram of Fc-$(Phz)_5$-OMFc in CH_2Cl_2/0.1 M [*n*-Bu_4N]PF_6. The current was sampled for the last 17 ms of a 57 ms pulse. Sweep rate, 10 mV s^{-1}; 'Drop time', 1 s.

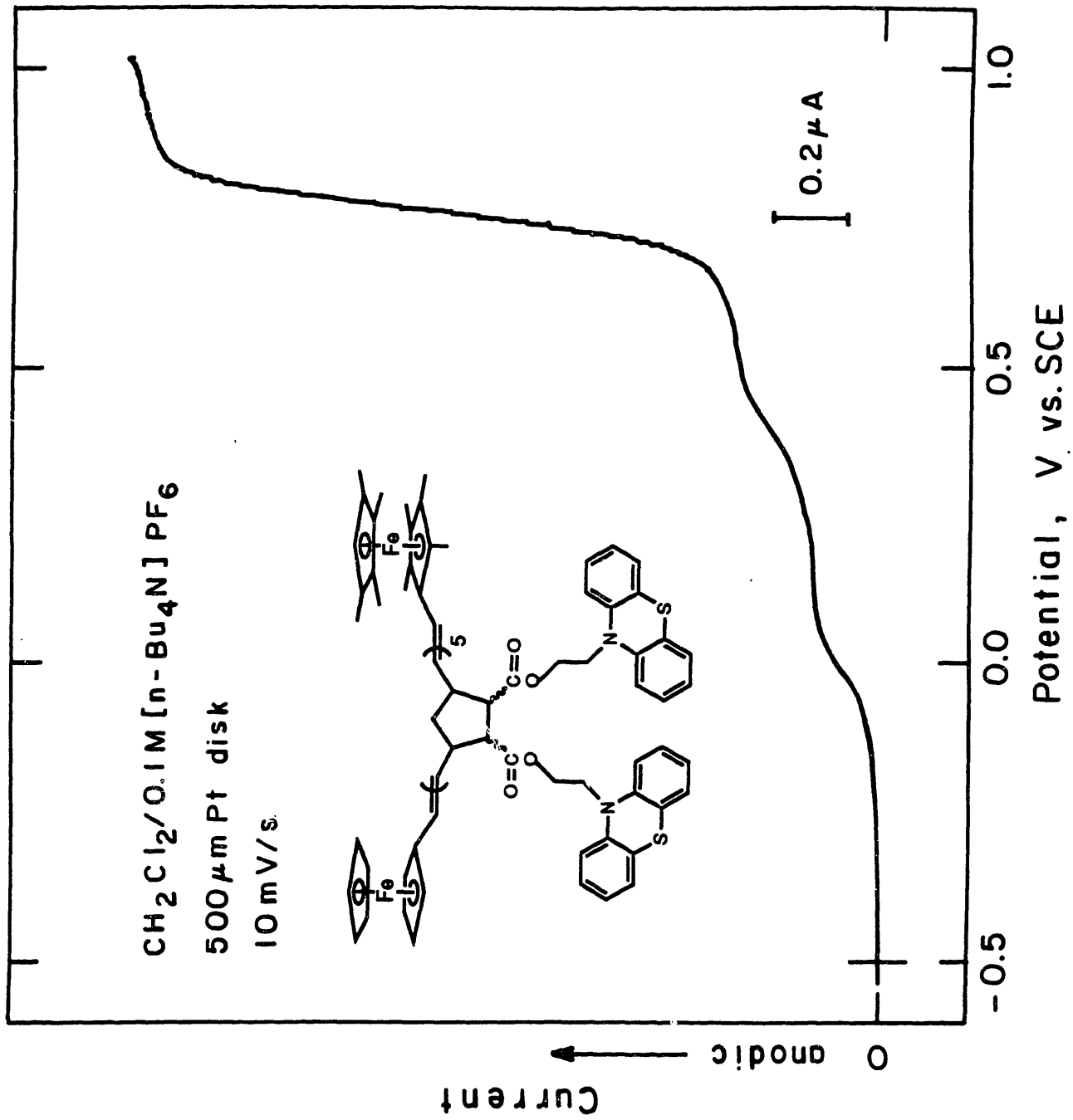
CH_2Cl_2/0.1M [n-Bu_4N] PF_6
500μm Pt disk
10 mV/s
0.2μA
Current
0 anodic
-0.5
0.0
0.5
1.0
Potential, V vs. SCE
Fe
Fe
5
C=O
O=C
O
O
N
N
S
S

Table IV. Data From Normal Pulse Voltammetric Oxidation of Polymers With Redox Active End Groups

	Fc-(Phz)$_5$			Fc-(Phz)$_5$-OMFc		
Component	i_{lim} nA	$E_{1/2}$[a] mV	slope[b] mV	i_{lim} nA	$E_{1/2}$ mV	slope mV
OMFc				9.5	5	-72
Fc	12	410	-70	10.3	380	-86
Phz	122	750	-56	101.2	750	-58
Diff. Coef. (cm^2 s^{-1})						
D_{obs}[c]	6.7×10^{-6}			5.2×10^{-6}		
D_{calc}[d]	4.8×10^{-6}			4.7×10^{-6}		

[a]vs. SCE. [b]slope of the plot E vs. $\log[(i_{lim} - i)/i]$. [c]Calculated from eq 6 using i_{lim} from Fc wave. [d]Calculated from the relation $D_i = D_j(MW_j/MW_i)^{0.55}$ based on eq 2, using ferrocene for the comparison; MW = 186, D = 2.4×10^{-5}.[54]

the basis, and at the oxidation potential of phenothiazine it can dump n = 10 electrons into the electrode. Viewed in this manner though, it must be remembered that the waveshape is that of a reversible, Nernstian one-electron couple.

Luminescent End Groups. Termination of living polymers with 1-pyrenecarboxaldehyde produces polymers with a lumophore located at the end of the chain. Polymers end-capped with luminescent molecules, and molecules capable of forming exiplexes have been prepared for studies of polymer dynamics in solution and in solids.[55] Information about many properties, such as polymer diffusion, chain mobility, cyclization, the effect of viscosity, or the local environment inside the polymer coil can be obtained from polymers capped with luminescent probes. Using probes with different lifetimes changes the timescale over which an event can be examined.

Another area of importance that can be studied is energy transfer and migration, and electron transfer within polymers.[55,56] Understanding the interactions between chromophores, donors, and acceptors is needed to build molecular systems that successfully separate charge and convert light into other usable forms of energy.

In the studies alluded to it is important to have a polymer sample that is as well-defined and narrowly disperse as possible. The qualities of ROMP make it well suited for application in this area. The work presented below is an initial step at examining redox polymers that have a pyrene

end group.

A group of polymers that have been prepared with pyrene capping end groups is shown in Chart VII. The polydispersity of the polymers was $(Fc)_{12}$-pyrene, 1.12; $(Phz)_{10}$-pyrene, 1.24; and $(Phz)_{10}(Nrb)_{70}$-pyrene, 1.08. The PDI values are comparable to those reported above for the (Fc) and (Phz) polymers. Furthermore, the molecular weights of the polymers vs. the polystyrene calibrant are consistent with the stoichiometry indicated for the homopolymers. The ^1H NMR spectra of all three polymers indicate the end groups are present in a 1:1 ratio, and the ratio of end group protons to olefinic protons agrees with that in the empirical formula. The pyrene capped $(Phz)_{10}(Nrb)_{70}$ was prepared from the same living polymer as the pivaldehyde capped polymer.

1-Vinylpyrene was prepared as a model of the lumophore in the polymer since the capping reaction produces a vinyl derivative from pyrenecarboxaldehyde. Polymers without a pyrene cap were also used in the study as models. These were $(Fc)_{12}$, and $(Phz)_{15}$, both of which had a *t*-butyl cap. $(Fc)_{12}$ was made from the same living polymer as $(Fc)_{12}$-pyrene.

The absorption, emission, and excitation spectra of 1-vinylpyrene are shown in Figure 16. In comparison to pyrene, the vinyl substituent causes a red shift of about 1300 cm^{-1} in absorption and emission spectra. The emission quantum yield for vinylpyrene is slightly greater, and is

Chart VII. Polymers prepared with a luminescent end group.

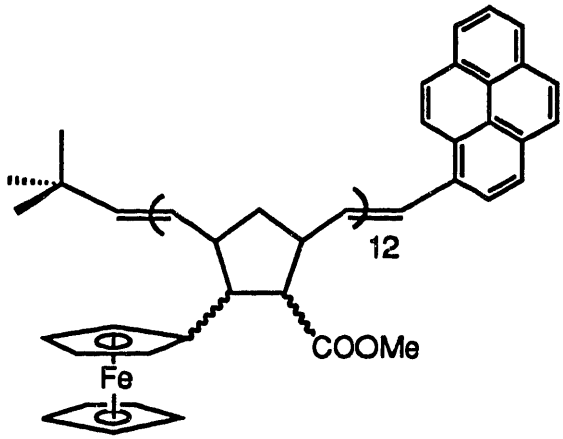

$(Fc)_{12}$-pyrene

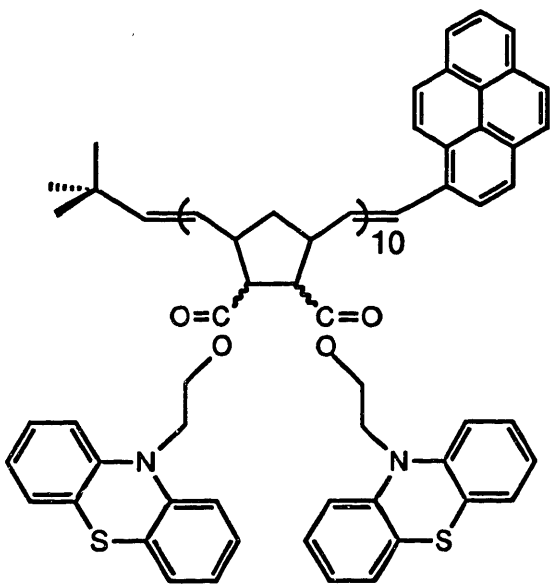

$(Phz)_{10}$-pyrene

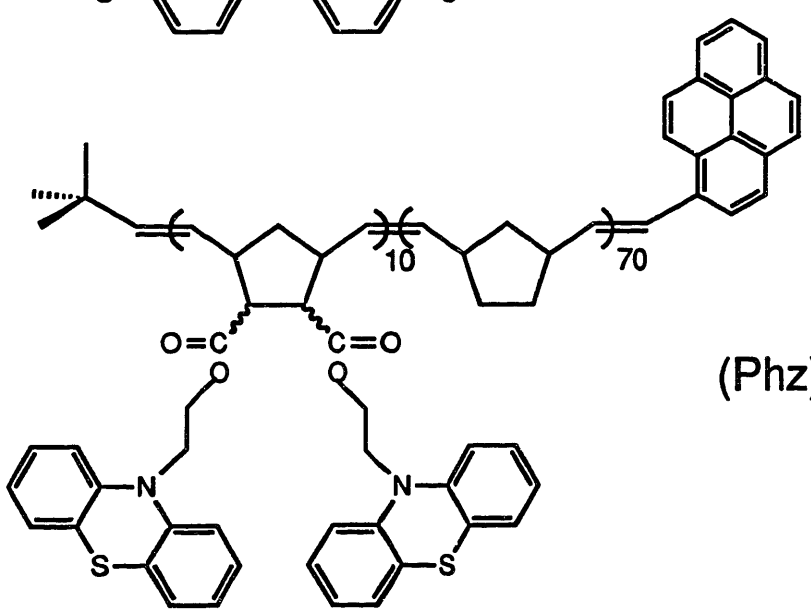

$(Phz)_{10}(Nrb)_{70}$-pyrene

Figure 16. The absorption, uncorrected excitation (λ_{em} = 440 nm), and uncorrected emission (λ_{ex} = 310 nm) spectra of 1-vinylpyrene in toluene at 5 μM concentration. The spectra have been normalized.

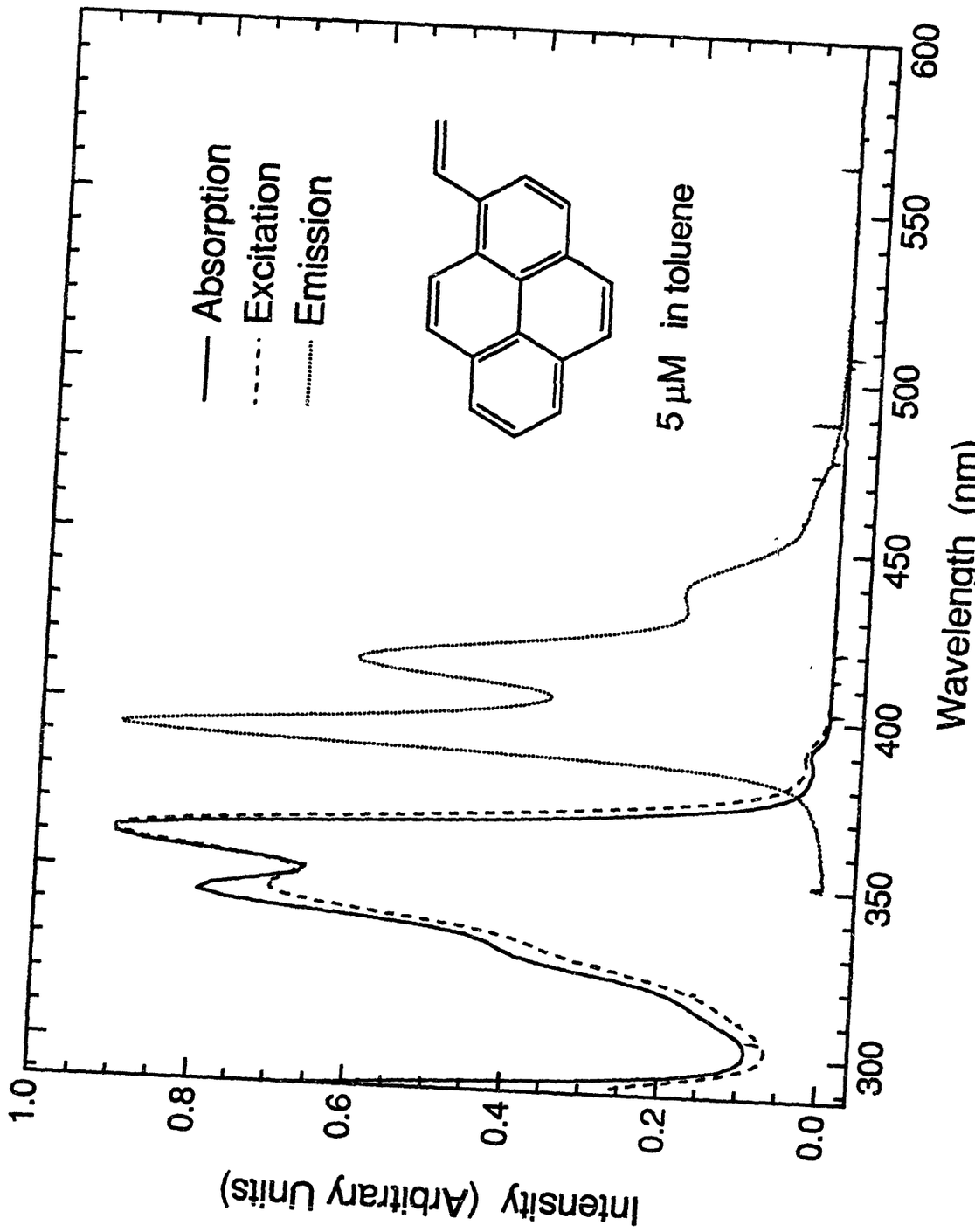
Absorption
Excitation
Emission
5 µM in toluene
Intensity (Arbitrary Units)
Wavelength (nm)
0.0
0.2
0.4
0.6
0.8
1.0
300
350
400
450
500
550
600

quenched less by O_2 than pyrene.[57] Like pyrene, vinylpyrene forms eximers, though higher concentrations of vinylpyrene are necessary to achieve their formation owing to its shorter singlet lifetime.

The absorption spectra of the pyrene-capped polymers in toluene are shown in Figure 17. Also, the sum of the absorption spectra for the constituents of the polymer are shown. Some subtle changes occur in the vinylpyrene spectrum when it is incorporated into a polymer. The bands have a lower absorbance and the relative absorbances change. The ferrocene band at 442 nm is unaffected in shape and intensity. The absorbance at 442 nm of a solution of known concentration agrees with the calculated absorbance value for twelve ferrocene groups with the extinction coefficient determined for the monomer.

The absorption spectra for the two Phz polymers, $(Phz)_{10}$-pyrene and $(Phz)_{10}(Nrb)_{70}$-pyrene, are identical, despite the very different primary structure. The matching spectra confirm that the degree of polymerization is controllable. These two polymers were prepared at different times but the end group to repeat unit ratio is the same. Comparing the absorbance spectra of the two Phz polymers with that of a solution containing a 3 to 2 molar ratio of vinylpyrene and $(Phz)_{15}$, so the ratio of phenothiazine units to pyrene is 20:1, shows there is a red shift of ~500 cm^{-1} in the lower energy bands in the pyrene-capped polymer. If the absorption spectrum of the Phz monomer is subtracted from

Figure 17. Absorbance spectra in toluene of (a) $(Phz)_{10}$-pyrene, $(Phz)_{10}(Nrb)_{70}$-pyrene, and a 3:2 solution of vinylpyrene and $(Phz)_{15}$, and (b) $(Fc)_{12}$-pyrene and a 1:1 solution of vinylpyrene and $(Fc)_{12}$.

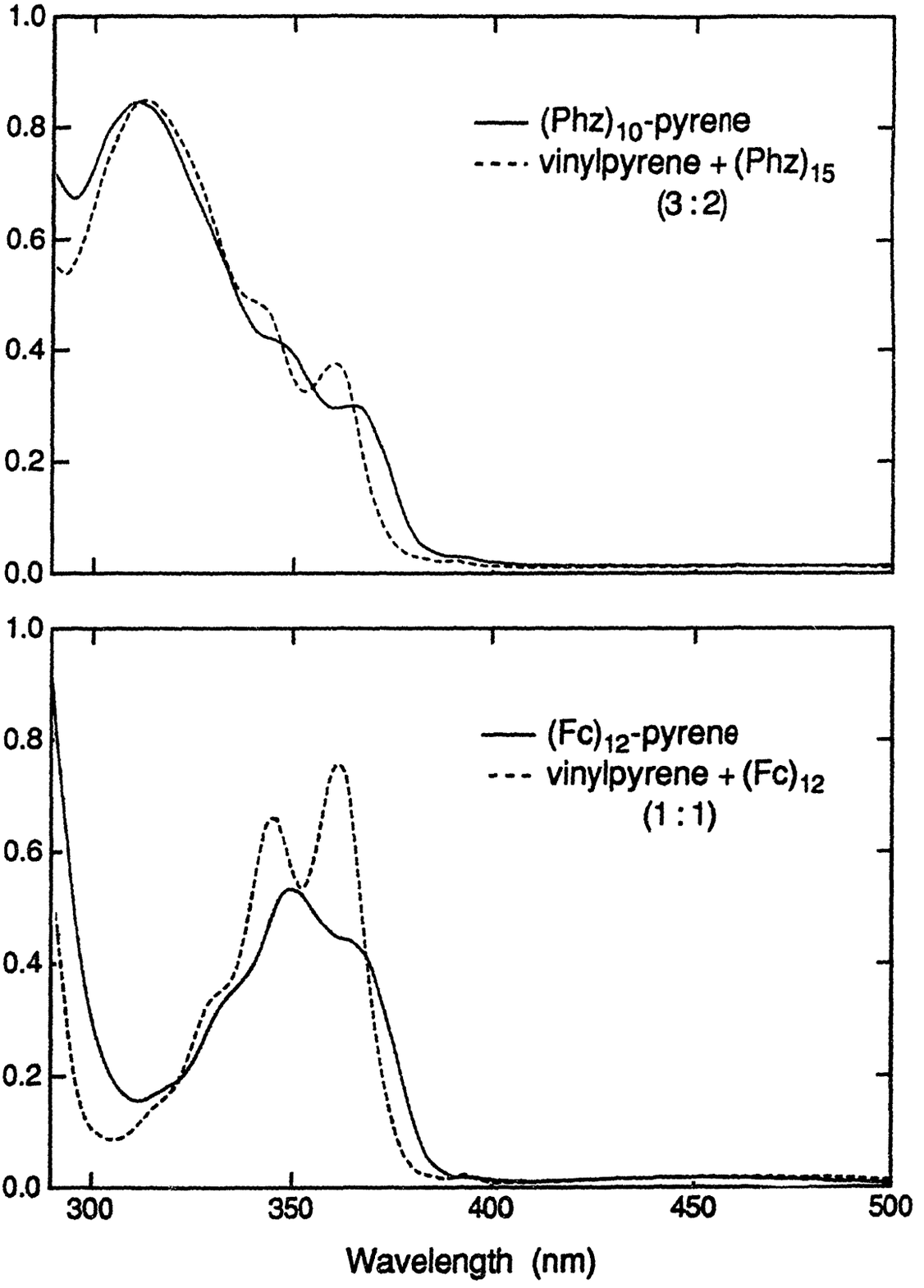
1.0
0.8
0.6
0.4
0.2
0.0
(Phz)10-pyrene
vinylpyrene + (Phz)15
(3 : 2)
1.0
0.8
0.6
0.4
0.2
0.0
(Fc)12-pyrene
vinylpyrene + (Fc)12
(1 : 1)
300
350
400
450
500
Wavelength (nm)

the spectrum of one of the pyrene-capped Phz polymers the resulting spectrum agrees closely with the spectrum of $(Fc)_{12}$-pyrene in the region 300-400 nm. The spectra show that the pyrene ground state is affected by the polynorbornene chain, but the degree to which the substituents on norbornene also affect it is uncertain.

Before considering the polymer emission, the absorption and emission properties of ferrocene and phenothiazine are considered first. Ferrocene absorbs about 5000 times less strongly than does vinylpyrene in the region 290-400 nm. Thus, ferrocene in $(Fc)_{12}$-pyrene will absorb a negligible amount of the excitation beam. Also ferrocene does not emit so it would not contribute to the emission spectrum if it was excited directly, by energy transfer, or by any other mechanism.

N-Alkylphenothiazine has its low energy absorption at 310 nm. This band tails into the region where the vinylpyrene absorption maxima occur. At a 20:1 ratio of phenothiazine to pyrene, in $(Phz)_{10}$-pyrene and $(Phz)_{10}(Nrb)_{70}$-pyrene the absorption of light by phenothiazine from 290 to 340 nm is substantial. At longer wavelengths, pyrene absorbs more strongly, for example in the range 360-380 nm pyrene absorbs ~90% of the light.

Phenothiazine emits light in the wavelength range 390-550 nm with λ_{max} = 440 nm, and so may contribute to the emission spectra of the polymer. The likelihood of detecting emission depends on the amount of light absorbed, and on the

percentage of absorbed photons that are emitted. The relative quantum yields of vinylpyrene and 10-methylphenothiazine and the Phz monomer were determined. Solutions of the three molecules were matched in absorbance at 330 nm with an optical density of 0.08. The relative quantum yields were found to be $\phi_{VP}/\phi_{10\text{-MePhz}} = 62$ and $\phi_{VP}/\phi_{\text{Phz mon.}} = 53$. These values are consistent with the ratio of the reported quantum yields of these molecules. 10-Methylphenothiazine has a low quantum yield, <0.01,[58] and pyrene is reported to have a quantum yield in the range 0.5-0.7.[59] Emission by phenothiazine will contribute to the polymer emission spectrum, but its contribution is minimized by exciting at wavelengths longer than 360 nm.

The emission spectra of the three polymers are shown in Figure 18, and the data are listed in Table V. Excitation at 370 nm yields emission spectra that are qualitatively the same, with the exception of a broad, low energy band at $\lambda_{max} = 518$ nm in the $(Phz)_{10}$-pyrene polymer. This band is absent in the $(Phz)_{10}(Nrb)_{70}$-pyrene block polymer that has 70 units of polynorbornene between Phz and the pyrene end group. The emission spectrum of $(Phz)_{10}$-pyrene was also examined in THF, where the low energy band is red-shifted by 920 cm^{-1} to 544 nm and lowered in intensity. The change in the relative emission intensities at 394 and 412 nm for $(Phz)_{10}$-pyrene between toluene and THF reflects the change induced in the absorption spectrum by the two solvents. At shorter wavelength excitation Phz emission begins to

Figure 18. Uncorrected emission spectra of (a) $(Phz)_{10}$-pyrene in toluene and THF, (b) $(Phz)_{10}(Nrb)_{70}$-pyrene in toluene, and (c) $(Fc)_{12}$-pyrene in toluene. The excitation wavelength was 370 nm. The spectra have been normalized.

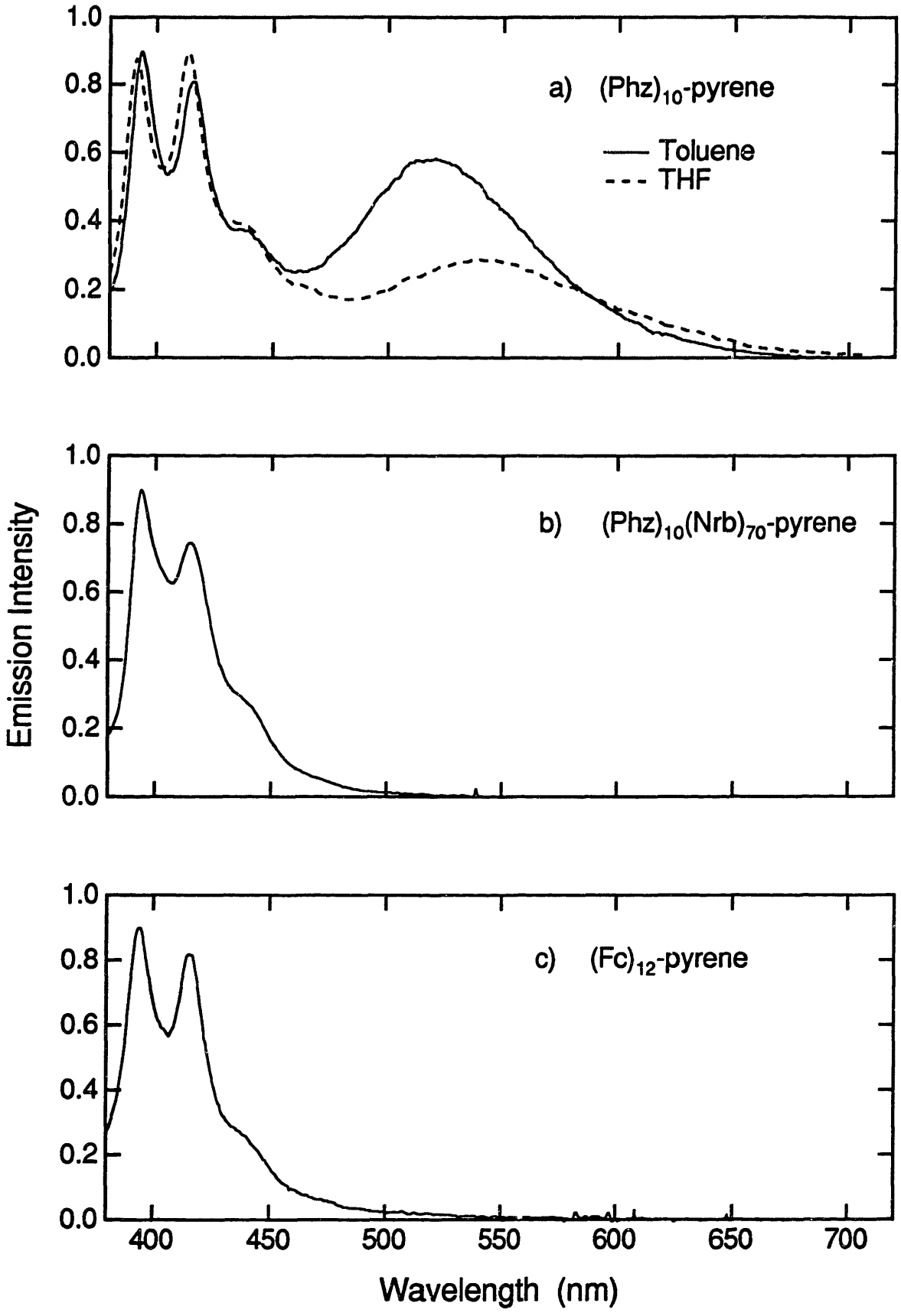
a) (Phz)10-pyrene
Toluene
THF
b) (Phz)10(Nrb)70-pyrene
c) (Fc)12-pyrene
Emission Intensity
Wavelength (nm)
1.0
0.8
0.6
0.4
0.2
0.0
400
450
500
550
600
650
700

Table V. Data From Emission and Excitation Spectra[a] of Polymers With Luminescent End Groups

Compound	Emission Max.[b] (relative int.)	Excitation Max.[c] (relative int.)	Excitation Max.[d] (relative int.)
vinylpyrene	394,415,437	330,347,363,391	
	(1.0,0.67,0.21)	0.38,0.78,1.0,0.04)	
$(Phz)_{10}$-pyrene	394,411,435,518	333,352,368,392	318,346,365,390
	(1.0,0.90,0.42,0.65)	(0.58,0.92,1.0,0.04)	(1.0,0.69,0.32,0.06)
$(Phz)_{10}$-pyrene[e]	394,415,436,544	330,351,366,390	315,342,360,400
	(1.0,1.0,0.42,0.30)	(0.62,0.96,1.0,0.02)	(1.0,0.54,0.25,0.03)
$(Phz)_{10}(Nrb)_{70}$-pyrene	395,416,436	331,352,368,392	
	(1.0,0.82,0.33)	(0.40,0.89,1.0,0.03)	
$(Fc)_{10}$-pyrene	395,416,434	320,332,350,364,390	
	(1.0,0.91,0.32)	(0.36,0.67,1.0,0.67,0.25)	

[a]in toluene at 298 K, spectra are uncorrected. [b]excitation wavelength 370 nm. [c]emission wavelength 440 nm. [d]emission wavelength 550 nm (toluene) and 590 nm (THF). [e]in THF

dominate the emission spectra of Phz polymers.

Excitation spectra of the samples were recorded by monitoring the emission at 440 nm. As shown in Figure 19, each of the polymers behaves differently. The $(Phz)_{10}$-pyrene excitation spectrum qualitatively resembles its own absorption spectrum, whereas for $(Phz)_{10}(Nrb)_{70}$-pyrene the excitation spectrum resembles the absorption spectrum of a pyrene chromophore. The excitation spectrum of $(Fc)_{12}$-pyrene also resembles its own absorption spectrum, but with a distinct enhancement in the band at 390 nm.

Excitation spectra obtained by monitoring the emission on the low energy side of the unique band in $(Phz)_{10}$-pyrene, at 550 and 590 nm in toluene and THF, respectively, are shown in Figure 20. The spectra show that the new, low energy emission band arises from excitation of pyrene, and not phenothiazine.

The relative excited-state lifetimes of the polymers compared to vinylpyrene were determined by a Stern-Volmer analysis of emission intensity quenching as a function of O_2 concentration. The Stern-Volmer equation for bimolecular quenching is:[60]

$$I_o/I = 1 + k_q\tau[Q] \qquad (7)$$

where I_o is the emission intensity in the absence of quencher, k_q is the bimolecular quenching rate constant, τ is the excited state lifetime for the molecule, and [Q] is the quencher concentration. For constant k_q the ratio of the slopes will be the ratio of the excited-state lifetimes.

Figure 19. Uncorrected excitation spectra of $(Phz)_{10}$-pyrene in (a) toluene and (b) THF, (c) $(Phz)_{10}(Nrb)_{70}$-pyrene in toluene, and (d) $(Fc)_{12}$-pyrene in toluene recorded by monitoring the emission at 440 nm. The spectra have been normalized.

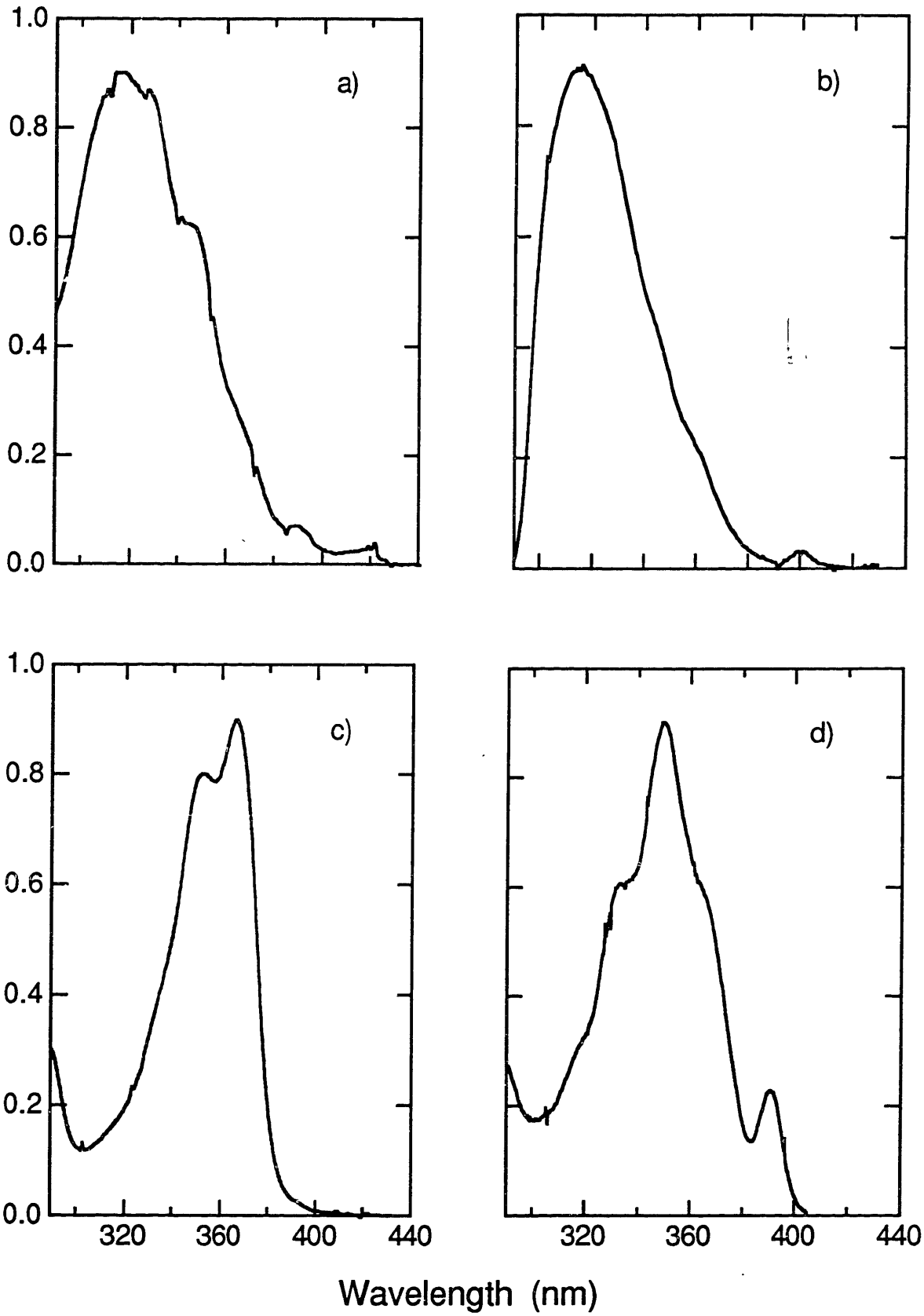
a)
b)
c)
d)
1.0
0.8
0.6
0.4
0.2
0.0
320
360
400
440
Wavelength (nm)

Figure 20. Uncorrected excitation spectra of $(Phz)_{10}$-pyrene in toluene and THF recorded by monitoring the emission at 550 and 590 nm, respectively. The spectra have been normalized.

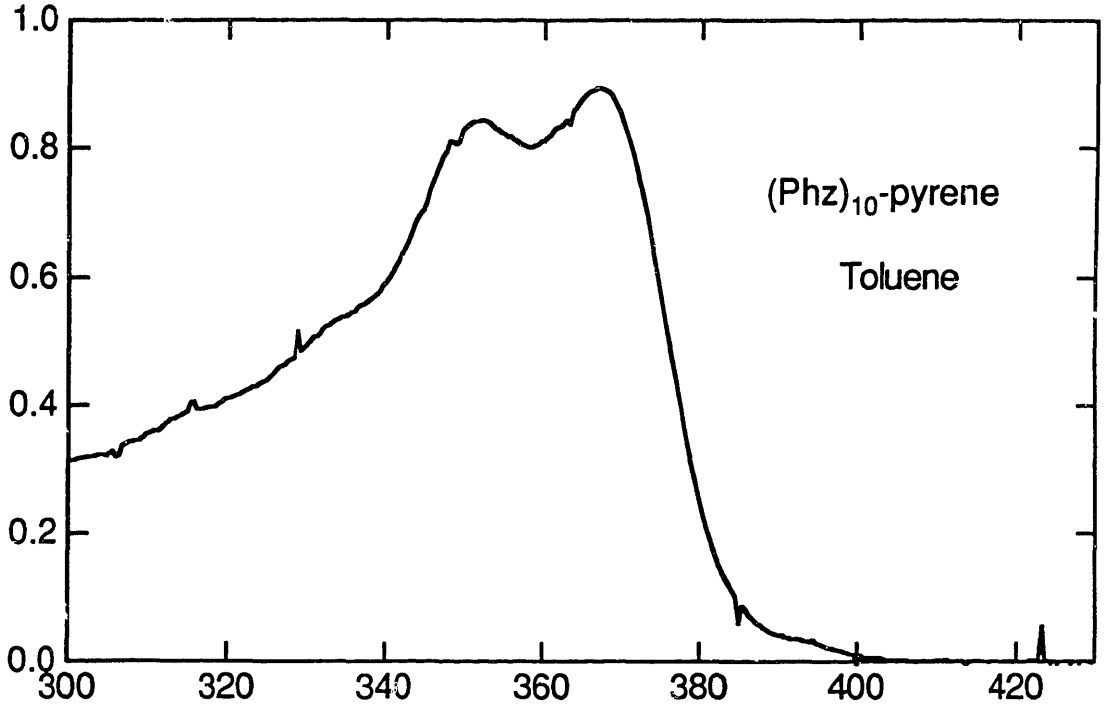
1.0
0.8
0.6
0.4
0.2
0.0
300
320
340
360
380
400
420
(Phz)10-pyrene
Toluene

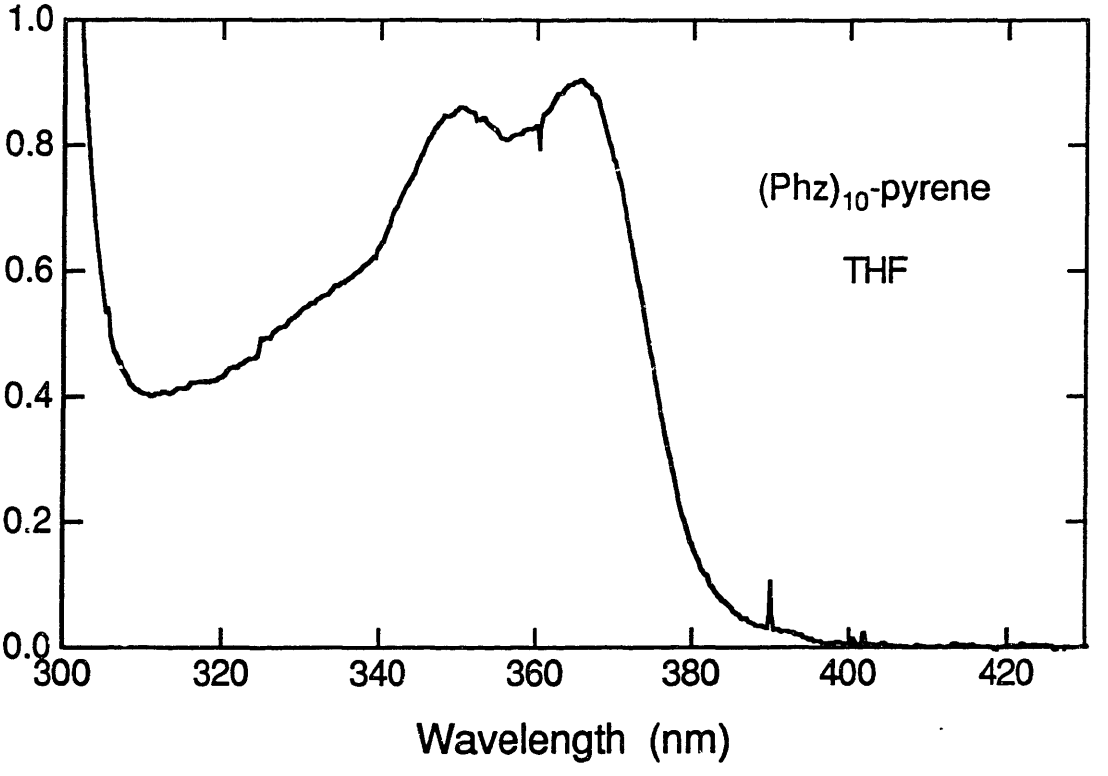
1.0
0.8
0.6
0.4
0.2
0.0
300
320
340
360
380
400
420
(Phz)10-pyrene
THF
Wavelength (nm)

Assuming O_2 quenching to have a constant k_q, Stern-Volmer quenching can thus give relative lifetimes of the pyrene species. The Stern-Volmer plots, shown in Figure 21, are linear and the slope of the plot for the polymers are smaller than for vinylpyrene. The relative lifetimes compared to vinylpyrene are listed in Figure 21.

Relative emission quantum yields show that fluorescence from vinylpyrene is quenched when it is located at the end of a phenothiazine or ferrocene polymer chain. Scheme V compares the pathways in the photophysical processes for $(Phz)_{10}$-pyrene and $(Phz)_{10}(Nrb)_{70}$-pyrene. When a Phz block is adjacent to the pyrene end group emission is quenched the most. In addition to quenching the pyrene emission intensity in $(Phz)_{10}$-pyrene, there is a new emission band at lower energy that is broad and without vibrational structure. The shift to lower energy and the decrease in intensity of this band with increased solvent polarity, together with its shape, suggest the red-shifted emission is from an exiplex.[61]

Attempts to form an exiplex from a mixture of the two lumophores, using vinylpyrene and 10-methylphenothiazine or the Phz monomer, were not successful. The emission spectra of a series of solutions that were 2.5 μM in vinylpyrene, and ranged from 0.2 mM to 50 mM in 10-methylphenothiazine were recorded. The ratio of phenothiazine to pyrene in these samples ranges from 80 to 20,000. The emission spectra were recorded for another series of solutions that

Figure 21. Stern-Volmer plots of 1-vinylpyrene, $(Phz)_{10}$-pyrene, $(Phz)_{10}(Nrb)_{70}$-pyrene, and $(Fc)_{12}$-pyrene obtained by the emission intensity quenching by O_2 in air-saturated and O_2-saturated solutions.

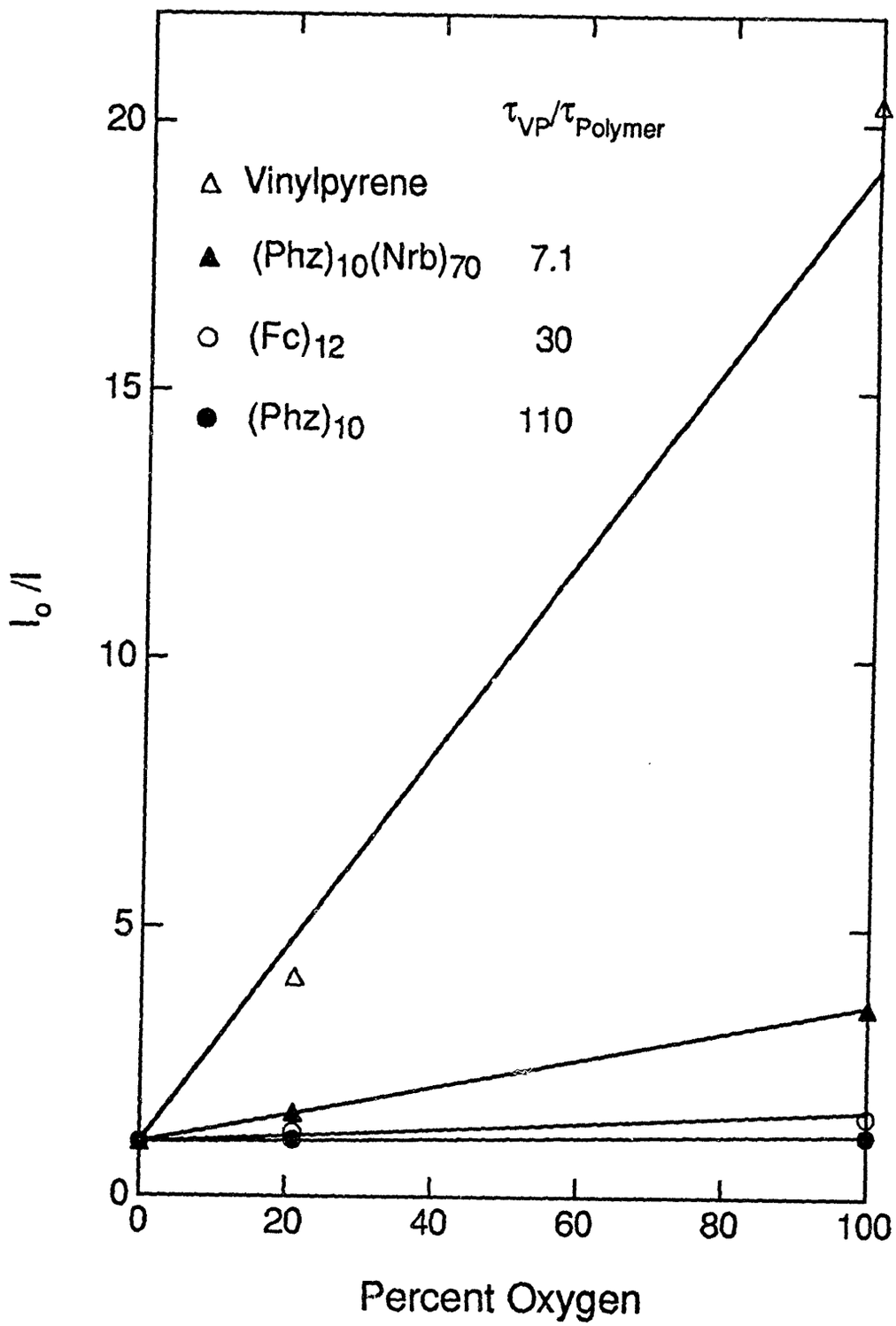
$\tau_{VP}/\tau_{Polymer}$
Vinylpyrene
$(Phz)_{10}(Nrb)_{70}$ 7.1
$(Fc)_{12}$ 30
$(Phz)_{10}$ 110
I_o/I
0
5
10
15
20
0
20
40
60
80
100
Percent Oxygen

Scheme V. Photophysical reaction pathways of $(Phz)_{10}$-pyrene (a) for selective excitation of pyrene at λ_{ex} > 355 nm and (b) for selective excitation of phenothiazine at λ_{ex} < 355 nm, and (c) $(Phz)_{10}(Nrb)_{70}$-pyrene at λ_{ex} > 355 nm. Radiative (⇝) and non-radiative (⟶) transitions.

a)

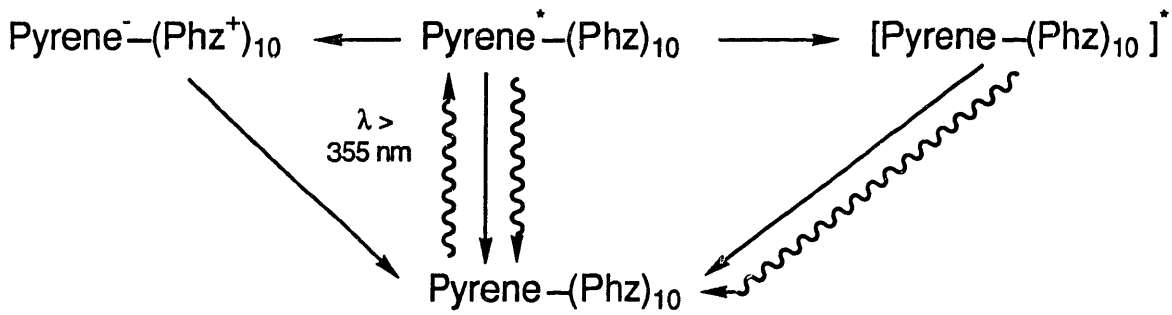
Pyrene⁻–(Phz⁺)10
Pyrene*–(Phz)10
[Pyrene–(Phz)10]*
λ > 355 nm
Pyrene–(Phz)10

b)

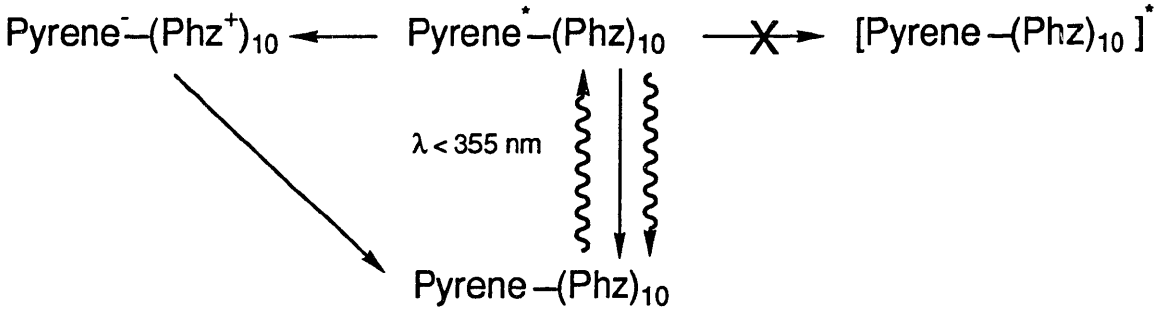
Pyrene⁻–(Phz⁺)10
Pyrene*–(Phz)10
[Pyrene–(Phz)10]*
λ < 355 nm
Pyrene–(Phz)10

c)

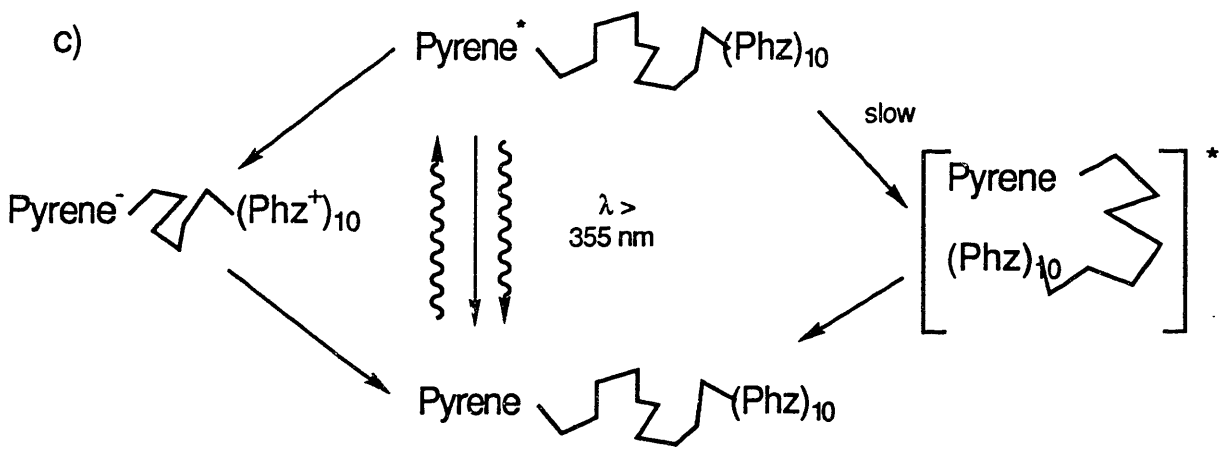
Pyrene*
(Phz)10
slow
Pyrene⁻
(Phz⁺)10
λ > 355 nm
Pyrene
(Phz)10
*
Pyrene
(Phz)10

were 5.0 μM in vinylpyrene and that had the same concentration range of Phz centers using the Phz monomer. As the concentration of phenothiazine was increased the only effect observed was quenching of the pyrene emission and then growth of the phenothiazine emission. There was no evidence of a broad, low energy band in solutions containing the separate lumophores. Phenothiazine polymers with a pyrene end group provide a special environment where within the lifetime of excited state pyrene the local phenothiazine concentration is high enough that the two can form an exiplex. But, the overall phenothiazine concentration, and absorption, is low enough that its emission will not dominate.

Exiplex formation between pyrene and phenothiazine has not been reported previously. However, pyrene exiplexes with amine donors have been widely studied,[62] and phenothiazine is known to quench emission by electron donation.[63]

Phenothiazine can be viewed on the one hand as a derivative of N,N-dialkylaniline, which is a classic example of an amine donor that forms exiplexes with pyrene. Or, since phenothiazine is an extended conjugated π system, it might form a sandwich pair donor-acceptor complex.[64] Furthermore, upon oxidation phenothiazine becomes more planar.[65] So, as charge transfer increases the oxidation state of phenothiazine, this should result in increased π overlap and a more stable donor-acceptor complex.

The exiplex bands in aromatic hydrocarbon-amine complexes

are typically red-shifted ~2500-4000 cm^{-1} and have enthalpies of formation of -10 kcal/mol. Ternary complexes that are 2:1 in quencher to lumophore have been observed and have an emission maximum shifted further to the red.[64] In comparison, the energy of the exiplex in $(Phz)_{10}$-pyrene is lower. The exiplex emission maximum is shifted more than 6100 cm^{-1} to lower energy from the singlet state energy of vinylpyrene. The exiplex energy can be calculated from the relation:[64]

$$E_E = h\nu_{max} = E_S + \Delta H_E - E_R \quad (9)$$

where E_S is the singlet energy, H_E is the enthalpy of formation of the exiplex, and E_R is the ground state repulsion energy. For pyrene and dimethylaniline, ΔH_E was experimentally determined to be -8 kcal/mol and from the equation, E_R was calculated to be 3 kcal/mol. Assuming E_R is similar for pyrene and phenothiazine, the enthalpy of formation is found to be -19 kcal/mol. This large value of enthalpy gain indicates there is a strong donor-acceptor interaction, or possibly more than one donor is interacting with pyrene. Considering the structure of the phenothiazine monomer this may be reasonable.

Excitation spectra in toluene and THF for the exiplex band of $(Phz)_{10}$-pyrene correspond to the absorption spectrum of vinylpyrene. Thus, the exiplex only forms upon excitation of pyrene. Judging from the similar singlet energies of pyrene and phenothiazine, energy transfer might occur in either direction. The lack of exiplex formation following

excitation of phenothiazine is probably due to its shorter lifetime. This means very few pairs of pyrene and phenothiazine units can approach each other within the lifetime of excited-state phenothiazine compared to the number of pairs that form exiplexes within vinylpyrene's excited-state lifetime.

Separating the block of phenothiazine from the pyrene end group by a 70 unit block of polynorbornene increases the lifetime of excited state pyrene by a factor of 16. Exiplex formation, if it occurs at all, occurs at a much slower rate. The cyclization rate of the chain is low enough that the chain ends are essentially not communicating during the excited state lifetime of pyrene. However, there is some mechanism by which the excited state is being quenched, since the lifetime is significantly shorter than for vinylpyrene.

The difference in the excitation spectra of $(Phz)_{10}$-pyrene and $(Phz)_{10}(Nrb)_{70}$-pyrene for emission at 440 nm is explained by considering the absolute quantum yields. Both lumophores emit at 440 nm, but pyrene emission is quenched by a factor of 16 times more in $(Phz)_{10}$-pyrene. With the pyrene emission quenched the phenothiazine emission is now apparent. For $(Phz)_{10}(Nrb)_{70}$-pyrene, the pyrene emission has a larger quantum yield and so the phenothiazine emission is much less apparent.

Pyrene emission can be quenched by electron donors[62] or acceptors,[66] by energy transfer,[67] or by itself,[32] depending

on the system. The relative redox energy levels of ferrocene, N-alkylphenothiazine and pyrene are given in Scheme VI. Excited state pyrene is not a strong enough reductant to act as an electron donor, but it is a strong enough oxidant to accept an electron from either ferrocene or phenothiazine. The driving force for the oxidation is:[68]

$$\Delta G = E'(D/D^+) - E'(A/A^-) - \Delta E_{oo} + (w_p - w_r) \qquad (8)$$

where E' is the redox potential of the donor or acceptor, ΔE_{oo} is the singlet excitation energy, and the last term represents the work necessary to bring the products and reactants together. For ferrocene ΔG is approximately -20 kcal/mol, and for phenothiazine, approximately -12 kcal/mol.

Excited state quenching by energy transfer requires good overlap between the emission spectrum of the excited molecule and the absorption spectrum of the quencher.[69] Ferrocene has a d-d absorption band within the emission spectrum of pyrene, whereas the tail absorption in phenothiazine overlaps with the onset of emission from pyrene.

The Fc block quenches emission from pyrene to an extent intermediate between the two Phz polymers, and no exiplex emission band is observed. Quenching by ferrocene may be through either electron transfer or energy transfer. The free energy change for electron transfer is favorable and large enough that rapid quenching would be expected.[62a] However, in a low dielectric solvent like toluene ion pair formation occurs at a slower rate.

Scheme VI. Energy diagram for the redox potentials of pyrene, phenothiazine, and ferrocene.

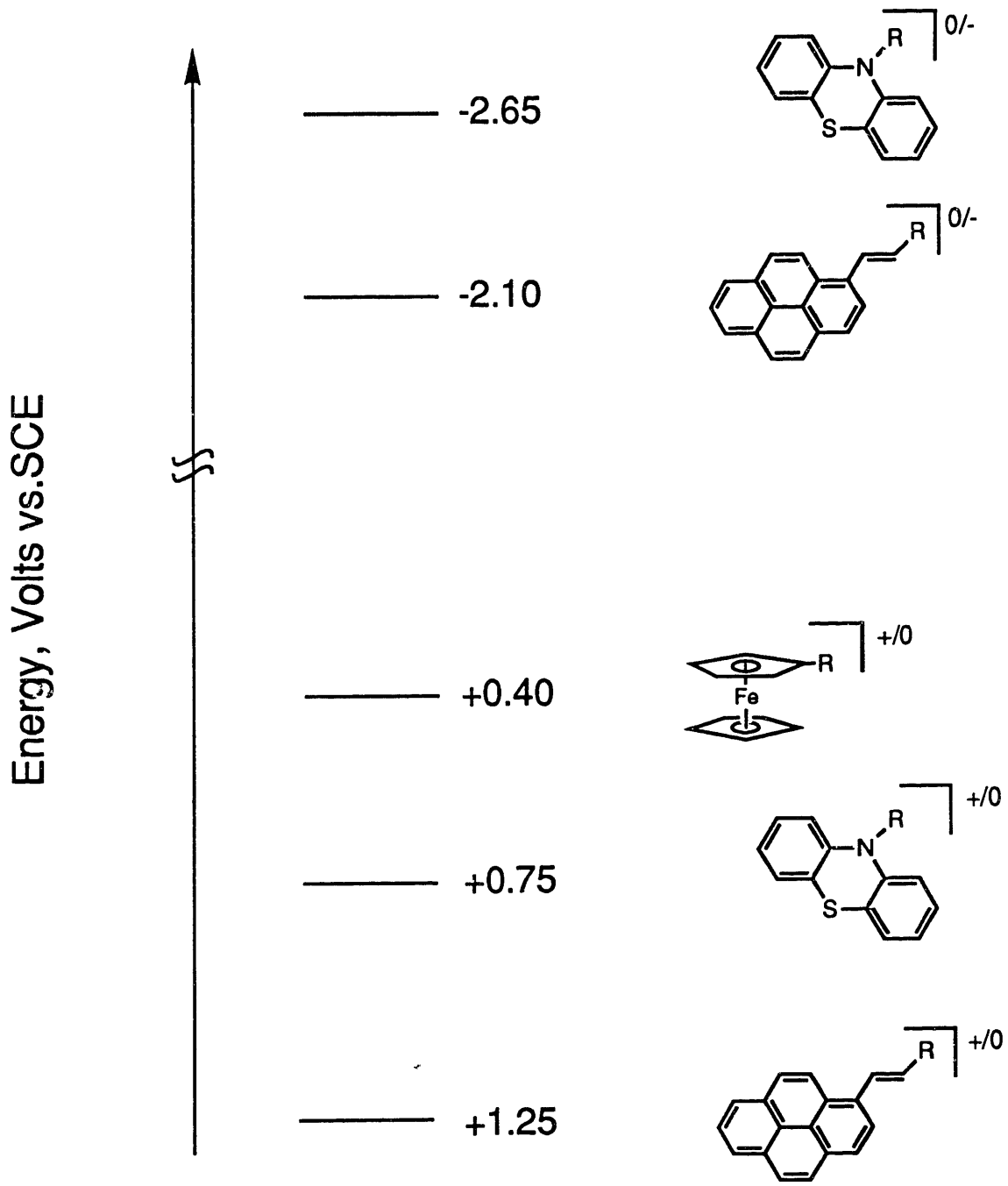
Energy, Volts vs.SCE
-2.65
-2.10
+0.40
+0.75
+1.25
0/-
0/-
+/0
+/0
+/0
R
N
S
Fe

Quenching by phenothiazine more likely occurs by electron transfer, to reduce excited-state pyrene. Exiplex formation indicates that a strong charge-transfer interaction occurs, and the spectral overlap required for efficient energy transfer is poor.

Conclusion

It has been established that ring opening metathesis polymerization with Mo alkylidene initiators of the type $Mo(CHR)(OR')_2(NAr)$ can be used to make redox-active polymers and block polymers. Despite their high formal oxidation state, **1** and **2** are difficult to reduce. With a reduction potential of -2.1 V vs. SCE, many redox-active molecules can be incorporated into a polymer without causing reductive decomposition of the Mo compound. Among living polymerization systems these Mo initiators tolerate the widest range of functional groups, allowing a great deal of freedom in the choice of redox polymers to make. With ROMP, the primary structure of the polymer, the block identity, block size, and block order, are all controllable through the manner of addition of monomer to the reaction. The utility of this system is augmented by the fact that norbornene derivatives serve as monomers. Compared with other strained cyclic olefins, norbornene derivatives are synthetically accessible and a variety of derivatives are commercially available.

The solution electrochemistry of these polymers in organic solvents (CH_2Cl_2, THF) is characterized by oxidative deposition. Normal pulse voltammetry allows quantitative evaluation of the current-voltage curves because the problems of precipitation associated with potential sweeps into the anodic wave are avoided. The termination reaction can be exploited to place a redox-active molecule or a

luminescent molecule at the end of the polymer chain. The redox molecule serves as a one-electron internal standard. The emission properties of the luminescent group varies with the primary structure of the polymer--phenothiazine groups only form exiplexes with pyrene when close to the pyrene end group--and the nature of the quencher present in the polymer.

With polymers made by ROMP, the primary structure of the chain is controllable, and the distribution about the average chain length is as narrow as can be achieved by polymer synthesis. These are a new class of redox polymers that can be fully-characterized prior to electrode surface confinement.

References

1. (a) Smith, D. K.; Tender, L. M.; Lane, G. A.; Licht, S.; Wrighton, M. S. *J. Am. Chem. Soc.* **1989**, *111*, 1099. (b) Shu, C-F.; Wrighton, M. S. *J. Phys. Chem.* **1988**, *92*, 5221.

2. Odian, G. *Principles of Polymerization;* Wiley: New York, NY, 1981.

3. (a) Rempp, P.; Merrill, E. *Polymer Synthesis;* Huethig & Wepf: Heidelberg, 1986; Chapter 5. (b) Gold, L. *J. Chem. Phys.* **1958**, *28*, 91.

4. (a) Flory, P. *J. Am. Chem. Soc.* **1940**, *62*, 1561. (b) Szwarc, M. *Nature* **1956**, *178*, 1168.

5. Szwarc, M. *Carbanions, Living Polymers, and Electron Transfer Processes;* Wiley: New York, NY, 1968.

6. Miyamoto, M.; Sawamoto, M.; Higashimura, T. *Macromolecules* **1984**, *17*, 265.

7. Sogah, D. Y.; Webster, O. W. *Macromolecules* **1986**, *19*, 1775.

8. (a) Kress, J.; Osborn, J. A.; Greene, R. M. E.; Ivin, K. J.; Rooney, J. J. *J. Am. Chem. Soc.* **1987**, *109*, 899. (b)

Gilliom, L. R.; Grubbs, R. H. *J. Am. Chem. Soc.* **1986**, *108*, 733. (c) Schrock, R. R. *J. Organomet. Chem.* **1986**, *300*, 249. (d) Murdzek, J. S.; Schrock, R. R. *Organometallics* **1987**, *6*, 1373.

9. Turett, W. L.; Johnson, D. R.; Roberson, I. M.; Montague, B. A. *J. Am. Chem. Soc.* **1960**, *82*, 2337.

10. Ivin, K. J. in *Encyclopedia of Polymer Science and Engineering*; Kroschwitz, J. I., Ed.; Wiley: New York, NY; Volume 9, p. 634.

11. Schrock, R. R. *Accnts. Chem. Res.* **1990**, in press.

12. Schrock, R. R.; Murdzek, J. S.; Bazan, G.; Robbins, J.; DiMare, M. *J. Am. Chem. Soc.*, in press.

13. Nugent, W. A.; Mayer, J. M. *Metal-Ligand Multiple Bonds*; Wiley: New York, NY, 1988; p. 234.

14. Zou, C.-F.; Wrighton, M. S. *J. Am. Chem. Soc.* **1990**, in press.

15. Wilbur, D. S.; Svita, Z. V. *J. Label. Compds. Radiopharm.* **1984**, *21*, 415.

16. Chapter II, Experimental Section.

17. Compton, S.; Wang, H. H.; Williams, J. M. *Inorg. Synth.* **1986**, *24*, 138.

18. Osgerby, J. M.; Pauson, P. L. *J. Chem. Soc.* **1958**, 650.

19. Nicolas, L.; Beugelmans-Verrier, M.; Guilhem, J. *Tetrahedron* **1981**, *37*, 3847.

20. Still, W. C.; Kahn, M.; Mitra, A. *J. Org. Chem.* **1978**, *43*, 2923.

21. Bard, A. J.; Faulkner, L. R. *Electrochemical Methods*; Wiley: New York, NY, 1980, Chapter 5.

22. Crowe, W. E.; Mitchell, J. P.; Gibson, V. C.; Schrock R. R., personal communication, 1990.

23. Evans, D. H.; O'Connell, K. M. *Electroanalytical Chem.* **1986**, *14*, 113.

24. Wimmer, F. L.; Snow, M. R.; Bond, A. M. *Inorg. Chem.* **1986**, *14*, 113.

25. Evans, D. H.; Busch, R. W.; *J. Am. Chem. Soc.* **1982**, *104*, 5057.

26. DiMare, M.; Crowe, W. E.; Bazan, G.; Schrock, R. R., manuscript in preparation.

27. Ref. 21, Chapter 11.

28. Bond, A. M.; Oldham, K. B. *J. Phys. Chem.* **1983**, *87*, 2492.

29. Liebmann, J. F.; Greenberg, A. *Chem. Rev.* **1976**, *76*, 311.

30. Moses, P. R.; Wier, L.; Murray, R. W. *Anal. Chem.* **1975**, *47*, 1882.

31. Jaegfeldt, H.; Kuwana, T.; Johansson, G. *J. Am. Chem. Soc.* **1983**, *105*, 1805.

32. Förster, V. Th.; Kasper, K. *Z. Electrochem.* **1955**, *59*, 976.

33. Fujihira, M.; Kamei, T.; Sakomura, M. *Abstracts of Papers*, 40th International Society of Electrochemistry Meeting, Kyoto, Japan; International Society of Electrochemistry: Zurich, Switzerland, 1989; Abstract 21-03-13-G.

34. Bazan, G. C.; Khosravi, E.; Schrock, R. R.; Feast, W.

J.; Gibson, V. C.; O'Regan, M. B.; Thomas, J. K.; Davis, W. D., submitted for publication, 1990.

35. Bazan, G., Schrock, R. R., personal communication, 1990.

36. Saito, J.; Waki, H.; Teramae, N.; Tanaka, S. *Prog. Org. Coatings* **1988**, *15*, 311.

37. Lattimer, R. P.; Schutten, H-R. *Anal. Chem.* **1989**, *61*, 1201A.

38. Riess, G.; Hurtrex, G.; Bahadur, P. In *Encyclopedia of Polymer Science and Engineering*; Kroschwitz, J. I., Ed.; Wiley: New York, NY, 1985: Volume 2, p.390.

39. Elias, H-G. *Macromolecules*; Plenum: New York, NY, 1984; Chapter 10.

40. Morèse-Séquéla, B.; St.-Jacques, M.; Renaud, J. M.; Prud'homme, *J. Macromolecules*, **1980**, *13*, 100.

41. Ref. 2, p. 32.

42. Ref. 21, Chapter 6.

43. Flanagan, J. B.; Margel, S.; Bard, A. J.; Anson, F. C.

J. Am. Chem. Soc. **1978**, *100*, 4248.

44. (a) Merz, A.; Bard, A. J. *J. Am. Chem. Soc.* **1978**, *100*, 3222. (b) Smith, T. W.; Kuder, J. E.; Wychik, D. *J. Polym. Sci.* **1976**, *14*, 2433.

45. Tanford, C. *The Physical Chemistry of Macromolecules;*

46. Aoki, K.; Akimoto, K.; Tokuda, K.; Matsuda, H.; Osteryoung, J. *J. Electroanal. Chem.* **1984**, *171*, 219.

47. Ref. 45, p. 362.

48. Burfield, D. R.; Lim, K-L. *Macromolecules* **1983**, *16*, 1170.

49. Ammar, F,; Savéant, J. M. *J. Electroanal. Chem.* **1973**, *47*, 115.

50. Saji, T.; Paseh, N. F.; Webber, S. E.; Bard, A. J. *J. Phys. Chem.* **1978**, *82*, 1101.

51. (a) Parry, E. P.; Osteryoung, R. A. *Anal. Chem.* **1965**, *37*, 1635. (b) Osteryoung, J. G.; Schreiner, M.M. *CRC Crit. Rev. Anal. Chem.* **1988**, *19*, S1.

52. Saito, Y. *Rev. Polarogr.* **1968**, *15*, 178.

53. Delahay, P. *New Instrumental Methods in Electrochemistry;* Interscience Publishers: New York, NY, 1954, p. 57.

54. Kadish, K. M.; Ding, J. Q.; Malinski, T. *Anal. Chem.* **1984**, *56,* 1741.

55. Guillet, J. *Polymer Photophysics and Photochemistry;* Cambridge University Press: Cambridge, 1985.

56. Strouse, G. F.; Worl, L. A.; Younathan, J. N.; Meyer, T. J. *J. Am. Chem. Soc.* **1989**, *111,* 9101.

57. McDonald, J. R.; Echols, W. E.; Price, T. R.; Fox, R. B. *J. Chem. Phys.* **1972**, *57,* 1746.

58. Kawanishi, Y.; Kitamura, N.; Tazuke, S. *J. Phys. Chem.* **1986**, *90,* 2469.

59. Murov, S. L. *Handbook of Photochemistry;* Marcel Dekker: New York, NY, 1973.

60. (a) Stern, O.; Volmer, M. *Physik. Z.* **1919**, *20,* 183. (b) Turro, N. J. *Modern Molecular Photochemistry;* Benjamin/Cummings: Menlo Park, CA, 1978; p. 246.

61. Weller, A. *Pure Appl. Chem.* **1968**, *16*, 115.

62. (a) Rehm, D.; Weller, A. *Isr. J. Chem.* **1970**, *8*, 259. (b) Weller, A. *Z. Phys. Chem. (Wiesbaden)* **1982**, *130*, 129.

63. Maestri, M.; Grätzel, M. *Ber. Bunsen-Gesell. Phys. Chem.* **1977**, *81*, 504.

64. Taylor, G. N.; Chandross, E. A.; Schiebel, A. H. *J. Am. Chem. Soc.* **1974**, *96*, 2693.

65. Hester, R. E.; Williams, P. J. *J. Chem. Soc. Perkin Trans. 2* **1981**, 852.

66. Tazuke, S.; Kitamura, N.; Kawanishi, Y. *J. Photochem.* **1985**, *29*, 123.

67. Hargreaves, J. S.; Webber, S. E. *Macromolecules* **1982**, *15*, 424.

68. Froelich, P.; Wehry, E. L. in *Modern Fluorescence Spectroscopy*; Wehry, E. L., Ed.; Plenum: New York, NY, 1976; Chapter 8.

69. Ref. 60, Chapter 9.

Chapter IV

Surface Confinement of Well-Defined Redox Active Polymers and Block Polymers by Unique Functionalities in the Polymers

Introduction

Using the methods presented in Chapter III, polymers have been prepared with groups capable of binding to electrode surfaces. In this chapter, the utility of applying these polymers as eletrode derivatizing reagents is discussed.

The binding of molecules to surfaces in order to modify the properties of the surface is an area of wide application. Many methods for attaching derivatizing reagents to surfaces have been developed. Research in the areas of chemically modified electrodes[1] and functionalized chromatographic supports[2] has particularly focused on attachment schemes for covalently bonding or adsorbing discrete molecules to surfaces. One of the more versatile methods is the coupling of silane derivatives to a surface via siloxane bond formation with a surface oxide layer.[3] This method is well-suited to electrode modification because of the presence of oxide surface layers on many electrode materials, such as Pt, $In(Sn)O_2$, Si, and C.[1] Surface-bound films made using siloxane linkages are very durable.

Silane coupling reagents that are di- or tri-functional can form a multilayered network, where some molecules are not directly bound to the surface. Mono-functional silane reagents though can form only one bond with the surface. Similarly, typical organic[4] or inorganic[5] reactions can be carried out between surface-bound and solution species to produce a modified surface through the formation of a covalent bond. If the reactant on a polymer prepared by

ROMP is the end group, then there would be only one unit of the reactant per polymer chain. Bond formation then leads to a unique covalent linkage between the surface and the polymer.

Specific adsorption of aromatic hydrocarbons[6] and quinones[7] onto C surfaces has also been used to prepare modified electrodes. The adsorption is usually a fast process, but with small molecules the attachment is reversible, and so has been relatively short-lived in the absence of adsorbate in the solution.[5]

These attachment schemes have been applied to binding molecular reagents to surfaces. Little work has been done using polymers that contain some of the functional groups listed above for electrode surface modification. Typically, polymers (either preformed or ones prepared in-situ) have been bound to electrodes by non-specific adsorption. They remain on the electrode, because they are not soluble in the electrolyte.

Using ROMP, functional groups that can bind to electrode surfaces can be readily incorporated into redox polymers. The surface binding groups can be incorporated into the polymer as a monomer or as an end group. In block polymers, the relative position of the surface linking group to the other components of the polymers can be changed by controlling the polymerization, as indicated in Scheme II of Chapter III.

What are the consequences of derivatizing electrodes with

redox polymers through a unique point of attachment? The relative position of the surface linking group within the polymer can lead to an oriented surface-bound polymer. It is worth investigating these polymers as a means of making surface structures that display supramolecular functions that arise because of the controlled orientation of the polymer layer.

Experimental

Chemicals. 4-(Fluoro)benzaldehyde and 4-pyridinecarboxaldehyde were obtained from Aldrich Chem. Co., and were purified by passage through a 5 cm column of activated alumina. 4-Pyridinecarboxaldehyde yellows after a few days of storage, it was freshly prepared each time. α-Bromo-*p*-tolualdehyde was recrystallized from Et_2O. (*endo, exo*)-2-Triethoxysilyl-5-norbornene and 4-[2-(trichlorosilyl) ethyl]pyridine were obtained from Petrarch Systems, Inc. (now HULS America, Inc.) and used as received. *p*-(Chloromethyl)phenyltrichlorosilane was obtained from PCR, Inc., Gainesville, FL, and used as received.

Polymer Synthesis and Characterization. The procedures for the synthesis and characterization of the polymers are given in the Experimental section of Chapter III.

Electrochemistry. Electrochemical experiments were done using conventional 3-electrode cells, using a Pine Instruments RDE 4 bipotentiostat modified for low current sensitivity. Traces were recorded on a Kipp and Zonen BD 91 X-Y recorder. The electrolyte was sparged with Ar or N_2 before use.

Pt electrodes were prepared and pretreated as described in Chapter II. Indium(tin) oxide (ITO) electrodes were made from 50 x 7 mm slabs of ITO coated on glass (Delta Technologies, Stillwater, MN) that were cut in thirds. The ITO surface was scrubbed with a warm soapy solution and rinsed copiously with water and dried before use. Glassy

carbon electrodes, 3 mm disks inlaid in a Teflon mount, were obtained from BAS: Bioanalytical Systems, West Lafayette, IN. The electrodes were polished before each experiment using 1 μm Metadi diamond polish (Buehler, Lake Bluff, IL) followed by sonication in MeOH for 10 min, and copious rinsing with the electrochemical solvent. n-Si electrodes were fabricated, pretreated, derivatized, and examined as described in Chapter II.

Synthesis. All chemicals used were reagent grade. Tetrahydrofuran (THF) was distilled from CaH_2 under N_2 immediately prior to use. Pyridine was stored over 4Å molecular sieves. Benzene was stirred with concentrated H_2SO_4, decanted, and distilled under N_2. Anhydrous Et_2O and the solvents used in chromatography were used as received. Silica gel, 230-400 mesh, from Aldrich Chemical Co. was used in chromatography. Ferrocenecarboxylic acid and 5-norbornene-2-methanol were obtained from Aldrich Chem. Co., and phosphorous pentachloride was obtained from Fluka AG. 5-Norbornene-2-methanol was distilled under N_2 before use. Octamethylferrocenecarboxaldehyde was generously provided by Dr. C-F. Zou of the Wrighton group.

^1H NMR spectra were recorded on either a Varian XL or Gemini 300 MHz FT spectrometer; ^{13}C NMR spectra were recorded on the same instruments at 75.4 MHz. Chemical shifts were calibrated by a residual solvent resonance relative to Me_4Si, δ 0.0. Electronic absorption spectra were obtained on a HP 8452A spectrophotometer using 1 cm

pathlength quartz cuvettes. Mass spectrometry was done on a Finnigan MAT System 8200 with a double focusing magnetic sector by electron impact (70 eV). Melting points were obtained with a Thomas capillary melting point apparatus, and are uncorrected. Elemental analyses were done by Schwartzkopf Microanalytical Lab, Woodside, NY.

5-Norbornene-(*endo, exo*)-2-(methoxycarbonyl)ferrocene. Ferrocenecarboxylic acid (2.1 g, 9.1 mmol) was added to 30 mL benzene in which PCl_5 (2.2 g, 10.0 mmol) was suspended. The red solution was stirred for 2 h at room temperature. The reaction mixture was filtered and the filtrate was concentrated in vacuo. The residue was taken up in hexane, washed with H_2O, dried over $MgSO_4$, filtered and the solvent was removed by rotary evaporation. The acid chloride was dissolved in THF and added to a three neck 100 mL flask fitted with a condenser, gas adaptor, septa, and a stir bar, that contained 30 mL THF, pyridine (1.5 mL, 20 mmol) and 5-norbornene-2-methanol (1.2 mL, 10 mmol). The solution was stirred at reflux for 20 h, then worked up with $CHCl_3$ and H_2O. Chromatography (1:19 ethyl acetate:hexane) yielded 1.60 g (52%) of product, which was recrystallized from Et_2O as orange prisms. The product was a 9:1 mixture of the endo and exo diastereomers as determined by ^1H NMR. R_f (1:19 EA:Hex) 0.34; MP 96-99°C; ^1H NMR (C_6D_6) δ 0.45 (1H, m), 1.05 (1H, m), 1.42 (1H, m), 1.62 (1H, m), 2.38 (1H, m), 2.57 (1H, m), 2.87 (1H, m), 3.87 (1H, m, -C*H*HO-), 4.04 (8H, m, -CH*H*O-, C_5H_5, $C_5H_2H_2$), 4.90 (2H, m, $C_5H_2H_2$), 5.95 (1H, m),

5.98 (1H, m); ^{13}C NMR (C_6D_6) δ 28.8, 38.2, 42.2, 44.1, 49.3, 67.4, 69.7, 70.3, 71.1, 80.2, 132.4, 137.7, 171.0; UV-vis (THF) λ_{max}/nm (log ε) 304 (2.99), 340 (sh), 442 (2.35); MS (relative abundance) 336 (M^+, 96), 270 (M - $C_5H_6^+$, 100), 230 ($FeC_{10}H_9CO_2H^+$, 95), 185 ($FeC_{10}H_9^+$, 11), 121 ($FeC_5H_5^+$, 25); Anal. Calcd for $C_{19}H_{20}FeO_2$: C, 67.88; H, 6.00; Fe, 16.61; Found: C, 67.97; H, 6.10; Fe, 16.83.

5-Norbornene-(endo, exo)-2-methoxy(methyloctamethylferrocene). According to the literature,[8] octamethylferrocenylmethyl cation (1.6 mmol) was reacted with sodium 5-norbornene-2-methoxide (1.8 mmol). The product showed 3 spots by TLC (20% Et_2O/hexane). Flash chromatography on silica (60Å) separated the bands, and the first was collected and concentrated by rotary evaporation to give 250 mg (33%) of a yellow solid. The solid could not be purified sufficiently for clean reaction with ROMP initiators.

The reaction was performed in two other ways, with the lithium alkoxide, prepared from n-BuLi and the alcohol, in place of the sodium alkoxide, and by reacting the cation with 5-norbornene-2-methanol, followed by diisopropyl amine. In all cases, yields were low and product recovery was difficult. A polymerization with this monomer was done with mixed success. Only some of the octamethylferrocene redox agent was incorporated into the polymer.

Results and Discussion

Functional groups capable of binding to electrodes have been incorporated into polymers prepared by ROMP as both a monomer and as end groups. The monomer employed was a trifunctional silane coupling reagent, triethoxysilyl-norbornene, (Si), shown in Chart II of Chapter III. The end groups used as surface linking agents were derived from the aldehydes pyrenecarboxaldehyde, pyridinecarboxaldehyde, and α-bromo-*p*-tolualdehyde, shown in Chart III of Chapter III, that were used to terminate the living polymerization.

Pyrene is one of a group of polycyclic aromatic molecules that irreversibly adsorbs to graphite surfaces.[5,6,7] The pyridine and benzylbromide end groups have been reacted with surfaces containing benzylchloride and pyridine groups, respectively. These surface linking reactions are similar to those used to derivatize chromatographic supports.[4]

Phenothiazine Polymers Containing Triethoxysilylnorbornene. Incorporating triethoxysilyl groups into the polymer via a monomer, triethoxysilylnorbornene, (Si), means that there will be a range in the number of (Si) groups per polymer chain. To minimize polymer cross-linking via siloxane bond formation a very small number of equivalents, 1 or 2, of the monomer was added to the living polymer. This means though that some polymer chains will not acquire a (Si) unit, while others will receive several. The different products, polymers with (Si) units and polymers without (Si) units, cannot be separated. However, only polymers with (Si) are

expected to bond to an electrode surface. Control experiments using polymers lacking (Si) groups were used to indicate whether such an assumption is true.

Several sets of (Si) containing polymers have been prepared. First, in the synthesis of the $(Phz)_5$ polymer with redox-active end groups, 2 equivalents of (Si) were added to the living 5mer, followed by octamethylferrocene-carboxaldehyde. The (Si) containing block polymer is shown in Chart I. Studies of this block polymer demonstrate that the 2 eq of (Si) added are adequate, and necessary, for surface attachment of the polymer.

First, as a comparison the behavior of the analog without (Si) will be considered. In the solution cyclic voltammetry of Fc-$(Phz)_5$-OMFc in CH_2Cl_2/electrolyte, the Phz wave shows reductive stripping, indicating the polymer precipitates or adsorbs upon oxidation. However, rereduction removes all of the material, and there is no accumulation of the polymer on the electrode. This is illustrated in Figure 1, where the electrode was poised at +0.95 V for 10, 20, and 30 s in consecutive sets of voltammograms. The stripping wave increases with the amount of charge consumed in the oxidation, but subsequent scans show that the cyclic voltammograms regain their original waveshape. Material does not accumulate on the electrode to result in either enhanced currents due to surface-confined material, or loss of activity, due to decomposition and fouling.

In contrast, soaking a Pt electrode (pretreated to have an

Chart I. Diblock Polymer of the Triethoxysilyl and Phenothiazine Monomers, With Redox-Active End Groups.

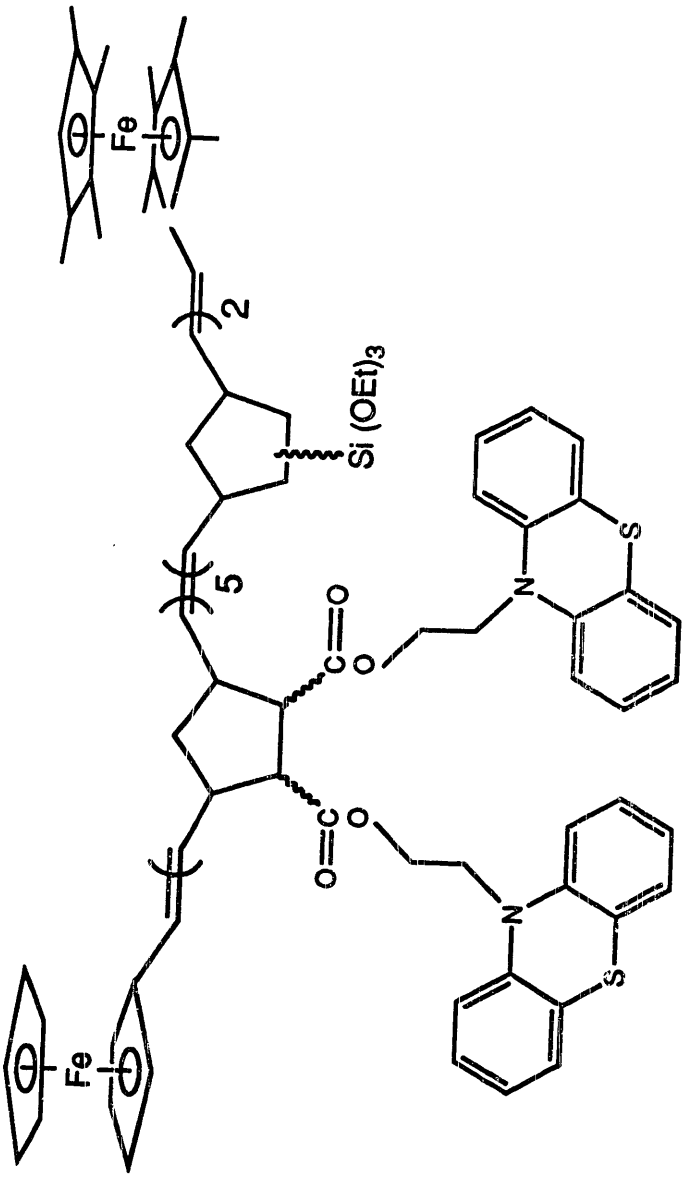

Fc-(Phz)$_5$-OMFc

Figure 1. Solution electrochemistry of Fc-$(Phz)_5$-OMFc, 0.06 mM, in CH_2Cl_2/0.1 M $[n\text{-}Bu_4N]PF_6$. In this consecutive series of voltammograms, the electrode potential was held at the positive limit for the specified time, 10, 20, and 30 s, respectively, and then cycled 3 times at 100 mV s^{-1}.

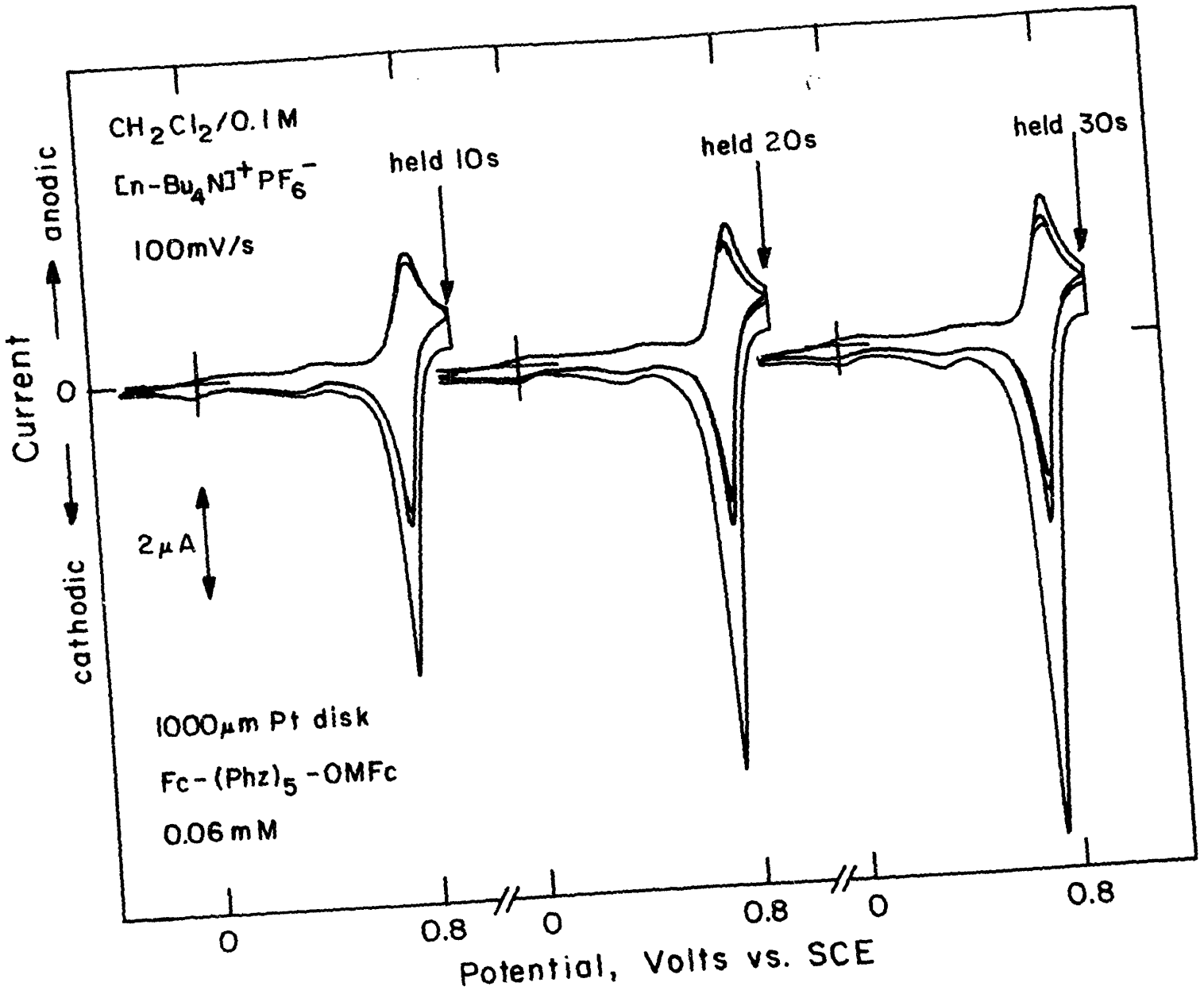
CH2Cl2/0.1M
[n-Bu4N]+PF6-
100mV/s
held 10s
held 20s
held 30s
Current
anodic
0
cathodic
2μA
1000μm Pt disk
Fc-(Phz)5-OMFc
0.06mM
0
0.8
0
0.8
0
0.8
Potential, Volts vs. SCE

oxide layer) in the presence of Fc-$(Phz)_5(Si)_2$-OMFc in a benzene solution for 14 h yielded a derivatized electrode. Cyclic voltammmograms shown in Figure 2 of the derivatized electrode in CH_2Cl_2/0.1 M [*n*-Bu_4N]PF_6 reveal persistent, redox waves for the Fc, Phz, and OMFc units of the polymer that are characteristic of a surface-bound species. In the same electrolyte medium, the non-(Si) containing polymer does not persistently adhere even after oxidative deposition.

The amount of material bound to the electrode surface is found by calculating the amount of charge in the faradaic wave. From the (Phz) wave, the coverage is 3×10^{-10} mol cm^{-2} of Phz units, or 3×10^{-11} mol cm^{-2} of polymer. A monolayer of a molecule such as ferrocene or iodide is ~1-2 $\times 10^{-10}$ mol cm^{-2}. For a polymer with 12 redox sites on average, a coverage of ~10^{-9} mol cm^{-2} of redox groups might be expected. However, enough about the structure of the bound polymer is not known to assess the apparent coverage of a monolayer. The size of the polynorbornene backbone and the surface area blocked from the solution by the polymer probably both contribute to lower coverages.

A set of longer Phz polymers prepared are shown in Chart II. Again, the batch of the living $(Phz)_{30}$ was split in half; one half was capped with N,N-dimethyl-*p*-(amino)-benzaldehyde, and the other half was treated with 2 eq of (Si) followed by *p*-(fluoro)benzaldehyde. Figure 3 shows the results of soaking pretreated Pt electrodes and $In(Sn)O_2$,

Figure 2. Scan rate dependence of the cyclic voltammetry for a Pt electrode derivatized with Fc-$(Phz)_5(Si)_2$-OMFc in CH_2Cl_2/0.1 M [*n*-Bu_4N]PF_6 from 100 to 1000 mV s^{-1} in 100 mV s^{-1} increments. The coverage of phenothiazine groups is 3×10^{-10} mol cm^{-2}, and of the polymer, 3×10^{-11} mol cm^{-2}.

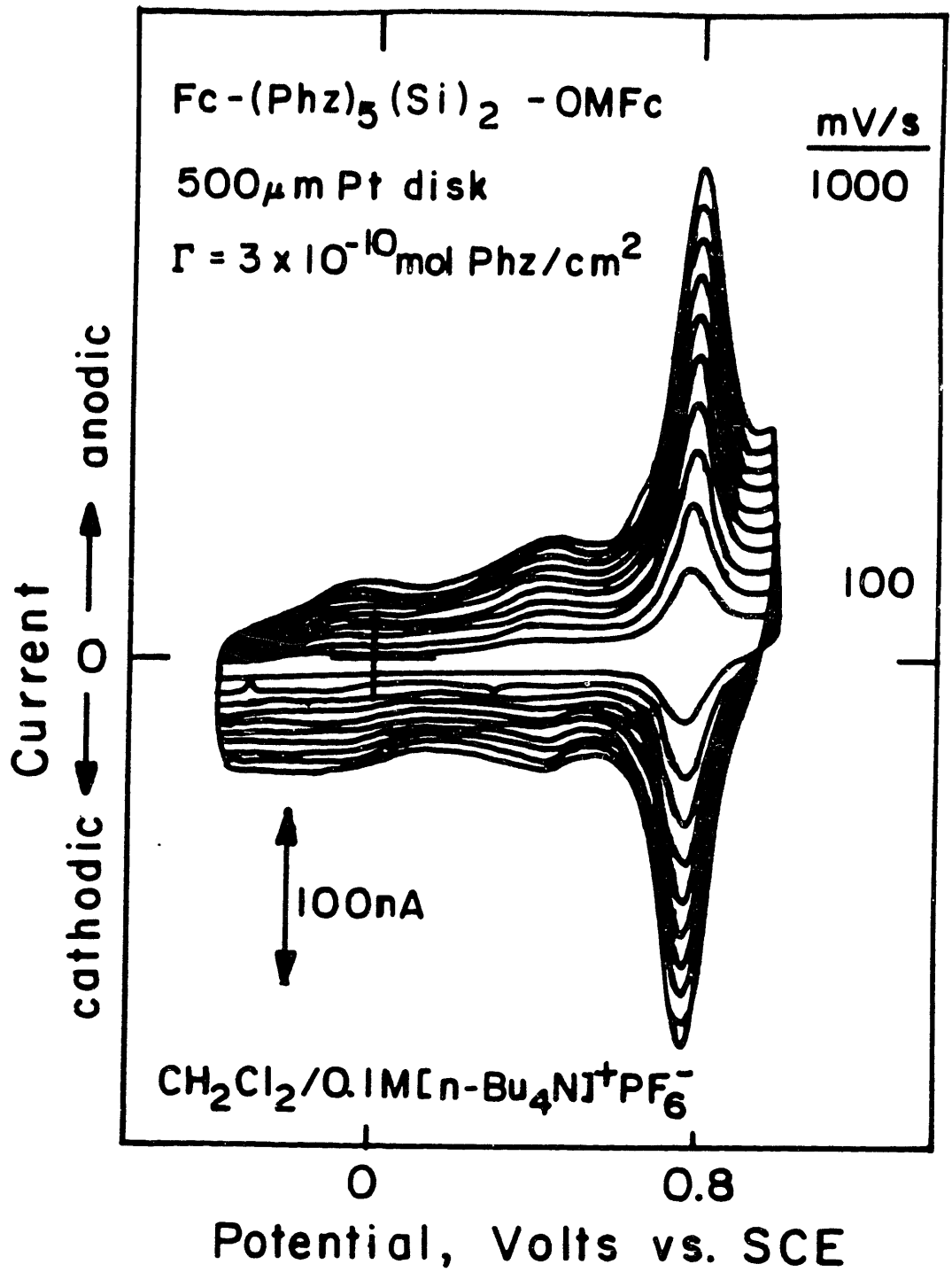
Fc-(Phz)5(Si)2-OMFc
500μm Pt disk
Γ = 3 x 10^-10 mol Phz/cm^2
mV/s
1000
100
100nA
CH2Cl2/0.1M[n-Bu4N]+PF6-
Current
cathodic
0
anodic
0
0.8
Potential, Volts vs. SCE

Chart II. Phenothiazine Polymer, and Block Polymer With the Triethoxysilyl Monomer, Made From the Same Living Polymer.

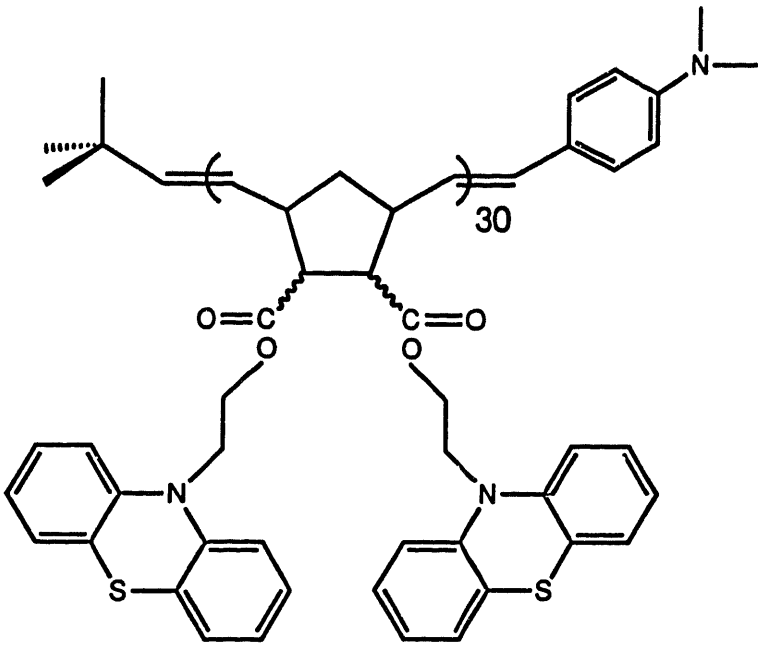

$(Phz)_{30}$

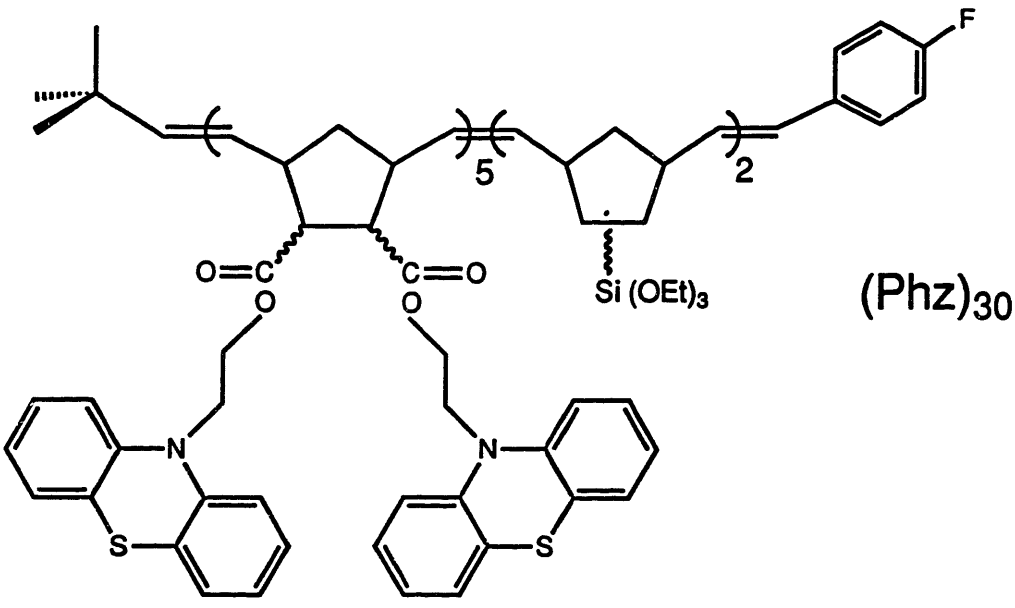

$(Phz)_{30}(Si)_2$

Figure 3. Cyclic voltammetry of (a) an ITO electrode that was soaked in a benzene solution of $(Phz)_{30}(Si)_2$ for 12 h, as a function of scan rate, (b) an ITO electrode that was soaked in a benzene solution of $(Phz)_{30}$ for 12 h, at 100 mV s^{-1}, (c) a Pt electrode soaked in a benzene solution of $(Phz)_{30}(Si)_2$ for 90 min, as a function of scan rate, and (d) a Pt electrode that was soaked in a benzene solution of $(Phz)_{30}$ for 8 h, at 100 mV s^{-1}. The coverage of phenothiazine on ITO was calculated to be 1 x 10^{-10} mol cm-2, and Pt, 5 x 10^{-10} mol cm^{-2}, corresponding to a coverage of the polymer of 8 x 10^{-12}, and 2 x 10^{-12} mol cm^{-2}, respectively.

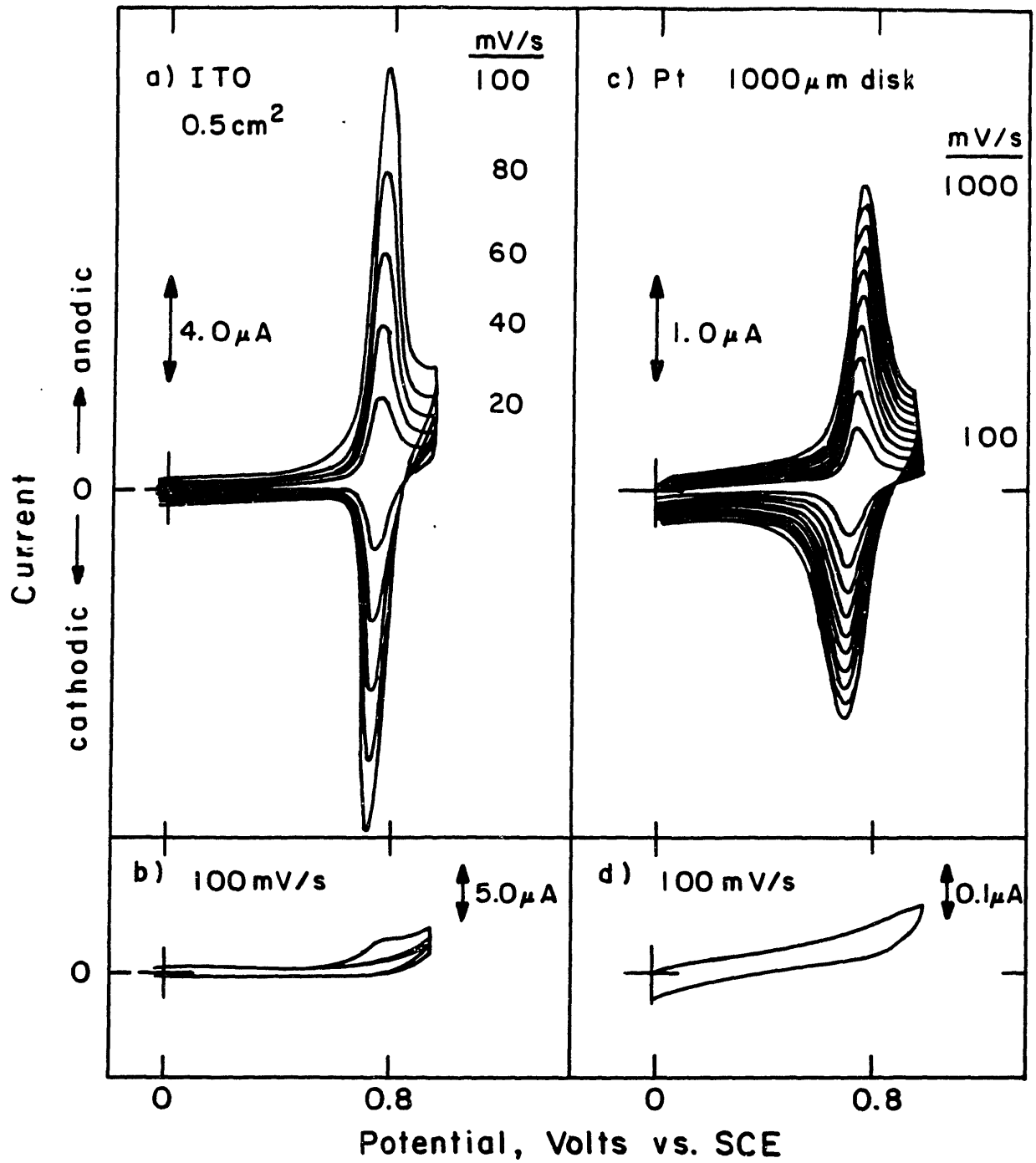
a) ITO
0.5cm²
mV/s
100
80
60
40
20
4.0μA
c) Pt 1000μm disk
mV/s
1000
100
1.0μA
b) 100mV/s
5.0μA
d) 100 mV/s
0.1μA
Current
cathodic
anodic
0
0
0.8
0
0.8
Potential, Volts vs. SCE

(ITO), electrodes in solutions of $(Phz)_{30}$ and $(Phz)_{30}(Si)_2$. A Pt electrode was soaked in the $(Phz)_{30}$ solution for 8 h, and another for 1.5 h in $(Phz)_{30}(Si)_2$. The ITO electrodes were soaked in the two solutions for 12 h. Only the polymer containing the (Si) block is found to yield a derivatized electrode. The coverages calculated were 5×10^{-10} and 1×10^{-10} mol cm^{-2} of Phz units for Pt and ITO, respectively. This corresponds to 8×10^{-12} and 2×10^{-12} mol cm^{-2} of polymer.

n-Si electrodes can also be derivatized with $(Phz)_{30}(Si)_2$. As shown in Figure 4, in the dark, no current flows at a derivatized electrode. Upon illumination with energetic enough photons (E > band gap = 1.1 eV) reversible cyclic voltammograms characteristic of a surface-bound redox couple are observed. The anodic peak potential is +380 mV vs. SCE, 370 mV negative of the redox potential of phenothiazine at a Pt electrode. This negative shift of the anodic wave represents the photovoltage, or the extent to which the light drives the oxidation of phenothiazine in a thermodynamically uphill sense. Turning off the light at the positive scan limit results in the reduction of phenothiazine in the dark, but no more charge passes upon further cycling in the dark. The coverage of Phz observed was 2.6×10^{-10} mol cm^{-2}, or 4×10^{-12} mol cm^{-2} of polymer.

Ferrocene Polymers Containing Triethoxysilylnorbornene. A complementary set of Fc/Nrb block polymers were made with different relative positions compared to a (Si) block.

Figure 4. (a) Cyclic voltammetric behavior of an n-Si electrode derivatized with $(Phz)_{30}(Si)_2$ in CH_2Cl_2/0.1 M *n*-Bu_4NPF_6 in the dark (- - - -), illuminated (————), and to the right, with light source turned off at the positive scan limit. (b) Scan rate dependence of the cyclic voltammetry for the same electrode of n-Si derivatized with $(Phz)_{30}(Si)_2$ under illumination. The coverage was 2.6 x 10^{-10} mol cm^{-2} of phenothiazine, or 4 x 10^{-12} mol cm^{-2} of polymer.

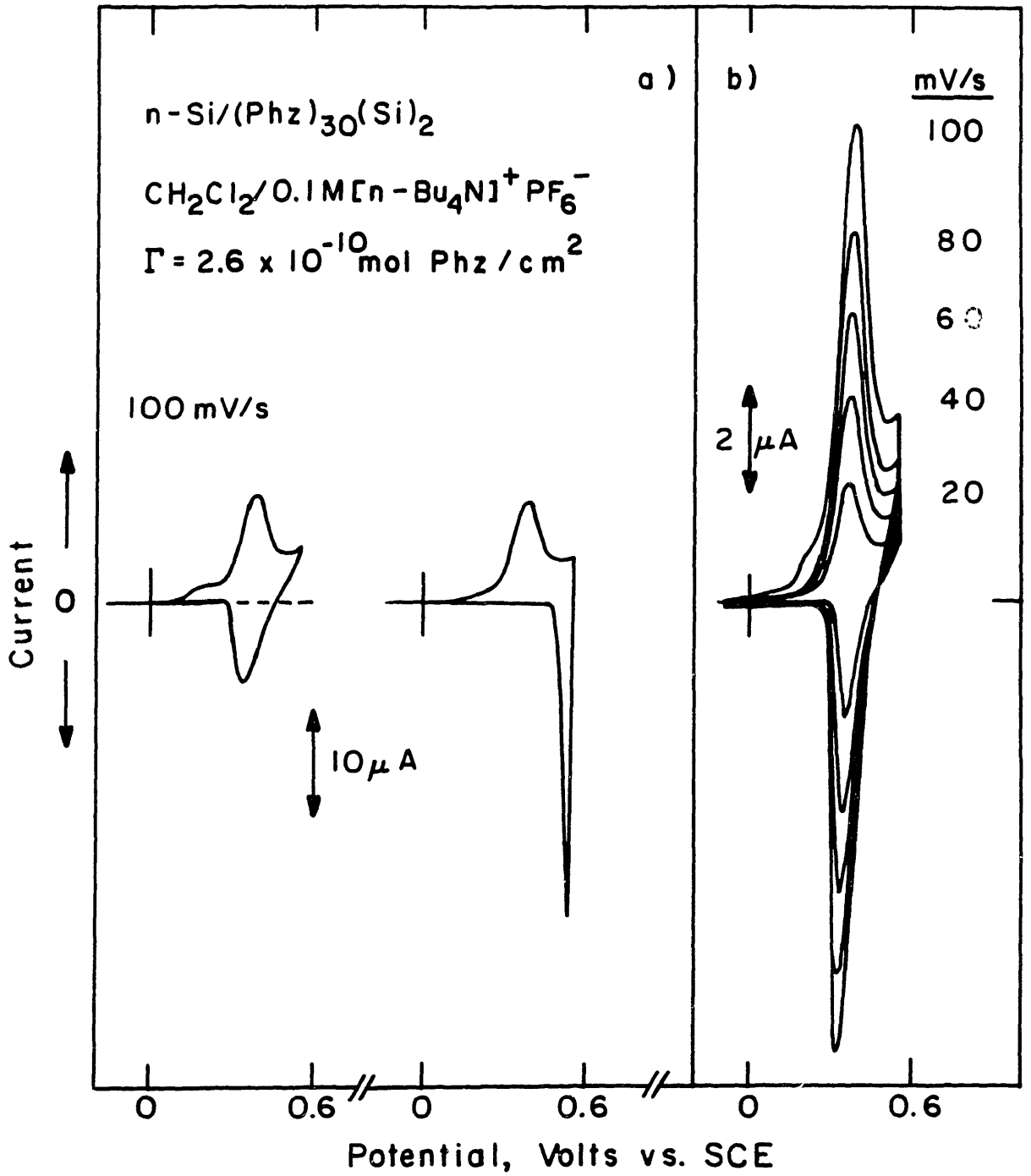
a)
b)
mV/s
100
80
60
40
20
n-Si/(Phz)30(Si)2
CH2Cl2/0.1M[n-Bu4N]+PF6-
Γ = 2.6 x 10-10 mol Phz/cm2
100 mV/s
2 μA
10 μA
Current
0
0
0.6
0
0.6
0
0.6
Potential, Volts vs. SCE

These polymers are shown in Chart III. Soaking pretreated Pt electrodes in benzene solutions of these polymers for 12 h yielded derivatized electrodes, while soaking electrodes in solutions of $(Fc)_{15}(Nrb)_{15}$ or $(Nrb)_{60}(Fc)_{15}$ for the same amount of time did not. Varying the position of the electroactive (Fc) block relative to the (Si) surface linking group and the (Nrb) block revealed no difference in the electrochemical behavior in CH_2Cl_2/electrolyte, as shown in Figure 5.

A triblock polymer containing two redox-active blocks, ferrocene and octamethylferrocene, and (Si) was prepared. This polymer is shown in Chart IV. The monomer containing octamethylferrocene could not be made in good yield nor could it be purified sufficiently well for use in the polymerization to make well-defined homopolymers. The block polymer did not yield the expected ratio of Fc to OMFc by ^1H NMR or by electrochemistry. Nonetheless, a triblock polymer was formed, and its electrochemical properties were examined.

The scan rate dependence of the cyclic voltammetry of this polymer, bound to a Pt electrode, in CH_2Cl_2, EtOH, and H_2O is shown in Figure 6. The amount of charge passed in the redox waves decreases by ~30% upon switching from CH_2Cl_2/electrolyte to EtOH/electrolyte. In H_2O/electrolyte very little faradaic current passes. The loss of the ability to pass charge in these films seems to be due to the presence of the polyalkylated ferrocene block, similar to

Chart III. Triblock Polymers Prepared With Ferrocene, Norbornene, and Triethoxysilyl Monomers.

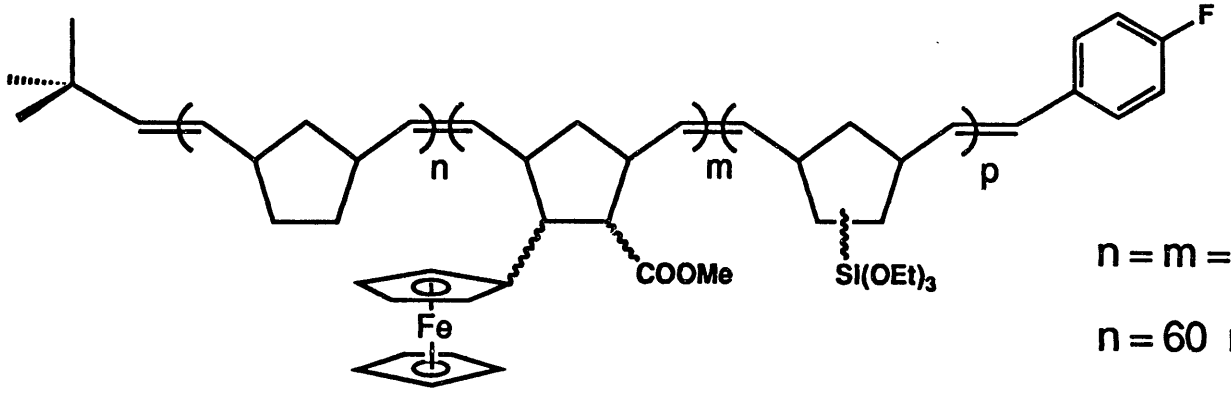

n = m = 30 p = 10

n = 60 m = 15 p = 1

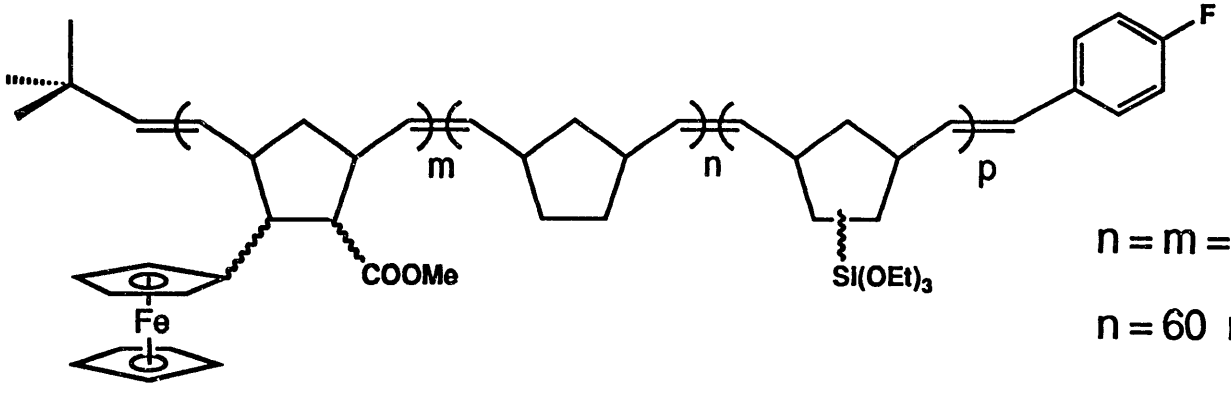

n = m = 30 p = 10

n = 60 m = 15 p = 1

Figure 5. Cyclic voltammetric behavior of Pt electrodes derivatized with $(Nrb)_{30}(Fc)_{30}(Si)_{10}$ and $(Fc)_{30}(Nrb)_{30}(Si)_{10}$ at 100 mV s^{-1} in CH_3CN/0.1 M [*n*-Ru_4N]PF_6.

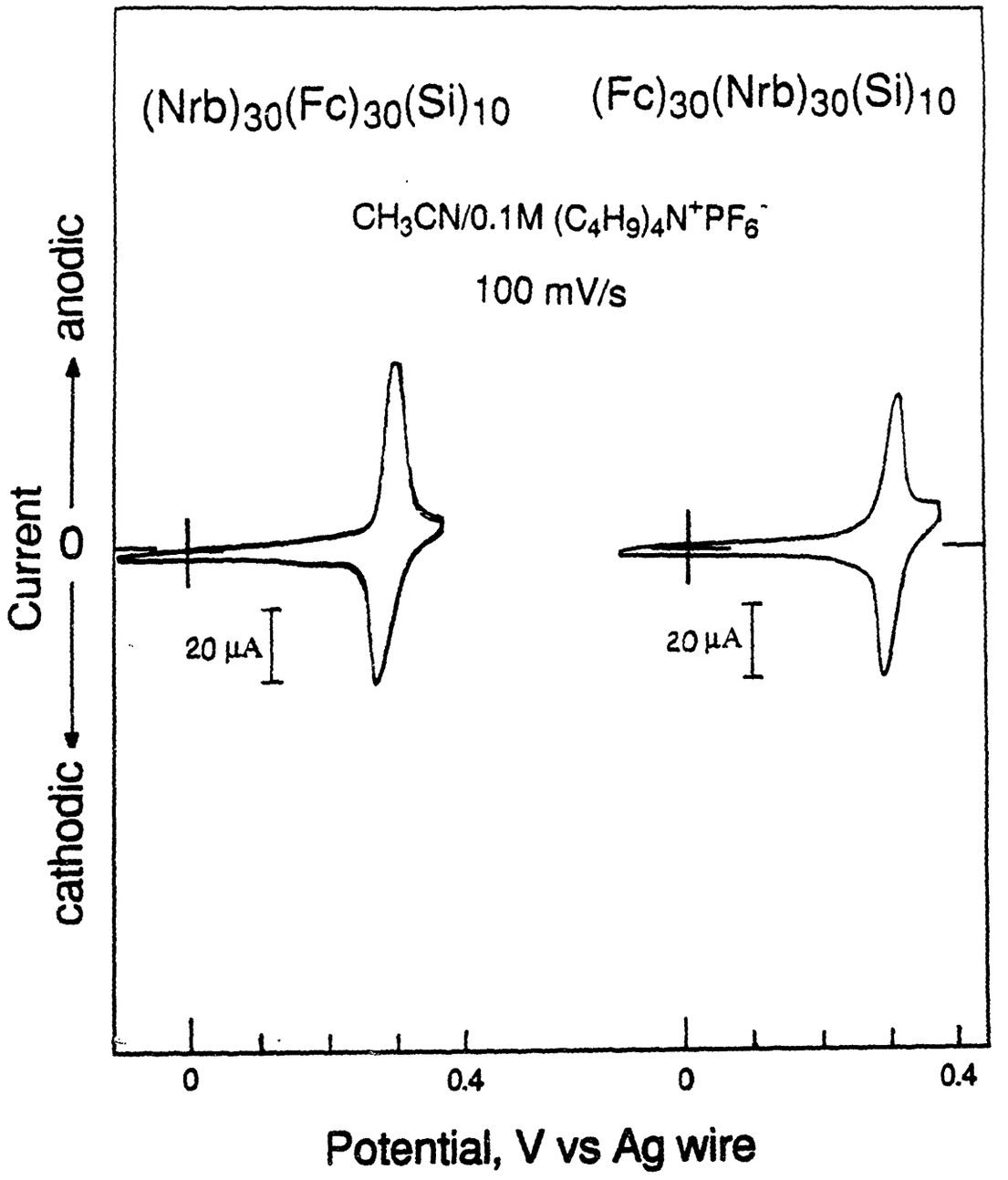
(Nrb)30(Fc)30(Si)10
(Fc)30(Nrb)30(Si)10
CH3CN/0.1M (C4H9)4N+PF6-
100 mV/s
Current
anodic
0
cathodic
20 µA
20 µA
0
0.4
0
0.4
Potential, V vs Ag wire

Chart IV. Triblock Polymer Prepared With Ferrocene, Octamethylferrocene, and Triethoxysilyl Monomers.

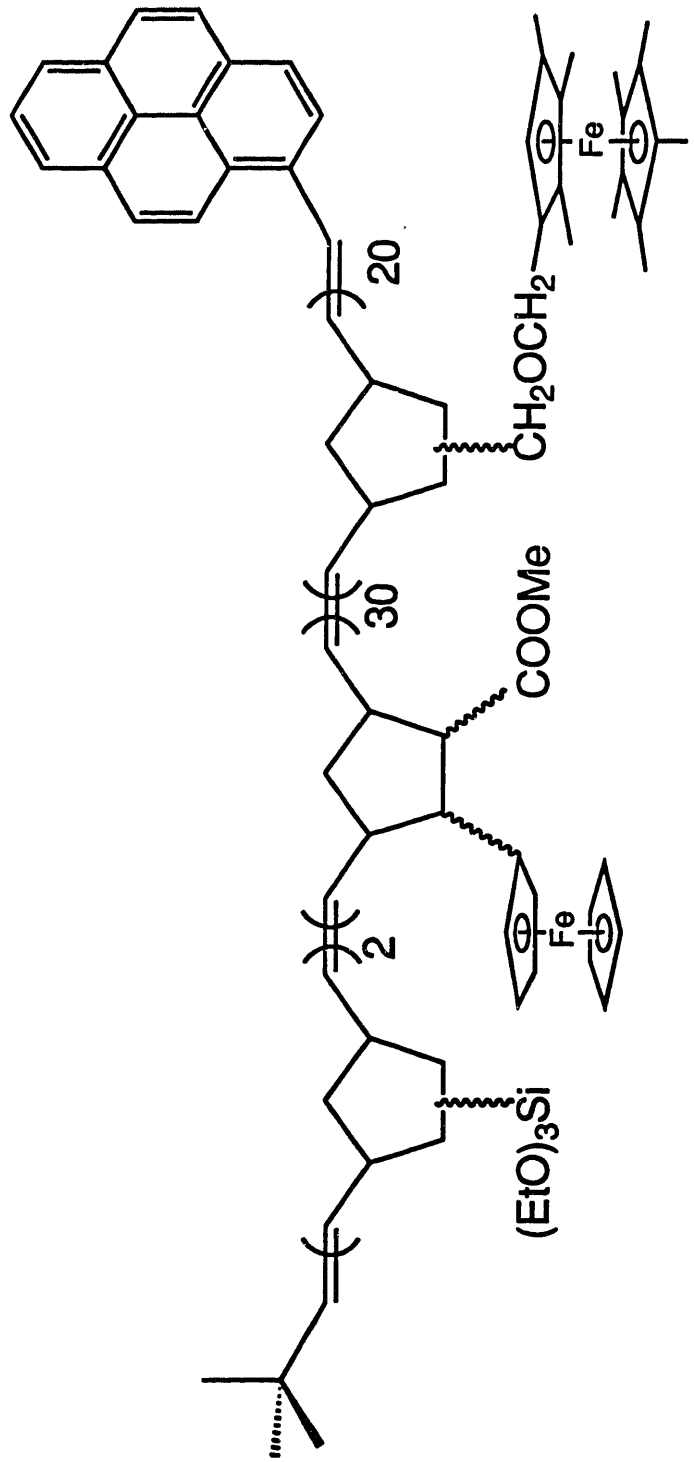

$(Si)_2(Fc)_{30}(OMFc)_{20}$

Figure 6. Solvent effects on the cyclic voltammetry of a Pt electrode derivatized with $(Si)_2(Fc)_{30}(OMFc)_{20}$-pyrene, that was prepared by soaking in a benzene solution of the polymer for 12 h, in CH_2Cl_2/0.1 M [*n*-Bu_4N]PF_6, EtOH/0.1 M [*n*-Bu_4N]PF_6, and H_2O/0.1 M $NaClO_4$. The coverage for the Fc wave in CH_2Cl_2/electrolyte is 1.1×10^{-10} mol cm^{-2}, and for the OMFc wave, 6×10^{-11} mol cm^{-2}.

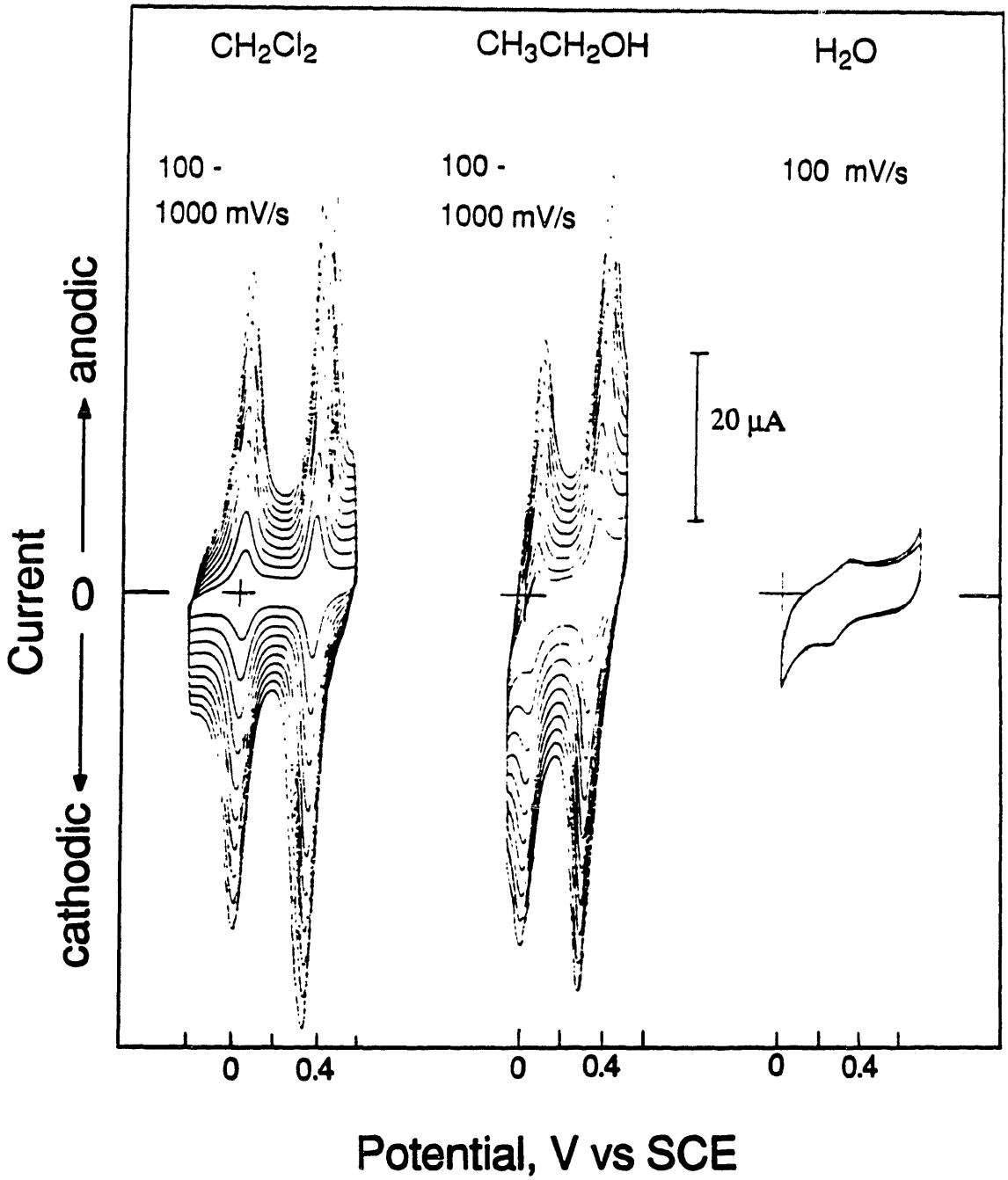
CH_2Cl_2
CH_3CH_2OH
H_2O
100 - 1000 mV/s
100 - 1000 mV/s
100 mV/s
20 µA
Current
anodic
0
cathodic
0
0.4
0
0.4
0
0.4
Potential, V vs SCE

the behavior observed for decaalkylferrocene films in H_2O/electrolyte as discussed in Chapter II. In comparison, the electrochemical response of surface-confined $(Nrb)_{15}(Fc)_{15}$, prepared by oxidative deposition from CH_2Cl_2/electrolyte, in CH_3CN, EtOH, and H_2O is shown in Figure 7. The amount of charge passed diminishes as the solvent becomes a poorer one for the polymer, but the electrochemical response is not shut off in an aqueous medium. In fact, compared to the response typically observed for ferrocene polymer films, the waveshape for $(Nrb)_{15}(Fc)_{15}$ is quite good; smooth symmetric waves are obtained instead of spikes, and the peak-to-peak separation remains small.

Polymers With A Pyrene End Group. Pyrene has a strong affinity for carbon surfaces. In small molecules, addition of a pyrene group allows one to attach molecules to C surfaces which otherwise would not adsorb. Soaking glassy carbon electrodes in benzene, THF, or CH_2Cl_2 solutions of polymers resulted in adsorption of the polymer independent of its composition. That is, polymers with and without the pyrene end group were found to adsorb to roughly the same extent. To test whether a pyrene group could overcome the polymer adsorption and displace it from the surface a competitive binding experiment was done. The polymers shown in Chart V were used. To 0.5 mL benzene was added 1 mg each of $(Fc)_{12}$ and $(Phz)_{15}$-pyrene, and in another solution $(Fc)_{12}$-pyrene and $(Phz)_{15}$. A 3 mm glassy carbon rod was

Figure 7. Solvent effects on the cyclic voltammetry for films of $(Nrb)_{15}(Fc)_{15}$ on a Pt electrode, prepared by oxidative deposition of the polymer from CH_2Cl_2/0.1 M [*n*-Bu_4N]PF_6, in CH_3CN/0.1 M [*n*-Bu_4N]PF_6, EtOH/0.1 M [*n*-Bu_4N]PF_6, and H_2O/0.1 M $NaClO_4$. The coverage observed for the Fc wave in CH_3CN/electrolyte is 8 x 10^{-10} mol cm^{-2}.

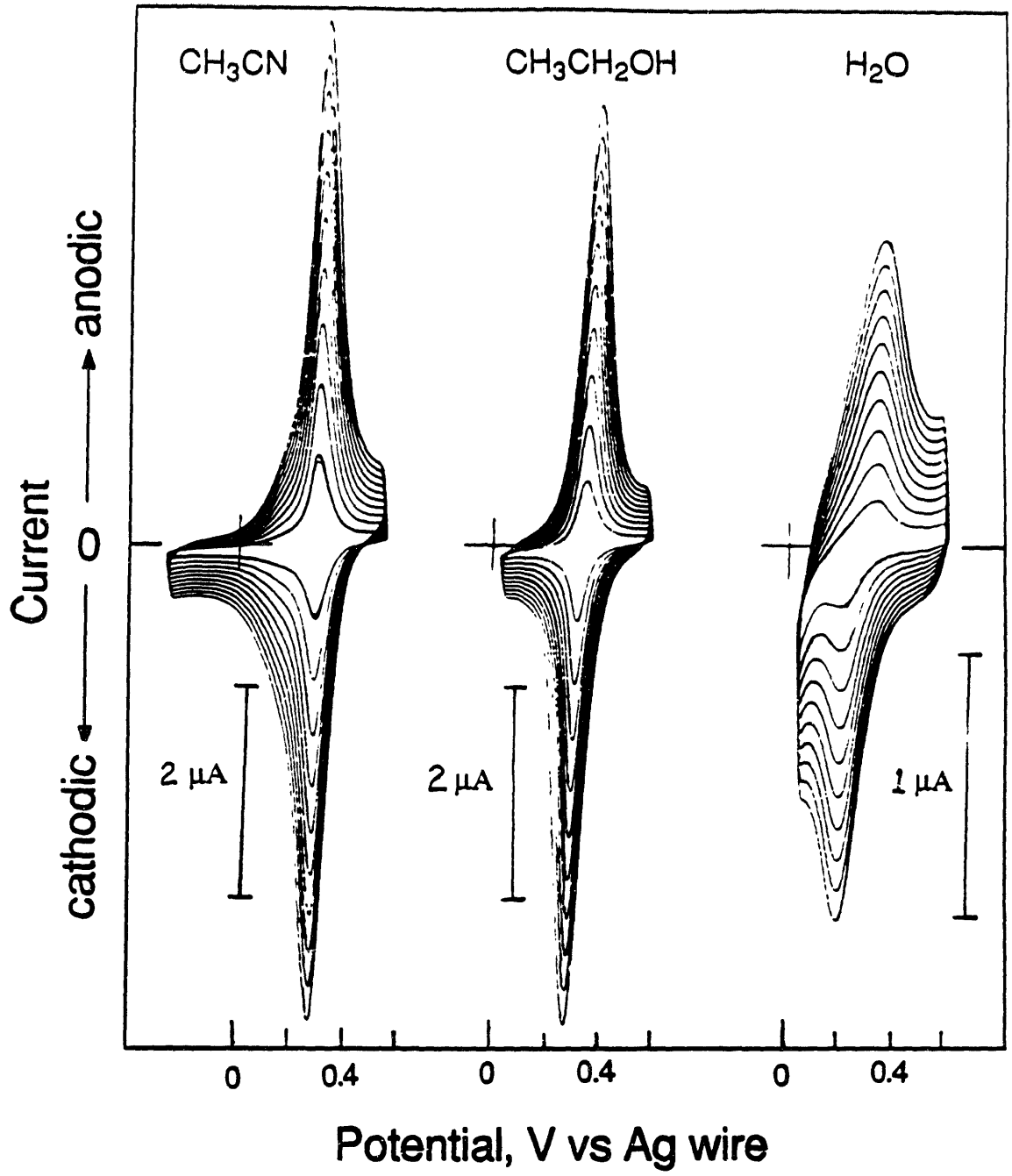
CH3CN
CH3CH2OH
H2O
Current
anodic
0
cathodic
2 μA
2 μA
1 μA
0
0.4
0
0.4
0
0.4
Potential, V vs Ag wire

Chart V. Polymers Prepared With Pyrene End-Groups Used For Adsorption To Carbon Surfaces.

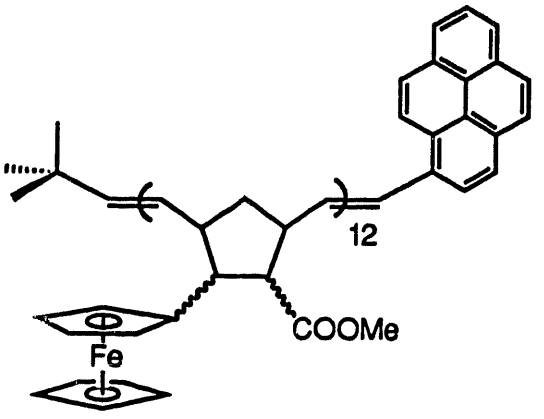

$(Fc)_{12}$-pyrene

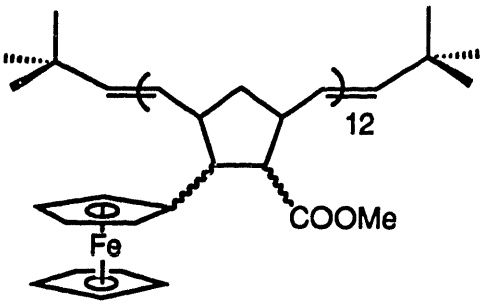

$(Fc)_{12}$

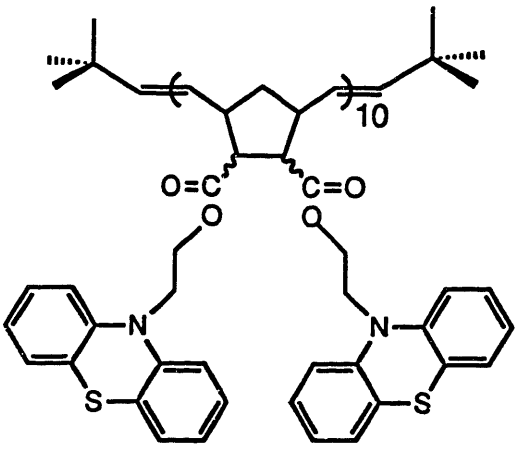

$(Phz)_{30}$

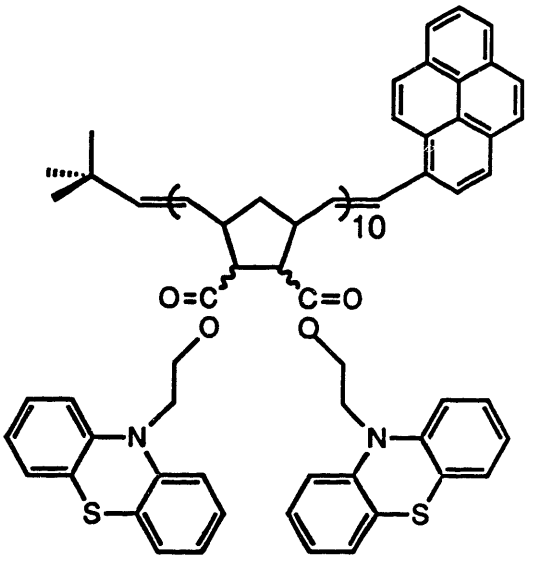

$(Phz)_{30}$-pyrene

cleaved, and the freshly exposed surfaces were soaked in the two solutions. The electrochemical response of the C electrodes was checked periodically. The results after 25 min, 10 h, and 55 h of soaking are shown in Figure 8. There is essentially no change in the relative coverage of the $(Fc)_{12}$ and $(Phz)_{15}$ polymers. The affinity of the pyrene for C surfaces did not overcome the adsorption of either polymer.

Surface Linking Reactions. Surface linking reactions between a nucleophile and an electrophile, where one is bound to the electrode and the other is a part of the polymer can provide covalently bound polymer molecules. The process is illustrated in Scheme I. This methodology was examined for two systems, shown in Chart VI, where the polymer or the surface each contain the nucleophile or the electrophile.

In the first system, ITO electrodes were treated with *p*-(chloromethyl)phenyltrichlorosilane and then soaked at room temperature in CH_2Cl_2 solutions containing $(Phz)_{10}$ or $(Phz)_{10}$-pyridine for 24 h. The electrochemical responses are shown in Figure 9. Also shown is the response from an ITO electrode dipped for 10 min into a solution in which *p*-(chloromethyl)phenyltrichlorosilane and $(Phz)_{10}$-pyridine had been reacted for 24 h. The treated ITO electrode that was soaked in $(Phz)_{10}$ solution shows very little faradaic current, whereas the treated electrode soaked in the solution with the Phz polymer with a pyridine end group

Figure 8. Competitive binding experiment between $(Fc)_{12}$-pyrene and $(Phz)_{15}$, and, $(Fc)_{12}$ and $(Phz)_{15}$-pyrene. Each half of a freshly cleaved 3 mm glassy carbon rod was immersed into a benzene solution containing one of the pairs of polymers (2 mg/mL). The rods were periodically removed from the soaking solution, rinsed thoroughly with benzene, and then checked for their electrochemical response in CH_2Cl_2/0.1 M [*n*-Bu_4N]PF_6. Following this, the rods were rinsed again and placed back into the soaking solution. The figure shows the electrochemical response after 25 min, 10 h, and 55 h of soaking time. The electrode area, estimated to be ~1.4 cm^2, is ill-defined due to the act of cleaving the rod.

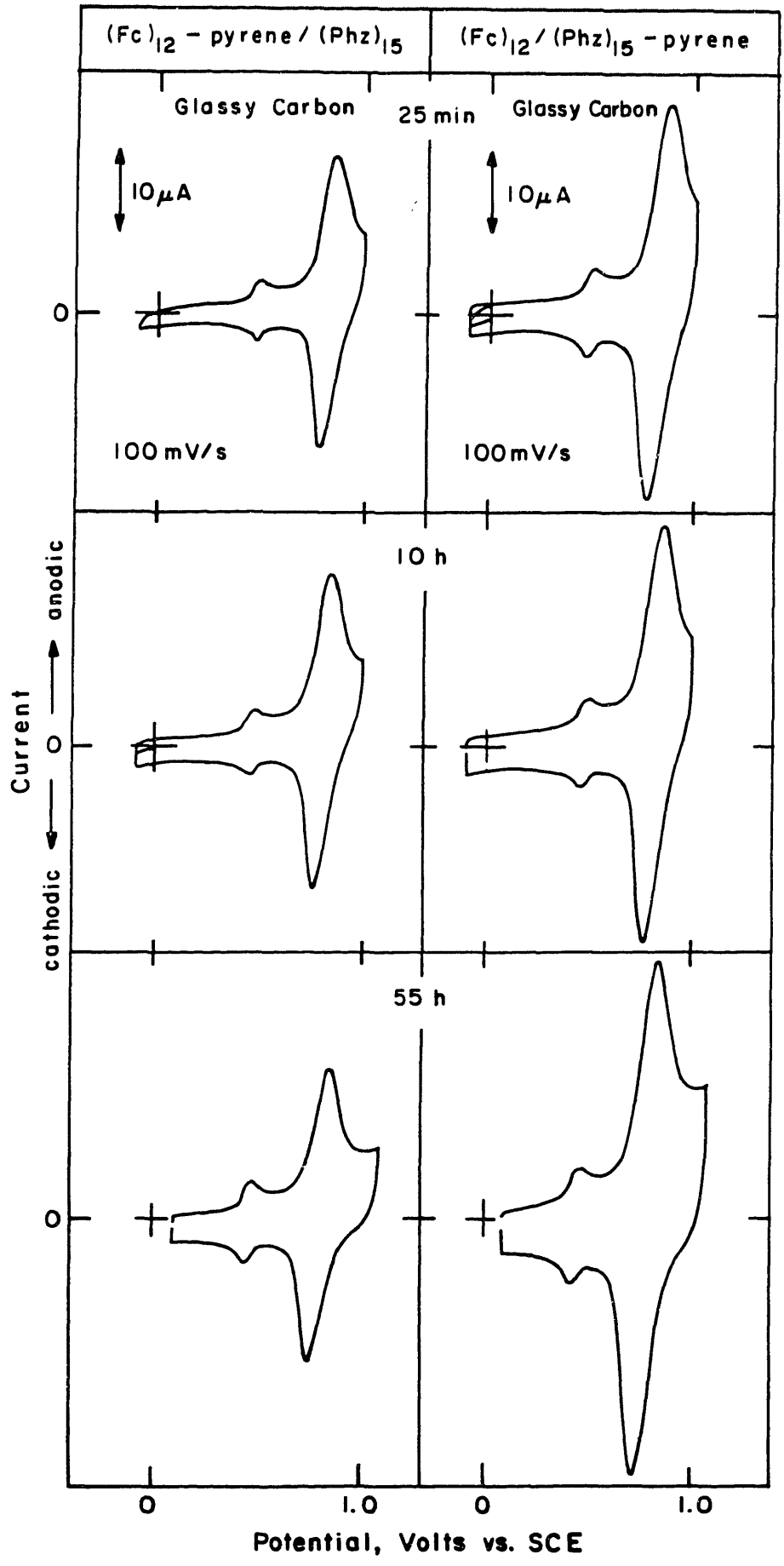
(Fc)12 – pyrene / (Phz)15
(Fc)12 / (Phz)15 – pyrene
Glassy Carbon
25 min
Glassy Carbon
10μA
10μA
0
100 mV/s
100 mV/s
10 h
Current
anodic
cathodic
0
55 h
0
0
1.0
0
1.0
Potential, Volts vs. SCE

Scheme I. Process For Linking a Polymer to a Surface Via Reaction Between a Surface-Bound Reagent and a Polymer-Bound Reagent.

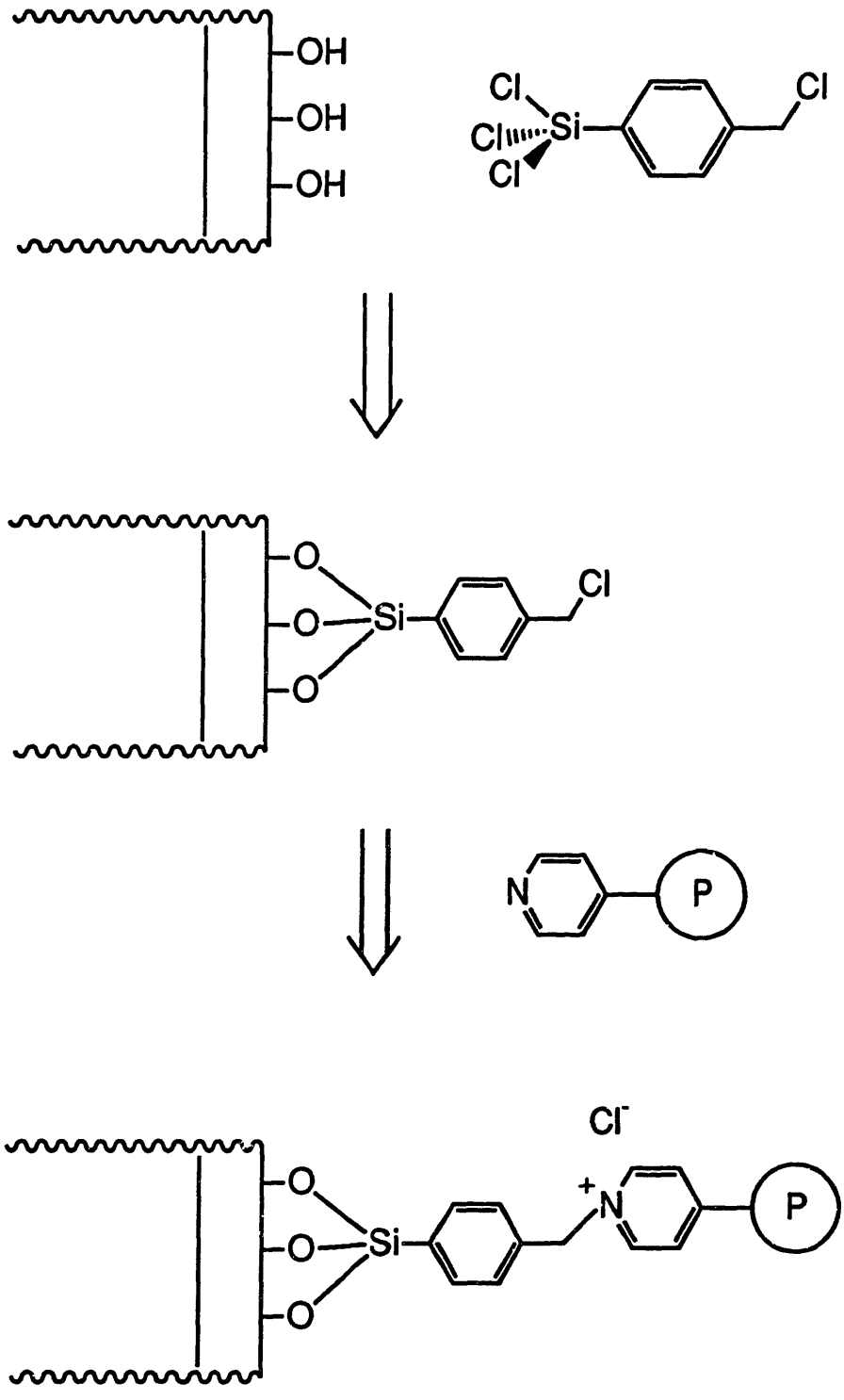
OH
OH
OH
Cl
Cl
Cl
Si
Cl
O
O
O
Si
Cl
N
P
Cl⁻
+
N
P
O
O
O
Si

Chart VI. Polymers Used in Surface Linking Reactions.

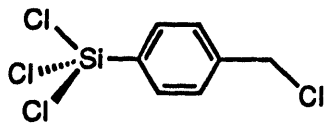
Cl
Cl
Cl
Si
Cl

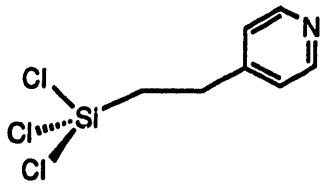
N
Cl
Cl
Cl
Si

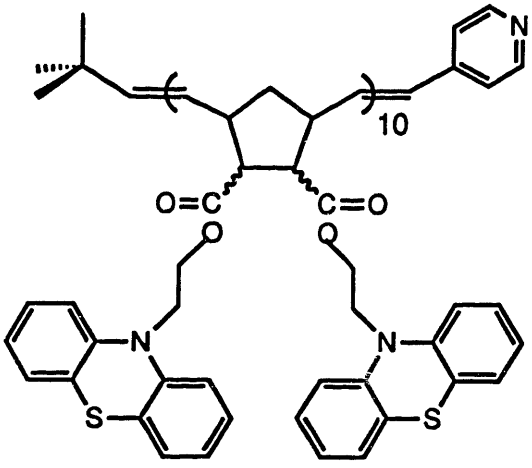
N
10
O=C
C=O
O
O
N
N
S
S

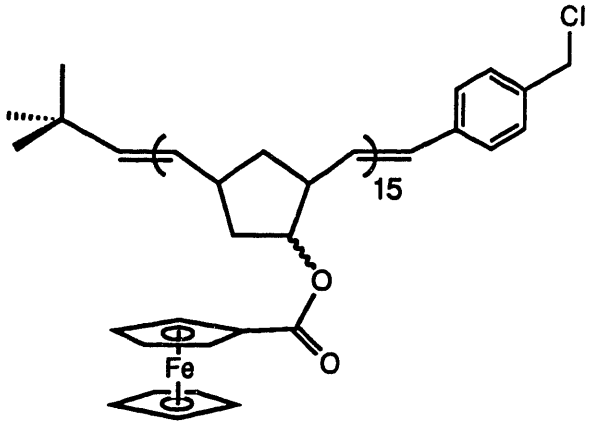
Cl
15
O
O
Fe

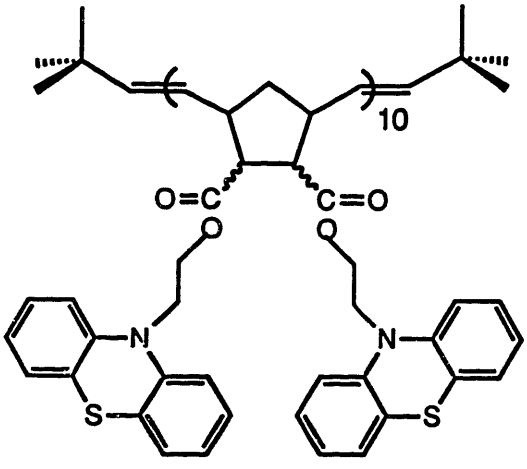
10
O=C
C=O
O
O
N
N
S
S

Figure 9. Cyclic voltammograms at 100 mV s^{-1} for (a) an untreated ITO electrode, (b) an ITO electrode treated with *p*-(chloromethyl)phenyltrichlorosilane, followed by a 24 h soak in a CH_2Cl_2 solution of $(Phz)_{10}$, (c) an ITO electrode treated with *p*-(chloromethyl)phenyltrichlorosilane, followed by a 24 h soak in a CH_2Cl_2 solution of $(Phz)_{10}$-pyridine, and (d) an ITO electrode soaked for 10 min in a solution of *p*-(chloromethyl)phenyltrichlorosilane and $(Phz)_{10}$-pyridine that had reacted for 24 h.

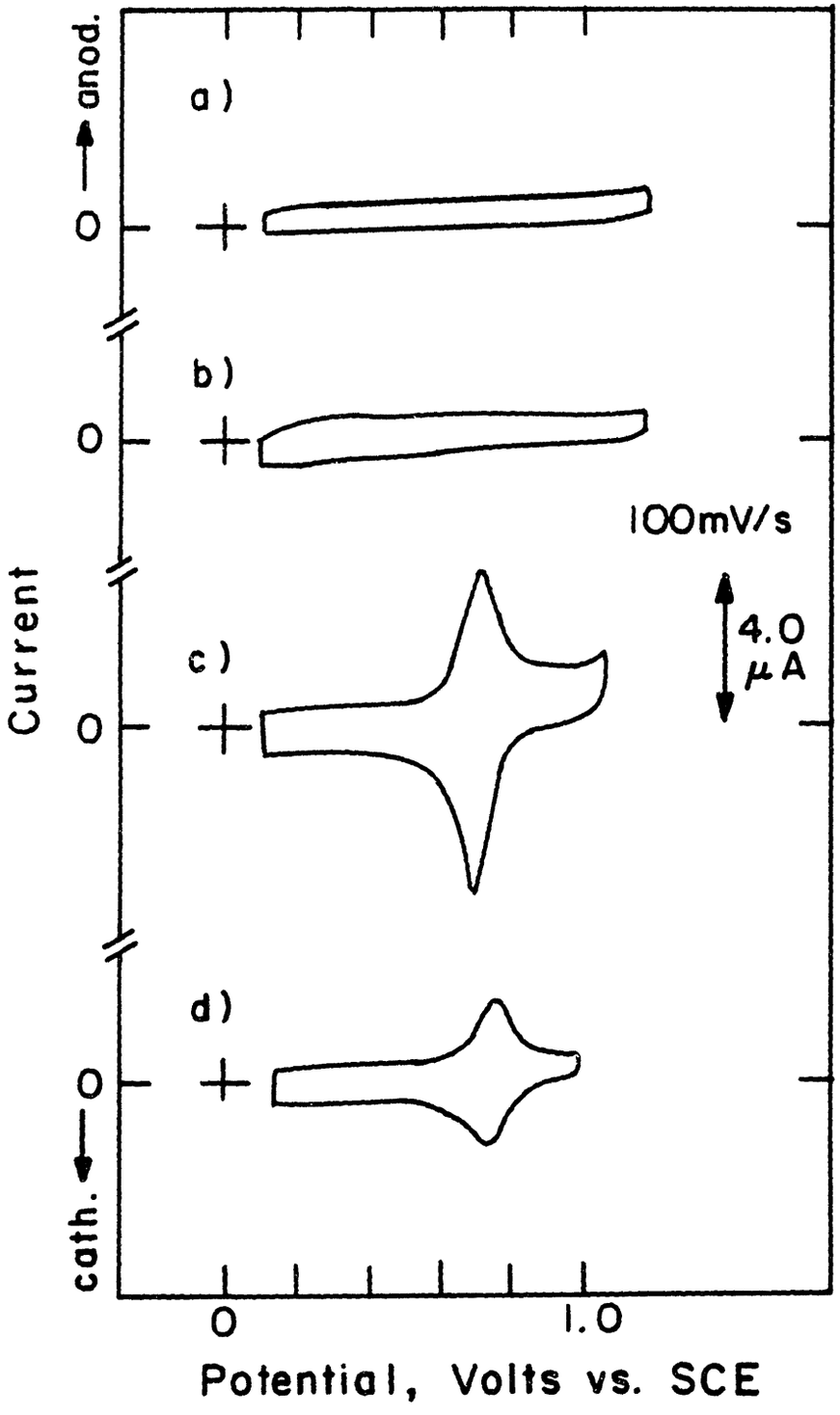
anod.
a)
0
b)
0
100mV/s
4.0
μA
Current
c)
0
d)
0
cath.
0
1.0
Potential, Volts vs. SCE

shows a persistent surface redox wave, with coverage of 1 x 10^{-10} mol cm^{-2} of Phz centers, of 5 x 10^{-12} mol cm^{-2} of polymer. The two reagents could be reacted prior to surface treatment, to produce what is effectively a triethoxysilyl end-capped polymer. Upon brief exposure of an ITO electrode to the solution of *p*-(chloromethyl)phenyltrichlorosilane and $(Phz)_{10}$-pyridine, a derivatized electrode was obtained, with a coverage of 3.3 x 10^{-11} mol cm^{-2} of Phz centers, or 2 x 10^{-12} mol cm^{-2} of polymer.

In the other system, a polymer made with the monomer 5-norbornene-2-(methoxycarbonyl)ferrocene, FcCE, was end-capped with an electrophile and the ITO surface was pretreated with 4-[2-(trichlorosilyl)ethyl]pyridine, to give a surface-bound pyridine. The synthetic route to the monomer is shown in Scheme II. Treated and untreated ITO surfaces, with and without a bound pyridine, were soaked in separate solutions of $(FcCE)_{15}$-benzylbromide for 24 h. The resultant electrochemical response is shown in Figure 10. There is a smaller coverage of FcCE on the untreated electrode corresponding to 6 x 10^{-12} mol cm^{-2} of FcCE, or 4 x 10^{-13} mol cm^{-2} of polymer. The pyridine treated surface soaked with $(FcCE)_{12}$-benzylbromide produced a derivatized electrode with larger coverage, 1.1 x 10^{-10} mol cm^{-2} of FcCE centers, or 8 X 10^{-12} mol cm^{-2} of polymer.

Scheme II. Synthetic Route to 5-Norbornene-2-(methoxycarbonyl)ferrocene.

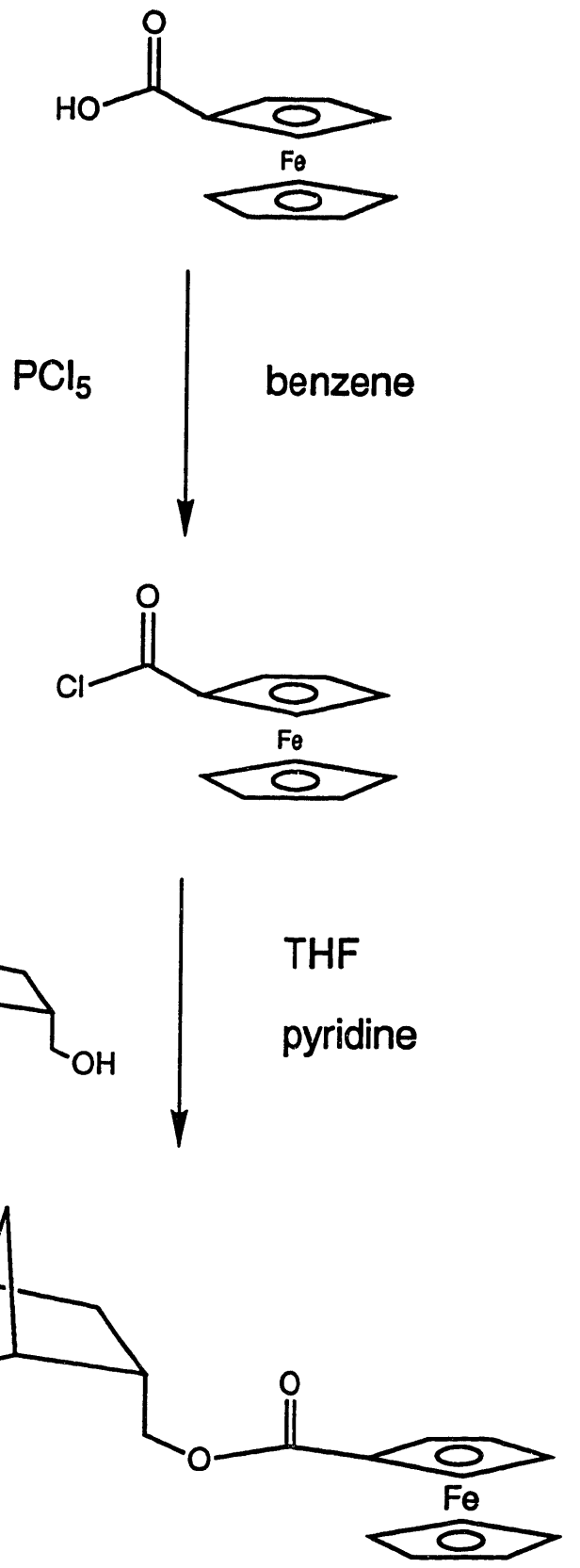
HO
O
Fe
PCl5
benzene
Cl
O
Fe
OH
THF
pyridine
O
O
Fe

Figure 10. Cyclic voltammograms at 100 mV s^{-1} for (a) an untreated ITO electrode that was soaked in $(FcCE)_{15}$-benzylbromide for 24 h, and (b) an ITO electrode treated with 4-[2-(trichlorosilyl)ethyl]pyridine, followed by a 24 h soak in $(FcCE)_{15}$-benzylbromide. The observed coverage of FcCE is 6 x 10^{-12} mol cm^{-2} in (a), and 1.1 x 10^{-10} mol cm^{-2} in (b).

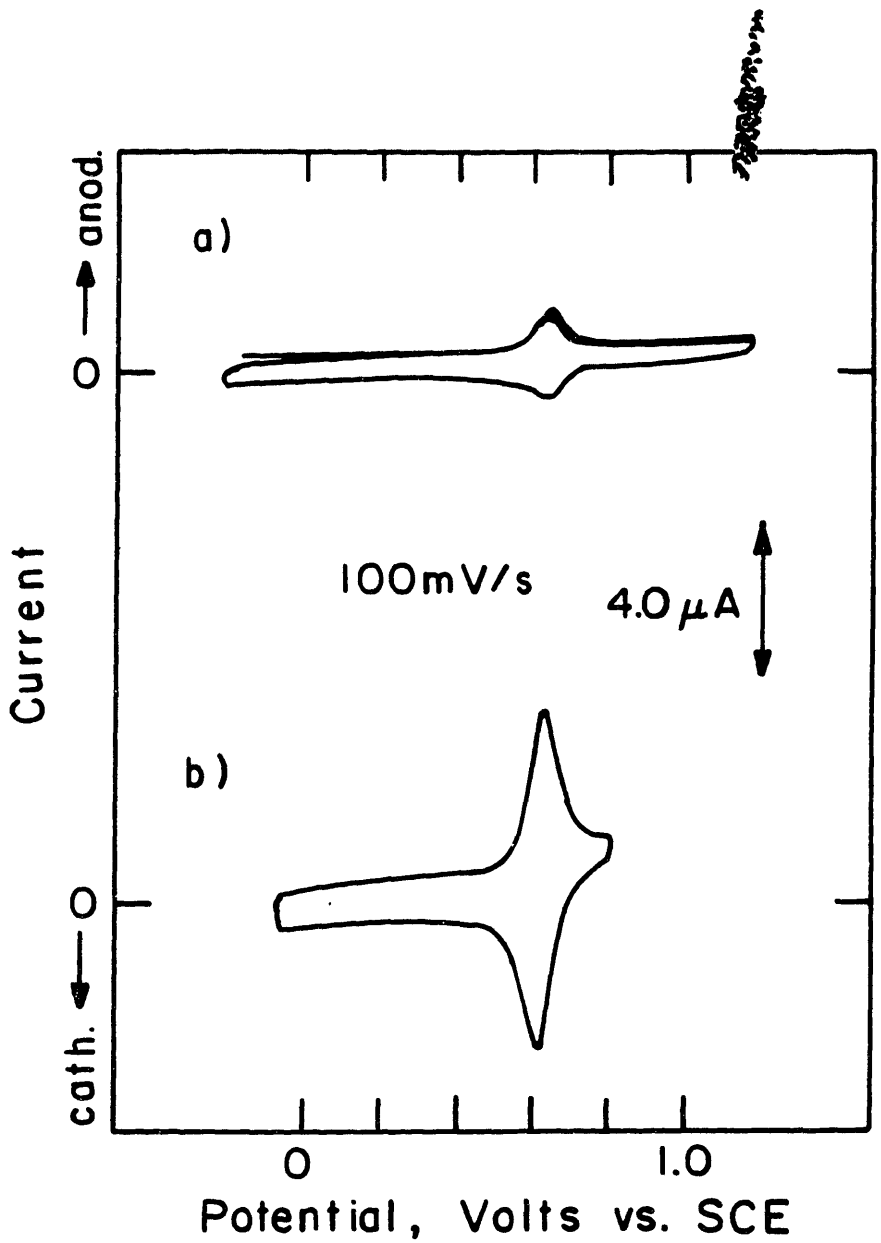
a)
b)
anod.
cath.
0
0
100mV/s
4.0 μA
Current
0
1.0
Potential, Volts vs. SCE

Conclusion

In the methods tried for derivatizing electrode surfaces with functionalized polymers none have produced multilayer coverages where the polymer has only a small portion of itself confined at the surface and the remainder chain-extended away from the surface. The same limiting coverages are observed in all cases, on the order of ~1 x 10^{-10} mol cm^{-2} of redox centers. (Si) containing polymers bind to Pt, ITO, and n-Si electrodes to give persistent films. For polymers as large as $(Phz)_{30}$, the (Si) group is solely responsible for the polymer binding to the electrode surface. Block polymers containing a polyalkylated ferrocene show large solvent effects compared to Fc/Nrb block polymers. Using pyrene capping groups to selectively adsorb to C surfaces is not effective. A single pyrene group cannot compete with the entire polymer for adsorption sites on C surfaces. Surface linking reactions between electrophiles, benzylhalides, and nucleophiles, pyridines, yield derivatized surfaces.

References

1. Murray, R. W. in *Electroanalytical Chemistry;* Bard, A. J., Ed.; Dekker: New York, NY, 1984; Volume 13, 191.

2. Deschler, U.; Kleinschmit, P.; Panster, P. *Angew. Chem. Int. Ed. Engl.* **1986**, *25*, 236.

3. *Silanes Surfaces and Interfaces;* Leyden, D. E., Ed.; Chemically Modified Surfaces, Volume 1; Gordon and Breach Science Publishers: New York, NY, 1986.

4. Tundo, P.; Venturello, P.; Angeletti, E. *J. Am. Chem. Soc.* **1982**, *104*, 6547.

5. Brown, A. P.; Anson, F. C. *J. Electroanal. Chem.* **1977**, *83*, 203.

6. Jaegfeldt, H.; Kuwana, T.; Johansson, G. *J. Am. Chem. Soc.* **1983**, *105*, 1805.

7. Brown, A. P.; Koval, C.; Anson, F. C. *J. Electroanal. Chem.* **1976**, *72*, 379.

8. Zou, C-F.; Wrighton, M. W. *J. Am. Chem. Soc.*, in press.

PART 2

AN INVESTIGATION OF THE CLAIMS OF COLD FUSION

Chapter V

Introduction to the Cold Fusion Episode

On March 23, 1989 in Salt Lake City, UT at a press conference held by the University of Utah, Martin Fleischmann and B. Stanley Pons announced their findings from an experiment attempting to induce deuterium nuclei to fuse inside a Pd lattice. The two are reported to have been conducting such experiments over the past five years, funding it themselves (~$100,000) and at first doing the work at home. The idea stemmed from puzzling results obtained in earlier experiments on the diffusion of hydrogen isotopes in palladium hydrides. According to Fleischmann, "[we thought] the idea was so stupid that nobody would want to fund it, but [we thought] the experiment had to be tried". Nonetheless, their claim of a net power output of 10 W cm^{-3} was followed by a period of world-wide interest in the testing of their claims.

The seemingly simple experiment consisted of the electrolysis of a D_2O/0.1 M LiOD solution in a pyrex flask using a Pd cathode and a Pt anode at moderate voltages and current densities. In the electrolysis, D (or H or T) is absorbed into the bulk of the Pd cathode until there is a D/Pd of about 1. Pons and Fleischmann wondered if two D nuclei might fuse under such conditions; their experiments indicated they did. When their measurements of nuclear particles produced did not yield the same fusion rate as calculated from the calorimetric experiments they

hypothesized there was a "hitherto unknown nuclear reaction" occurring. To those who study nuclear physics, the nuclear reactions are considered 'known', and furthermore they wondered why Pons and Fleischmann were still alive, given the success of the experiment. The flux of nuclear radiation from D-D fusion at the rates necessary to produce the level of excess heat they claimed is lethal.

At that first press conference the only details learned by interested or puzzled experimenters were that Pd, Pt, and D_2O were used in a vacuum-jacketed cell. But despite the lack of information the race was on to duplicate the experiment. From ad-hoc interdisciplinary research teams to garage tinkerers, innumerable workers set off to see if fusion energy was finally to be a reality. The first thing to do was to get some Pd and D_2O. Companies began to run advertisements highlighting the materials needed for cold fusion experiments. But those who did not act quickly found that the stock shelves were empty. Less than a week after the press conference the major commercial suppliers in the US had sold out of Pd. At MIT the purchase of D_2O was restricted to prevent unsupervised experimentation. The supply of Pd was of interest to more than just those in the labs. On the Futures Market the price of Pd was driven up by speculators to ~30% over its pre-"cold fusion" price.

* * *

On March 23, 1989, in Cambridge, MA, a group of students and post-docs from the Wrighton group had assembled at the Thirsty Ear Pub in Ashdown House. The TV, tuned to the evening news program silently flashed its images to a room filled with the sounds of the stereo and the conversational din. Dr. Richard Crooks though caught notice of Pons and Fleischmann on the screen, but before the TV sound could be turned up the story was over. The group concluded that if this news was important they would read about it in Friday's newspaper.

By Saturday, several Wrighton group members had joined up with a staff scientist at the Plasma Fusion Center, Marcel Gaudreau, and his battery of undergraduates from Theta Delta Chi for a day of experimenting. The details of the Utah experiment, however, were still unknown. They still had not reported the composition of the electrolyte solution, the electrochemical parameters or the time needed to produce the effect. Undaunted, electrochemical cells were set up in a shielded area and a neutron detector situated above the cell. The electrolyses were carried out at higher and higher voltages, but there were no indications of fusion. The final measure tried was a series of 7000 V pulses of several μs duration. The ionized material formed a green plasma near the electrodes, but there was no evidence that anything

unusual, such as fusion, might be occurring. The session ended, at 6:00 AM, in futility.

Monday morning, as Vince Cammarata, Dick Crooks, Martin Schloh and myself were reviewing the scant facts in the newapapers and wondering what to try next, we received a phone call from Marcel: he was in Utah at Pons' laboratories, and full of information. By late afternoon we had driven across Massachusetts and New Hampshire and procured D_2O, LiD for the preparation of the electrolyte, and the last 6 mm rod of Pd at Johnson Matthey. (The office of Johnson Matthey lies within the shadow of the Seabrook Nuclear Power Plant.) That evening our first four cells were assembled and the electrolyses started.

These experiments were set up in the far corner of a 50' x 50', three story vault with 6' concrete walls. This area was awaiting the arrival and installation of the new Tokomak reactor, but for the time being was the site for the cold fusion in a test tube experiments. During the first days interested and curious onlookers visited throughout the day. In that first week copies of the two papers, from Pons and Fleischmann and Jones *et al* were received by fax, and a tape of the CNN coverage of the press conference was obtained. Shortly thereafter a proposal for funding and support was drafted and submitted, and there was discussion of making a trip to the University of Utah.

After the burst of activity and excitement came a gradual letdown as the number of negative reports increased. Our experiments were shut down after another generation of cells had been designed and run, and while in the midst of preparing a third generation cell. Since there was no evidence of nuclear processes or anomalous heat and no new experimental details revealed by Pons and Fleischmann it was time to leave this experiment. In the meantime a second type of experiment had been set up at Brookhaven National Laboratories.

Following the announcement by Pons and Fleischmann a puzzling question was by what mechanism the reaction could be taking place. Among the speculations was the idea that muons in cosmic rays might be a catalyst. Muon catalyzed D-D fusion, first discovered in 1954, has been studied with renewed interest recently. In fact, the term "cold fusion" was originally applied to this muon-induced fusion reaction. In these reactions, though, the target that the muon source irradiates is a chamber of gaseous or liquid D_2/T_2. Heavy mass elements are known to capture muons efficiently, so the presence of the cathode would seem to be inhibitory. However, the muon capture cross-sections in a hydrided metal were not known, and it was postulated that D-μ formation followed by muon-induced fusion could procede within this metal hydride lattice. Professor Min Chen, from the MIT

Physics Department, proposed the experiment to test this idea. One of the few muon sources in the world is located at Brookhaven, and space on the muon line was available.

* * *

There were many who criticized Pons and Fleischmann for announcing their findings in a press conference rather than in the usual scientific forums. In their defense, it's their risk, and besides, how can you regulate a breakthrough? However, dramatic public press announcements raise the expectations of the audience. Newscasts showed file footage of the ocean surf, commenting that according to Pons' and Fleischmann's result the ocean could supply enough deuterium to fuel energy plants for a long, long, long time. So, on the other hand, they have a responsibility to both the scientific community and to the public. To other scientists they owe research that can be reproduced, and that has been substantiated by proper control experiments. And towards the public they should act in accordance with the trust in which they receive their financial support.

This rings idealistic, and more and more it is. There can be a variety of competing motives involved. It is too simple to harangue Pons and Fleischmann for going public, there was much more at stake than just a scientific finding. They and the university could expect to gain financially by this as others have recently done with patented university research.

Situations in science where conflicts of interest arise are a larger issue, but not appropriately discussed here.

The way in which *other* scientists worked after their announcement, in following up their claim in terms of its merit as a scientific finding did not follow the usual process either. Work done in the labs responded to new information on an almost daily basis. A variety of networks carried news and information as fast as one could take it in. Each morning certain newspapers, especially the Wall Street Journal, the New York Times and the Washington Post were paged through for announcements and reports. As the press called around to the researchers for their stories they became sources themselves as they passed along what they had found out from others. Alliances were forged as each group wanted to learn about what went on in the "closed scientific sessions" or the "closed press conferences". Bulletin boards on computer networks served as a source of information, theories, idle speculation, worries, and jokes. Summaries and detailed commentary of the proceedings of 'cold fusion' sesions at conferences were posted in these bulletin boards. Some groups posted manuscripts of papers they were submitting to journals.

These networks, of computers and fax machines, and the daily newspaper are not how one typically hears of scientific findings, and press conferences are not typically held to

announce one's work. Although, in the beginning of the cold fusion episode holding a press conference was the norm. Confirming results were announced, or theoretical explanations were summarized to the roomful of reporters for dissemination. This practice did not continue long however as those who spoke out so quickly realized errors in their work and were soon retracting their statements. Conducting "science by press conference" became a derogatory cliche for this whole episode.

After one year, what is the status of the cold fusion research? Pons and Fleischmann appeared at a couple of scientific meetings early on and then six months after their first announcement presented new results at the International Society of Electrochemistry Meeting in Kyoto, Japan. These results did not seem to convert either the skeptics or the believers. They have yet to publish a second paper. Nor have results from ^{4}He assays of their cathodes been released yet, though these were due in October 1989.

At the National Cold Fusion Institute, set up adjacent the campus of the University of Utah in August, 1989, with funds appropriated by the Utah Legislature to develop the technology, they are working to reproduce the effect. The Director, Dr. H. Rossi, interviewed after four months of operation stated that so far none of the cells were producing excess heat--it is a bit unnerving.

Other groups are trying to understand some anomalous heat bursts, neutron bursts, and the source for some of the high ^3H levels reported. As yet none of these events are correlated. There are grants available to investigate these anomalous events (no one is calling it fusion). In the outcome, these anomalous effects intrigue some, but practical electrolytic fusion power is not to be.

For all the effort expended in this episode some lessons have been learned. The value of circumspection and patience, of not proclaiming success before careful checks have been made is one lesson. Also, the value of experience, in this case embodied in the multidisciplinary teams that assembled to try to duplicate the experiment, is appreciated.

Most lessons needed to be relearned. Foremost among them is the issue of control experiments. A fundamental part of any experimental study are the controls. Unfortunately for Pons and Fleischmann, they made their announcement without doing any control experiments, such as using H_2O in place of D_2O, to solidify and help verify their claim. Other lessons concerned reproducibility and instrument calibration. Some relearned these, to their chagrin, in the days following a press conference they had held.

Other research groups, inspired by the claims from Utah, have been led to try other methods to induce fusion. Two of these new attempts at fusion, at Brookhaven National

Laboratories, and at Nagoya University, Japan, which have yielded evidence of nuclear fusion products, are one beneficial result of the Utah claims, though still no practical energy sources have been found.

This episode could be studied by historians of science, pyschologists and sociologists, as it provided a glimpse at the often supressed side of the workings of science. The upshot is all of this activity will be preserved in books and TV programs; the authors and producers are now covering the grounds, picking what memories they can out of those involved. In retrospect though it is difficult to recall the flow of events with daily resolution, and without the influence of later events.

The public will probably recall this episode as Discover magazine sums it up: "the biggest science story of the year, and its biggest flop". To those in science, some lessons have been learned, but it is time to return to our work.

* * *

At MIT, a group made from the Chemistry, Physics, and Materials Science and Engineering Departments and the Plasma Fusion Center came together to examine the claims of Pons and Fleischmann about nuclear fusion occuring in D_2O electrolysis cells using Pd cathodes. The experiments are described in Chapters VI and VII. A sociological account of this

experiment has been written in the August, 1989 issue of Boston Magazine.

Chapter VI presents experiments intended to duplicate the conditions of the experiment reported by Pons and Fleischmann to try to reproduce their result.

In Chapter VII, an experiment performed at Brookhaven National Laboratories using the muon source to irradiate metal hydrides is presented. The rationale for this experiment was that muons present in cosmic rays were suggested to be the agent inducing fusion in the metal hydrides. This hypothesis was tested under a controllable and high muon flux, where the equivalent of several days of natural irradiation by cosmic muons could be achieved in minutes.

Chapter VI

Measurement and Analysis of Neutron and Gamma Ray Emission Rates, Other Fusion Products, and Power in Electrochemical Cells Having Pd Cathodes[a]

[a]The work described in this chapter represents a collaborative effort and has been submitted for publication in the Journal of Fusion Energy. The co-authors are: David Albagli, Vince Cammarata, Richard M. Crooks, Martin O. Schloh, and Mark S. Wrighton, from the Department of Chemistry; X. Chen, Catherine Fiore, Marcel J. P. Gaudreau, C. K. Li, Paul Linsay, Stanley C. Luckhardt, Ronald R. Parker, Richard D. Petrasso, and Kevin W. Wenzel, from the Plasma Fusion Center; and Ron Ballinger and I. Hwang, from the Department of Nuclear Engineering and the Department of Materials Science and Engineering.

Chapter Outline

Introduction

Solid State Chemistry of Pd

Experimental

Electrodes and Electrolyte Solutions

Pd-D Loading Factor

Results and Discussion

1 Phase I Experiments

2. Phase II Cell and Calorimeter Configurations

A. Cell

B. Calorimeter

3. Phase II Power Measurements

4. Radiation Measurements

A. Neutron Measurements

B. γ-Ray Measurements

5. Fusion Product Analysis

A. Gas Phase

B. Liquid Phase

C. Solid Phase

6. Surface Analysis of Pd Cathodes

7. Critique of the γ-Ray Spectroscopy

8. Comments on Calorimetry

A. Refinements

B. Critique of the Calorimetric Results

Conclusion

References

Introduction

There have been three recent reports of nuclear fusion processes occurring at room temperature inside metal lattices.[1-3] Two of these[2,3] report only very low levels of neutron emission, and although perhaps important from a fundamental viewpoint, they hold no promise of scale-up as a viable commercial energy source. However, the claim of Fleischmann, Pons, and Hawkins[1] (FPH) involves large and easily detectable levels of excess power and nuclear fusion products. It is to the latter report that these experiments were addressed.

FPH reported electrochemical experiments that resulted in the generation of excess heat, tritium, and neutron emission.[1] They concluded that the rate of excess heating and the presence of typical fusion products could only be accounted for by invoking a heretofore unknown nuclear fusion process since the quantity of fusion products detected was many orders of magnitude lower than expected on the basis of the claimed power output. The reports from FPH have centered on the generation of excess heat in electrochemical cells containing Pd cathodes, Pt anodes, and $LiOD/D_2O$ electrolyte solutions, operated at current densities in the range 8-512 mA/cm^2 and at voltages between 2-10 V. The FPH radiation measurements have been critiqued,[4] having been found to contain serious omissions and inaccuracies. As a result of this analysis the γ-ray spectroscopic results have been retracted by Fleischmann,[5] and later reasserted[6] along lines

which still contain equally fundamental errors.[4b] At present there are two additional reports[7,8] which corroborate the level of excess heating reported by FPH, and one report of fusion products.[9] Importantly, there has been no report of excess heat generation correlated with observation of fusion products from the same cell despite efforts to exactly replicate the FPH experiment. Modifications to the FPH experiment intended to enhance the reported effects have similarly failed to yield excess heat or fusion products.[10] In addition to research activity among experimentalists there has been considerable effort directed towards a theoretical understanding of processes that might be responsible for cold fusion, but the consensus has generally been negative.[10-13]

The purpose of this investigation was to replicate as nearly as possible the experimental procedure of FPH. Accordingly, we have used information from the refereed scientific literature[1,6] or presented by FPH at scientific meetings in designing these experiments.[14,15] Furthermore, in determining what represents relevant evidence for nuclear fusion, we have focused our measurements and analyses on D-D fusion branches, Table I,[16] eq A-C. However, our measurements are sensitive to fusion products generated by all of the reactions shown in Table I except eq F.

At high temperatures eq A and B, Table I, have branching ratios of about 50%,[16] while eq C is suppressed by $\sim 10^7$. These branching ratios are energy dependent and may not apply to fusion reactions at low energy, although similar results

Table I. Nuclear Fusion Reactions[a]

Reaction	Equation
A	$D + D \rightarrow n$ [2.45 MeV] + ^{3}He [0.82 MeV]
B	$D + D \rightarrow H$ [3.02 MeV] + T [1.01 MeV]
C	$D + D \rightarrow \gamma$ [23.8 MeV] + ^{4}He [0.08 MeV]
D	$D + {}^{6}Li \rightarrow n$ [2.96 MeV] + ^{7}Be [0.43 MeV]
E	$D + {}^{6}Li \rightarrow {}^{4}He$ [11.2 MeV] + ^{4}He [11.2 MeV]
F	$D + {}^{6}Li \rightarrow H$ [4.39 MeV] + ^{7}Li [0.63 MeV]
G	$D + {}^{7}Li \rightarrow n$ [13.36 MeV] + ^{8}Be [1.67 MeV]
	$\rightarrow n$ [13.36 MeV] + ^{4}He [0.85 MeV] + ^{4}He [0.85 MeV]
H	$D + {}^{7}Li \rightarrow \gamma$ [16.7 MeV] + ^{9}Be [0.02 MeV]
I	$D + {}^{7}Li \rightarrow p + {}^{8}Li$ (endoergic, −1.01 MeV)
	$\rightarrow \rightarrow p + {}^{4}He$ [8.05 MeV] + ^{4}He [8.05 MeV]
J	$D + {}^{7}Li \rightarrow T + {}^{6}Li$ (endoergic, −1.81 MeV)

[a]From Reference 16.

have been measured for low energy, muon-catalyzed fusion.[17] Fleischmann[15] has suggested that eq C might be enhanced in cold fusion, and that it could be responsible for the presence of excess power in the absence of commensurate levels of neutrons and tritium.

The first phase (Phase I) of these experiments was begun shortly after the announcement of cold fusion by FPH. Because of the limited time available for implementation of Phase I, the techniques and error limits were relatively crude. Nevertheless, the level of sensitivity was sufficient for detecting the magnitude of excess power and neutron emission claimed by FPH. Phase I experiments are summarized in Results and Discussion, Section 1.

The second phase (Phase II) of the investigation featured improved accuracy and data acquisition, and a more thorough analysis of the Pd cathodes, electrolyte solutions, and effluent gases for fusion products. The cells were analyzed by the following means: 1) constant temperature calorimetry; 2) neutron counting and γ-ray spectroscopy; 3) mass spectral analysis of ^4He in effluent gases, and ^4He and ^3He within the Pd lattice; 4) tritium analyses of the electrolyte solutions; and 5) X-ray photoelectron spectroscopy of the Pd cathode surface.

Within the estimated levels of accuracy, which are given in individual sections of this report, no evidence was found of any excess power output, fusion products, or any other

evidence of nuclear fusion occurring in electrochemical cells modeled after those described by FPH.[1,14,15]

Solid State Chemistry of Pd.

The absorption of H or D by metallic Pd has been extensively investigated.[18,19] The face-centered cubic Pd host lattice expands as H or D atoms begin occupying octahedral sites and forming PdH_n or PdD_n solid solutions.[20] Recent theoretical calculations of the structure of H or D in Pd clusters[21] and in bulk Pd[22] suggest that even at the very high H or D concentrations postulated to exist in PdD_2, the equilibrium distance between two D atoms is ~0.2 Å larger than the D_2 intramolecular spacing of 0.74 Å.[22]

Below 300 °C, the PdH_n or PdD_n homogeneous solid solution can exist in two phases; a hydrogen-poor α phase and a hydrogen-rich β phase. Values for the maximum H/Pd ratio at which the α phase can exist, α_{max}, and for the minimum H/Pd ratio necessary to form the β phase, β_{min}, are $\alpha_{max} = 0.008$ and $\beta_{min} = 0.607$ at 25 °C.[19] At T = 25 °C and P = 1 atm the maximum H/Pd loading ratio which can be achieved by gas charging is about 0.7.[23] Electrolytically prepared hydrides with H/Pd loading ratios as high as 0.9 have been reported, however these materials are unstable at ambient conditions and slowly lose hydrogen upon standing.[23] In practice the maximum D/Pd ratio that can be obtained by electrolysis of D_2O varies with the conditions of the electrolysis and on the pretreatment of the Pd cathode. However, for cathodes which

have been equilibrated with air at T = 25 °C and P = 1 atm, a value in the range D/Pd = 0.7-0.8 is widely accepted.[19] It has been estimated that the flux of H into Pd upon electrolysis of H_2O is ~10^{16} molecules/cm^2-s.[24] Based on this value and the dimensions of the Pd cathodes, Tables II and III, we can estimate the time needed to reach a loading of D/Pd ~0.7 to be about 215 h for Phase I and 33 h for Phase II electrodes.

In addition to absorbing hydrogen isotopes, electrolytic Pd/D_2O-electrolyte solutions exhibit an inverse isotope effect. That is, the higher mass isotopes will concentrate in the liquid phase relative to either the gas or solid phase.[27,28] Therefore, upon extended electrolysis in D_2O electrolyte solutions in which hydrogen and tritium are present at low concentration, the solution phase will become enriched in the heavier isotopes and the Pd cathode will become enriched in the lighter isotopes. When determining the tritium content of cells thought to be generating tritium by nuclear processes, the presence of tritium above the background level may only indicate preferential concentration of tritium in the solution by the normal separation process described above.

Experimental

Specific experimental details relating to calorimetry, nuclear measurements, and the assays of fusion products are reported in individual sections.

Table II. Phase I Cell Parameters

Cell	Electrode Size (cm) Preparation	Electrolyte Current Density Range (mA/cm^2)[a]	Start (m/d/y)	Stop (m/d/y)
A	0.64 x 2.5 solvent rinse	0.1 M LiOD 35-175	3/27/89	5/19/89
B	0.64 x 2.5 solvent rinse	0.1 M LiOD[b] 35-175	3/27/89	5/19/89
C	0.10 x 2.5 solvent rinse	0.1 M LiOD 64-950	3/28/89	4/19/89
E	0.64 x 2.5 700°C/vacuum	0.1 M LiOD 35	3/28/89	4/7/89
F	0.64 x 2.5 700°C/vacuum	0.1 M LiOD 40-280	4/1/89	5/19/89

[a]The current density was periodically varied between these limits for the duration of the experiment.

[b]2 M $LiNO_3$ added after 3 days.

Table III. Phase II Cell Parameters

Parameter	H_2O Cell	D_2O Cell
Cathode	Pd Rod 0.1 x 9 cm	Pd Rod 0.1 x 9 cm
Anode	Pt wire 0.5 x 70 cm	Pt wire 0.5 x 70 cm
Electrolyte	0.25 M LiOH/H_2O	0.25 M LiOD/D_2O
Volume	55 mL	55 mL
Current	196 ± 2 mA	195 ± 2 mA
Current Density	69 mA/cm^2	69 mA/cm^2
Voltage	2.86 ± 0.03 V	2.88 ± 0.03 V
Start Time	4/20/89 (9:45 h)	4/20/89 (18:30 h)
Stop Time	4/29/89 (16:15 h)	4/29/89 (16:15 h)
Duration	223 h	213 h

Preparation of Electrodes and Electrolyte Solutions.

A Pd (99.96%) rod (0.64 x 10 cm) (Johnson Matthey/Aesar, Seabrook, NH) was cut into four 2.5 cm long sections and used in Phase I experiments, Table II. Pd wire 0.1 cm in diameter (Engelhard, Iselin, NJ) was used in the remaining Phase I experiments and in Phase II. The pretreatment of Phase I cathodes is shown in Table II. Phase II cathodes were degassed by heating to 725 °C in vacuum prior to use. Pt (99.99%) anodes were fashioned from 0.1 cm wire (Johnson Matthey/Aesar, Seabrook, NH).

The D_2O/LiOD electrolyte solutions were prepared by addition of LiD powder (98% D; Alfa Products, Danvers, MA) to D_2O (Phase I: 99.9% D, lot number F11G; Phase II: 99.8% D, lot number F7962; Cambridge Isotope Laboratories, Medford, MA) under an inert atmosphere. The H_2O/LiOH electrolyte solutions were prepared by mixing glass distilled H_2O (EM Science, Cherry Hill, NJ) and LiOH (Alfa Products, Danvers, MA) in air.

Pd-D Loading Factor.

To ascertain a lower bound on the loading factor reached at the end of the Phase II experiments the Pd cathodes were degassed by heating and the evolved gas collected. Under the conditions of degassing, T = 260 °C, P = 1 atm, the ratio H/Pd is known to fall to ~0.02.[25] The Pd rods were heated until degassing ceased, about 1 h, and the loading factors were calculated based on the volume of gas expelled, and independently by the change in weight of the Pd rods. The

average loading ratios were found to be 0.75 ± 0.05 and 0.78 ± 0.05 for the D and H loaded cathodes respectively. These values indicate that during Phase II experiments the cathodes were loaded with D or H near the maximum level, and were well into the Pd β phase. Similar analyses of some Phase I rods indicated slightly lower D/Pd loading in the range 0.6-0.7.

Results and Discussion

1. Phase I Experiments.

The Phase I experiments were begun within a few days of the announcement of cold nuclear fusion. The hastily assembled Phase I apparatus allowed simple calorimetry, neutron counting, and γ-ray spectroscopy.

The single compartment glass cells were suspended in air and contained D_2O/0.1 M LiOD, Pd rod cathodes, and helically wound Pt wire anodes (~0.1 x 20 cm) mounted coaxially with the Pd cathode. Gases generated during electrolysis were vented through a mineral oil bubbler fitted with a drying tube to prevent contamination of D_2O by atmospheric H_2O. The Pd cathode pretreatment, duration of electrolysis, electrolyte concentration, and range of current densities are shown in Table II. The measured D/Pd loading factor in the cathodes tested was ~0.62 ± 0.05 indicating these cathodes were in the Pd β phase.

Cell temperature was monitored by continuously recording the voltage of a chromel-alumel thermocouple in thermal contact with the exterior wall of each cell. The

relationship between temperature and power was calibrated by inserting a 15 ohm resistor into the cell and recording the temperature rise as a function of electrical power dissipated in the resistor. The calibration was nearly linear over the temperature range of interest and had a slope of 0.2 W/°C. Variations in cell temperature of 1.5 °C were easily detectable, making the resolution of the Phase I calorimeter ~0.3 W. For 0.4 x 10 cm Pd rod cathodes operating at 64 mA/cm^2 FPH reported an excess power of 1.4 W/cm^3.[1] Based on the volume of the Phase I electrodes, and assuming similar excess power gain for these slightly larger diameter cathodes, we expected to observe at least 1.1 W of excess power, a value within the resolution of our calorimeter. However, over the course of the Phase I experiments we did not observe any changes in cell temperature except those related to changes of input power level, electrolyte volume, ambient temperature, and other experimental variables.

Neutron emission was measured using a moderated BF_3 detector which was absolutely calibrated with a Pu/Be source emitting $1.5 \times 10^6 \pm 6 \times 10^4$ n/s.[29] During calibration the geometry of the source relative to the Phase I detector, D_n1, closely approximated that of the electrochemical cells and detector. The measured background rate of the detector was 0.7 ± 0.02 cts/min which is equivalent to a source strength of 216 n/s at a distance of 1 m between the source and the detector; in Phase I this distance ranged from 30 cm to 1 m. For the closest cell, the minimum detectable neutron source

rate would have been 19 n/s. FPH[1] have reported the rate of neutron emission from their cells as 3.2×10^4 n/s-cm^3 for a 0.4 x 10 cm Pd rod operated at 64 mA/cm^2. Normalized to the volume of the Phase I Pd cathodes this corresponds to a source strength of ~2.6×10^4 n/s, or about 1×10^2 above the background level. Accordingly, the level of neutron emission from any "fusing cell" is easily within the detection limit of D_n1.

Figure 1 shows the BF_3 detector counting rate measured during a period of 10 days commencing at the beginning of the electrolysis of cells C and E. The average neutron count rate during the time that the cells operated was 0.7 cts/min. This rate was identical to the background count rate measured after electrolysis was stopped and the cells removed from the room where the experiments took place. Neutron measurements were continued until all cells were disconnected, but throughout this time the background count rate always equaled the average count rate.

FPH[1] originally reported observation of a 2.22 MeV γ-ray line originating from neutron-capture-on-hydrogen, eq 1.

$$n + p \rightarrow D + \gamma \text{ [2.22 MeV]} \qquad (1)$$

They contended that the neutron radiation in their experiment was generated according to eq A, Table I. More recently FPH[6] have suggested that their γ-ray peak actually resides at 2.5 MeV, and is not due to neutron-capture-on-hydrogen. However,

Figure 1. Neutron count rates during Phase I experiments detected using a moderated BF_3 detector (D_n1). Each point corresponds to an 8 hour average. The geometry and efficiency of the detector is described in Section 1.

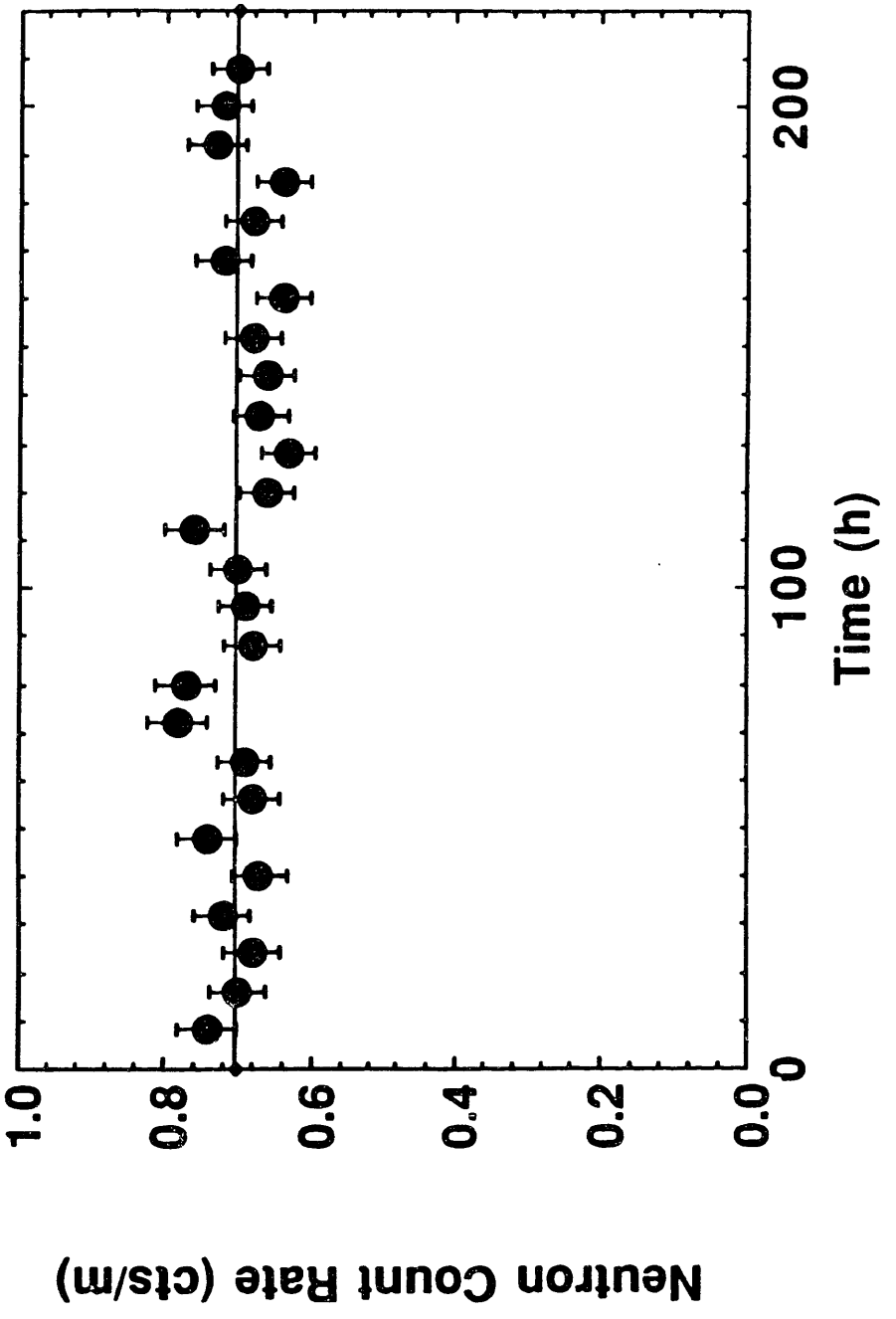
Neutron Count Rate (cts/m)
1.0
0.8
0.6
0.4
0.2
0.0
0
100
200
Time (h)

they are unable to assign this feature to a nuclear process or to account for its unphysical shape.[4b] We measured the γ-ray spectrum in the vicinity of our electrochemical cells with a 3 in. x 3 in. NaI(Tl) crystal spectrometer system over the ranges 0-3 MeV and 0-30 MeV. Water was interposed between the cells and the spectrometer to thermalize the neutrons and permit observation of γ-rays generated according to eq 1. A complete description of the spectrometer, calibration procedure, and an analysis of the FPH data are given in Sections 4 and 7. The important result is that during Phase I experiments no spectral features were detected in the γ-ray spectra except those corresponding to background processes.

FPH[1] reported the presence of tritium in electrochemical cells generating excess power which they ascribed to the presence of a nuclear fusion reaction, eq B, Table I. We also searched for tritium by periodically removing 1-2 mL samples of electrolyte from Phase I cells and analyzing by a procedure detailed in Section 5. However, we did not detect a level of tritium significantly above the measured background level of 300 ± 50 dpm/mL in Phase I cells at any time during electrolysis.

In summary, we analyzed cells modeled after those described by FPH for excess power, neutron and γ-ray emission, and tritium content. Our error limits in all cases would have permitted us to detect the magnitude of changes FPH have contended occur in cells undergoing cold fusion. However, in

Phase I experiments we were unable to reproduce the effects reported by FPH, and we did not observe any evidence for excess power generation or any other nuclear fusion processes.

2. Phase II Cell and Calorimeter Configurations.

A. Cell. The cell used for Phase II experiments is shown in Figure 2a. This design was chosen because it is essentially the same as that employed by FPH.[1] A Pd cathode is supported in the center of the cylindrical Pyrex cell by two Teflon guides. Electrical contact to the cathode was achieved by spot welding a length of Teflon-wrapped Pt wire to the top of the Pd cathode. The Pt anode and a Teflon-coated nichrome heating element are wound helically around two concentric rings of Pyrex tubes. This configuration provided a distributed, axially symmetric heat source and reduced thermal gradients in solution compared to systems using small asymmetrically disposed heating elements. Two tubes in the inner ring, which support the anode, serve as feedthroughs for the temperature monitors. The heater feedback was monitored by a Pt RTD thermometer accurate to 0.1 °C (Omega Engineering, Stamford, CT) enclosed in a thin-walled glass tube filled with mineral oil to ensure good thermal contact between the RTD thermometer and the electrolyte solution. The temperature of the cell was monitored by a similarly configured chromel-alumel thermocouple.

Figure 2. Phase II calorimeter. (a) Cross sectional view of the Phase II cell. The cell height is about 12 cm. (b) Block diagram of the logic of the feedback control system. (c) Test calibration of the calorimeter. The power input to the cell from a standard resistive heat source is plotted against power measured with the constant temperature calorimeter. The input power is accurate within 3%.

(a)

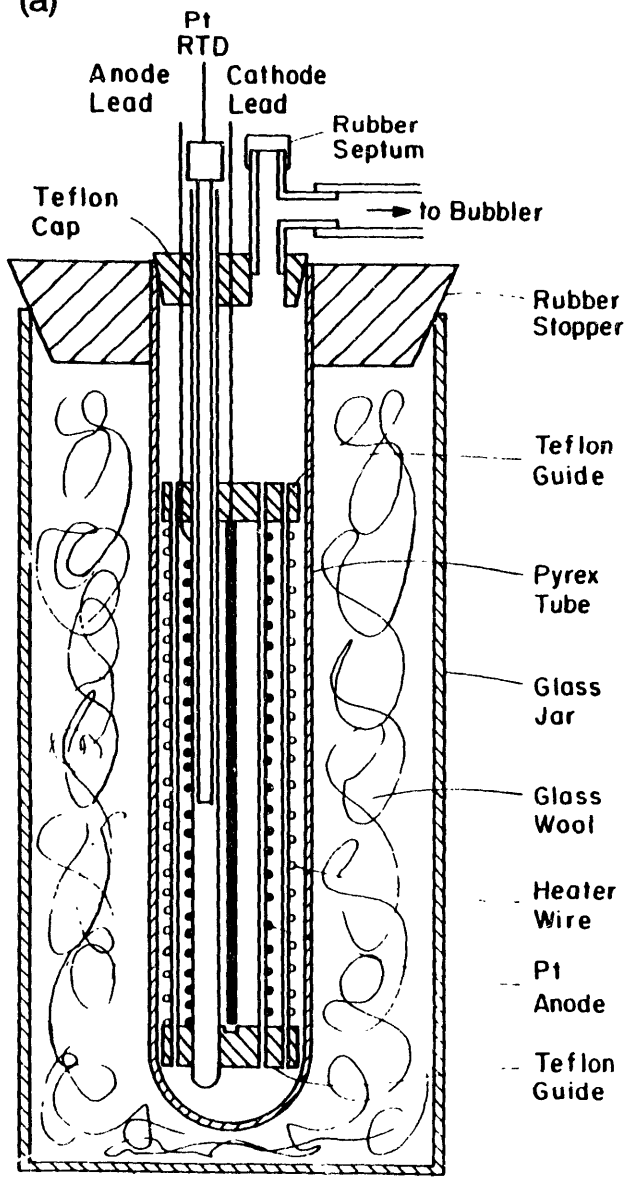
Pt
RTD
Anode
Lead
Cathode
Lead
Rubber
Septum
Teflon
Cap
to Bubbler
Rubber
Stopper
Teflon
Guide
Pyrex
Tube
Glass
Jar
Glass
Wool
Heater
Wire
Pt
Anode
Teflon
Guide

(b)

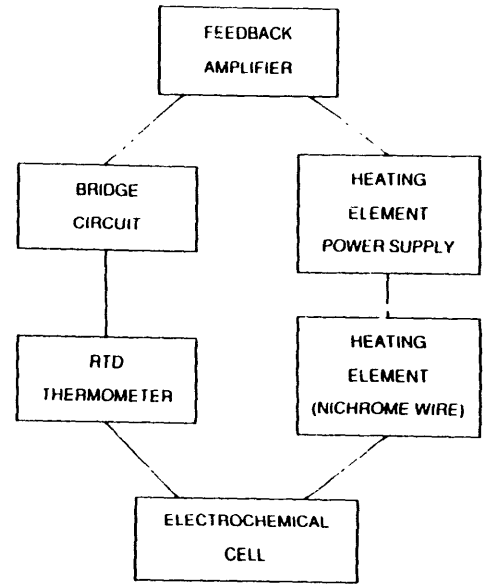
FEEDBACK
AMPLIFIER
BRIDGE
CIRCUIT
HEATING
ELEMENT
POWER SUPPLY
RTD
THERMOMETER
HEATING
ELEMENT
(NICHROME WIRE)
ELECTROCHEMICAL
CELL

(c)

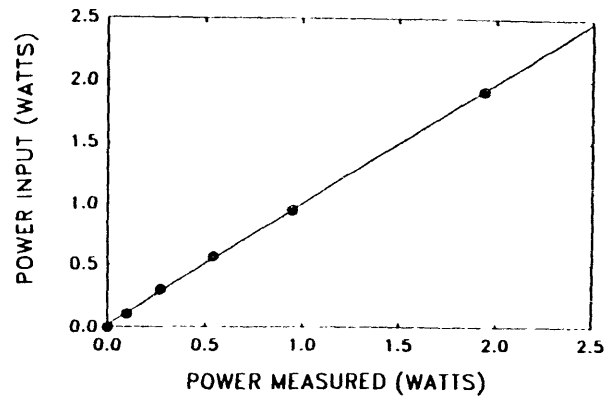
POWER INPUT (WATTS)
2.5
2.0
1.5
1.0
0.5
0.0
0.0
0.5
1.0
1.5
2.0
2.5
POWER MEASURED (WATTS)

The cell was filled with electrolyte solution to a level several centimeters above the top of the upper Teflon support. This ensured that the Pd cathodes, which can act as a D_2/O_2 or H_2/O_2 recombination catalyst, would not be directly exposed to gas in the cell headspace. In addition, this extra volume reduced the need for frequent additions of solvent to replenish that which evaporated or was electrolyzed. As described in Section 3, we found that correction for steady power drifts caused by loss of solvent was possible, but that frequent additions of fresh solvent appeared to cause a decrease in cell power which was more difficult to account for.

Additional holes present in the Teflon supports permitted outflow of the electrolysis gases. However, these holes did not completely eliminate the formation of large bubbles within the cell. Gases were permitted to leave the cell through a mineral oil bubbler vented through a drying tube to prevent contamination of the D_2O-containing electrolyte by atmospheric H_2O. D_2O or H_2O was added to the cells by injection through a gas tight rubber septum. The cell was placed in a glass jar containing glass wool to reduce thermal convection and ensure a fixed thermal transport rate from the cell into the surrounding constant temperature bath.

B. Calorimeter. Phase II experiments utilized a constant temperature calorimeter having a sensitivity of about 40 mW. Constant cell temperature was maintained using

a temperature feedback control system connected to the heating element, Figure 2b. Power fluctuations generated in the cell were detected as changes in the applied heating power. In operation, the temperature signal was compared to a reference setpoint and a correction signal was generated proportional to the difference between the setpoint and the cell temperature. The correction signal was amplified and used to drive a heating element. The cell operating temperature, T_c, was typically 46 °C.

During experimental runs the following cell parameters were continually monitored: T_c; bath temperature, T_b; cell voltage and current, V_c, I_c; and heater voltage and current, V_h, I_h. The data were A/D converted with a multiplexed Hewlett-Packard auto-ranging high precision digital voltmeter, and the thermocouple was referenced to an electronic reference junction. All resulting digital data were stored on disk at a sample period of, typically, 120 s.

3. Phase II Power Measurements.

Under steady state, isothermal conditions the input power to the cell consisted of the cell power, $P_c = I_c V_c$, the heater power $P_h = I_h V_h$, plus any unknown anomalous power in the cell, P_x. Power was lost from the cell through two dominant channels, thermal transport, P_{th}, and loss of the electrolysis products H_2 (or D_2) and O_2, P_e. Thermal transport to the external constant temperature bath took place through a layer of dead air space packed with glass

wool and to a lesser extent to the ambient atmosphere through the top of the cell. Evolution of the reaction products, D_2 and O_2, consumed power at a rate given by $P_e = V_e I_c$, where V_e is the potential associated with the enthalpy change of the electrolysis of water. Recombination of the gaseous products will effectively reduce P_e, and is a significant source of error for calorimetry in open cells when the degree of recombination is not measured. Under steady state conditions the cell power balance equation is given by eq 2.

$$P_h + P_c + P_x = P_{th} + P_e \qquad (2)$$

If thermal gradients in the cell are sufficiently small, as discussed below, and if recombination is negligible, then at constant I_c and V_c, eq 2 reduces to eq 3.

$$P_x + P_h = \text{Constant} \qquad (3)$$

This equation allows the unknown power, P_x, to be determined. If P_x increases, then the feedback control system of the calorimeter reduces P_h to maintain T_c constant.

As a test of our calorimetric method we measured the values of $V_e^{D_2O}$ and $V_e^{H_2O}$. In this experiment T_c was brought to its normal operating value by application of only P_h. When the electrolysis was switched on, P_h decreased to compensate for the power due to Joule heating, $P_c - P_e$, which

is always present in electrochemical cells. By application of eq 4,

$$P_h^o = P_h^f + [P_c-(V_e \times I_c)] \quad (4)$$

where P_h^o and P_h^f are the heater powers before and after the electrolysis is turned on, we can experimentally determine V_e. The results of this experiment gave $V_e^{D_2O} = 1.57$ V and $V_e^{H_2O} = 1.41$ V, compared to the theoretical values which are 1.53 V and 1.48 V, respectively.[30] This measurement indicates that short time scale changes in P_x can be detected with ~5% accuracy.

A significant source of error in calorimetric measurements is the formation of thermal gradients in the cell. For the cell design shown in Figure 2a, streaming of small gas bubbles formed as a result of electrolysis caused sufficient mixing to eliminate thermal gradients. However, when the cell current density was reduced below ~18 mA/cm^2 detectable errors in the cell power balance appeared. In all of the experiments reported here, current densities higher than 18 mA/cm^2 were used. A test of the calorimeter calibration was carried out at $I_c = 0$ using a heating element immersed in the cell. To eliminate thermal gradients during this testing, N_2 was bubbled into the bottom the cell at a rate intended to simulate electrolytic bubbling. Calibration tests using the standard heat source were found to be accurate to within 3% as shown in Figure 2c.

To test for the presence of anomalous power generation in D_2O-containing electrolyte solutions as compared to H_2O-containing electrolyte solutions, the two Phase II cells described in Section 2 were run for approximately 200 hours under galvanostatic conditions, Table III. The cell parameters, I_c, T_c, V_c, and P_h are shown for a 1.2 h period near the end of the run, Figure 3. The data for P_h indicate that there is no significant difference in heat generation between the D_2O cell and H_2O cell to within the 40 mW sensitivity of the calorimetry. Moreover, no excess power was found in any of the cells. The excess power claimed by FPH[1] for 0.1 cm diameter cathodes at 64 mA/cm^2 would be about twice the sensitivity of our calorimeter and if present would have been detectable.

The comparison experiment described above took place over a short period in comparison to the time scale of evaporation and electrolytic decomposition of the solvent. Data which demonstrates the long term stability of the Phase II parameters, I_c, V_c, and T_c, are shown in Figures 4a and 5a. However, measurement of P_h over a 100 h period, Figure 6, indicates a significant drift caused by the reduction of solvent volume. We demonstrated that this drift was due to solvent loss rather than to an unknown power source, P_x, by calibrating P_{th} as a function of electrolyte solution volume. When enough solvent was added to the D_2O cell to compensate for that lost to electrolysis at the end of the 100 h period shown in Figure 6, P_h returned to within 20% of its original

Figure 3. Time history of the Phase II cell current, I_c; temperature, T_c; voltage, V_c; and heater power, P_h; during a 1.2 h period after approximately 200 h of electrolysis.

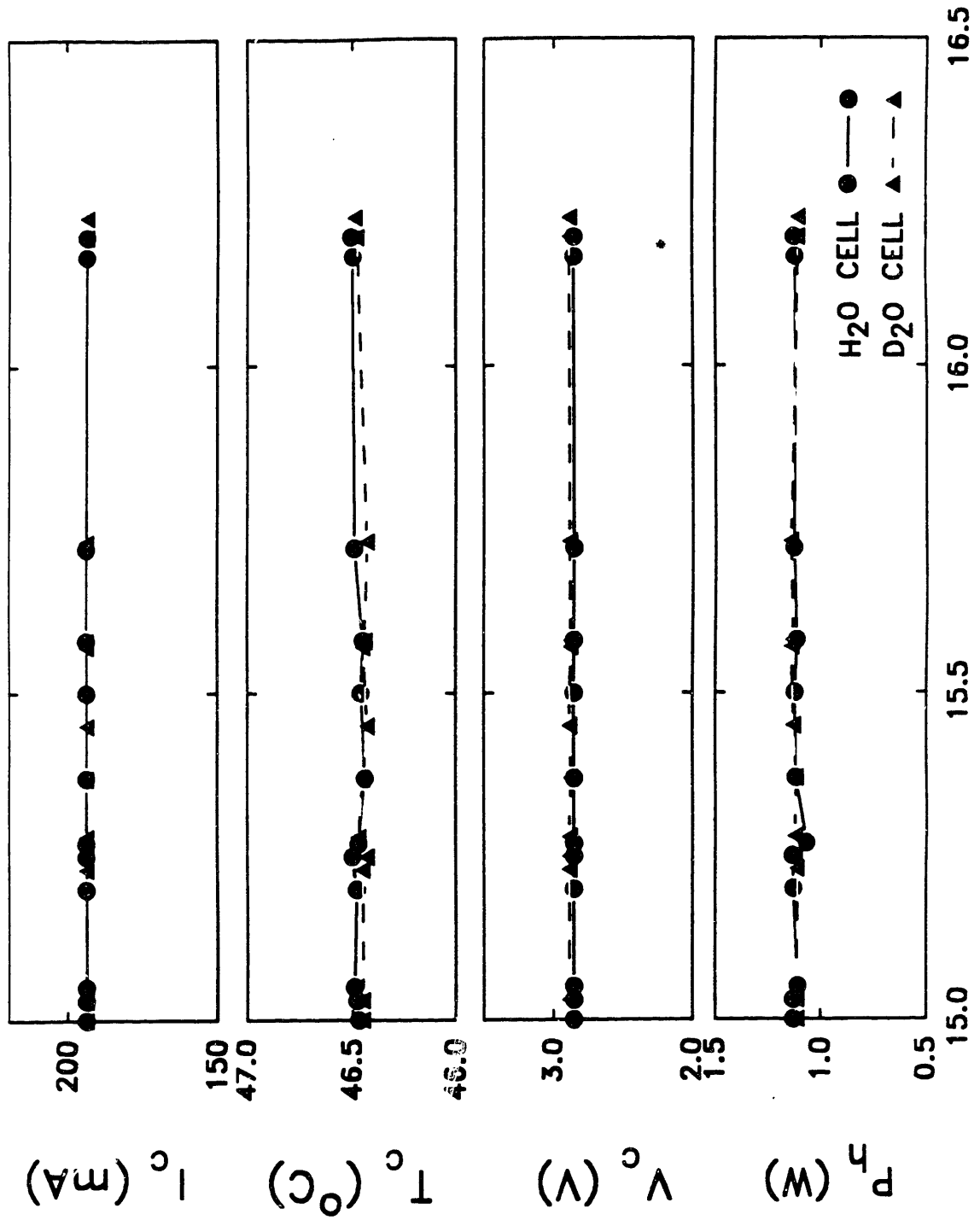
I_c (mA)
200
150
T_c (°C)
47.0
46.5
46.0
V_c (V)
3.0
2.0
1.5
P_h (W)
1.0
0.5
15.0
15.5
16.0
16.5
TIME (h)
H_2O CELL
D_2O CELL

Figure 4. (a) Time history of the cell current, I_C; voltage, V_C; and temperature, T_C, for the Phase II H_2O cell (22:00 h, 4/25/89 - 04:00 h, 4/29/89). At 65 h the set point for the cell temperature was changed from 46.8°C to 46.2°C. (b) Time history of the "anomalous" power, P_X, in the H_2O cell. These data have been time averaged over 1 h blocks. The base line drift caused by solvent loss has been subtracted.

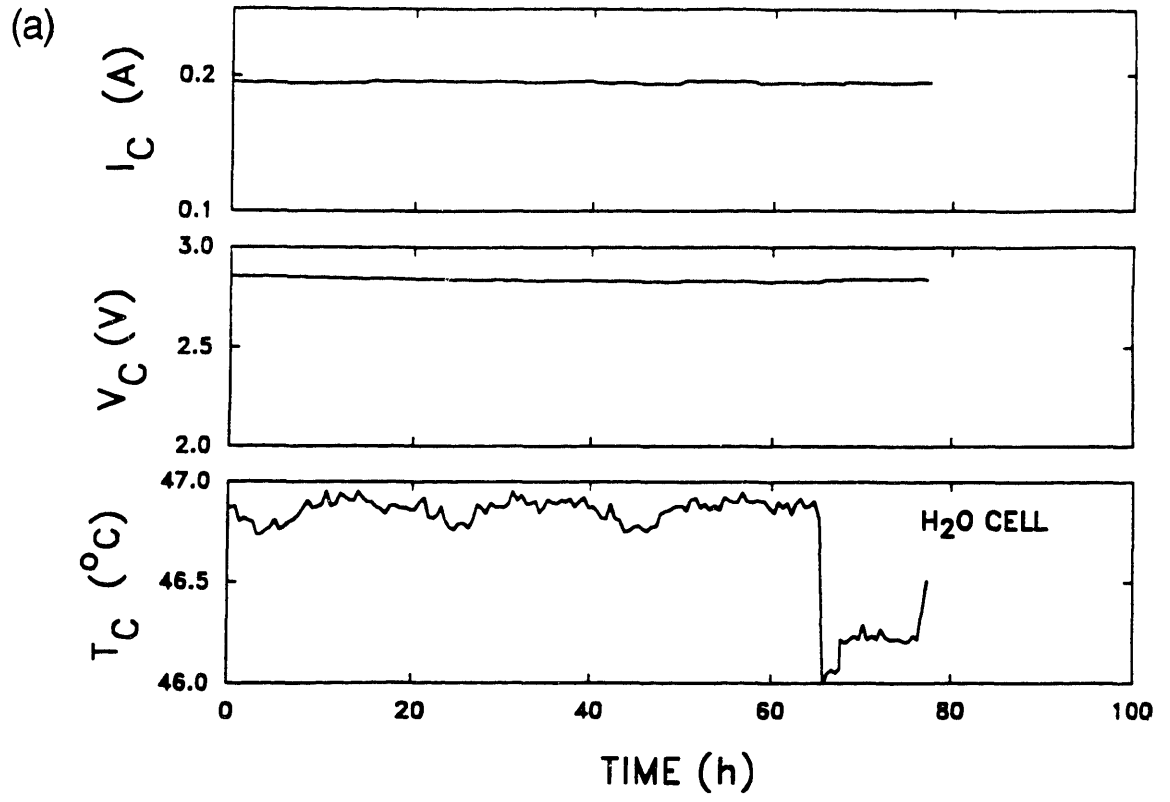
(a)
I_C (A)
0.2
0.1
3.0
V_C (V)
2.5
2.0
47.0
T_C (°C)
46.5
46.0
H_2O CELL
0
20
40
60
80
100
TIME (h)

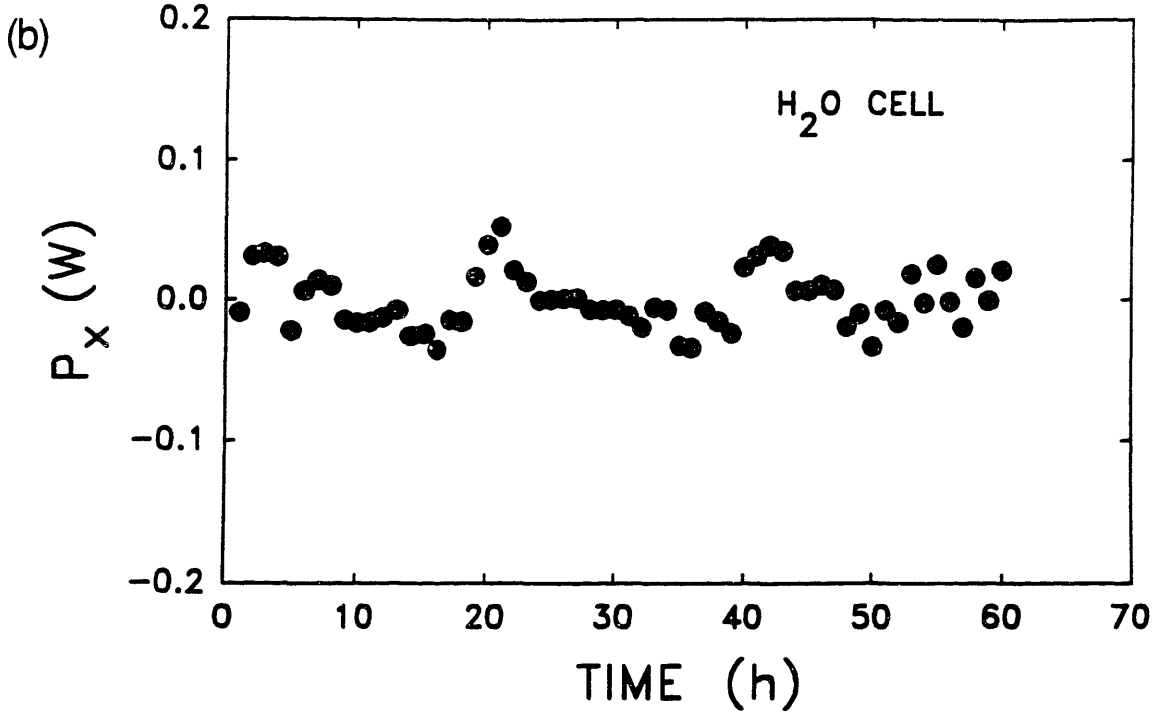
(b)
0.2
0.1
0.0
−0.1
−0.2
P_x (W)
H_2O CELL
0
10
20
30
40
50
60
70
TIME (h)

Figure 5. (a) Time history of the cell current, I_C; voltage, V_C; and temperature, T_C, for the Phase II D_2O cell (8:00 h, 4/23/89 - 3:00 h, 4/28/89). At 15 h the set point for the cell temperature was changed from 46.7 °C to 46.0 °C. (b) Time history of the "anomalous" power, P_X, in the D_2O cell. These data have been time averaged over 1 h blocks. The base line drift caused by solvent loss has been subtracted.

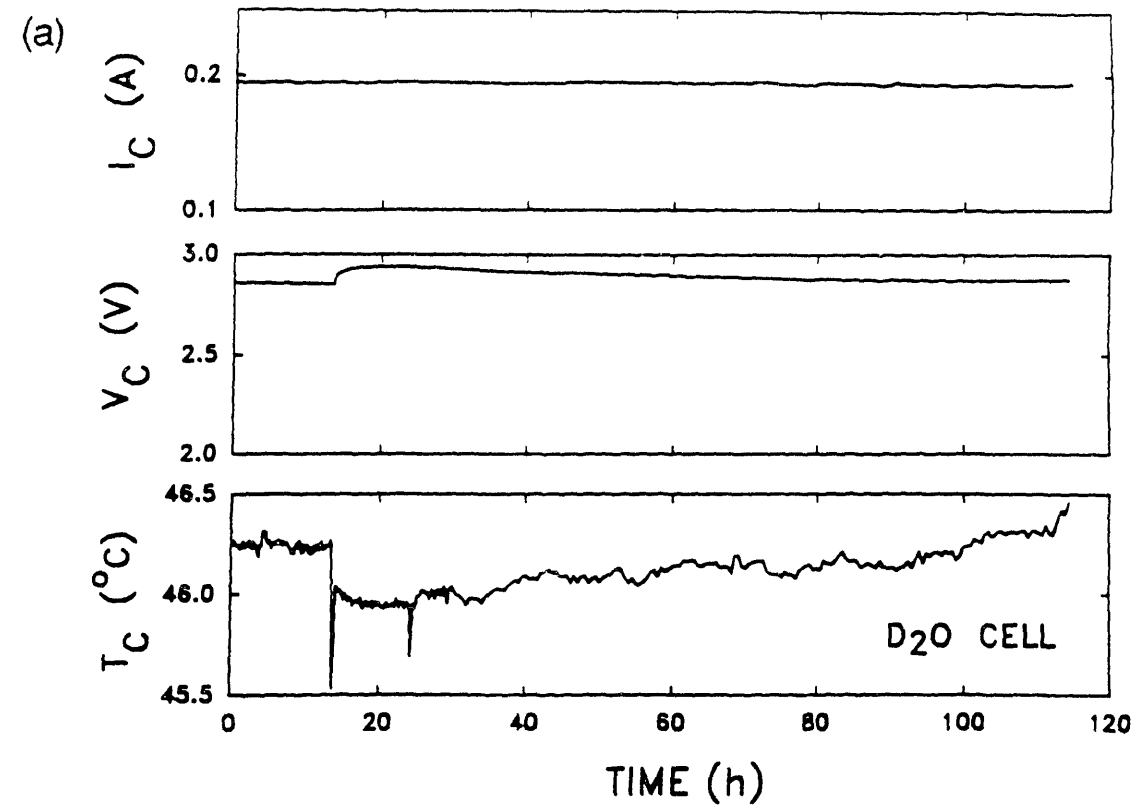
(a)
I_C (A)
0.2
0.1
V_C (V)
3.0
2.5
2.0
T_C (°C)
46.5
46.0
45.5
D_2O CELL
0
20
40
60
80
100
120
TIME (h)

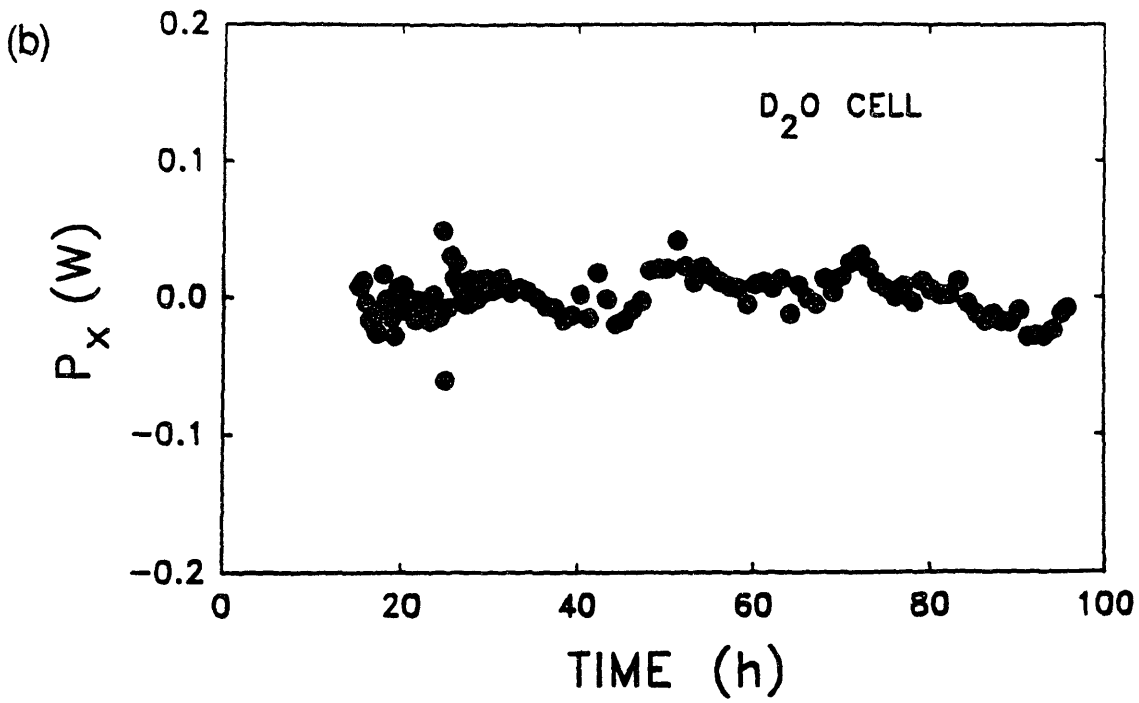
(b)
P_x (W)
0.2
0.1
0.0
−0.1
−0.2
D_2O CELL
0
20
40
60
80
100
TIME (h)

Figure 6. Time history of the calorimeter heater power over a 100 h period of electrolysis for the D_2O cell (8:00 h, 4/24/89 - 12:00 h, 4/28/89). The increase in P_h at 16 h into the run was caused by addition of 5 mL of D_2O to the cell, and the fluctuation 8 h later was intentionally introduced as a time calibration mark. At 3 h the rate of data aquisition was reduced and the trace appears lighter.

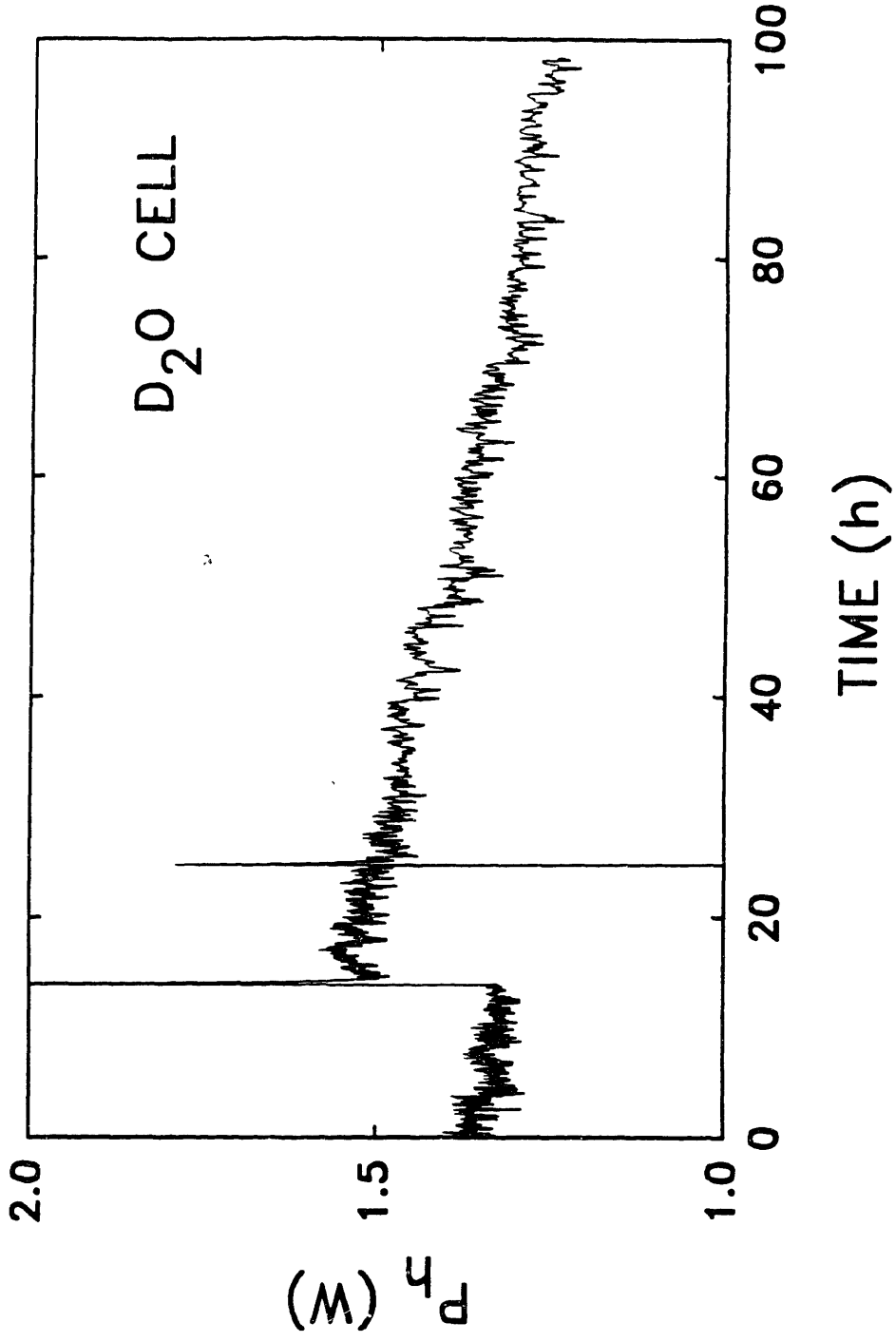
D_2O CELL
P_T (W)
2.0
1.5
1.0
0
20
40
60
80
100
TIME (h)

value. If the total volume of solvent lost over the course of the experiment had been taken into account, including that lost to evaporation, P_h would have been even closer to its original value.

In addition to the steady drift, a high frequency component was also observed in P_h. The magnitude of the high frequency oscillation decreased significantly when the electrolysis reaction was turned off. The long time variation of P_h can best be seen by smoothing the high frequency oscillations using digital filtering, and correcting the sloping baseline by fitting the drift with a linear function and subtracting from the signal, Figures 4b and 5b. The data show a slowly fluctuating power level in both the H_2O and D_2O cells, but neither show evidence of sustained power production at the levels claimed by FPH.[1] For the current density used here FPH reported a power level of 79 mW, a level above the fluctuation level present in Figures 4b and 5b. The low level power fluctuations apparent in Figures 4b and 5b may be caused by a number of processes. For example, gas recombination, bubble trapping, or droplet formation. These effects are discussed in Section 8.

4. Radiation Measurements.

A. Neutron Measurements. The Phase I neutron detector, D_n1, was discussed in Section 1. This detector was operated in a similar configuration in Phase II, however an additional detector, D_n2, was also

present and integrated into the computer data acquisition system. D_n2 was calibrated with the source described in Section 1 and was found to be somewhat less sensitive than D_n1. For D_n2 the average count rate recorded was 0.8 cts/min, Figure 7, which corresponds to a minimum detectable source rate of 42 n/s at the nearest cell (20 cm) and to 10^3 n/s at the farthest one (100 cm). D_n1 was recalibrated using a smaller distance between the source and the detector, however the average background count rate did not change from that found in Phase I, 0.7 cts/min. This corresponds to a minimum detectable signal of 60 n/s from cells which were typically 37 cm from the detector.

The neutron rate reported by FPH was 3.2×10^4 n/s-cm^3. A neutron rate of this magnitude would have appeared on D_n2 as a count rate of between 40 and 1000 times background level, and 650 times background on D_n1. Such signals would have been easily observable, yet no increase in signal above background occurred in either phase of our experiment. While the neutron detectors used were somewhat insensitive and would not have been capable of making a measurement at the level reported by Jones,[2] they were more than adequate to measure an effect as large as that reported by FPH.[1,6]

B. γ-Ray Measurements. The gamma radiation was monitored by two 3 in. x 3 in. NaI(Tl) scintillation detectors. Detector 1, $D_\gamma1$, covered the energy range from 0

Figure 7. Neutron count rates before and during Phase II experiments detected using a moderated BF_3 detector (D_n2). Each point corresponds to an 8 hour average. The geometry and efficiency of the detector is described in Section 4.

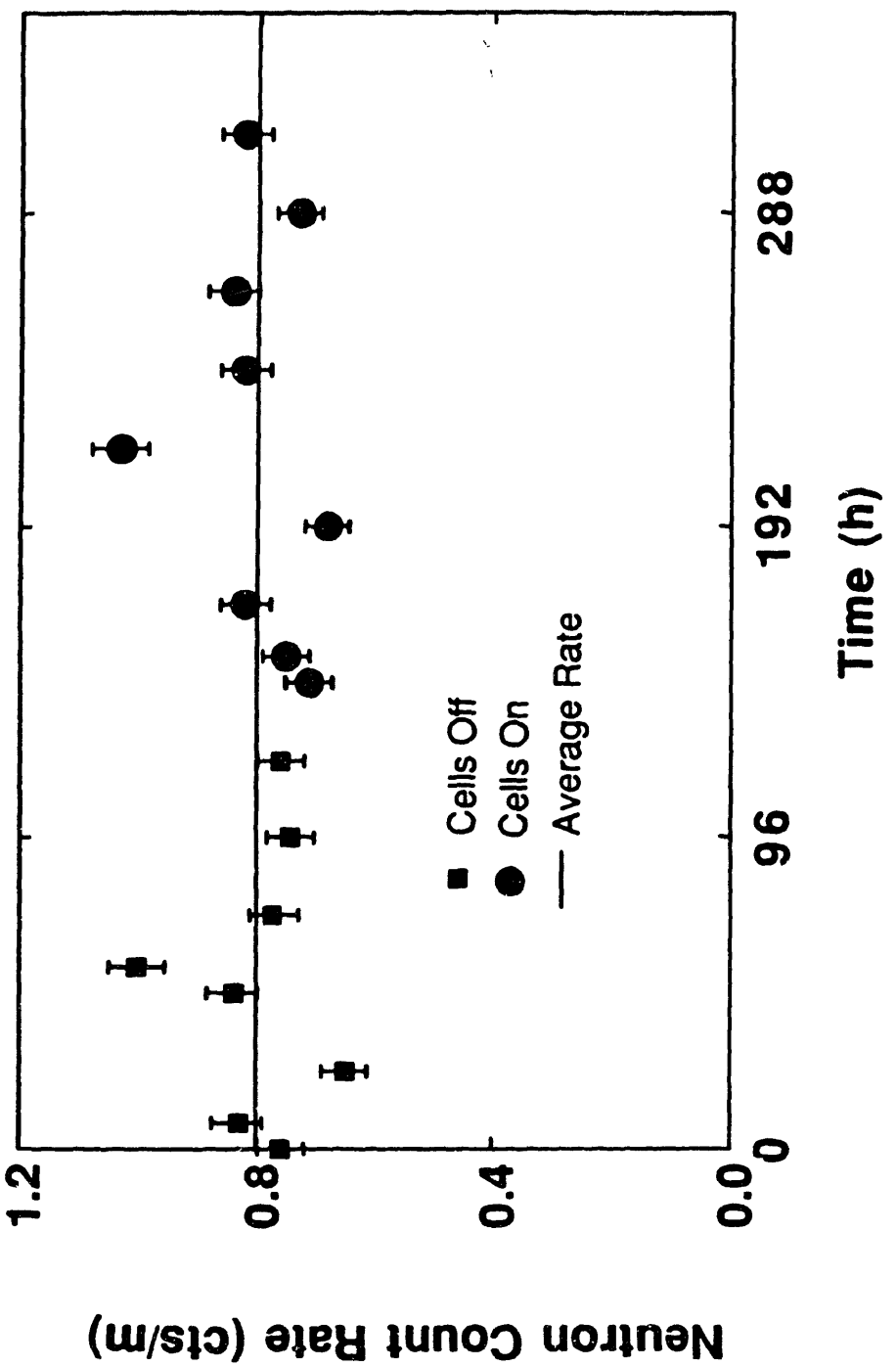
Neutron Count Rate (cts/m)
1.2
0.8
0.4
0.0
0
96
192
288
Time (h)
Cells Off
Cells On
Average Rate

to 3 MeV for measurement of the purported 2.22 MeV neutron-capture-on-hydrogen γ-ray. Detector 2, $D_\gamma 2$, covered the energy range from 0 to 30 MeV for measurement of the 23.8 MeV γ-ray from eq C, Table I. The two detectors were located underneath the water tank containing the electrolysis cells, and were collimated with about 10 cm of lead shielding. The detectors viewed the cells through approximately 5 cm of water and 1 cm of plastic. The γ spectra were stored continuously in RAM and dumped to disk every 100 minutes.

The sensitivity of $D_\gamma 1$ to the neutron-capture γ-rays was experimentally measured with a 1.5×10^6 n/s (Pu/Be) neutron calibration source placed in the center of the water tank. The measured gamma rate was about 1700 cts/MeV-s at 2.22 MeV, Figure 8a. Given the background rate of 0.7 cts/MeV-s at this energy, Figure 8b, the minimum detectable rate was about 200 n/s. The sensitivity of $D_\gamma 2$ to 23.8 MeV photons was estimated based on the background γ-rate, the detector efficiency, and the detector geometry. For the background rate of 0.02 cts/MeV-s at 23.8 MeV, Figure 9, and for a detector efficiency of ~50% for these photons in a 3 in. x 3 in. NaI(Tl) crystal, the detector can measure a γ rate of ~10 photon/s generated in the cell.

After nearly two months of monitoring Phase I and Phase II cells, no increase in the γ emission rate above the background level was observed. This sets the upper limits on the rates of the reactions corresponding to eq A and C, Table I, to be 200 reactions/s and 10 reactions/s respectively.

Figure 8. γ-ray spectra measured with a 3 in. x 3 in. NaI(Tl) scintillation detector (Dγ1) covering the energy range 0-3 MeV. (a) A neutron-capture-on-hydrogen spectrum obtained with a 1.5 x 10^6 n/s (Pu/Be) calibration neutron source submerged in water. Appearing are the (n,γ) peak (2.22 MeV), a Compton edge (1.99 MeV), and the first and second escape peaks. (b) Background γ-ray spectrum. The background γ-rate at 2.22 MeV is about 0.7 cts/MeV-s. Using the neutron-capture γ-ray experiment as a calibration, a 200 n/s source can increase the γ rate at 2.22 MeV by ~25% above the background.

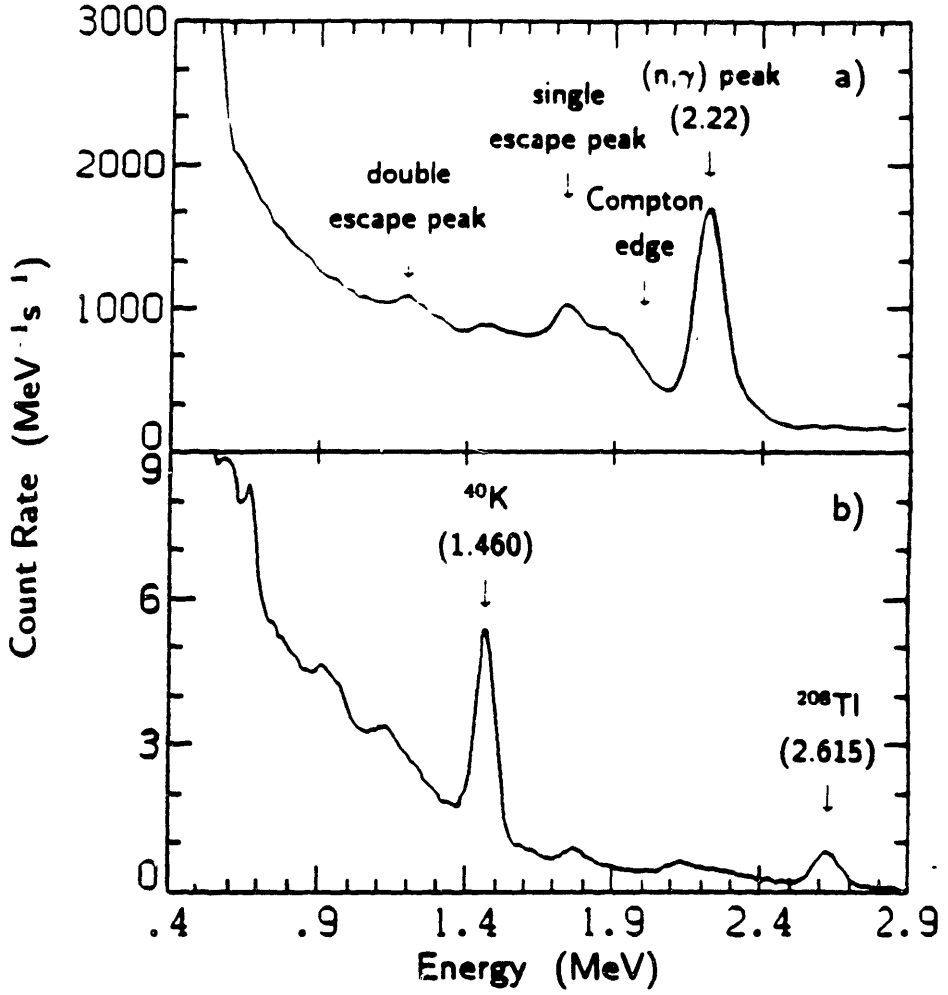
3000
2000
1000
0
9
6
3
0
Count Rate (MeV⁻¹s⁻¹)
(n,γ) peak
(2.22)
a)
single
escape peak
double
escape peak
Compton
edge
40K
(1.460)
b)
208Tl
(2.615)
.4
.9
1.4
1.9
2.4
2.9
Energy (MeV)

Figure 9. A background γ-ray spectrum measured with a NaI(Tl) detector ($D_\gamma 2$), covering the energy range 0-30 MeV. Based on the background γ-rate at 23.8 MeV, and for a ~50% detection efficiency for these γ-rays, the detector is sensitive to a γ rate of 10 photon/s from Phase II cells.

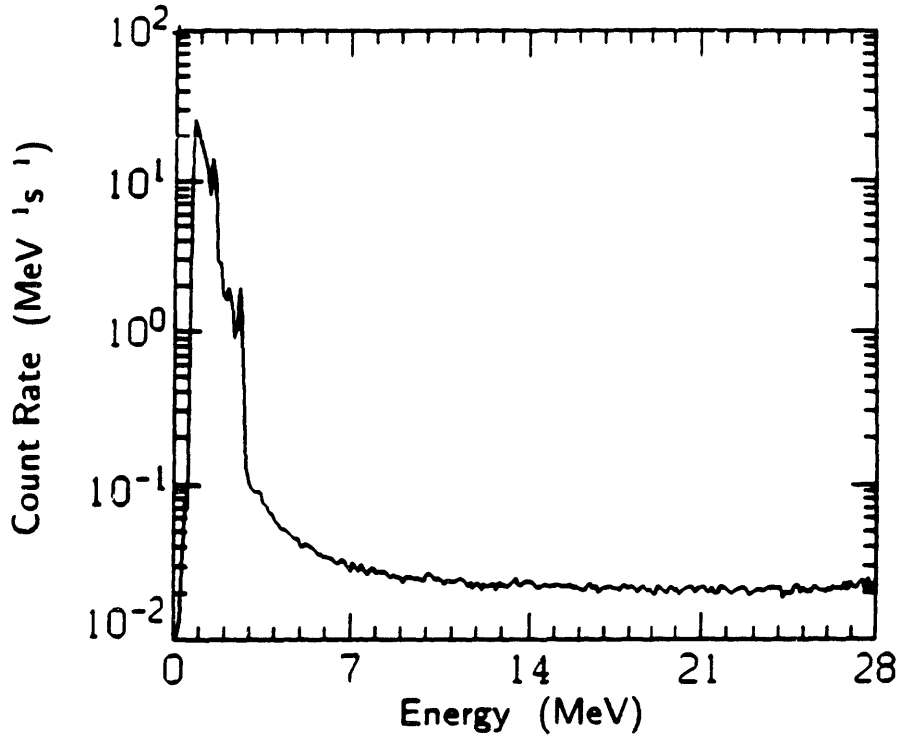
10^2
10^1
10^0
10^{-1}
10^{-2}
Count Rate (MeV ^{1}s ^{1})
0
7
14
21
28
Energy (MeV)

The maximum reaction rate sets an upper limit on excess power arising from eq A, Table I, of ~10^{-9} W/cm^3 in Phase II cells. This value is significantly more sensitive than calorimetric power measurements, and suggests that the presence of γ radiation would be a more convincing indicator of nuclear fusion than calorimetric excess power measurements. Based on the maximum reaction rate for eq C, Table I, we can also set a maximum fusion power limit of ~10^{-9} W/cm^3. However this energy should not appear as heat in the electrochemical cell, barring a new mechanism that couples energy into the Pd lattice, since most of the energy would be carried off by the photon.

5. Fusion Product Analysis.

Detailed experiments designed to detect the presence of any fusion products generated in Phase II cells have been performed. It is the unambiguous detection of fusion products, rather than excess heat, that is a definitive test for cold fusion in Pd cathodes. Furthermore, as described below, the presence of fusion products is generally a more sensitive test for fusion power generation than the calorimetric methods described by here and by others.[1,7,8] In this section the results of experiments designed to detect fusion products in effluent gases, electrolyte solutions, and inside Pd cathodes will be described.

A. Gas Phase. Electrochemical cells generating excess heat have been reported to evolve concentrations of ^{4}He

significantly higher than background levels.[31] Mass spectral analysis of gas evolved from Phase II cells was undertaken to detect the presence of ^4He, a fusion product associated with eq C, E, and G, Table I. Importantly, this analysis is only sensitive to fusion processes occurring on Pd surfaces, because the diffusion coefficient of He inside Pd is too low to permit internally generated He to escape into the solution.[32]

A Finnigan MAT 8200 double-focussing, high resolution mass spectrometer was used for analysis of ^4He and D_2 in the effluent gas of the electrolyzing Phase II cells. Gas samples were drawn with gas-tight syringes and injected into an evacuated glass tube attached to the inlet system of the high resolution mass spectrometer. The nominal resolution required to resolve the ^4He and D_2 mass peaks, 4.0026 amu and 4.028 amu respectively, is about 158. The resolution of our instrument was 500, sufficient to easily resolve the two mass peaks.

The data shown in Figure 10 were taken over the mass range 3.9-4.1 amu. Figure 10a shows a spectrum of ambient air taken from the room where the cells were operated. Air samples taken from other locations showed the same peak magnitude, which we infer corresponds to the natural abundance of He in air, 5 ppm.[33] The result of a mass spectral analysis of the effluent gas from the electrolyzing Phase II D_2O cell is shown in Figure 10b. As expected for cells containing D_2O the mass peak for D_2 is off-scale,

Figure 10. Mass spectral analysis of gas samples taken from: (a) ambient laboratory air; (b) the effluent gas stream of an operating D_2O cell. The mass range shown is from 3.9 to 4.1 amu. The peak height of ^4He (4.0026 amu) is the same in both samples, ~5 ppm, indicating that no ^4He above the background level is produced in the D_2O-containing cell.

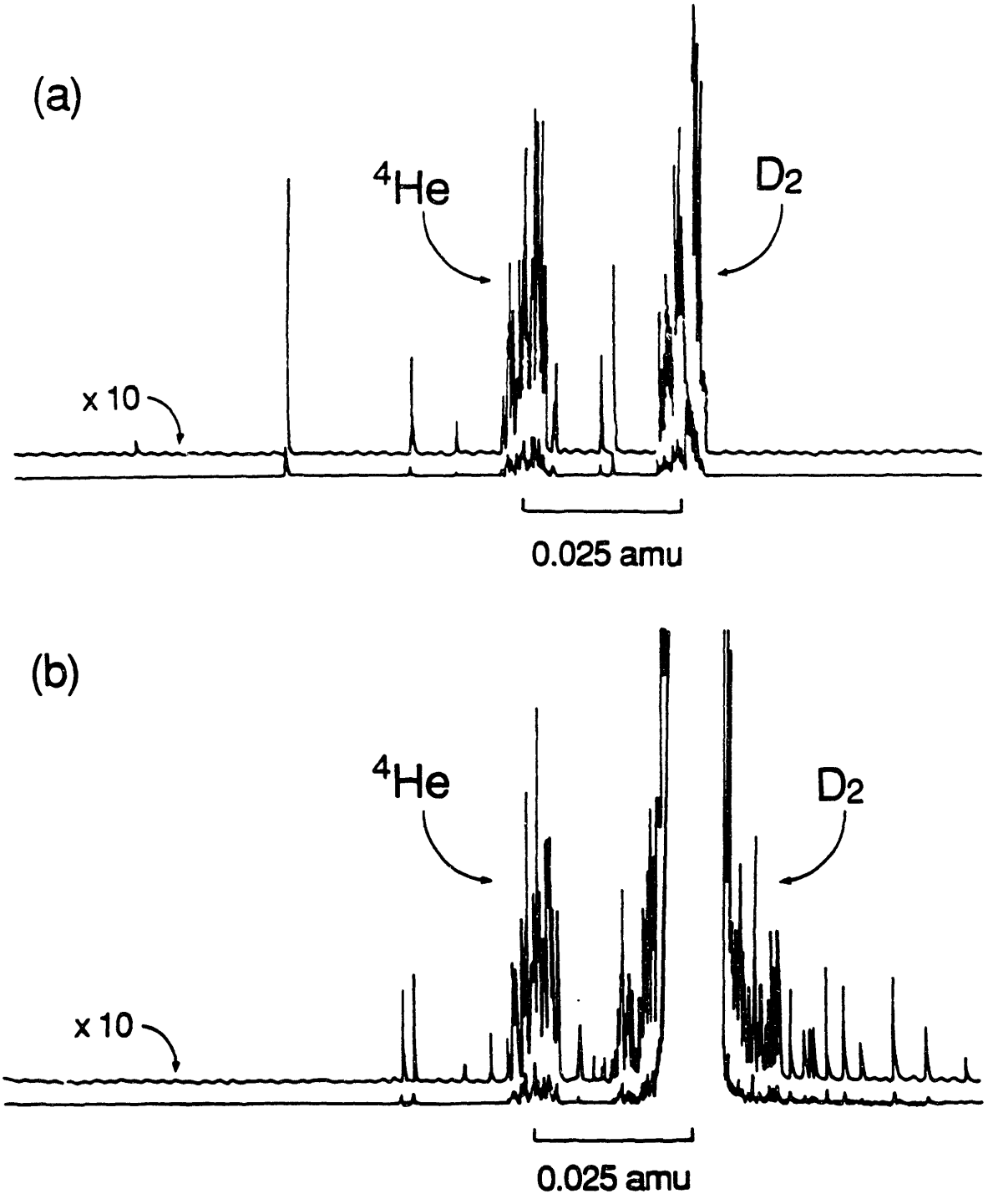
(a)
^{4}He
D_2
x 10
0.025 amu
(b)
^{4}He
D_2
x 10
0.025 amu

however the height of the ^4He peak is identical to that shown in Figure 10a indicating that within the estimated detection limit, ~1 ppm above background, no excess ^4He is produced in the electrolyzing cell. It is possible to relate the fusion power level associated with eq C, Table I, to the detection limit of this ^4He assay. Assuming all ^4He is formed at the Pd surface, and using the energy released in eq C, Table I, and the rate of electrolysis, Table III, fusion power generation at a maximum rate of ~28 W/cm^3 could occur at the level of sensitivity of the ^4He mass spectral assay. However, since most of the energy is carried off by the γ-ray, most fusion energy would not appear as heat in the cell.

B. Liquid Phase. Control and electrolyte samples were analyzed for tritium at the M.I.T. Radiation Protection Office using a Packard Model 2000 CA Liquid Scintillation Counter. 1 mL of sample was added to 10 mL of Packard Opti-Fluor scintillation fluid (Packard Instrument Co., Grove, IL). The samples were dark-adapted for one hour, and then each sample was counted for 2 min. Calibration was achieved by means of a quench correction curve using tritium standards of known concentration. The minimum detectable tritium level was 40 dpm/mL. Results for samples from Phase II experiments are given in Table IV.

The background tritium level in the D_2O used for Phase II experiments was specified by the manufacturer to be less than 5 $\mu Ci/kg$ which corresponds to 1.9×10^{-10} M tritium or 1.2×10^4 dpm/mL. The experimentally determined background

Table IV. Phase II Tritium Data

Sample	Scintillations (dpm/mL)
H_2O	45 ± 9
H_2O/0.25 M LiOH	
before electrolysis	73 ± 7
after 223 h electrolysis[a]	63 ± 10
D_2O	111 ± 17
D_2O/0.25 M LiOD	
before electrolysis	101 ± 11
after 214 h electrolysis[a]	138 ± 16

[a]See Table III.

level of tritium corresponded to ~100 dpm/mL. Analysis of the electrolyte solution from Phase II H_2O- and D_2O-containing cells showed no significant increase in tritium concentration after more than 200 hours of electrolysis, Table IV.

It is possible to relate the magnitude of fusion power which would be dissipated as heat in Phase II cells by Pd electrodes undergoing fusion according to eq B, Table I, to the concentration of tritium present in the electrolyte solutions. However, the accuracy of such an analysis is limited in open cells, since some atomic tritium may catalytically react and form molecular tritium, DT or T_2, at the Pd electrode surface rather than exchange with D_2O to form TDO. Nevertheless, using the half life of tritium and the cell parameters listed Table III, the power released by the tritium branch of D-D fusion for our detection sensitivity can be estimated. In closed cells, this calculation sets the maximum fusion power limit for eq B, Table I at $\sim 10^{-7}$ W/cm^3. However, in the open cells, tritium may be lost prior to the assay and the actual power level could be higher, underscoring the advantages of using a closed cell configuration.

C. Solid Phase. If He were formed by a nuclear fusion process, eq C, Table I, it would be immobilized in the Pd metal. Experiments designed to measure the diffusion coefficient of He in PdT_n have verified that diffusion in that medium is negligible as well.[32] Detection of a significant level of He in the metal would constitute

important evidence for cold fusion. In this section we discuss the He analysis of Phase I Pd cathodes.

The presence of He in the metal electrodes was detected using mass spectrometric techniques. Samples, 10-30 mg, were cut from the Pd electrodes and the apparatus described in Refs. 34 and 35 was used to melt the Pd and collect all escaping gases. The gas sample was then cryogenically separated and the remaining He was analyzed by mass spectrometry. The resulting ^3He and ^4He mass peaks were compared with standards for calibration.

A He assay of one of the Phase I samples was obtained,[36] with the result that no enhancement of ^3He or ^4He above background levels was detected. This analysis was performed on samples taken from a Pd cathode that had undergone 21 days of electrolysis in 0.1 M $LiOD/D_2O$ electrolyte solution. The results, Table V, indicate that no He above the background level was generated in the Pd cathode.

The He assay provides an upper limit on the average fusion power produced from eq C, Table I. The He assay of the Pd electrode provides a typical sensitivity of $n_{He} = 4 \times 10^{11}$ atoms/cm^3. The upper limit on fusion energy production is obtained by multiplying the sensitivity by the heat of reaction, Q_{He}. For the ^4He branch $Q_{He} = 23.88$ MeV/reaction or 3.8×10^{-12} J/reaction or 267 Gcal/mol of reaction product. To obtain the average detectable fusion power, the volumetric heat of reaction is divided by the duration of the experiment, Δt, eq 5.

Table V.

Results of the He Analysis of Phase I Pd Cathodes.[a]

Sample Description	Mass (mg)	^{3}He (atoms/sample)	^{4}He
Before Electrolysis			
Pd Cathode 1	13.60	$<1\times10^8$	2×10^8
Pd Cathode 2	18.52	$<1\times10^8$	1×10^8
After 21 Days of Electrolysis in D_2O Electrolyte[b]			
Pd Cathode 3	12.29	$<1\times10^8$	1×10^8
Pd Cathode 4	12.64	$<1\times10^8$	4×10^8

[a]See Ref. 36.

[b]See Table II.

$$P_{D+D\rightarrow{}^4He} = \frac{n_{He} Q_{He}}{\Delta t} \qquad (5)$$

Using the detection sensitivity, heat of reaction, and taking a typical time interval for the electrolysis run to be Δt = 250 h, the average detectable fusion power by the He assay method is $P_{D+D\rightarrow{}^4He} < 2\ \mu W/cm^3$. A similar analysis for the power from the ^3He fusion branch, eq A, Table I, yields $P_{D+D\rightarrow{}^3He} < 3\ \mu W/cm^3$. The He assay technique is approximately 10^3 times more sensitive than calorimetric measurements that can typically detect heat variations in the 10 mW range. However, for the analyses discussed in this section, only the ^3He fusion branch will result in solution heating, since the energy associated with the γ-ray of the ^4He fusion branch will be carried out of the cell.

6. Surface Analysis of Pd Cathodes. The Pd cathodes were observed to undergo physical changes in Phase I and II experiments. For example, the electrodes expanded, fissures developed, and the color of the surface varied. To understand the nature of these compositional changes an elemental surface analysis (X-ray photoelectron spectroscopy, XPS) was undertaken.

A Surface Science SSX-100 spectrometer was used to obtain the XPS spectra. The instrument was calibrated to Au ($4f_{7/2}$) = 84.0 eV binding energy. Depth profiling was done by sputtering the surface with an Ar ion gun operated with the chamber backfilled with Ar to 2.4×10^{-7} Torr.[37]

Cathode samples from the Phase II D_2O and H_2O cells, and an unused Pd sample were examined by XPS over the range of binding energies 0-1000 eV. After each analysis a portion of the surface was removed by Ar^+ sputtering to establish a depth profile of contaminants in the surface region. The spectrum shown for a used Pd cathode, Figure 11a, was recorded after 15 s of Ar^+ sputtering. Peaks corresponding to C, O, F, Si, As, Na, Zn, Mg and Pt are present, but the peak expected for Pd peak is absent. This result indicates that the important catalytic properties associated with a clean Pd surface are obscured in a used cathode since the escape depth of a photoelectron is about 50 Å.[38] After 12 min of Ar^+ sputtering peaks arising from Pd emerged, and after 45 min the surface spectrum appeared essentially identical to the spectrum of a fresh Pd sample, Figure 11b. Surface-bound Li originating in the electrolyte might be expected to be present, but does not appear presumably because XPS is not very sensitive to this element.

The source of surface impurities from electrolytes was not thoroughly investigated, however we speculate that they originated in the cell materials. For example, Si, As, and Na are present in the Pyrex,[39] and these elements can be leached from the glass in aqueous base.[40] The presence of Pt on the Pd cathode suggests dissolution of Pt at the anode followed by deposition on the cathode.[41] It is likely that C and F originate in the internal Teflon supports. Whatever their source, changes in surface composition of the Pd

Figure 11. (a) XPS spectrum of the Pd cathode from the Phase II D_2O cell after ~200 h of electrolysis. The surface of the sample was Ar^+ sputtered for 15 s before analysis. (b) XPS spectrum of a fresh Pd sample.

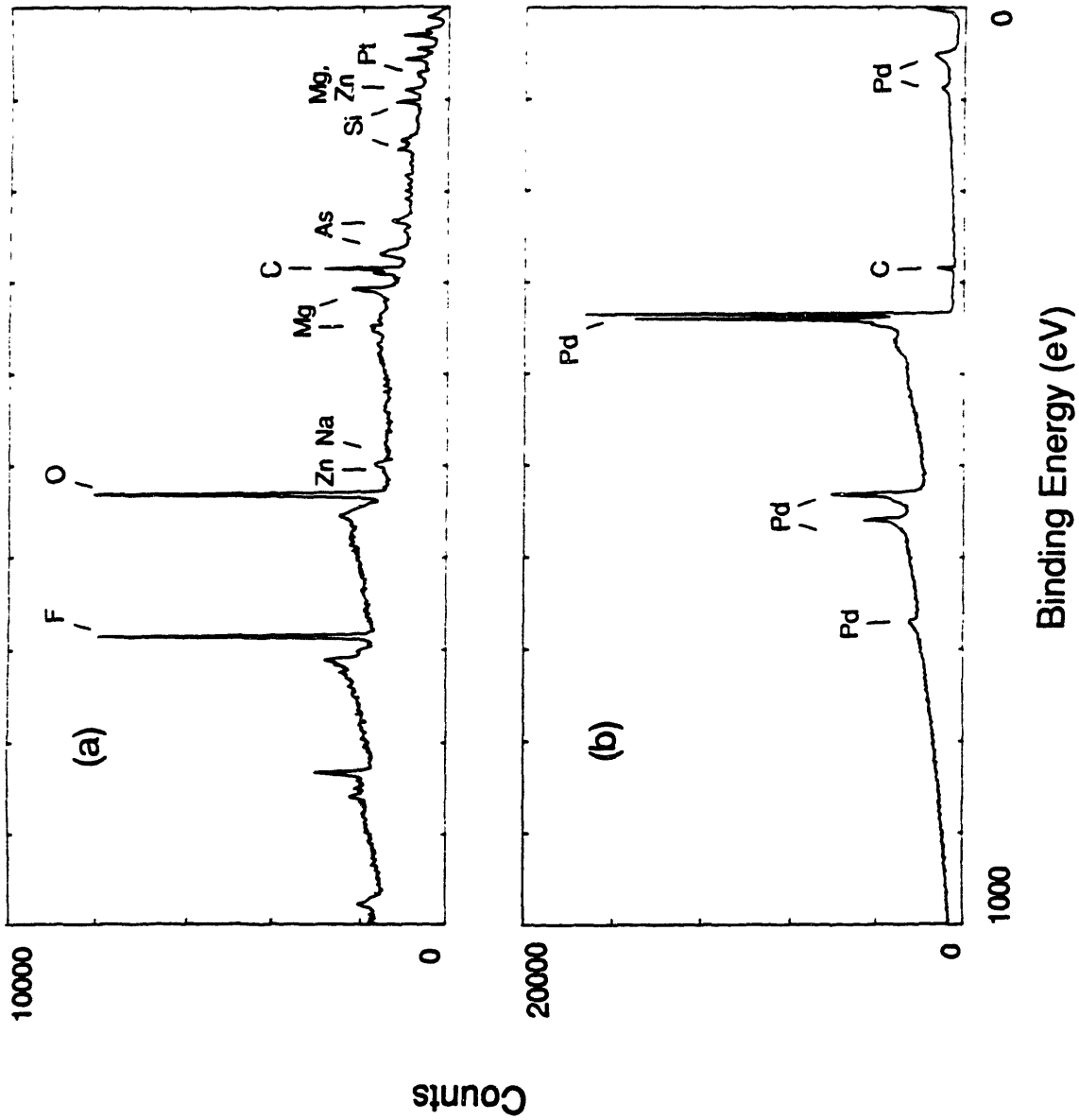
(a)
F
O
Zn Na
Mg
C
As
Si Zn
Mg
Pt
10000
0
(b)
Pd
Pd
Pd
C
Pd
20000
0
1000
0
Counts
Binding Energy (eV)

cathode shown by the spectra in Figure 11 will exert time dependent changes in parameters critical to calorimetry and the composition of PdD_n. For example, changes in surface structure will affect the cell voltage, V_c, and therefore the level of power, P_c, dissipated in the cell. In addition, it is known that certain adsorbates can change the maximum ratio of D/Pd in electrochemically charged Pd cathodes.[42]

7. Critique of the γ-ray spectroscopy.

Two sets of γ-ray spectra have been published by FPH as supporting evidence for solid state fusion of deuterons in their experiment.[1,6] In the first spectrum, presented in their original paper and errata,[1] they showed a signal peak centered at 2.22 MeV, Figure 12a. They contend that this signal line originated from neutron-capture-on-hydrogen, eq 1, and therefore was proof of neutron generation in their electrolysis cells. Several fundamental inconsistencies have been found in this spectrum. First, the linewidth of the signal line corresponds to a NaI detector resolution of about 2.5% at 2.2 MeV. But based on classical works on NaI scintillation detectors, on our own measurement of γ-rays from neutron-capture in water using 3 in. x 3 in. NaI detectors, and on their own detector calibration with 1.33 and 1.46 MeV γ lines, their detector resolution at 2.2 MeV should be 4-5%. Second, no Compton edge is present in their spectrum, Figure 12a, and it should be distinctly prominent at 1.99 MeV, as shown in Figure 8a. Third, there are several natural background γ lines located near 2.2 MeV. Consequently, the

Figure 12. γ signals presented by FPH[1] as supporting evidence of nuclear fusion in electrochemical cells. (a) A reproduction of the purported 2.22 MeV neutron-capture-on-hydrogen γ-ray line.[1] As was pointed out previously,[4a] the resolution of their NaI spectrometer would be about 2.5% based on this linewidth. With such resolution, one would expect to see a clearly defined Compton edge at 1.99 MeV. No edge is evident. Also, a resolution of 2.5% is inconsistent with their spectral resolution (Table 1b of ref. 4a). Because of these inconsistencies, we argue that this signal is an instrumental artefact. (b) A reproduction of the FPH spectrum which contains a 2.496 MeV signal line (peak 7).[6] We argue that the signal line is an instrumental artifact because its lineshape is unphysical.[4b] Also, we believe the ^{208}Tl (2.61 MeV) line is peak 6 instead of peak 8, as has been identified by FPH. Therefore the purported signal line is at about 2.8 MeV instead of 2.496 MeV. Furthermore, there is no significant difference between the sink (background) and the tank (cell) spectra at 2.2 MeV, near peak 5. This sets an upper limit on the neutron production rate of 400 n/s from the heat-producing cell. This limit is a factor of 100 smaller than the neutron rate FPH claim to have actually observed.[1]

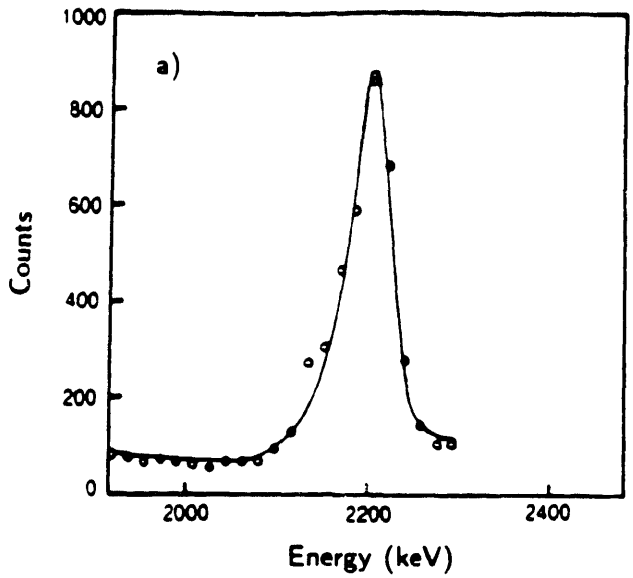
a)
Counts
Energy (keV)
1000
800
600
400
200
0
2000
2200
2400

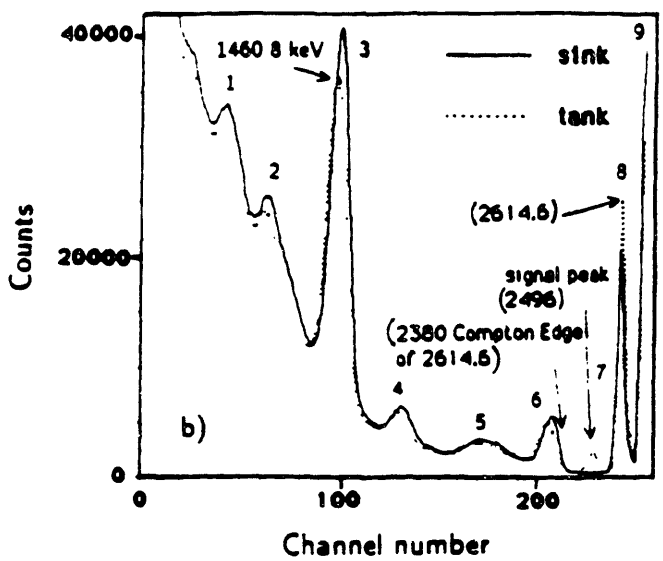
b)
Counts
Channel number
1460.8 keV
sink
tank
(2614.6)
signal peak
(2496)
(2380 Compton Edge
of 2614.6)
1
2
3
4
5
6
7
8
9
40000
20000
0
100
200

background rate near E = 2.2 MeV should be of about the same magnitude as their signal line. The unusually low γ-ray background shown in their spectrum suggests that their signal line cannot be located at 2.2 MeV. Based on these arguments, it was concluded that the FPH signal line is an instrumental artifact unrelated to a γ reaction, and that its energy location is unlikely to be 2.2 MeV.[4a]

In response to the above criticism FPH published a second spectrum, Figure 12b, which is a full γ-spectrum claimed to be measured over a cell generating excess heat at a rate of 1.7-1.8 W.[6] In the new spectrum they identified a signal line at an energy of 2.496 MeV (peak 7, Figure 12b) rather than at 2.22 MeV. They are not able to identify the physical processes which generates this 2.496 MeV γ-ray, but they contend that the signal line is still evidence of some unspecified nuclear reaction occurring in their cell. It has been pointed out[4b] that this new signal line has a shape which is unphysical, and concluded that it is not a true γ line. Furthermore, based on the identification of background lines in their spectrum, we determined that they have misidentified the ^{208}Tl (2.61 MeV) line, and therefore their energy calibration is incorrect.[4b] With the correct energy calibration, their signal peak actually resides at about 2.8 MeV rather than 2.496 MeV. We believe that the high energy peaks (peaks 7-9, Figure 12b) are caused by defects in the upper channels of their spectrum analyzer. Nevertheless, one crucial observation can be made by comparing the FPH spectra

measured over a heat producing cell and that measured over a sink 5 m away: no observable change exists in the γ rate at 2.22 MeV (in the vicinity of peak 5, Figure 12b). Quantitatively, based on the controlled neutron experiment in water and the FPH γ data in the energy range near 2.22 MeV, we can set an upper limit on the neutron production rate of about 4×10^2 n/s from their cell.[4b] This bound is a factor of 100 smaller than the rate FPH claim to have actually observed with their neutron detector.[1] Therefore, we conclude that FPH did not observe neutrons or γ-rays from their electrochemical cells.

8. Comments on Calorimetry.

A. Refinements. There are a number of error sources present in the calorimetry described here. Some of these are inherent to long-term electrochemical calorimetry,[43] but others can be minimized through careful choice of the calorimeter used and electrolysis conditions. Since the design of the calorimeter was intended to resemble that of FPH, it is likely that many of the difficulties encountered here could also have been present in their experiments. In this section several important aspects of high resolution, long-term electrochemical calorimetry will be discussed.

In open cell calorimetry one significant error arises from energy loss due to unintentional recombination of the electrolysis gases, D_2 and O_2, eq 6.

$$2D_2 + O_2 \rightarrow 2D_2O \qquad (6)$$

Catalytic recombination will take place at Pd or Pt surfaces in either the gas or the liquid phase. As pointed out in part B of this section, the magnitude of the excess power reported by FPH,[1] and others[7,8] is usually lower than or comparable to the heat accompanying chemistry released according to eq 6. Other important deficiencies of vented cells include energy losses due to evaporation, fluctuations of electrolyte level, and atmospheric contamination of electrolyte solutions.

Some of the problems associated with open cell calorimetry can be adequately addressed by intentional recombination of electrolysis gases in a closed cell configuration. In closed cells all heat released according to eq 6 can be accounted for since no reaction products are permitted to escape the calorimeter. Furthermore, difficulties associated with solution losses to evaporation and electrolysis are not present in closed cells. These losses will affect the thermal mass of the calorimeter and the cell resistance. For example, the thermal drift detected in our calorimeter, Figure 6, was caused by time dependent changes in thermal power loss, P_{th}. The cell resistance, which is determined by the electrode geometry and the concentration of electrolyte will also be affected by solution loss, since the time dependent increase in electrolyte concentration will serve to lower the cell

resistance, thereby reducing the total cell power, P_c. In addition, if the electrolyte level falls so as to reduce the active surface area of either electrode, the current density, and therefore P_c, will increase.[44] Evaporative losses will affect power measurements in much the same manner.

The cell materials are another serious source of error in electrochemical calorimetry. As discussed in Section 6, glass is sparingly soluble in alkaline solutions,[40] Pt can transfer from the anode to the cathode,[41] and low molecular weight $(CF_2)_x$ can leach out of Teflon.

There are several other problems which are likely to have adverse effects on electrochemical calorimetry. For example, gas vented from our cells frequently ceased to flow for extended time periods. This effect was caused by formation of large gas bubbles which became trapped under the upper and lower Teflon supports, Figure 2a. The effect of bubble formation is similar to that of solvent loss by evaporation or electrolysis. Phase changes within the Pd lattice ($\alpha_{Pd} \rightarrow \beta_{Pd}$), time dependent changes in electrode surface roughness, temperature gradients caused by ineffective stirring, inadequate methods of power calibration, and redistribution of electrolyte in the cell caused by condensation and droplet formation all represent deficiencies in calorimetry.

Considering the higher resolution afforded by many of the fusion product assay techniques compared to heat-based calorimetry, we feel that demonstration of cold fusion will

be better served by focusing detection efforts on fusion products rather than power measurements.

B. Critique of the Calorimetric Results. An important aspect of the FPH experiment stems from the claim that thermal power was generated with a magnitude of several W/cm^3, and that this level of power is orders of magnitude larger than can be accounted for by chemical processes. Analysis of the calorimetry data presented in Tables 1 and 2 of Ref. 1, shows that the above claims are incorrect and not supported by the data. The excess heat reported, more correctly the excess power, P_x, is less than or approximately equal to the energy associated with the chemistry of eq 6. Table VI contains data from Ref. 1 concerning the cathode dimensions; current density; total cell current; excess power, P_{ex}; recombination power, P_{rec} (1.53 V x I_c); and the ratio of the excess power to recombination power, P_{ex}/P_{rec}. Table VI shows that in seven out of nine cases $P_{ex} < P_{rec}$. In one of the remaining cases the value of P_{ex} was scaled by an unspecified method from a cathode length of 1.25 cm to a length of 10 cm. In the other case, the difference between P_{ex} and P_{rec} may not be significant considering the numerous error sources inherent to open cell calorimetry. This analysis indicates that the calorimetry data reported by FPH do not support the claim that "It is inconceivable that this [power] could be due to anything but nuclear processes."[1]

Table VI.

Analysis of FPH Calorimetry Data.

Cathode Dimension (cm)	Current Density (mA/cm^2)	Cell Current (mA)	Excess Power, P_{ex} (W)	Recombination Power, P_{rec} (W)	P_{ex}/P_{rec}
0.1x10	8	25	0.0075	0.0385	0.19
0.1x10	64	201	0.079	0.31	0.25
0.1x10[a]	512	1610	0.65	2.48	0.26
0.2x10	8	50	0.036	0.077	0.46
0.2x10	64	402	0.493	0.619	0.79
0.2x10[a]	512	3220	3.02	4.96	0.61
0.4x10	8	101	0.15	0.155	0.97
0.4x10	64	804	1.75	1.24	1.41
0.4x10[a]	512	6430	26.8	9.90	2.71

[a]Data scaled from 1.25 cm length cathodes to 10 cm length [Ref.1].

Conclusions

Experiments intended to duplicate those reported by FPH[1] have been designed and implemented. Analyses of these experiments are broad-based and include measurements of neutron and γ radiation, power, and fusion products. In all cases the minimum detection limits in these experiments are better than or equivalent to those reported by FPH. Importantly, the level of fusion products present is by far a more sensitive indicator of nuclear fusion reactions than are the relatively insensitive heat-based measurements which form the foundation of the claim of cold nuclear fusion put forth by FPH.[1] At our level of sensitivity, which in some cases corresponds to a level 10^7 times better than the rate of excess heating claimed by FPH, no evidence for nuclear fusion processes or any excess power generation in electrochemical cells containing D_2O and Pd cathodes was detected. Furthermore, based on the analysis[4] of the FPH γ spectra we conclude that FPH, contrary to their claims,[1,6] did not detect neutrons or γ-rays from their "excess heat-producing" cells.

References

1. Fleischmann, M.; Pons, S.; Hawkins, M. *J. Electroanal. Chem.* **1989**, *261*, 301; and erratum, **1989**, *263*, 187.

2. Jones, S. E.; Palmer, E. P.; Czirr, J. B.; Decker, D. L.; Jensen, G. L.; Thorne, J. M.; Taylor, S. F.; Rafelski, J. *Nature* **1989**, *338*, 737.

3. DeNinno, A.; Frattolillo, A.; Lollobattista, G.; Martinia, L.; Martone, M.; Mori, L.; Fodda, S.; Scaramuzzi, F. *Europhys. Lett.* **1989**, *9*, 221.

4. a) Petrasso, R. D.; Chen, X.; Wenzel, K. W.; Parker, R. R.; Li, C. K.; Fiore, C. *Nature* **1989**, *339*, 183. b) Petrasso, R. D.; Chen, X.; Wenzel, K. W.; Parker, R. R.; Li, C. K.; Fiore, C. *Nature* **1989**, *339*, 667.

5. a) Fleischmann, M. 175th Meeting of the Electrochemical Society, Los Angeles, California, May 1989, "As we have repeatedly pointed out, we are well aware of the deficiencies of these [γ-ray] spectra". b) Maddox, J. *Nature* **1989**, *340*, 15.

6. Fleischmann, M.; Pons, S.; Hawkins, M.; Hoffman, R. J. *Nature* **1989**, *339*, 667.

7. Appleby, A. J.; Srinivasan, S.; Kim, Y. J.; Murphy, O. J.; Martin, C. R. presented at the Workshop on Cold Fusion Phenomena, Santa Fe, NM, May 23-25, 1989.

8. Belzner, A.; Bischler, U.; Crouch-Baker, S.; Gur, T. M.; Lucier, F.; Schreiber, M.; Huggins, R.A. presented at the Workshop on Cold Fusion Phenomena, Santa Fe, NM, May 23-25, 1989.

9. Wolf, K. L.; Packham, N.; Shoemaker, J.; Cheng, F.; Lawson, D. presented at the Workshop on Cold Fusion Phenomena, Santa Fe, NM, May 23-25, 1989.

10. a) *Meeting Abstracts*, Workshop on Cold Fusion Phenomena, Santa Fe, NM, May 23-25, 1989. b) *Abstracts Selected for Poster Sessions*, Workshop on Cold Fusion Phenomena, Santa Fe, NM, May 23-25, 1989.

11. Horanyi, G. *Electrochim. Acta* **1989**, *34*, 889.

12. Koonin, S. E.; Nauenberg, M. *Nature* **1989**, *339*, 690.

13. Leggett, A. J.; Baym, G. *Nature* **1989**, *340*, 45.

14. 179th American Chemical Society National Meeting, Dallas, TX, April, 1989.

15. 175th Meeting of the Electrochemical Society, Los Angeles, CA, May 1989.

16. McGowan, F. K. *et al*, *Nuclear Data Tables* **1969**, *A6*, 353. b) ibid, **1970**, *A8*, 199.

17. Jones, S. E. *Nature* **1986**, *321*, 127.

18. Graham, T. *Phil. Trans. R. Soc. (London)* **1866**, *156*, 415.

19. Lewis, F. A. *The Palladium Hydrogen System*; Academic: London, 1967 and references therein.

20. Worsham, J. E., Jr.; Wilkinson, M. K.; Shull, C. G. *J. Phys. Chem. Soln.* **1957**, *3*, 303.

21 Lohr, L. L. *J. Phys. Chem.* **1989**, *93*, 4697.

22. Sun, Z.; Tománek, D. *Phys. Rev. Lett.* **1989**, *63*, 59.

23. Smith, D. P. *Hydrogen in Metals*; The University Of Chicago Press: Chicago, IL, 1948.

24. Ref. 19, p 37.

25. Ref. 19, p.22.

26. Wicke, E.; Brodowsky, H.; Züchner, H. In *Hydrogen in Metals II*; Alefeld, G.; Völkl, J., Eds.; Topics in Applied Physics; Springer-Verlag: Berlin, 1978; Vol. 29, p 88.

27. Sicking, G. *Ber. Bunsenges. Phys. Chem.* **1972**, *76*, 790.

28. Ref. 26, p. 96.

29. (a) Reilly, W. F. M. S. Thesis, Massachusetts Institute of Technology, Cambridge, MA, 1959. (b) Anderson, M. E. *Nucl Appl.* **1968**, *4*, 142.

30. Hoare, J. P. In *Standard Potentials in Aqueous Solutions*; Bard, A. J.; Parsons, R.; Jordan, J., Eds.; Dekker: New York, NY, 1985; Chapter 4.

31. Walling, C.; Simons, J. *J. Phys. Chem.* **1989**, *93*, 4693.

32. (a) Thomas G. J.; Mintz, J. M. *J. Nucl. Mat.* **1983**, *116*, 336. (b) Schober, T. In *Hydrogen in Disordered and Amorphous Solids*; Bambakidis, G.; Bowman, R. C., Jr.; Plenum: New York, NY, 1986; p 377-396.

33. *CRC Handbook of Chemistry and Physics*; Weast, R. C., Ed.; CRC Press: Boca Raton, FL, 1985; p F156.

34. Kurz, M. D.; Jenkins, W. J; Hart, S. R. *Nature* **1982**, *297*, 6, 43.

35. Kurz, M. D.; Jenkins, W. J.; Schilling, J. C.; Hart, S. R. *Earth Planet. Sci. Lett.* **1982**, *58*, 1.

36. He analyses were carried out by Brian Oliver, Roketdyne Division, Rockwell International, Canoga Park, CA.

37. *Handbook of X-ray Photoelectron Spectroscopy*; Perkin-Elmer Corp., Eden Prairie, MN.

38. Seah, M. P.; Dench, W. A. *Surface and Interface Analysis* **1979**, *1*, 2.

39. Boyd, D. C.; Thompson, D. A. *Kirk-Othmer Encyclopedia of Chemical Technology*; Wiley: New York, NY, 1980; p 807-880.

40. *The Corning Laboratory Catalogue*; Corning Science Products, Corning, NY, 1988; p T7.

41. (a) Malachesky, P.; Jasinski, R.; Burrow, B. *J. Electrochem. Soc.* **1967**, *114*, 1104. (b) Vasina, S. Ya.; Petrii, O. A.; Safanov, V. A. *Elektrokhimiya* **1981**, *17*, 270.

42. Maoka, T.; Enyo, N. *Electrochim. Acta* **1981**, *26*, 607.

43. Sherfey, J. M.; Brenner, A. *J. Electrochem. Soc.* **1958**, *105*, 665.

44. Bard, A. J.; Faulkner, L. R. *Electrochemical Methods*; Wiley: New York, NY, 1980; Chapter 3.

Chapter VII

Measurements of Neutron Emission Induced by Muons Stopped in Metal Deuteride Targets[a]

[a]The work described in this chapter represents a collaborative effort and has been submitted for publication in the Journal of Fusion Energy. The co-authors are, from MIT: D. Albagli, V. Cammarata, M. Schloh, and M. S. Wrighton, from the Department of Chemistry; M. Chen and S. G. Steadman, from the Department of Physics and Laboratory for Nuclear Science; M. P. J. Gaudreau, S. C. Luckhardt, and R. R. Parker, from the Plasma Fusion Center; K. Kwok, from the Nuclear Reactor Laboratory; C. Thieme, from the Francis Bitter National Magnet Laboratory; and from Brookhaven National Laboratory: D. I. Lowenstein, from the Alternating Gradient Synchrotron Department; R. Debbe, from the Department of Physics; and J. J. Reilly, from the Department of Applied Science.

Introduction

Recently, three papers have reported[1-3] observation of D-D fusion in metal deuterides. These claims have been examined in many experimental,[4,5] computational[6,7] and theoretical[8,9] studies. A possible mechanism explaining cold fusion that has been presented is the catalysis of D-D fusion by naturally occurring negative muons from cosmic rays.[9] In this theory it was suggested that in fully saturated metal hydrides, muons might be shielded from capture by heavy element nuclei because of the band structure of this solid. The largest muon catalyzed fusion turnover rate observed has been 150 fusion reactions per muon in a liquefied mixture of D_2 and T_2.[10] However, the result of exposing metal hydrides to muons is not documented. To investigate the possibility of muon catalyzed fusion in metal hydride targets, an experiment with deuterated Pd, Ti and Y was conducted on a muon beam line at the Alternating Gradient Synchrotron (AGS) at Brookhaven National Laboratory. Presented in this Chapter is the apparatus, targets used and analysis of a representative experimental run.

Experimental Apparatus

A diagram of the the AGS muon facility is shown in Figure 1. Approximately 1.5×10^{13} protons are accelerated to 30 GeV every 2.5 s and then slowly extracted out of the AGS to the experimental target stations for 1.0-1.25 s. A fraction of the AGS protons (typically 5×10^{11}) are split off to the muon beam experimental

Figure 1 Simplified diagram of the BNL AGS muon facility.

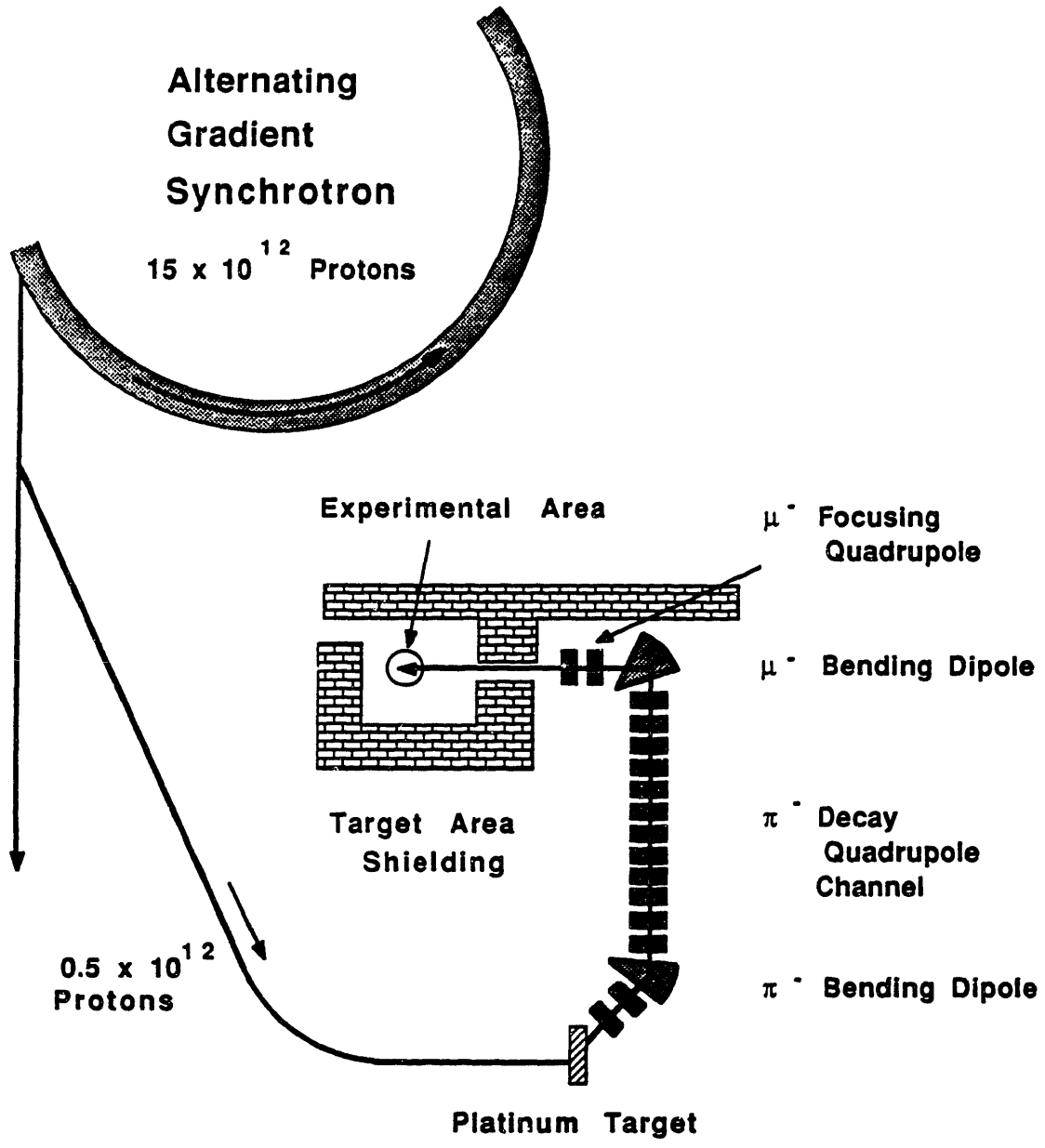
Alternating
Gradient
Synchrotron
15 x 10^12 Protons
Experimental Area
μ⁻ Focusing
Quadrupole
μ⁻ Bending Dipole
Target Area
Shielding
π⁻ Decay
Quadrupole
Channel
0.5 x 10^12
Protons
π⁻ Bending Dipole
Platinum Target

area where they are focused onto a 10 cm long Pt target. The secondary particles produced are then captured in the muon beam line. A portion of the pions produced in the collision enter the beam line, where they are first momentum selected by a dipole magnet and then allowed to decay into muons in a quadrupole channel. The muons are momentum selected to 80 MeV/c by a dipole magnet and focused by quadrupole magnets directly before entering the concrete, steel and lead shielding structure of the experimental target area.

A diagram of the target area is shown in Figure 2. The 2 x 2 cm collimated muon beam is defined by a fast coincidence plastic scintillator hodoscope. An incident muon event is defined by a coincidence of the S1, S2, and S3 scintillators within a gate width of 10 ns. The defined beam size at the target is approximately 4 cm^2. A "muon stop" is counted if the muon is not subsequently detected at the veto counter, S4, situated behind the target. The thin plastic scintillators have efficiencies near unity for both fast muons and electrons. The difference in the range of photomultiplier pulse heights between the electrons and the muons permitted discrimination between the two. From this measurement, we conclude that the electron contamination in the beam was less than 25%. A degrader (0.5 cm of Pb) was placed between the S2 and S3 scintillators to slow down the muons in the beam in order to maximize the number of muons that stop in the target.

The target and the veto counter, S4, were located in a tube along the axis of a drum containing 2 coaxial rings of ^3He

Figure 2 Simplified diagram of the muon target area and the electronic diagnostics.

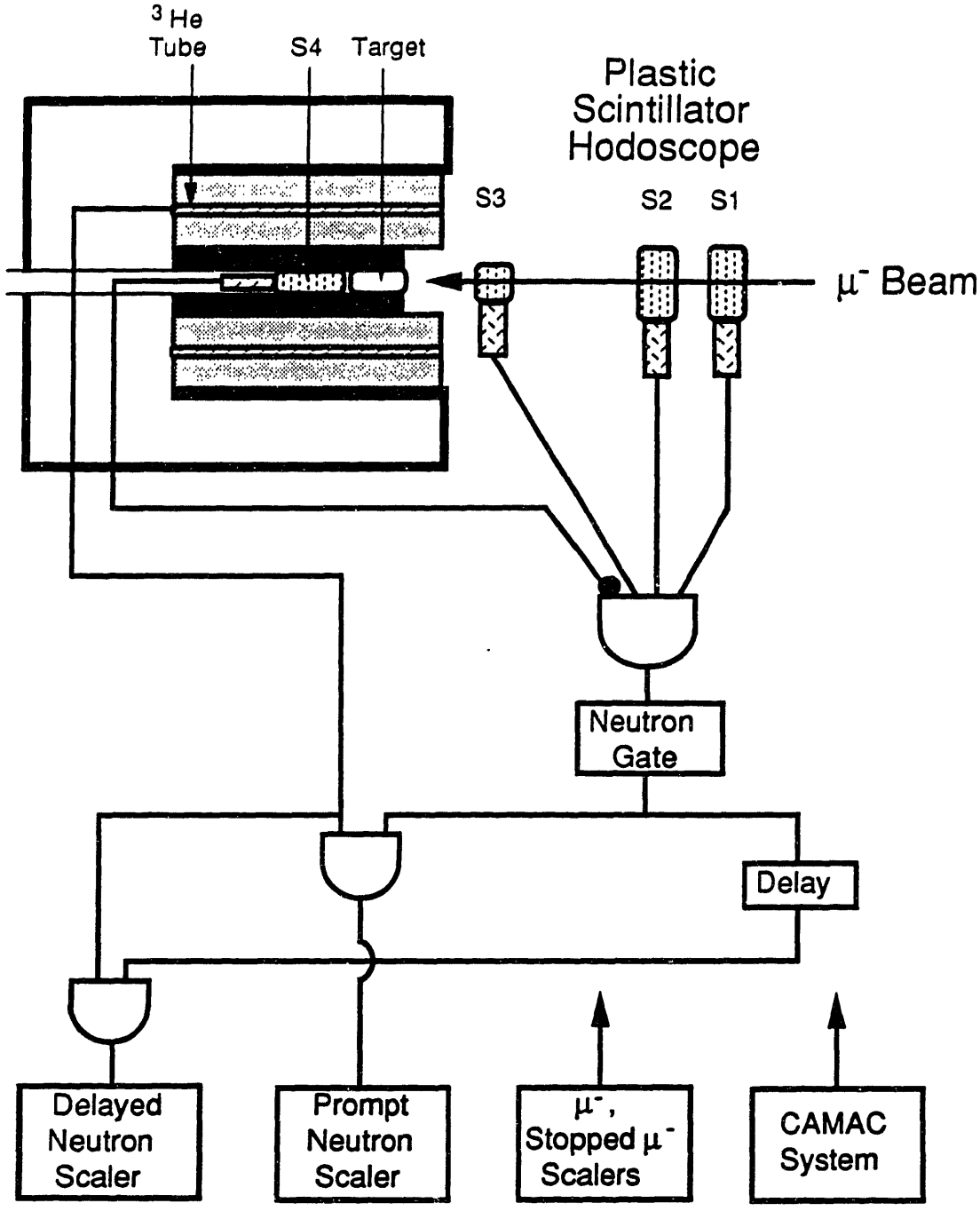
^{3}He Tube
S4
Target
Plastic Scintillator Hodoscope
S3
S2
S1
μ⁻ Beam
Neutron Gate
Delay
Delayed Neutron Scaler
Prompt Neutron Scaler
μ⁻, Stopped μ⁻ Scalers
CAMAC System

detectors. A cross section of the array of ^{3}He detectors is shown in Figure 3. The detector array was constructed of 20 high pressure (4 atm fill pressure) 2.5 x 38 cm ^{3}He tubes inserted in a cylindrical block of polyethylene moderator which was wrapped with a layer of Cd. The polyethylene block was situated in a steel drum, the void space inside was filled with polyethylene beads, and the drum was wrapped with more Cd sheets. The neutron counting efficiency obtained was high because, in addition to the large neutron absorption cross-section of ^{3}He, the detector had a nearly 4π steradian geometry. Background neutrons were further minimized by the concrete and polyethylene built into the structural shielding surrounding the target area.

Since the neutron background from the AGS during a beam pulse was about 1000 cts/s, an electronic gate of typically 50 μs was opened for neutron counting immediately after a muon stop was registered. The background count rate between beam pulses was much lower (<1 cts/s) than during a pulse. Even with this synchronous detection scheme, the random background neutron rate was large enough to cause an overestimate in the ratio of neutrons to stopped muons. To correct for this, the random neutron coincidence rate was measured by opening a second gate of the same width after a 180 μs delay beyond the muon stop.[11] The real neutron count was then determined by the difference between the prompt, and delayed, gated neutron counts. The neutron detector signals were also pulse height and time delay analyzed by a microcomputer controlled CAMAC system.

Figure 3 Cross section of the ^{3}He neutron detector with the calibration source, ^{252}Cf, and the NaI(Tl) gamma detector.

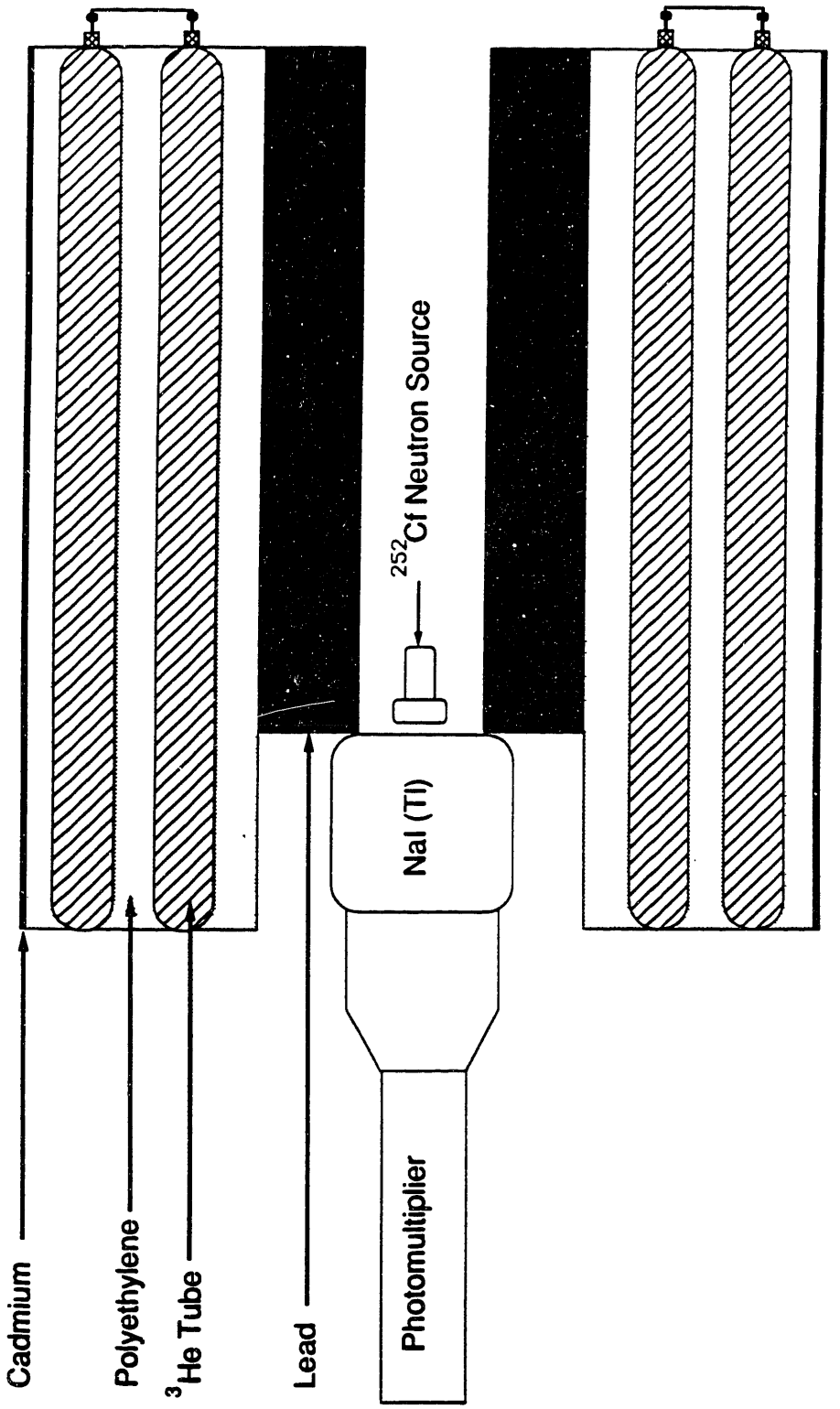
Cadmium
Polyethylene
^{3}He Tube
Lead
Photomultiplier
NaI (Tl)
^{252}Cf Neutron Source

Calibration of the Detector. A ^{252}Cf source was used to determine the counting efficiency and the response time of the ^{3}He detector array. The setup used to calibrate the neutron detector is shown in Figure 3. ^{252}Cf has a half life of 2.65 y and a branching ratio of 96.9% for alpha decay to ^{248}Cm, which has a half life of 4.7 x 10^5 y and thus does not produce any significant neutrons or gammas. The other 3.1% branch undergoes spontaneous fission, which on the average simultaneously produces 2.5 neutrons per event. The absolute neutron emission rate is 2000 ± 50 n/s. In addition, prompt gammas with a total energy of about 7 MeV are emitted for each fission event.

The absolute neutron counting efficiency was determined by counting the number of neutrons from the ^{252}Cf at different positions in the detector. The maximum efficiency observed was 20%, with the source located at the center of the ^{3}He detector. At the spot where the target was positioned, the efficiency was 14 ± 1%. This location was chosen to reduce the systematic error due to positioning of the target and the S3 and S4 scintillation counters.

The time response of the ^{3}He detector was measured using the time difference between the signal of the prompt gammas recorded by a NaI(Tl) detector, and the signal of the moderated neutrons in the ^{3}He detector. The time delay between the NaI(Tl) gamma pulse and the ^{3}He pulse is plotted in Figure 4. A fit to the form $e^{-t/\tau}$ determines τ = 53 μs. These measurements are consistent with rough calculations that assume that the neutrons are moderated in the polyethylene just before reaching the detector, and only a very

Figure 4 ^{3}He neutron detector response time to a ^{252}Cf source. The response time was fitted to an exponential decay; the time constant was found to be 53 μs. The characteristics of the fission reaction are discussed in the text.

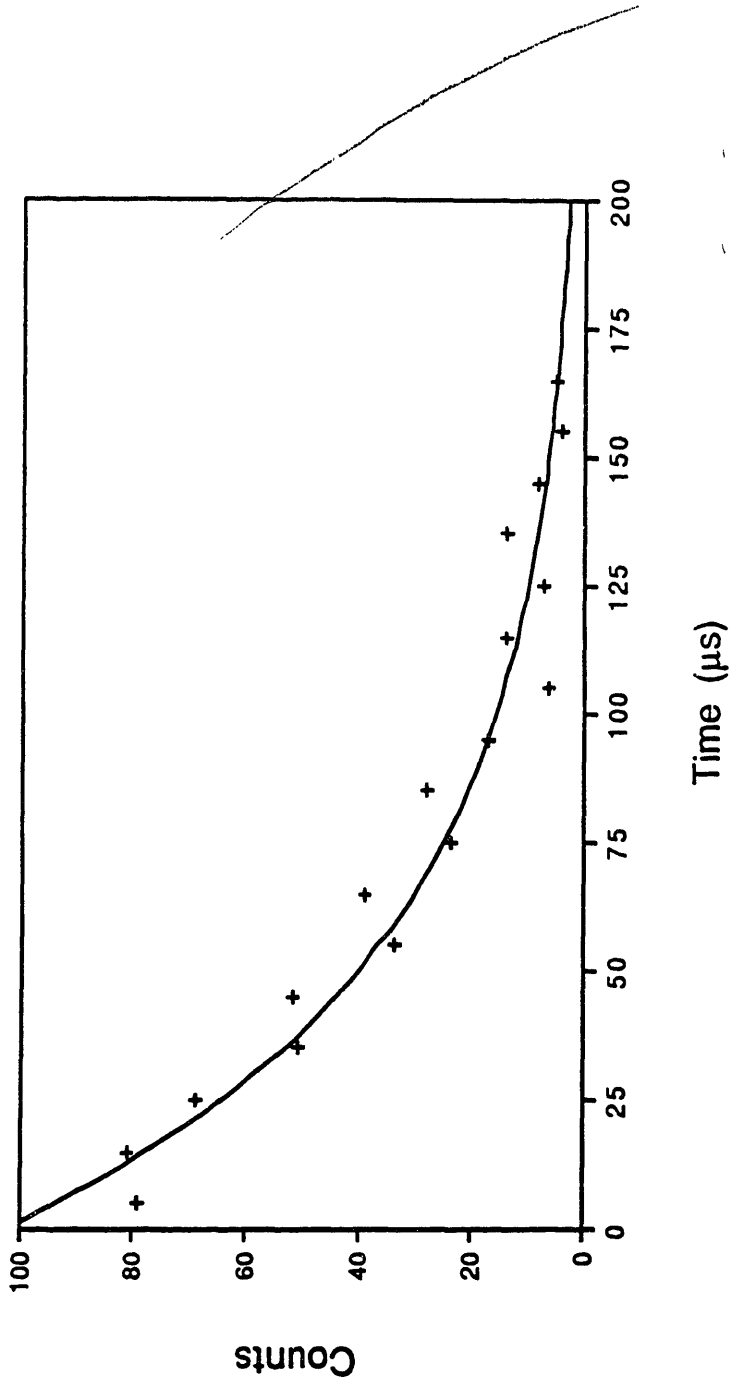
Counts
0
20
40
60
80
100
0
25
50
75
100
125
150
175
200
Time (μs)

few random walk collisions occur.

Pulse height analysis of the ^{3}He signal for three conditions, (a) with prompt, gated neutrons, (b) with the ^{252}Cf source, and (c) with self-triggered neutrons, is shown in Figure 5. The self-triggered neutrons represent all neutrons, synchronized or not, with stopped muons. The shape of all three spectra are similar and agree with the detector specifications.[12] These data provide strong evidence that neutrons, and not gammas or other particles, were being counted.

Target Preparation. A variety of targets were prepared and tested:

1) Palladium (annealed and cold worked)
2) Palladium pressure-loaded with deuterium to $PdD_{0.7}$
3) Palladium electrolytically-loaded with deuterium to $PdD_{0.7}$
4) Palladium in an active D_2O electrolysis cell
5) Titanium shavings
6) Titanium shavings pressure-loaded with deuterium to TiD_2
7) Yttrium pressure-loaded with deuterium to YD_3
8) Empty plastic or glass sample containers

In general, the pressure-loaded metal deuterides were prepared at elevated temperatures and pressures using standard procedures.[13] The deuterium content was calculated by the increase in mass of the samples. The electrolytically-loaded palladium targets were prepared in 0.1 M $LiOD/D_2O$. The loading process of the 6.4 mm rod was monitored for evidence of cold fusion.[4] Some

Figure 5 ^{3}He pulse height spectra for: (a) prompt, gated neutrons, (b) the neutron calibration source, ^{252}Cf, and (c) self-triggered neutrons.

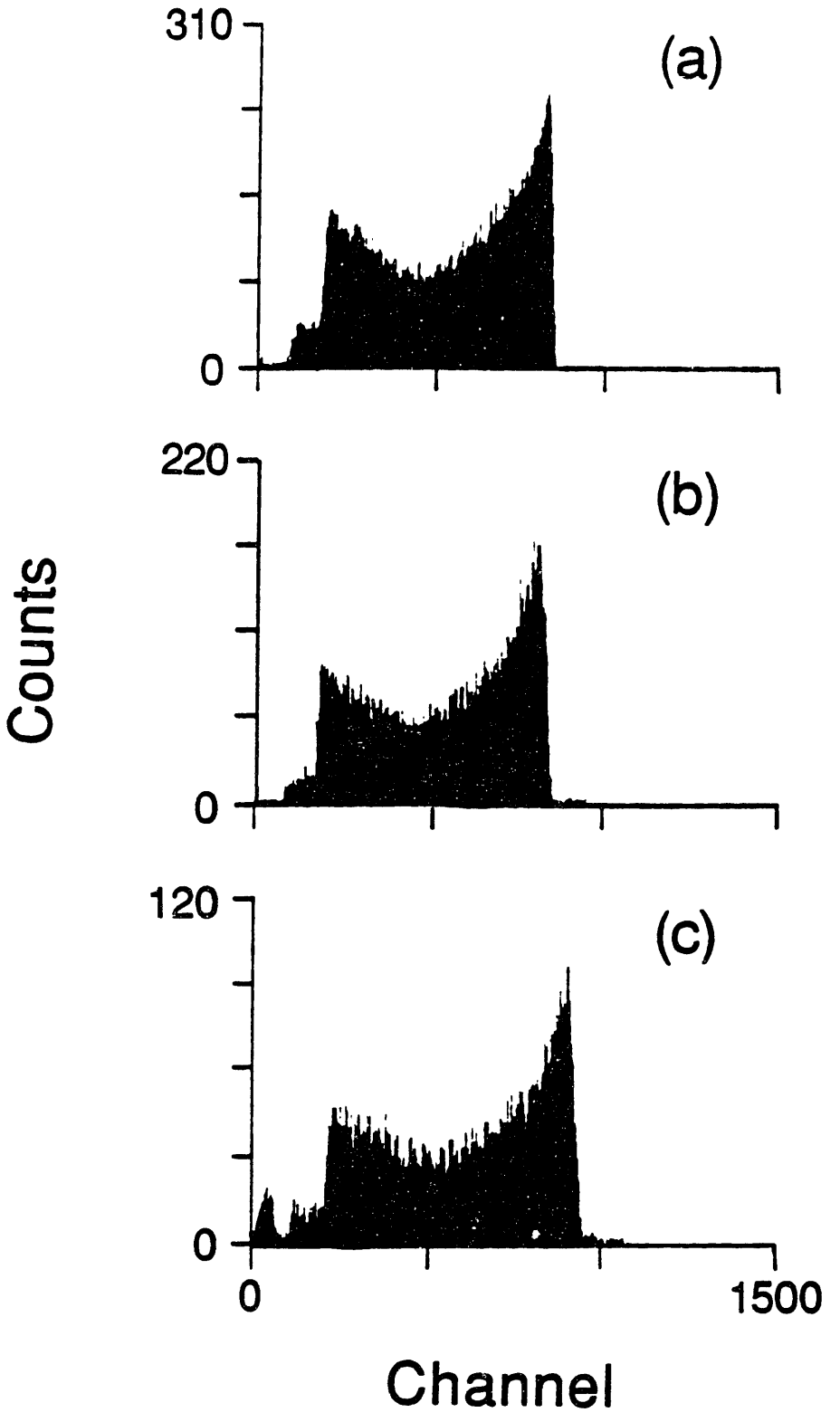
310
(a)
0
220
(b)
Counts
0
120
(c)
0
0
1500
Channel

palladium targets were annealed under vacuum just below the melting point.

Results and Discussion

A typical result is found in runs comparing palladium and palladium deuteride targets. The deuterated target was a 1 cm thick stack of four pressure-loaded $PdD_{0.7}$ sheets, prepared from Pd samples that were annealed near its melting point, producing millimeter-sized crystals. Data were acquired over 13 min. The plastic scintillator counts were:

Total μ^- in the beam

$S1 \cdot S2 \cdot S3 = 43,669$

Total μ^- stopped in target

$S1 \cdot S2 \cdot S3 \cdot \overline{S4} = 18,693$

Since the single rates in S1, S2, S3 and S4 are low, ~100/s, and the coincidence gate width is small, 10 ns, the random coincidence rate in either measurement is negligible. The fact that the stopped muons, $S1 \cdot S2 \cdot S3 \cdot \overline{S4}$, are 43% of the spatially defined muon beam, $S1 \cdot S2 \cdot S3$, indicates the beam is sufficiently degraded.

The ungated neutron count was 319,648. The 50 μs gated count was 3,804 and the 180 μs delayed gated count was 1237. The real neutron count is thus the difference of these two numbers, or 2,567. Since the neutron detector efficiency was 14 ± 1% (syst.), and approximately 39% of the neutrons fall outside the 50 μs gate, (see Figure 4) the absolute neutron count was 30058. The ratio of real neutrons to stopped muons was 1.61 ± 0.02 (stat.).

Similarly, data taken with a palladium target without deuterium shows that the ratio of the real neutrons to stopped muons was 1.65 ± 0.02 (stat.). Systematic errors in both ratios (target with and without deuterium), due to mechanical alignment, ^{3}He detection efficiency, effects due to gate width, and subtraction of the random neutron counts, are estimated to be 30%, but are similar for the different targets. The resultant systematic error on the the difference of the two ratios is estimated to be 15%, since many systematic errors cancel out. The neutron count per stopped muon due to deuterium being present in the metal is thus 0.0 ± 0.03 (stat.) with a systematic error of ± 0.25 absolute.

Experimental runs were made in which the temperature of a pressure-loaded palladium target was monitored with a linear thermistor fixed directly to the metal. No detectable temperature difference, 26 ± 0.5 °C, was measured over the time the target was exposed to the muon beam, and after the beam had been shut off.

The electrolyte solution from the electrolysis cell target was analyzed for excess tritium, a product of D-D fusion, by liquid scintillation counting.[14] The minimum detectable level was 35 dpm, and no change above the background level of 100 ± 14 dpm was observed.

Similar neutron measurements made with Ti and Y deuterated targets yielded results within the above absolute error bar, 1.5 ± 0.5 (absolute) neutrons per stopped muon.

Conclusion

From the difference in the measured number of neutrons yielded per stopped muon in deuterated and non-deuterated palladium targets, it is concluded that muon catalyzed fusion occurs at a rate of 0.0 ± 0.03 (stat.) ± 0.25 (syst.) neutrons per stopped muon. The observed ratio is consistent with the capture of muons by the heavy element nuclei,[15] within experimental error. Together with the temperature and tritium measurements, these data do not support the notion of cosmic ray induced muon catalyzed fusion in palladium deuteride, $PdD_{0.7}$.

References

1. Fleischmann, M.; Pons, B. S.; Hawkins, M. *J. Electroanal. Chem.* **1989**, *261*, 301, and erratum, **1989**, *263*, 187.

2. Jones, S. E.; Palmer, E. P.; Czirr, J. B.; Decker, D. L.; Jensen, G. L.; Thorne, J. M.; Taylor, S. F.; Rafelski, J. *Nature*, **1989**, *338*, 737.

3. DeNinno, A.; Frattolillo, A.; Lollobattista, G.; Martinia, L.; Martone, M.; Mori, L.; Fodda, S.; Scaramuzzi, F. *Europhys. Lett.* **1989**, *9*, 221.

4. Albagli, D.; Ballinger, R.; Cammarata, V.; Chen, X.; Crooks, R. M.; Fiore, C.; Gaudreau, M. J. P.; Hwang, I.; Li, C. K.; Linsay, P.; Luckhardt, S. C.; Parker, R. R.; Petrasso, R. D.; Schloh, M. O.; Wenzel, K. W.; Wrighton, M. S. *J. Fusion Energy*, submitted.

5. Gai, M.; Rugari, S. L.; France, R. H.; Lund, B. J.; Zhao, Z.; Davenport, A. J.; Isaacs, H. S.; Lynn, K.G. *Nature*, **1989**, *340*, 29.

6. Koonin, S. E.; Nauenberg, M. *Nature*, **339**, 690 (1989).

7. Z. Sun and D. Tománek, *Phys. Rev. Lett.*, **63**, 59 (1989).

8. Leggett, A. J.; Baym, G. *Nature* **1989**, *340*, 45.

9. Guinan, M. W.; Chapline, G. F.; Moir, R. W. Preprint, submitted to *Phys. Rev. Lett.*.

10. (a) Jones, S. E. *Nature* **1986**, *321*, 127. (b) Jones, S. E.; Anderson, A. N.; Caffrey, A. J.; Van Siclen, C. DeW.; Watts, K. D.; Bradbury, J. N.; Cohen, J. S.; Gram, P. A. M.; Leon, M.; Maltrud, H. R.; Paciotti, M. A. *Phys. Rev. Lett.*, **1986**, *56*, 588.

11. Suchannek, R. G.; Young, S. J.; Sheridan, J. R. *Rev. Sci. Instrum.*, **1975**, *46*, 1037.

12. Knoll, G. F. *Radiation Detection and Measurement*; Wiley: New York, 1979; p 533.

13. *Metal Hydrides*; Mueller, W. M.; Blackledge, J. P.; Libowitz, G. G., Eds.; Academic: New York, NY, 1968 and references therein.

14. Chapter VI, Results and Discussion, Section 6 B.

15. Gershtein, S. S.; Ponomarev, L. I. In *Muon Physics*; Hughes V. W.; Wu, C. S., Eds.; Academic: New York, NY, 1975; Vol. 3, p 141-233.